

**Toxicology of Functionalized Nanomaterials in Fishes**

by

Lindsey Colleen Felix

A thesis submitted in partial fulfillment of the requirements for the degree of

Doctor of Philosophy

in

PHYSIOLOGY, CELL AND DEVELOPMENTAL BIOLOGY

Department of Biological Sciences  
University of Alberta

© Lindsey Colleen Felix, 2016

## ABSTRACT

Engineered nanomaterials (NMs), tiny synthetic materials having at least one dimension between one and one hundred billionths of a metre, are increasingly being developed for and incorporated into a myriad of commercial, consumer, and industrial applications due to their unique and tailorable properties. Widespread and expanding production and use of engineered NMs implies that they will enter aquatic environments through accidental (e.g. down-the-drain disposal of NM-containing consumer products) or intentional (e.g. groundwater remediation efforts) anthropogenic release and thus have the potential to interact with and adversely affect living organisms like fishes. My research aimed to identify the physical and chemical properties intrinsic to the NMs themselves (e.g. surface coatings or functional groups) and extrinsic environmental factors (e.g. solar radiation) that modulate NM toxicity using fish model systems. Several functionalized and nonfunctionalized metal oxide and carbon-based NMs were characterized using appropriate analytical instruments and techniques. The information derived from these studies was used to better understand the interactions between NMs and biological systems and to accurately evaluate and interpret the toxicological effects resulting from exposure. Zebrafish (*Danio rerio*) embryos were exposed to a range of NM concentrations (0.1-2000 mg/L) under laboratory and more environmentally realistic conditions for up to seven days, multiple endpoints indicative of toxicity (e.g. alterations in gene expression, delayed development, incidences of malformation, increased antioxidant enzyme activity, lethality, lipid peroxidation, etc.) were assessed, and the potential

mechanisms underlying noted toxicity were elucidated. Moreover, a combination of flow cytometry and laser scanning confocal microscopy was used to investigate the cellular uptake mechanisms of NMs and to determine their subsequent fate within rainbow trout (*Oncorhynchus mykiss*) gill epithelial cells. The work presented here represents the first comprehensive, explicit, and systematic evidence-based report on the toxicology of functionalized NMs in fishes and some of the major findings were as follows. Most NMs adsorbed to or settled on the embryonic zebrafish while some traversed the chorion and sorbed to the developing fish within the chorionic membrane. However, the NMs located on the external larval surface could not be distinguished from those that may have been internalized by the animal using *in vivo* methods. Further *in vitro* measurements demonstrated that these surface-bound NMs were actively taken up into rainbow trout gill epithelial cells via clathrin-mediated endocytosis and became localized within lysosomal compartments. Surface functionalization was found to affect the characteristics of certain carbon-based NMs resulting in differential responses and thus played a key role in determining their toxicity at different levels of biological organization. Furthermore, the surface coating was shown to lessen the severity of reactive oxygen species induced effects of metal oxide NMs on embryo-larval zebrafish and toxicity was reported to depend on ultraviolet light exposure. Taken together, improved knowledge and understanding of the factors that modulate NM toxicity and the mechanisms by which NMs cause effects will facilitate accurate toxicological assessments by researchers and thus allow risk assessors to better predict the potential impact of engineered NMs when they are unintentionally or purposefully released into the aquatic environment.

## PREFACE

This thesis is an original work by Lindsey Colleen Felix. The research project, of which this thesis is a part, received research ethics approval from the University of Alberta Animal Care and Use Committee. The following protocols governed this research: AUP00000001 (2012-2016); Effects of Nanoparticle Exposure on Zebrafish, Trout and Cardinal tetras Development and Physiology AUP Protocol #566 Fate and effects of Nanomaterials in the Aquatic environment (2008-2012).

Some of the research conducted for this thesis forms part of an international research collaboration, led by Professor G.G. Goss at the University of Alberta, with Professor G.G. Goss being the lead collaborator at the University of Alberta. I (Lindsey C. Felix) performed the majority of the work presented in this original Ph.D. thesis. However, some parts of this thesis were the result of collaborative efforts and thus, the terms “we” and “our” are used throughout this thesis. I was invited to submit parts of **Chapters 1 and 6** for possible publication as a book chapter. **Chapters 2 and 3** have been published in Environmental Science and Technology and Carbon peer-review journals, respectively. **Chapters 4 and 5** will be submitted for possible publication in peer-review journals. The bibliographical details for each data chapter are listed below and indicated at the beginning of each corresponding data chapter. The roles of all authors for each data chapter along with specific experimental contributions of certain co-authors are briefly described below:

### **Chapter 2:**

Felix, L.C., Ortega, V.A., Ede, J.D., Goss, G.G., 2013. Physicochemical characteristics of polymer-coated metal oxide nanoparticles and their toxicological effects on zebrafish (*Danio rerio*) development. Environmental Science and Technology 47(12), 6589–6596. doi: 10.1021/es401403p.

LCF, VAO, and GGG conceived and designed the experiments. LCF, VAO, and JDE performed the experiments. LCF analyzed the data. GGG contributed analysis tools, materials, and reagents. LCF and GGG wrote the manuscript. LCF, VAO, JDE, and GGG drafted and revised the manuscript. All experiments performed in Chapter 2 are the result of my individual efforts with the following exceptions: LCF and VAO collaboratively collected dissolution data and JDE took confocal microscope images.

### **Chapter 3:**

Felix, L.C., Ede, J.D., Snell, D.A., Oliveira, T.M., Martinez-Rubi, Y., Simard, B., Luong, J.H.T., Goss, G.G., 2016. Physicochemical properties of functionalized carbon-based nanomaterials and their toxicity to fishes. Carbon 104, 78–89. doi: 10.1016/j.carbon.2016.03.041.

LCF, JDE, and GGG conceived and designed the experiments. LCF, JDE, DAS, and TMO performed the experiments. LCF analyzed the data. YM-R, BS, JHTL, and GGG contributed analysis tools, characterization data, materials, and/or reagents. LCF and GGG wrote the manuscript. LCF, JDE, DAS, TMO, YM-R, BS, JHTL, and

GGG drafted and revised the manuscript. All experiments performed in Chapter 3 are the result of my individual efforts with the following exceptions: JDE provided cell viability data while DAS and TMO assisted with some data collection.

**Chapter 4:**

Felix, L.C., Folkerts, E.J., He, Y., Goss, G.G. Poly (acrylic acid) polymer coating mitigates hydroxyl radical-mediated effects of titanium dioxide nanoparticles in developing zebrafish (*Danio rerio*). To be submitted.

LCF and GGG conceived and designed the experiments. LCF, EJJ, and YH performed the experiments. LCF analyzed the data. GGG contributed analysis tools, materials, and reagents. LCF and GGG wrote the manuscript. LCF, EJJ, YH, and GGG drafted and revised the manuscript. All experiments performed in Chapter 4 are the result of my individual efforts, including construction of the apparatus, with the following exceptions: EJJ and YH collected thiobarbituric acid reactive substances and gene expression data, respectively.

**Chapter 5:**

Felix, L.C., Ortega, V.A., Goss, G.G. Cellular uptake and intracellular localization of poly (acrylic acid) nanoparticles in a rainbow trout (*Oncorhynchus mykiss*) gill epithelial cell line. To be submitted.

LCF, VAO, and GGG conceived and designed the experiments. LCF performed the experiments and analyzed the data. GGG contributed analysis tools, materials, and reagents. LCF and GGG wrote the manuscript. LCF, VAO, and GGG drafted and revised the manuscript.

## ACKNOWLEDGEMENTS

First and foremost I would like to acknowledge my advisor, Dr. Greg Goss, and my committee members, Dr. Keith Tierney and Dr. James Stafford, for providing an immeasurable amount of guidance and support throughout my program. I am now a more confident arguer, presenter, researcher, and writer because of them. I have had many incredible opportunities and experiences under their supervision. Words cannot express how much I appreciate their sound advice, encouragement, and expertise. I would also like to thank my internal/external examiner, Dr. John Seubert, and my external examiner, Dr. Caren Helbing, for taking the time to read this thesis, attending my PhD defense, and providing constructive criticism.

I am grateful to the Natural Sciences and Engineering Research Council of Canada and the University of Alberta for noticing my efforts and subsequently awarding me the Postgraduate Scholarship (Doctoral) and Queen Elizabeth II Graduate Scholarships (Masters and Doctoral), respectively. I would not have made it this far without the abovementioned financial support.

I would also like to recognize the many collaborators and colleagues who contributed to the work presented in this thesis. Many thanks to Dr. Darren Anderson of Vive Crop Protection Inc., Dr. Cynthia Goh from the University of Toronto, Dr. Yadienka Martinez-Rubi and Dr. Benoit Simard from the National Research Council of Canada, and Dr. John Luong from the University College Cork for generously donating and providing an extensive characterization of the materials for these studies. Thank you to Arlene Oatway, Dr. Andrew Waskiewicz, and Dr. Kathy Magor

from the University of Alberta and Geraldine Barron and Dr. Xuejun Sun from the Cross Cancer Institute for help with microscope imaging. Thanks to Dr. Niels Bols from the University of Waterloo for providing the fish gill cell line, Dr. Shuangquan Zhang and Madeleine Jensen-Fontaine from the University of Alberta for instrument analysis, Aleah McCorry and Jesse Edgington from the Biological Sciences Animal Services for fish care, and undergraduate students, Dana Snell, Taiane Oliveira, and Muhammad Raza for contributing their time and efforts toward facilitating my projects. My PhD dissertation has been strengthened because of your involvement.

Furthermore, I am thankful to the members of the Goss lab, past and present, who have made my time at the University of Alberta both enjoyable and memorable. I am particularly appreciative of my collaborations and friendships with Dr. David Boyle, Erik Folkerts, Dr. James Ede, Dr. Kimberly Ong, Van Ortega, and Dr. Yuhe He. Your willingness to read drafts, offer suggestions for improvement, and provide advice, encouragement, support, and training along the way did not go unnoticed.

Last but not least, I would like to give special thanks to my family. To my parents, Alice and Richard Felix, thank you for your unconditional love, emotional and financial support, and for inspiring me to “get my education.” To my sister, Janeen Felix, thanks for encouraging me to maintain a healthy, balanced lifestyle and for reminding me that I am only human and therefore I should not be so hard on myself. I am especially indebted to my nephew, Ryker Samson, born the same year I began my graduate studies, whose rapid growth has motivated me to complete my PhD degree. Finally, I would like to express my gratitude to my loving and patient fiancé, Andrew Sova, whose faith in me never faltered. I love you all very much.

## TABLE OF CONTENTS

LIST OF TABLES .....	xii
LIST OF FIGURES .....	xiii
LIST OF ABBREVIATIONS .....	xv

### CHAPTER 1

Introduction.....	1
1.1 INTRODUCTION .....	2
1.2 TRANSPORT, TRANSFORMATION, AND FATE OF NANOMATERIALS .....	5
1.2.1 Environmental.....	5
1.2.2 Biological.....	7
1.2.2.1 Absorption and uptake .....	8
1.2.2.2 Distribution, metabolism, and excretion .....	14
1.3 FACTORS MODULATING NANOMATERIAL TOXICITY .....	16
1.3.1 Size, agglomeration, and charge .....	17
1.3.2 Dissolution .....	19
1.3.3 Surface functionalization.....	21
1.3.4 Natural organic matter .....	22
1.3.5 Ultraviolet light .....	23
1.4 CHALLENGES IN NANOTOXICITY TESTING .....	25
1.5 TOXICITY ASSESSMENT OF NANOMATERIALS .....	30
1.5.1 Cerium oxide nanomaterials.....	31
1.5.2 Iron oxide nanomaterials .....	34
1.5.3 Titanium dioxide nanomaterials.....	35
1.5.4 Zinc oxide nanomaterials .....	36
1.5.5 Single-walled carbon nanotubes .....	38
1.5.6 Cellulose nanocrystals .....	39
1.6 <i>IN VIVO</i> AND <i>IN VITRO</i> FISH MODELS .....	40
1.6.1 Zebrafish embryo.....	41
1.6.2 Rainbow trout gill epithelial cell line .....	42
1.7 THESIS GOALS .....	43

### CHAPTER 2

Physicochemical characteristics of polymer-coated metal oxide nanoparticles and their toxicological effects on zebrafish ( <i>Danio rerio</i> ) development.....	44
--	----

<b>2.1 INTRODUCTION .....</b>	<b>45</b>
<b>2.2 MATERIALS AND METHODS .....</b>	<b>47</b>
2.2.1 Synthesis of polymer-coated nanoparticles .....	47
2.2.2 Physicochemical characterization of polymer-coated nanoparticles .....	48
2.2.3 Polymer-coated metal oxide nanoparticle dissolution .....	49
2.2.4 Rearing facility and embryo production.....	50
2.2.5 Zebrafish embryo toxicity assay .....	51
2.2.6 Lethal and sublethal endpoints.....	52
2.2.7 Nanoparticle interaction with zebrafish embryo .....	53
2.2.8 Statistical analysis .....	55
<b>2.3 RESULTS AND DISCUSSION .....</b>	<b>55</b>
2.3.1 Physicochemical characterization of polymer-coated nanoparticles .....	55
2.3.2 Polymer-coated nanoparticle dissolution.....	57
2.3.3 Lethality tests on zebrafish embryos and post-hatch larvae.....	61
2.3.4 Sublethal effects on zebrafish .....	63
2.3.5 Nanoparticle interaction with zebrafish embryo .....	65
 <b>CHAPTER 3</b>	
<b>Physicochemical properties of functionalized carbon-based nanomaterials and their toxicity to fishes .....</b>	<b>70</b>
<b>3.1 INTRODUCTION .....</b>	<b>71</b>
<b>3.2 EXPERIMENTAL.....</b>	<b>74</b>
3.2.1 Nanomaterial production and functionalization.....	74
3.2.2 Preparation of nanomaterial test suspensions.....	75
3.2.3 Physicochemical characterization of nanomaterials.....	76
3.2.4 Zebrafish holding facility and collection of viable embryos .....	78
3.2.5 Cell culture .....	79
3.2.6 Whole-animal effects of nanomaterial exposure to zebrafish.....	79
3.2.7 Cellular effects of nanomaterial exposure to channel catfish cells.....	80
3.2.8 Molecular effects of nanomaterial exposure to zebrafish .....	81
3.2.9 Statistical analysis .....	82
<b>3.3 RESULTS AND DISCUSSION .....</b>	<b>83</b>
3.3.1 Physicochemical characteristics of functionalized nanomaterials .....	83
3.3.2 Whole-animal effects .....	89
3.3.3 Cellular effects.....	95
3.3.4 Molecular effects .....	97
<b>3.4 CONCLUSIONS .....</b>	<b>100</b>

## **CHAPTER 4**

<b>Poly (acrylic acid) polymer coating mitigates hydroxyl radical-mediated effects of titanium dioxide nanoparticles in developing zebrafish (<i>Danio rerio</i>) .....</b>	<b>102</b>
<b>4.1 INTRODUCTION .....</b>	<b>103</b>
<b>4.2 MATERIALS AND METHODS .....</b>	<b>105</b>
<b>4.2.1 Nanoparticle sources and preparation of suspensions .....</b>	<b>105</b>
<b>4.2.2 Production of hydroxyl radicals by nanoparticles.....</b>	<b>106</b>
<b>4.2.3 Coexposure of zebrafish embryos to nanoparticles and simulated sunlight.....</b>	<b>107</b>
<b>4.2.4 Survival, hatching success, and malformation .....</b>	<b>108</b>
<b>4.2.5 Thiobarbituric acid reactive substances assay .....</b>	<b>108</b>
<b>4.2.6 Catalase, total glutathione, superoxide dismutase, and protein assays</b>	<b>109</b>
<b>4.2.7 Gene expression profiles.....</b>	<b>110</b>
<b>4.2.8 Statistical analysis .....</b>	<b>111</b>
<b>4.3 RESULTS AND DISCUSSION .....</b>	<b>112</b>
<b>4.3.1 Hydroxyl radical generation .....</b>	<b>112</b>
<b>4.3.2 Whole-animal effects .....</b>	<b>114</b>
<b>4.3.3 Tissue and biochemical effects.....</b>	<b>117</b>
<b>4.3.4 Molecular effects .....</b>	<b>121</b>
<b>CHAPTER 5</b>	
<b>Cellular uptake and intracellular localization of poly (acrylic acid) nanoparticles in a rainbow trout (<i>Oncorhynchus mykiss</i>) gill epithelial cell line .....</b>	<b>124</b>
<b>5.1 INTRODUCTION .....</b>	<b>125</b>
<b>5.2 METHODS .....</b>	<b>129</b>
<b>5.2.1 Nanoparticle synthesis, stock preparation, and characterization .....</b>	<b>129</b>
<b>5.2.2 Fluorescent biomarkers, transport inhibitors, and organelle stains.....</b>	<b>130</b>
<b>5.2.3 Cell culture and seeding of cells.....</b>	<b>132</b>
<b>5.2.4 Efficacy of endocytosis inhibitors .....</b>	<b>133</b>
<b>5.2.5 Nanoparticle uptake and inhibition of endocytotic pathways .....</b>	<b>134</b>
<b>5.2.6 Flow cytometry analysis of uptake in live cells .....</b>	<b>134</b>
<b>5.2.7 Laser scanning confocal microscopy of fixed and live cells .....</b>	<b>135</b>
<b>5.2.8 Statistical analysis .....</b>	<b>136</b>
<b>5.3 RESULTS .....</b>	<b>137</b>
<b>5.3.1 Physicochemical properties of nanoparticle suspensions.....</b>	<b>137</b>
<b>5.3.2 Uptake and intracellular localization of nanoparticles .....</b>	<b>139</b>
<b>5.4 DISCUSSION .....</b>	<b>144</b>
<b>5.5 CONCLUSIONS .....</b>	<b>153</b>

**CHAPTER 6**

**Conclusions and future directions..... 154**

**6.1 CONCLUSIONS AND FUTURE DIRECTIONS..... 155**

**6.1.1 General conclusions ..... 156**

**6.1.2 Recommendations for future research..... 162**

*6.1.2.1 Evaluate nanomaterial toxicity under environmentally realistic conditions ..... 163*

*6.1.2.2 Assess functionalized nanomaterial phototoxicity at the cellular level ..... 164*

*6.1.2.3 Examine cellular uptake and fate of nanomaterials by several approaches..... 165*

*6.1.2.4 Explore the toxicokinetics of functionalized nanomaterials using fish ..... 166*

**6.1.3 Outlook..... 167**

**WORKS CITED ..... 169**

**APPENDICES..... 216**

**Supplemental Tables..... 216**

**Supplemental Figures ..... 222**

**Supplemental Text ..... 246**

*Appendix I ..... 246*

*Appendix II..... 247*

*Appendix III ..... 250*

## LIST OF TABLES

<b>Table 1-1. General characteristics of the metal oxide- and carbon-based NMs examined in this thesis.....</b>	<b>33</b>
<b>Table 5-1. Physicochemical characteristics of NP suspensions.....</b>	<b>138</b>
<b>Table S2-1. Product information provided by Vive Crop Protection Inc. ....</b>	<b>216</b>
<b>Table S2-2. pH values of vnCAP exposure suspensions .....</b>	<b>217</b>
<b>Table S2-3. Trace metal content present in NP stock suspensions.....</b>	<b>218</b>
<b>Table S2-4. Lethal concentration 50 values and 95% confidence intervals .....</b>	<b>219</b>
<b>Table S3-1. Gene-specific primers for zebrafish.....</b>	<b>220</b>
<b>Table S4-1. Gene-specific primers for zebrafish.....</b>	<b>221</b>

## LIST OF FIGURES

Figure 1-1. Schematic of possible endocytotic pathways utilized by NPs to enter RTgill-W1 cells .....	11
Figure 1-2. Diagram showing the interrelationship between antioxidant defense enzymes, ROS, and oxidative damage.....	26
Figure 1-3. Diagram of the functionalized NMs examined in this thesis.....	32
Figure 2-1. Graphical abstract.....	44
Figure 2-2. Dissolution of polymer-coated NPs.....	58
Figure 2-3. pH-dependent dissolution of polymer-coated ZnO NPs.....	60
Figure 2-4. Cumulative percent survival of NP exposed zebrafish.....	62
Figure 2-5. Percent hatch of MeO NP exposed zebrafish.....	64
Figure 2-6. Sorption of CeO <sub>2</sub> NPs to zebrafish embryos.....	67
Figure 2-7. Sorption of vnCAP-NR to zebrafish embryos.....	68
Figure 3-1. Physicochemical properties of functionalized SWCNT and CNC test suspensions over time .....	85
Figure 3-2. Trace metals present SWCNT and SLS test suspensions.....	88
Figure 3-3. Cumulative percent survival of zebrafish exposed to SWCNT and CNC test suspensions.....	91
Figure 3-4. Percent hatch of zebrafish exposed to SWCNT and CNC test suspensions .....	93
Figure 3-5. The viability of channel catfish cell lines after <i>in vitro</i> CNC exposure .....	96
Figure 3-6. Changes in gene expression patterns following exposure to SWCNT and CNC test suspensions.....	99
Figure 4-1. Graphical abstract.....	102
Figure 4-2. Generation of OH• by NPs.....	113
Figure 4-3. Percent hatch of zebrafish exposed to NPs in the absence (-) or presence (+) of illumination .....	116
Figure 4-4. Lipid peroxidation in zebrafish larvae.....	118
Figure 4-5. Cat activity, TG level, and Sod activity in co-exposed zebrafish larvae.....	120
Figure 4-6. Changes in zebrafish gene expression patterns following NP and UV light co-exposure.....	122
Figure 5-1. Effects of pharmacological inhibitors on the association of fluorescently labelled biomolecules with RTgill-W1 cells.....	140
Figure 5-2. Effect of endocytosis inhibitors on the association of 3-9 nm NPs with RTgill-W1 cells .....	141
Figure 5-3. LSCM images revealed NP association with RTgill-W1 cells.....	142
Figure 5-4. LSCM images of negative control cells .....	143
Figure 5-5. Three-dimensional rendering of RTgill-W1 cells following a 1 h exposure to 25 µg/mL NPs (red) .....	145
Figure 5-6. Association of NPs with lysosomes of RTgill-W1 cells.....	146
Figure 5-7. Three-dimensional rendering of RTgill-W1 cells following coexposure to 10 µg/mL NPs (red spheres) and LTY (green spheres).....	147
Figure S2-1. Schematic diagram of polymer-coated NP synthesis .....	222

<b>Figure S2-2. TEM images of MeO NPs .....</b>	<b>223</b>
<b>Figure S2-3. Time-dependent changes in hydrodynamic diameter.....</b>	<b>224</b>
<b>Figure S2-4. Time-dependent changes in polydispersity index .....</b>	<b>225</b>
<b>Figure S2-5. Time-dependent changes in zeta potential.....</b>	<b>226</b>
<b>Figure S2-6. Cumulative percent survival of free metal exposed zebrafish .....</b>	<b>227</b>
<b>Figure S2-7. Length of 72 hpf zebrafish larvae.....</b>	<b>228</b>
<b>Figure S3-1. A schematic diagram of the oxidation process .....</b>	<b>229</b>
<b>Figure S3-2. Optical properties of SWCNT and SLS test suspensions.....</b>	<b>230</b>
<b>Figure S3-3. Screening of endogenous control genes and genes of interest by polymerase chain reaction amplification .....</b>	<b>231</b>
<b>Figure S3-4. Representative TEM images of SWCNTs and CNCs .....</b>	<b>232</b>
<b>Figure S3-5. Ammonia concentration in SWCNT suspension.....</b>	<b>233</b>
<b>Figure S3-6. Adsorption of NF-SWCNTs to zebrafish embryos and larvae .....</b>	<b>234</b>
<b>Figure S3-7. Changes in endogenous control gene expression patterns following exposure to SWCNT and CNC test suspensions .....</b>	<b>235</b>
<b>Figure S4-1. Schematic of experimental design and endpoints examined.....</b>	<b>236</b>
<b>Figure S4-2. Representative micrographs of 144 hpf larvae.....</b>	<b>237</b>
<b>Figure S4-3. Screening of endogenous control genes and genes of interest by polymerase chain reaction (PCR) amplification .....</b>	<b>238</b>
<b>Figure S4-4. Representative TEM images of NPs .....</b>	<b>239</b>
<b>Figure S4-5. Physicochemical characteristics of NP suspensions over time.....</b>	<b>240</b>
<b>Figure S4-6. Percent survival of zebrafish exposed to NPs in the absence (-) or presence (+) of UV illumination .....</b>	<b>241</b>
<b>Figure S4-7. Malformations caused by NP and UV light co-exposure.....</b>	<b>242</b>
<b>Figure S4-8. Uncoated TiO<sub>2</sub> NPs absorb at wavelengths used for TG (412 nm), Sod (450 nm), TBARS (531 nm), Cat (560 nm), and protein (562 nm) assay measurements.....</b>	<b>243</b>
<b>Figure S4-9. NP interference with biochemical assay components, without (-) and with (+) analyte .....</b>	<b>244</b>
<b>Figure S4-10. Changes in endogenous control gene expression patterns .....</b>	<b>245</b>

## LIST OF ABBREVIATIONS

\* Terms are abbreviated after first use within each chapter.

1G8	channel catfish B-cell line
28S.3	channel catfish T-cell line
2-DR	2-deoxy-D-ribose
3B11	channel catfish B-cell line
<i>α-ttp</i>	<i>alpha-tocopherol transport protein</i> , zebrafish gene
ALS	ammonium lignin sulfonate
ALS-SWCNT(s)	ammonium lignin sulfonate wrapped single-walled carbon nanotube(s)
ANOVA	analysis of variance
APS	ammonium persulfate
bs	bent spine
BSA	bovine serum albumin
Cat	catalase, antioxidant enzyme
<i>cat</i>	<i>catalase</i> , zebrafish gene
CavME	caveolae-mediated endocytosis
CMDR	CellMask Deep Red plasma membrane stain
CME	clathrin-mediated endocytosis
CNC(s)	cellulose nanocrystal(s)
CNT(s)	carbon nanotube(s)
-CO	carbonyl group
-COO <sup>-</sup>	carboxylate anion
COO <sup>-</sup> -CNC(s)	carboxylated cellulose nanocrystal(s)
COOH-30-SWCNT(s)	carboxylic acid functionalized at 30 °C single-walled carbon nanotube(s)
COOH-40-SWCNT(s)	carboxylic acid functionalized at 40 °C single-walled carbon nanotube(s)
COOH-50-SWCNT(s)	carboxylic acid functionalized at 50 °C single-walled carbon nanotube(s)
CPZ	chlorpromazine
CTb	cholera toxin B subunit
CTb-FITC	cholera toxin B subunit, fluorescein isothiocyanate conjugate
DAPI	4',6-diamidino-2-phenylindole
ddH <sub>2</sub> O	double-distilled water
Dex	dextran
Dex-FL	10 kDa dextran, fluorescein conjugate
DL	detection limit
DLS	dynamic light scattering
DMSO	dimethyl sulfoxide
DTW	dechlorinated tap water
E	amplification efficiency

<i>eflα</i>	<i>elongation factor 1 alpha</i> , zebrafish gene
Ex/Em	excitation/emission wavelengths
F	forward primer sequence
FAAS	flame atomic absorption spectrometer
FBS	fetal bovine serum
FETEM	field emission transmission microscopy
<i>gclc</i>	<i>glutamate-cysteine ligase catalytic subunit</i> , zebrafish gene
GN	genistein
<i>gpx1a</i>	<i>glutathione peroxidase 1a</i> , zebrafish gene
GSSG	glutathione disulfide
GTPase	guanosine triphosphatase
H <sub>2</sub> O <sub>2</sub>	hydrogen peroxide
<i>hif1ab</i>	<i>hypoxia-inducible factor 1 alpha subunit b</i> , zebrafish gene
hpf	hour(s) post fertilization
<i>hsp70</i>	<i>heat shock protein 70 kDa</i> , zebrafish gene
ICP-MS	inductively coupled plasma mass spectroscopy
ICP-OES	inductively coupled plasma optical emission spectrometer
L-15 medium	Leibovitz L-15 cell culture medium
LC50	lethal concentration 50 value
LSCM	laser scanning confocal microscope
LTY	LysoTracker Yellow-HCK-123
LVTEM	low voltage transmission electron microscopy
MCC	microcrystalline cellulose
MeO	metal oxide
MP	macropinocytosis
NCBI	National Center for Biotechnology Information
NF-SWCNT(s)	nonfunctionalized single-walled carbon nanotube(s)
NM(s)	nanomaterial(s)
NP(s)	nanoparticle(s)
NR	Nile red
NRC	National Research Council of Canada
PAA	poly (acrylic acid)
PBS	phosphate buffered saline
PBS/BSA	PBS containing 0.05% bovine serum albumin
PCR	polymerase chain reaction
pe	pericardial edema
PI	propidium iodide
polymer-coated TiO <sub>2</sub> NP(s)	poly (acrylic acid)-coated titanium dioxide nanoparticle(s)
polymer NP(s)	poly (acrylic acid) nanoparticle(s)
qPCR	quantitative polymerase chain reaction
R	reverse primer sequence
RCF	relative centrifugal force

ROS	reactive oxygen specie
rpm	revolutions per minute
RTgill-W1	rainbow trout gill epithelial cell line
O <sub>2</sub> <sup>-</sup>	superoxide anion(s)
OECD	Organisation for Economic Co-operation and Development
-OH	hydroxyl group
OH•	hydroxyl radical
SEM	standard error of the mean
SLS	sodium lignin sulfonate
SLS-SWCNT(s)	sodium lignin sulfonate wrapped single-walled carbon nanotube(s)
Sod	superoxide dismutase, antioxidant enzyme
<i>sod2</i>	<i>superoxide dismutase 2</i> , zebrafish gene
SWCNT(s)	single-walled carbon nanotube(s)
TBARS	thiobarbituric acid reactive substances
TEM	transmission electron microscopy
TEP	1,1,3,3-tetraethoxypropane
Tf-FL	transferrin from human serum, fluorescein conjugate
TG	total glutathione
TiO <sub>2</sub> NP(s)	titanium dioxide nanoparticle(s)
TMS	tricaine methanesulfonate
Trypsin/EDTA	trypsin containing 0.05% ethylenediaminetetraacetic acid
uncoated TiO <sub>2</sub> NP(s)	uncoated titanium dioxide nanoparticle(s)
USD	United States dollar
UV	ultraviolet
vn	Vive Nano Inc. (now Vive Crop Protection Inc.)
vnCAP	poly (acrylic acid) nanocapsule
vnCAP-NR	poly (acrylic acid) nanocapsule loaded with Nile red
vnCeO <sub>2</sub>	poly (acrylic acid)-coated cerium oxide nanoparticle
vnFe <sub>2</sub> O <sub>3</sub>	poly (acrylic acid)-coated iron oxide nanoparticle
vnTiO <sub>2</sub>	poly (acrylic acid)-coated titanium dioxide nanoparticle
vnZnO	poly (acrylic acid)-coated zinc oxide nanoparticle
WN	wortmannin
yse	yolk sac edema
ζ potential	zeta potential

# **CHAPTER 1**

## **Introduction**

## 1.1 INTRODUCTION

Hailed by many as the next industrial revolution (Kumar and Jee, 2013), the rapidly expanding interdisciplinary field of nanotechnology involving the controlled manipulation of matter at the nanoscale is critical to advances in several areas including agriculture, construction, electronics, energy, environment, food, manufacturing, materials, medicine, pharmaceuticals, robotics, transport, and security (Sharma et al., 2015). The field of nanotechnology has boomed since the Nobel Laureate and quantum theorist, Richard Feynman, first introduced the concept back in 1959 during his renowned speech titled “There is plenty of room at the bottom” (Feynman, 1959), which opened the door to immense possibilities at the atomic scale. Fifteen years later, physicist Norio Taniguchi coined the term nanotechnology in his conference paper titled “On the basic concept of nano-technology” (with a hyphen) (Taniguchi, 1974) and in 1990, the first nanotechnology-related journal called “Nanotechnology” began to publish articles. Nanotechnology is now a multibillion-dollar per annum industry (Schultz et al., 2014) and research is being conducted globally. According to BCC Research, the worldwide market for nanotechnology-based products was worth ~26 billion United States dollars (USD) in 2014 and this market research company predicts that nanotechnology will generate ~64 billion USD by the year 2019 (BCC Research, 2014). From more than 60,000 articles related to nanotechnology available on PubMed in May 2016, half were published in the last five years indicating a considerable interest in this field. The advancement of nanotechnology will lead to the precise control and manipulation of

atoms and molecules that make up all physical matter (Yih and Moudgil, 2007). Traditional manufacturing uses a top-down approach to make small objects from larger components, whereas bottom-up nanotechnology employs the fundamental aspects of molecular recognition directed self-assembly to build nanoscale objects atom by atom (Singh et al., 2013). Several national research institutions (e.g. National Institute of Nanotechnology, CA), manufacturing industries (e.g. Applied Nanotools, CA), and government-funded initiatives (e.g. National Nanotechnology Initiative, USA) have been established to facilitate the research and development of nanotechnology-based applications and products. As a result, many multi-disciplinary concerted and coordinated efforts have been made to address the environmental health and safety concerns related to nanoscale devices, materials, and structures including Environment Canada, the European Commission for Standardization, the Organisation for Economic Co-operation and Development (OECD), the World Health Organization, and the Natural Sciences and Engineering Research Council of Canada, National Research Council of Canada and the Business Development Bank of Canada Nanotechnology Initiative, which has funded much of my research.

Introduced over a decade ago (Donaldson et al., 2004), nanotoxicology is an emerging multidisciplinary branch of toxicology that evaluates the safety of engineered nanomaterials (NMs) by assessing their effects on living organisms (Oberdörster et al., 2005b). Gallud and Fadeel (2015) have suggested that NMs should be defined as “materials that can interact with biological systems at the nanoscale.” Although there is still no ‘one-size-fits-all’ definition of a NM (Gallud and Fadeel, 2015), the European Commission’s recommended regulatory definition is

a step forward (European Commission, 2011). For the purposes of this thesis, an engineered NM is defined as a tiny synthetic material having at least one dimension between one and one hundred billionths of a metre, which can include a nanoparticle that has three nanoscale dimensions, as well as a nanotube and a nanocrystal that have one dimension extending one hundred nanometers or more (International Organization for Standardization, 2015); the term NM will be used consistently throughout this chapter for clarity. Due to their small size, NMs exhibit unique colloidal properties and functions that differ from their bulk counterparts (Schultz et al., 2014). For example, NMs have a high surface area-to-volume ratio, and hence have more exposed atoms on their surfaces compared to bulk materials (Pietrojusti et al., 2014). Therefore, potential NM effects may not be predicted by conventional toxicological approaches (Shvedova et al., 2016). The volume of nano-products and thus nano-wastes are increasing at a much faster rate than toxicological information is being generated by nanotoxicologists and analyzed by regulators (Reinsborough and Sullivan, 2011).

Here, I will highlight some of the key aspects of my research including the factors that modulate the transport, transformation, and fate of NMs in the environment and their ensuing interactions with biological systems. Then, I will discuss the challenges facing nanotoxicologists and regulators that seek to minimize and predict the potential risk associated with NMs when they are inadvertently or intentionally released into the environment. Finally, I will provide an exclusive toxicological assessment of the model NMs used in my studies, describe my *in vivo* and *in vitro* fish model systems, and present the goals of my thesis.

## **1.2 TRANSPORT, TRANSFORMATION, AND FATE OF NANOMATERIALS**

Given that there are over 1800 nanotechnology-based consumer products currently available on the market (Vance et al., 2015), these and other nano-enabled or nano-enhanced applications will inevitably end up in the environment and interact with living organisms at some point during their product life cycle (Mitrano et al., 2015). It is noteworthy that non-engineered NMs derived from sources including dust storms, forest fires, and volcanic eruptions are naturally found in the environment (Grillo et al., 2015). The potential transport, transformation and fate of engineered NMs in the environment will be discussed in the first subsection below.

### **1.2.1 Environmental**

The increased production of manufactured NMs means that they will come in contact with the environment through various routes including the use, recycling, and/or disposal of nanotechnology-based consumer products, discharge of effluent from wastewater treatment and industrial processing plants, controlled release of nanoformulations for environmental remediation efforts (Dhar Dwivedi et al., 2015), and/or accidental production or transport spills (Gottschalk and Nowack, 2011). Nanoadditives in food, personal care, and other household products that are flushed as feces/urine, washed off skin, or poured down the drain enter wastewater treatment plants and subsequently the environment as treated effluent liberated into surface waters or as incinerated wastes, landfill solids, or biosolids derived from sewage sludge applied to agricultural land (Weir et al., 2012). Wastewater treatment plant

processes may effectively remove carbon-based NMs from effluent whereas metal and metal oxide NMs may persist and be discharged into freshwater environments (Gottschalk and Nowack, 2011). There is limited information available on the behaviour of NMs in incinerated wastes, and data regarding NMs in landfill leachate is scant (Bolyard et al., 2013). Certain NMs like zerovalent iron are typically injected directly into the subsurface environment to remediate groundwater contaminated with chlorinated solvents (Gottschalk and Nowack, 2011). The release of NMs in aerosol sprays is instantaneous when applied, whereas NM escape from emulsions or suspensions is expected within hours (Gottschalk and Nowack, 2011). Immediate release of NMs embedded in plastic or polymer matrices is improbable; however, the products themselves may be used outside or end up in landfills and degrade or be transformed upon exposure to environmental conditions (Mitrano et al., 2015). Exterior paint containing NMs, for example, can wash off facades by rainwater, enter storm water runoff, and be transported to aquatic environments (Gottschalk and Nowack, 2011). Most NMs released from disposed products are present in matrix-bound form, but some can be freed by mechanical abrasion and material aging, and exist as individual NMs in the environment (Gottschalk and Nowack, 2011). Upon release into the environment, NM-containing products may be exposed to natural sunlight and degrade due to thermal and photooxidative processes (Gottschalk and Nowack, 2011). Other abiotic factors including ionic strength, natural organic matter (NOM) and pH are known to facilitate the transformation of NMs in aquatic environments (Dhar Dwivedi et al., 2015). Moreover, biotic interactions with plants, fungi and microorganisms can also affect NM transformation

(Dhar Dwivedi et al., 2015). The behaviour of NMs in the aqueous phase may also be influenced by rainfall or other weather events, that change the hydrology of NOM, suspended particles, and salinity of natural waters (Handy et al., 2008a; Mitrano et al., 2015). Furthermore, some NMs may settle in the water column and interact with benthic organisms while those that remain suspended will be transported considerable distances in the environment (Baalousha et al., 2008). Currently, analytical methods and techniques that detect and quantitatively monitor manufactured NMs in different environmental compartments are lacking; therefore, reliable data regarding realistic environmental concentrations of NMs is scarce (Gottschalk and Nowack, 2011). Arguably, most nanotoxicity tests are not designed to assess the potential hazards of NMs using environmentally relevant concentrations but are aimed instead at elucidating the mechanisms underlying NM toxicity (Krug, 2014). Although the actual environmental concentrations and production/use quantities of NMs are largely unknown, modeled or predicted estimates have been reported elsewhere (Cowie et al., 2014; Gottschalk et al., 2010; 2009; 2013; Piccinno et al., 2012). It is clear that aquatic organisms will likely be or have been exposed to engineered NMs, potentially resulting in negative impacts on ecosystem health.

### **1.2.2 Biological**

Toxicokinetics is a term used to describe how a substance (e.g. a NM) enters the body (i.e. absorption) and its fate afterward (i.e. distribution, metabolism, and excretion) (Shi et al., 2013). Direct interaction and interference of engineered NMs with biological systems are expected because the sizes of NMs and cellular

machinery are comparable (Shvedova et al., 2016). NMs are too big to be taken up by ion or other transporters, and although passive diffusion cannot be ruled out as a possible uptake mechanism for certain lipophilic NMs (Handy et al., 2008a), most are likely internalized by cells via active processes (Faille et al., 2012; Firdessa et al., 2014; Kuhn et al., 2014). In the following subsections, I will discuss the toxicokinetics of NM transportation, the interactions between NMs and living systems, and the fate of NMs both *in vitro* and *in vivo*. Specifically, I will introduce potential cellular transport pathways for NMs (absorption) and their fate inside cells, describe how cell uptake processes are studied and identify specific pathways involved, and finally, explore the distribution, metabolism, and excretion of NMs. It is noteworthy that the information provided in the subsections below is largely derived from either established mammalian or emerging fish model systems. Although there are many fundamental similarities among mammals and fishes (see section 1.6), differences between these vertebrates can vary considerably and some mammalian-specific traits cannot be assessed with fish model systems (Cataño and Gómez-Lechón, 2005). Moreover, distribution, metabolism, and excretion processes are beyond the scope of this thesis and are thus not discussed in great detail. The excretion process will be revisited in **Chapter 6**.

### ***1.2.2.1 Absorption and uptake***

The term absorption describes how NMs translocate from the external environment or initial site of exposure to the internal milieu of a biological system (Li et al., 2010). Many studies have reported that NMs enter the human body either

directly from injection (e.g. subcutaneous, intramuscular, etc.) or indirectly via pulmonary (i.e. inhaled into the lungs), oral (i.e. consumption of contaminated food or drink), and/or dermal (i.e. interaction between NMs and skin) exposure (Li et al., 2010). Two important processes are necessary for absorption to occur at the cellular level: a NM must first adsorb onto or come in close spatial proximity to the cell surface and secondly, the NM has to be internalized into the cell (Landfester and Ostafin, 2008).

All eukaryotic cells utilize endocytotic processes to communicate with the extracellular environment (Oh and Park, 2014). Endocytosis is an energy-dependent process by which cells internalize nutrients and signalling molecules allowing them to acquire energy and talk to each other, respectively (Oh and Park, 2014), and is the major route of NM translocation across cell membranes (Behra et al., 2013). Endocytosis has been thoroughly characterized in mammalian cells (Engqvist-Goldstein and Drubin, 2003) and is generally classified into phagocytosis or cell eating of large particles and pinocytosis or cell drinking of fluids, solutes and suspensions containing small particles (Khalil et al., 2006; Kou et al., 2013). Mammalian phagocytic cells including dendritic cells, macrophages, monocytes, neutrophils and mast cells utilize phagocytosis to internalize materials  $> 0.5 \mu\text{m}$  in size including bacteria, yeast and dead cells (Khalil et al., 2006; Oh and Park, 2014). Using the rat basophilic leukemia (RBL)-2H3 mast cell line, Ede et al. (2015) reported a strong association between fluorescein isothiocyanate-functionalized rosette nanotubes and immunoglobulin E receptors (Fc $\epsilon$ RI) located on the cell membrane surface, and confirmed internalization of these carbon-based materials.

Pinocytosis occurs in all types of cells (Khalil et al., 2006) and functions to absorb biological fluids from the extracellular environment (Oh and Park, 2014). Pinocytosis is typically divided into four morphologically distinct pathways including clathrin-mediated endocytosis (CME), caveolae-mediated endocytosis (CavME), macropinocytosis (MP), and clathrin- and caveolae-independent endocytosis (Kou et al., 2013); the latter pathway is beyond the scope of this thesis and thus will not be discussed further. CME, CavME, and MP routes are distinguished by the composition of the vesicular coat (if present), the size of the formed vesicle, the proteins involved, the fate of the internalized ligand, and the cell type (Khalil et al., 2006; Kou et al., 2013). Conversely, the intracellular fate of a NM depends on the endocytotic pathway selected for transport into the cell (Kou et al., 2013). Some aspects of CME, CavME, and MP pathways are summarized below and depicted in **Figure 1-1**.

The initial step of internalization through CME is the binding of a ligand (e.g. a NM, low-density lipoprotein, etc.) to an extracellular receptor that triggers the invagination of a clathrin-coated pit and subsequent formation of a clathrin-coated vesicle (~100-150 nm in diameter; pH 7.0) (Khalil et al., 2006). Once the cytosolic coat protein clathrin depolymerizes forming an early endosome, the internalized ligand may dissociate from its receptor due to the slightly acidic pH (6.5) of the vesicle (Khalil et al., 2006). Both ligand and receptor are then sorted to their appropriate subcellular destination including the Golgi apparatus, nucleus, or back to the cell surface (Khalil et al., 2006). The early endosome matures and eventually delivers its cargo to a lysosome (Khalil et al., 2006), which is an acidic

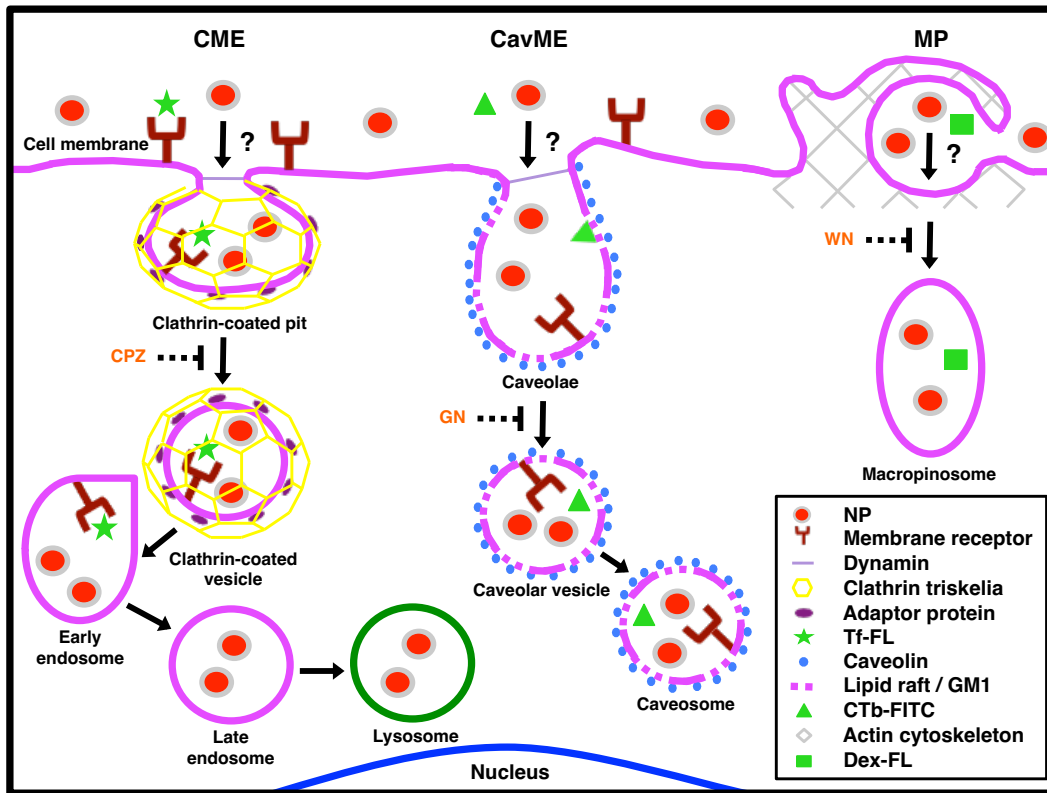


**Figure 1-1. Schematic of possible endocytotic pathways utilized by NPs to enter RTgill-W1 cells.** Potential mechanisms of NP uptake include: CME involving clathrin-coated vesicles containing extracellular receptors and NPs that shed their coating to form endosomes that later fuse with lysosomes, CavME where NPs interact with cell membrane lipid raft invaginations called caveolae and become trapped within caveolar vesicles that form caveosomes, and MP which is facilitated by actin that acts as a scaffold allowing the cell membrane to engulf NPs and extracellular fluid into macropinosomes (Kou et al., 2013). CME and CavME are considered receptor-mediated endocytosis (Oh and Park, 2014). Adaptor proteins are located between the lipid membrane and the clathrin lattice (Popova et al., 2013). CPZ, GN, and WN inhibit CME, CavME, and MP pathways, respectively (dos Santos et al., 2011; Greulich et al., 2011; Singh et al., 2012). Fluorescently labelled proteins including Tf-FL and CTb-FITC are known to be internalized by CME and CavME pathways, respectively (dos Santos et al., 2011; Kuhn et al., 2014), whereas fluorescent polysaccharides like Dex-FL use the MP pathway (Li et al., 2015).

membrane-bound organelle present in animal cells that enzymatically degrades macromolecules (Luzio et al., 2007).

The non-acidic and non-digestive CavME pathway has been implicated in the transport of bacterial toxins, certain viruses, glycosphingolipids, NMs and pathogens into the cell (Khalil et al., 2006; Kou et al., 2013). In CavME, caveolae detach from the plasma membrane into the cytosol forming a caveolar vesicle (~50-60 nm in size) enriched in the endogenous coat protein caveolin (Khalil et al., 2006). These coated vesicles or caveosomes are internalized more slowly than endosomes involved in the CME pathway and since ligands do not experience a drop in pH they can be directly trafficked to the Golgi apparatus or endoplasmic reticulum, thereby bypassing acidification and enzymolysis in the lysosome (Khalil et al., 2006).

The MP pathway involves growth factors and other signals that stimulate evagination of the plasma membrane through outward-directed polymerization of the actin cytoskeleton (Khalil et al., 2006). These cell surface ruffles often pinch off to form large irregularly shaped uncoated macropinosomes ( $\leq 5 \mu\text{m}$  in size) that contain fluid and macromolecules (Khalil et al., 2006). The fate of macropinosomes is cell-type specific (Khalil et al., 2006). In macrophages, for example, macropinosomes are trafficked to the center of the cell, shrink by the loss of fluid, become more acidic, and then fuse with lysosomes whereas in human A431 cells, macropinosomes recycle back to the cell surface (Khalil et al., 2006). Although recent reports suggest that cells utilize multiple endocytotic pathways to internalize NMs (Firdessa et al., 2014; Monti et al., 2015; Suen and Chau, 2013), many cell-NM systems remain unexplored.

Researchers typically use a combination of inhibitors and fluorescent markers (molecular probes) to determine whether the corresponding pathway plays a role in the cellular internalization of NMs and to study the fate of NMs within a cell, respectively (Kou et al., 2013). Since endocytosis is an energy-dependent process, low temperature and ATPase inhibitors like sodium azide can be used to distinguish non-endocytotic pathways (Kou et al., 2013). The inhibitors chlorpromazine (CPZ), genistein, and wortmannin are commonly employed to block CME, CavME, and MP pathways, respectively (Mercer and Helenius, 2009; Nabi and Le, 2003; Zhang and Monteiro-Riviere, 2009), to confirm whether the corresponding pathway was exploited by NMs to enter cells. However, these pharmacological inhibitors may induce nonspecific effects and efficiencies vary across different cell types (Dutta and Donaldson, 2013). For example, CPZ can inhibit both CME and clathrin-independent endocytosis in some cells leading to unintended consequences (Dutta and Donaldson, 2013). Therefore, fluorescent markers have been routinely used alongside endocytosis inhibitors to confirm the internalization pathway involved and to provide more convincing evidence (Kou et al., 2013). Transferrin, cholera toxin B subunit, and dextran are known to be internalized through CME, CavME, and MP pathways, respectively (Liu et al., 2010; Patel and Insel, 2009; Santos et al., 2000), and are thus commonly used as markers of these pathways (Kou et al., 2013) when conjugated to fluorescent molecules (fluorophores). However, these markers may use different pathways upon entering a cell lacking specific endocytotic machinery (Kou et al., 2013) such as caveolin/caveolae-deficient HepG2 cells (Fujimoto et al., 2000). Cellular uptake of fluorescently labelled NMs can be visualized by two- and

three-dimensional computer-rendered confocal microscope imaging (Kou et al., 2013) and quantified by flow cytometry (Firdessa et al., 2014). Organelle dyes including non-fixable LysoTracker can be used to detect the co-localization of fluorescently labelled NMs in live cells using confocal microscopy (Van der Velden et al., 2013). Although evidence supporting NM uptake by cells is mounting (Firdessa et al., 2014; Kuhn et al., 2014; Monti et al., 2015), it is debatable whether cellular internalization is a prerequisite for toxicity (Li et al., 2015c). Are NMs internalized by cells, and if so, by which endocytotic pathway(s) and what is their ultimate subcellular fate? These research questions are explored in **Chapter 5**. I hypothesize that NMs enter cells via endocytosis; however, uptake is both cell type-specific and governed by a variety of NM properties including size, charge and surface functional groups (Kou et al., 2013; Oh and Park, 2014), which makes pinpointing an exact mechanism by which NMs are internalized difficult.

#### ***1.2.2.2 Distribution, metabolism, and excretion***

Distribution, metabolism, and excretion of NMs in fish is poorly understood and information about these mechanisms is lacking (Handy et al., 2008a). Once a brachial epithelial cell internalizes individual or small groups of NMs (Farkas et al., 2011), the next step in biological uptake is the transcellular transport through the cell to the blood (Handy et al., 2008a). Due to their small size, NMs can then be transported throughout the body via the circulatory system and may be stored in different organs with consequential bioaccumulation (Wang et al., 2013). Although knowledge of the body distribution of NMs in fish is hindered by labour intensive and

time-consuming techniques (e.g. electron microscopy) for the measurement of NMs in tissues, fluorescently labelled NMs are increasingly being utilized in pharmacokinetic studies to fill these gaps (Handy et al., 2008a). The gills, gut, kidneys, and liver are considered to be the primary target organs for NM toxicity in fish (Handy et al., 2008a). Since a fish must have a continuous flow of water passing over its gills, NMs in liquid phase could directly interact with gill lamellae (Handy et al., 2008a). In addition, NM contaminated water drunk by freshwater fish could access to the gut mucosa and subsequently the liver and kidneys (Handy et al., 2008a). Metabolism of xenobiotics (i.e. substances foreign to the body) predominantly occurs in the liver of fish and, to a lesser extent, in the kidney (Bury et al., 2014). Assuming that NMs reach the liver and that metabolic processes affect NMs, dissolution of metal oxide NMs (see section 1.3.2) may occur while carbon-based NMs could be hydroxylated, oxidized, or reduced by phase I enzymes (e.g. cytochrome P450 monooxygenases) leading to phase II conjugation events (Handy et al., 2008a). The NM may not even be metabolized if it is small enough or if it already has a hydrophilic surface (Handy et al., 2008a). Engineered NMs and other substances that originate in the blood are excreted mainly via the gills, kidney, and liver into the surrounding water, urine, and bile/feces, respectively (Handy et al., 2008a). Apart from branchial or renal clearance, biliary excretion into the bile is expected to be the most likely mechanism involved in the removal of NMs or NM metabolites from a fish (Handy et al., 2008a). It remains unknown whether vesicles within gill epithelial cells are trafficked from the basolateral membrane to the apical membrane and it is unlikely that NMs larger than a few nanometers would be able to

traverse the glomerular filtration barrier (Handy et al., 2008a). Clearance from hepatocytes involves the fusion of secretory vesicles at the plasma membrane, and given that these vesicles are ~200 nm in size, exocytosis of NMs or NM metabolites via the biliary system is plausible (Hampton et al., 1988; Handy et al., 2008a). Clearly, more detailed information about the toxicokinetics of NMs in fishes (and mammals) is needed and warrants further study.

### **1.3 FACTORS MODULATING NANOMATERIAL TOXICITY**

The characteristics of both the NM and environment are important in determining NM toxicity. Over the last decade, nanotoxicologists have gained a better understanding of the physical and chemical characteristics of NMs and have identified certain properties that modulate NM toxicity to aquatic organisms. Several factors affect cellular import mechanisms, intracellular trafficking, nano-bio interactions, and toxicity of NMs; the most important determinants are predestined by the NM itself or its surrounding environment (Firdessa et al., 2014; Nel et al., 2009). Some interrelated factors intrinsic to the NMs themselves (size, agglomeration, charge, dissolution, and surface functionalization) and extrinsic environmental factors including NOM and ultraviolet (UV) light that modulate NM toxicity are discussed in the following subsections.

### 1.3.1 Size, agglomeration, and charge

Monitoring the sizes of NMs at the beginning, middle, and end of the experimental period is essential to better predict their distribution, bioavailability, and fate in aquatic environments (Schultz et al., 2014). The size of a NM largely determines its interaction with biological systems (Jiang et al., 2009). Many studies have suggested that size matters when it comes to NM internalization by cells or organisms (Shang et al., 2014), and NMs above a certain threshold size may not be able to traverse biological membranes, such as the protective chorion surrounding embryonic fish (Rawson et al., 2000). As mentioned above (see section 1.2.2.1), the size of the formed cellular vesicle (i.e. clathrin-coated vesicle, caveosome, or macropinosome) that engulfs a NM depends on the selected endocytosis pathway (Kou et al., 2013). Large particles ( $\leq 5 \mu\text{m}$ ) are likely internalized via MP, whereas smaller particles ( $\leq 150 \text{ nm}$ ) may be taken up via CME or CavME pathways (Kou et al., 2013). However, NM size does not solely govern cellular uptake and some researchers suggest that agglomeration and surface charge also play important roles (Kühnel et al., 2009; Sokolova et al., 2013). According to the Derjaguin-Landau-Verwey-Overbeek theory, particles tend to agglomerate or flocculate when attractive forces (e.g. van der Waals) dominate repulsive forces (e.g. electrostatic), which destabilizes the suspension (Derjaguin and Landau, 1941; Verwey and Overbeek, 1948). Agglomeration reduces both the specific surface area of the NM available for nano-bio interactions and the stability of the NM suspension (i.e. the likelihood that NMs will remain suspended in an aqueous medium) (Schultz et al., 2014). Large NM

agglomerates that form in aqueous solutions will likely settle and concentrate at the bottom of exposure vessel where adherent cells, benthic organisms, and embryos are located (Schultz et al., 2014). Various abiotic (e.g. solution pH, ionic strength, and divalent ions) and biotic (e.g. NOM) factors influence NM agglomeration kinetics (Ghosh et al., 2010; Jiang et al., 2009). Agglomeration is suppressed when the solution pH is far from the point of zero charge because repulsive electrostatic forces overpower attractive van der Waals forces (Jiang et al., 2009). The electrostatic double layer surrounding a NM expands and its surface charge increases in low ionic strength medium (Jiang et al., 2009), similar to the dechlorinated tap water used in my research. Divalent calcium and magnesium ions present in natural waters are also known to induce NM agglomeration (Handy et al., 2008a).

Cationic NMs show a high affinity for negatively charged cytomembranes due to electrostatic interactions with cells (Wilhelm et al., 2003), resulting in rapid entry (Kou et al., 2013). Cationic polymer NMs may leak from lysosomes and become localized in the perinuclear region due to the proton-sponge effect (Boussif et al., 1995). This hypothesis suggests that polycations become protonated in acidic cellular vesicles which causes an influx of chloride ions and water leading to lysosomal swelling and rupture, thus providing an escape route for internalized cargo (Boussif et al., 1995). Cationic polymer NMs and lipids have therefore been utilized as carriers in gene delivery applications to enhance the release of DNA into the cytosol prior to lysosomal degradation, thus allowing the gene to reach the nucleus (Khalil et al., 2006). At physiological pH, hydrophobic interactions and hydrogen bonds may facilitate the binding of NMs with no charge to cell membranes (Vandamme and

Brobeck, 2005), whereas hydrophilic polymer coatings can prevent interactions between charge-neutral NMs and cells leading to less adsorption (Kou et al., 2013). The large anionic domains of the cell surface should repel negatively charged NMs (Patil et al., 2007), like those tested in my research. However, anionic NMs have been proposed to cluster at positive sites (e.g. on proteins) favouring adsorption of other like-charged NMs to the plasma membrane (Wilhelm et al., 2003). Anionic poly (acrylic acid) polymers tend to agglomerate in acidic media and repel each other at neutral pH, the latter repulsive interaction results in less mucoadhesion compared to cationic dendrimers (Vandamme and Brobeck, 2005). How do size, agglomeration, and surface charge affect NM toxicity? This research question is examined in **Chapters 2-4**. Are size, agglomeration, and surface charge the only parameters that determine which cellular transport pathway will be chosen? This research question is considered in **Chapter 5**. I hypothesize that size, agglomeration, and charge have a controlling influence on NM toxicity because these properties largely determine nano-bio interactions (Nel et al., 2009).

### **1.3.2 Dissolution**

High dissolution rates or release of ionic metal over time would be expected for metallic NMs as a result of their large surface area per unit mass (Miao et al., 2010). The increased flux of metal and metal oxide NMs in consumer products has raised concern as to whether the release of these NMs and their accompanying dissolved metal ions will negatively impact the aquatic environment (Schultz et al., 2014). It has been well documented that most heavy metals including cadmium, lead,

nickel, and zinc are toxic to aquatic organisms (Govind and Madhuri, 2014) and sublethal exposures are known to adversely affect an organism's endocrine system (Georgescu et al., 2011), growth (Farkas et al., 2002), and reproduction (Ebrahimi and Taherianfard, 2011). Many nanotoxicological studies have identified dissolution of metallic NMs and the subsequent shedding of free metal ions as the primary mode of toxicity to freshwater and marine organisms (Franklin et al., 2007; Miao et al., 2010; Schultz et al., 2012) while other reports suggest that observed toxicities in fishes were not exclusively attributed to dissolved metal species (Bai et al., 2010; Hao et al., 2013). Since aqueous exposure medium contains both metal-based NMs and dissolved metal ions, observed toxicity is usually the result of a combination of both components (Ma et al., 2013). Humic or fulvic acid, NM agglomerates, small molecules, and surface coatings from the exposure medium can potentially impede dissolution rates by blocking NM surfaces (Liu and Hurt, 2010; Merdzan et al., 2014), thereby abrogating toxic effects. Conversely, high temperature and low pH both increase dissolution rates of metal NM colloids (Liu and Hurt, 2010). Miao et al. (2010) observed that by decreasing the pH of a metal oxide NM suspension from 9 to 7, the maximum total metal ion concentration increased by nearly 100 times. Since suspensions change as NMs aggregate, bind to molecules, and translocate across biological membranes, analytical techniques such as dialysis are commonly employed to measure changes in total dissolution over time (Schultz et al., 2014). Are noted effects dissolution-based or NM-specific? This research question is answered in **Chapters 2 and 3**. I hypothesize that surface coatings increase the stability of NMs in suspension and reduce NM dissolution, thereby mitigating free metal effects because

polymers can soak up contaminating metal ions (see section 1.3.3) (Yang et al., 2012).

### **1.3.3 Surface functionalization**

The development of functionalized NMs is central to the advancement of nanotechnology (Subbiah et al., 2010). Various chemical methods have been employed to synthesize functionalized NMs specifically for use in many fields including agricultural and biomedical sciences (Liu and Lal, 2015; Subbiah et al., 2010; Xu et al., 2014). Functionalization is a technique employed by chemists and material scientists to conjugate (i.e. physically attach or adsorb) chemical moieties like carboxylic acid functional groups or polymers onto the surfaces of NMs to tailor their properties to fit specific applications (Meng et al., 2009; Priestly et al., 2014; Subbiah et al., 2010). Carboxylic acid groups can be used to tune the hydrophobicity or hydrophilicity of the NM surface (Leung et al., 2011). Hydrophobic NMs have a higher affinity for the phospholipid bilayer than hydrophilic NMs and are thus expected to be efficiently internalized by a cell (Kou et al., 2013). Furthermore, hydrophilic polymers can suppress the interactions between the NM core and the cell surface (Kou et al., 2013). Wrapping polymers around carbon-based NMs reduces their agglomeration tendencies by diminishing the attractive van der Waals forces between individual materials (Star et al., 2001), rendering them compatible with other matrices (Subbiah et al., 2010). Dispersibility of certain carbon-based NMs can be improved through covalent attachment of functional groups or noncovalent adsorption of polymers onto their surfaces (Zhao and Liu, 2012). Some polymer

coatings function to minimize or prevent dissolution of free metal ions released from metal NMs via chelation (Yang et al., 2012) while others can envelop NMs with UV absorbing capabilities and repress substrate availability for free radical production without affecting their desired photocatalytic properties (Smijs and Pavel, 2011). Another form of functionalization involves the encapsulation with a polymer rather than adsorption onto the NM surface (Subbiah et al., 2010). Polymeric NMs composed of biocompatible polymers have been extensively studied for use as nano-sized carriers of various formulations (e.g. drugs, fungicides, insecticides, etc.) in controlled delivery applications while metal NMs are tunable and can serve as vehicles for tracers or contrast agents in medical imaging applications (Liu and Lal, 2015; Subbiah et al., 2010; Xu et al., 2014). Chemical functionalization of NMs is expected to broaden their scope of potential applications but may also be used to modify NM toxicity. Therefore, functionalized NMs should be carefully examined for any undesirable changes in toxicity. Does surface functionalization modulate NM toxicity? This research question is investigated in **Chapters 2-4** and is the major focus of my thesis. I hypothesize that polymer coatings mitigate NM toxicity because they complex dissolved ions and capture reactive radicals, both known mediators of NM toxicity (Smijs and Pavel, 2011; Yang et al., 2012).

#### **1.3.4 Natural organic matter**

Ubiquitous in natural waters, NOM is a heterogeneous, anionic matrix (Dhar Dwivedi et al., 2015) formed during the microbial decomposition of plants and animals (Grillo et al., 2015). The biopolymers and degraded products (i.e. humic and

fulvic acids) that make up NOM vary in composition and molecular weight, and are negatively charged due to carboxylic and phenolic functional groups (Dhar Dwivedi et al., 2015). It is well known that NOM can form an ecocorona around the NM surface that functions to minimize or prevent agglomeration through repulsive electrostatic and/or steric interactions (Ghosh et al., 2010). This ecocorona can affect NM bioavailability to and biopersistence in aquatic organisms, and thus modulates NM toxicity (Byrne et al., 2013; Westmeier et al., 2016). Van Hoecke et al. (2011) observed that NOM adsorbed to the surfaces of metal oxide NMs and suggested that their toxicity was reduced through a decrease in the bioavailability of these materials to algae (*Pseudokirchneriella subcapitata*). In the same manner, NOM can adsorb to a metal oxide NM and inhibit its dissolution by blocking the interaction between the NM surface and water molecules (Ma et al., 2013). Although NOM is not the subject of this thesis, I am collaborating with Dr. Kimberly Ong, Dr. David Boyle, Dr. James Ede, Dr. Guibin Ma, Dr. Jonathan Veinot, and Dr. Greg Goss to publish research related to the ameliorating effects of humic acid on NM-induced developmental toxicity in fish.

### **1.3.5 Ultraviolet light**

Stratospheric ozone provides an important protective shield against the harmful components of solar radiation including UVC (200-280 nm) and UVB (280-320 nm) wavelengths shorter than 290 nm (Charron et al., 2000); UVA (320-400 nm) wavelengths pass through the ozone layer (Prasad, 2012). The inevitable release of manufactured NMs into the environment has raised concern as to

whether nonionizing UV radiation will mediate deleterious health effects. Most nanotoxicity tests are performed in laboratories under controlled conditions, which are considered effects or mechanistic-oriented studies (Mitrano et al., 2015; Schultz et al., 2014). However, certain NMs may be inert under ambient fluorescent laboratory lighting and become toxic due to UV-induced transformations in the environment (Wiesner et al., 2009). Fluorescent lamps that illuminate laboratories emit negligible or no UV radiation (Safari et al., 2015), yet certain NMs are wide band-gap semiconductors (Li et al., 2015b). When a semiconductor absorbs enough energy, i.e. photon energy must be at or above the band gap energy of the material, from sources like natural sunlight a valence electron is bumped up to the conduction band resulting in a free electron and a positively charged area or hole (Ma et al., 2012). This electron-hole pair reacts with dissolved oxygen and water in an aqueous environment to efficiently produce reactive oxygen species (ROS) (Ma et al., 2012) including hydrogen peroxide, hydroxyl radicals, and superoxide anions (Cerutti, 1985). These ROS contain unpaired valence electrons that make them highly reactive and capable of inducing severe cellular damage (Dahle and Arai, 2015). Moreover, certain nanoscale semiconductors can convert harmful organic contaminants into carbon dioxide and water due to their photocatalytic properties (Iqbal et al., 2016; Mahlambi et al., 2015). The photoreactivity of metal oxides with a cerium, iron, titanium, or zinc core (see sections 1.5.1-1.5.4) (Khan et al., 2015; Valdiglesias et al., 2016) are directly related to their UV-induced toxicities and thus may be the primary mechanism of toxicity under environmentally realistic conditions (Ma et al., 2013). Although endogenously produced ROS play a central role in normal cellular

metabolic processes (Weydert and Cullen, 2009), high intracellular concentrations of ROS generated by nanoscale semiconductors that undergo oxidation may overwhelm the antioxidant defense system resulting in irreversible damage to carbohydrates, membrane lipids, nucleic acids, and proteins (Riley, 1994). Therefore, an enzymatic antioxidant system has evolved to ameliorate ROS-induced adverse effects (Riley, 1994). The vital roles of defense enzymes including catalase, glutathione peroxidase, and superoxide dismutase, and antioxidants such as glutathione in the mitigation of oxidative stress on DNA, lipids, and proteins have been extensively reviewed (Gutteridge, 1995; Kelly et al., 1998; Sies, 2007). **Figure 1-2** shows a diagrammatic representation of the relation among the antioxidant defense system, ROS, and oxidative damage. Improved knowledge of the unique properties of nano-sized band gap semiconductors will enhance our understanding of their potential phototoxic effects and facilitate proper risk assessment (Schultz et al., 2014). Does UV light mediate the phototoxicity of nanoscale semiconductors, and if so, do polymer coatings mitigate this effect? A novel experimental methodology has been employed in **Chapter 4** to tackle these research questions. I hypothesize that the polymer coating that envelops the NM will mitigate toxicity because it inhibits the formation of ROS by preventing the direct contact between the NM surface, oxygen, and water (Smijs and Pavel, 2011).

#### **1.4 CHALLENGES IN NANOTOXICITY TESTING**

Regulation of NMs is still in its infancy (Ngarize et al., 2012). At present, there are few NM-specific regulations, and most of these involve reporting

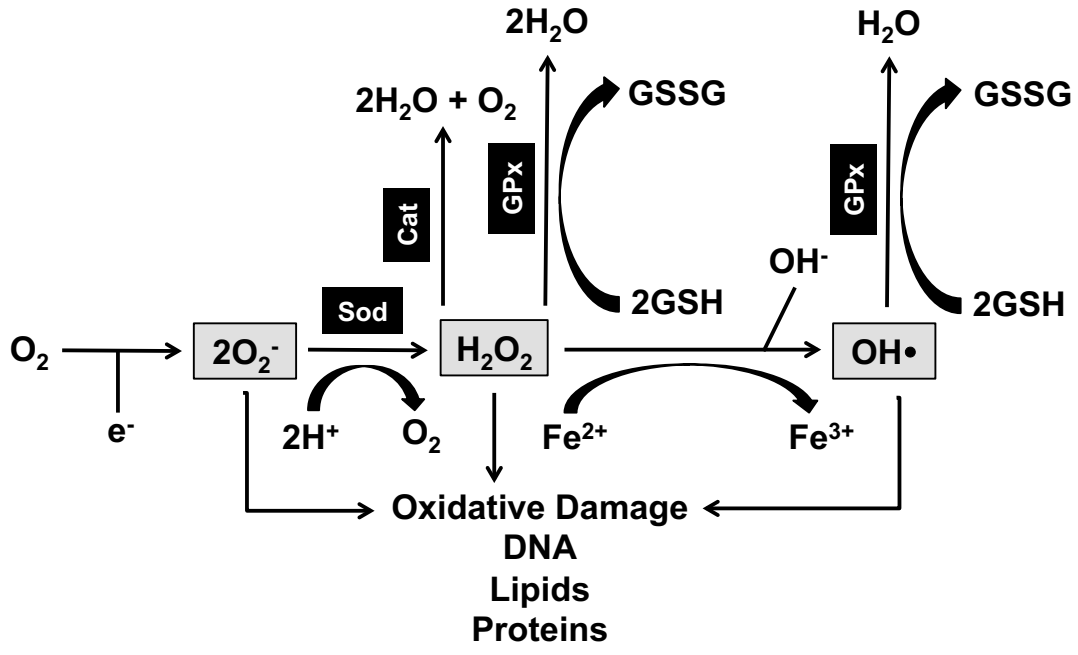


**Figure 1-2. Diagram showing the interrelationship between antioxidant defense enzymes (black), ROS (gray), and oxidative damage.** Free radicals including superoxide anions ( $O_2^-$ ) are catalyzed to hydrogen peroxide ( $H_2O_2$ ) by superoxide dismutase (Sod).  $H_2O_2$  are converted into water through the action of catalase (Cat) or glutathione peroxidase (GPx).  $H_2O_2$  not detoxified by these processes can be further reduced to hydroxyl radicals ( $OH^\bullet$ ) through the Fenton reaction and then converted into water, using GSH as a reductant. All ROS are capable of inducing oxidative damage to DNA, lipids, and proteins. Adapted from Yuan et al., 2012.

requirements for any substantial new use of the base material (CEPA, 2015). However, most NMs are regulated in the same manner as their corresponding bulk counterparts (Pitkanen et al., 2014). Moreover, risk assessment of NMs remains at the development stage (Pitkanen et al., 2014). Although no comprehensive, explicit, and systematic evidence-based guideline for the risk assessment of NMs currently exists (Pitkanen et al., 2014), a couple of guidance documents are available (OECD, 2012a; SCENIHR, 2009). The combination of hazard and exposure is the major determinant of risk (Pitkanen et al., 2014). Toxicity testing plays a fundamental role in hazard evaluation (Warheit and Donner, 2010); however, knowledge of environmental exposure is limited (Gottschalk and Nowack, 2011). Accurate and efficient toxicity testing is necessary to determine whether NMs should fall under regulations mandated for traditional bulk chemicals (Schultz et al., 2014). Conventional *in vivo* and *in vitro* toxicity tests for traditional chemicals are commonly employed due to their familiarity and interpretability (Balbus et al., 2007). However, these traditional testing methods may not be suitable for NMs and could lead to an inaccurate assessment of toxicity and thus risk (Schultz et al., 2014). Several OECD test guidelines and guidance documents for traditional chemicals can be generally applied to NMs; however, some need to be adapted or newly developed to address endpoints more suited for NM testing (Rasmussen et al., 2016). One NM-specific OECD test guideline exists, which provides direction for sample preparation and dosimetry for NM testing (OECD, 2012b). Furthermore, NM-specific issues including appropriate characterization methods/techniques (Rasmussen et al., 2016), bio- and small

molecule interactions (Nel et al., 2009), and assay interference (Ong et al., 2014a) are not covered in present guidelines or guidance documents.

It is highly debated whether conventional methods originally designed for soluble chemicals are appropriate for non-dispersible colloidal materials like most NMs (Schultz et al., 2014). Characterization of NM properties should be as comprehensive as possible to ensure that results are accurate, reliable, reproducible, and interpreted correctly for the establishment of regulations related to NM safety (Jiang et al., 2009). The measurement of every possible NM characteristic is quixotic (Jiang et al., 2009). Therefore, a list of physicochemical properties has been identified by the Working Party on Manufactured Nanomaterials that must be addressed in nanotoxicological studies including size, charge, surface chemistry, and photocatalytic activity (Rasmussen et al., 2016); discussed in detail above (see section 1.3). These and other NM properties should be characterized in the exposure medium (Schultz et al., 2014). Dynamic light scattering (DLS) is a well established, non-invasive analytical technique that is often employed to measure the size, size distribution, and charge of NM agglomerates in a dispersed medium (Boluk and Danumah, 2014); however, this characterization method has certain disadvantages. For example, the data obtained from DLS does bias toward large particles that scatter more light than small particles (Murdock et al., 2008) and this technique may not provide meaningful size distribution measurements for high aspect ratio or cylindrical-shaped NMs (Rasmussen et al., 2016).

Due to their small size and large surface area to volume ratio, NMs can adsorb and effectively sequester soluble molecules including carbohydrates, growth factors,

hormones, and nutrients from biological media that may be essential to an organism's survival (Brunner et al., 2010; Schultz et al., 2014). Biomolecules and small soluble molecules including salts/ions, serum proteins, and vitamins present in cell culture medium will inevitably interact with NMs forming a biomolecular corona that cloaks the NM surface and can change its agglomeration kinetics, making characterization of NMs in physiological matrices difficult (Baolog et al., 2015; Monopoli et al., 2012; Schultz et al., 2014). Furthermore, complex biological fluid might also induce NM agglomeration and certain NMs can adsorb to and thus deplete essential micronutrients like folic acid from these multicomponent aqueous matrices, potentially leading to reduced cell viability (Guo et al., 2008; Kühnel et al., 2009).

High-throughput *in vitro* assays are widely used by toxicologists to quantitatively determine the biochemical and physiological responses of organisms to xenobiotics (Shukla et al., 2010). Although researchers have begun to realize that NMs can interfere with standard toxicity assays, the majority of published nanotoxicology literature fails to report or account for potential NM-assay interference (Ong et al., 2014a; Petersen et al., 2014). Intrinsic optical absorbance or fluorescence of NMs, adsorption of NMs to assay components, and high NM concentrations increase the likelihood of NM-assay interference, which can lead to false-positive results and an inaccurate assessment of toxicity will ensue (Ong et al., 2014a; Schultz et al., 2014). Due to their quantum properties, nanoscale semiconductors typically absorb or fluoresce at wavelengths in the UV region, which may overlap with the wavelength monitored in the assay (Kroll et al., 2012). As mentioned above, NMs can adsorb to molecules and this interaction may hinder the

proper transformation of indicator molecules used in classic endpoint assays (Wörle-Knirsch et al., 2006). The final NM concentration present in a biological sample may not be lowered by repeated washes, centrifugations, or filtrations that attempt to remove non-internalized NMs adsorbed onto tissue and cell surfaces; therefore, controlling for NM interference with assay measurements is essential (Ong et al., 2014a). Nanotoxicologists have begun to collaborate with cell biologists, chemists, engineers, material scientists, and physicists to explore the role of different physicochemical properties in determining NM toxicity and, by introducing appropriate controls into their experimental design (e.g. different NM sizes, ionic metal, and surface coatings alone), researchers are now more equipped conceptually and methodologically to accurately assess and interpret their results (Schultz et al., 2014). A number of informative literature reviews have been published in recent years that present a series of recommendations aimed at alleviating some of the challenges associated with nanotoxicity testing (Baun et al., 2008; Ong et al., 2014a; Petersen et al., 2014; Schultz et al., 2014; Taurozzi et al., 2011). Taken together, a variety of factors must be considered by nanotoxicologists to make accurate toxicological assessments. As a result, regulators, who seek to minimize risk, will be able to extrapolate useful information from these well designed and executed studies to better predict NM toxicity.

## **1.5 TOXICITY ASSESSMENT OF NANOMATERIALS**

Nanotoxicologists need to have a keen understanding of biology, chemistry, and physics to make accurate and meaningful toxicological assessments (Schultz et al., 2014). Of the 1827 nanotechnology-based consumer products currently available on the market, 175 products were identified to contain either metal oxide or carbon-based NMs (Vance et al., 2015), which are the model NMs used in my research and the most widely studied among nanotoxicologists. Five of the major OECD priority NMs (OECD, 2010), cerium oxide ( $\text{CeO}_2$ ), iron oxide ( $\text{Fe}_2\text{O}_3$ ), titanium dioxide ( $\text{TiO}_2$ ), zinc oxide ( $\text{ZnO}$ ), and single-walled carbon nanotubes (SWCNTs), as well as one novel non-priority NM, cellulose nanocrystals (CNCs), are examined in this thesis (**Figure 1-3; Table 1-1**). In the following subsections, I will discuss the applications and products that incorporate each of the abovementioned nonfunctionalized NMs, the unique physicochemical properties that modulate their toxicity, and summarize recent research illustrating their toxic effects on aquatic organisms, including algae, invertebrates, and vertebrates. Studies of NM toxicity on human health using mammalian model systems are not the subject of this thesis and have thus been excluded. The intention here is not to provide an exhaustive review of the nanotoxicological literature, but rather to draw attention to the wide diversity of NMs and their effects across multiple levels of biological organization.

### **1.5.1 Cerium oxide nanomaterials**

Ceria or  $\text{CeO}_2$  NMs have received much attention in recent years due to their use in catalyst, ceramic coating, fuel/glass additive, and fuel cell applications (Dahle and Arai, 2015). These NMs are commonly used in catalytic converters of motor

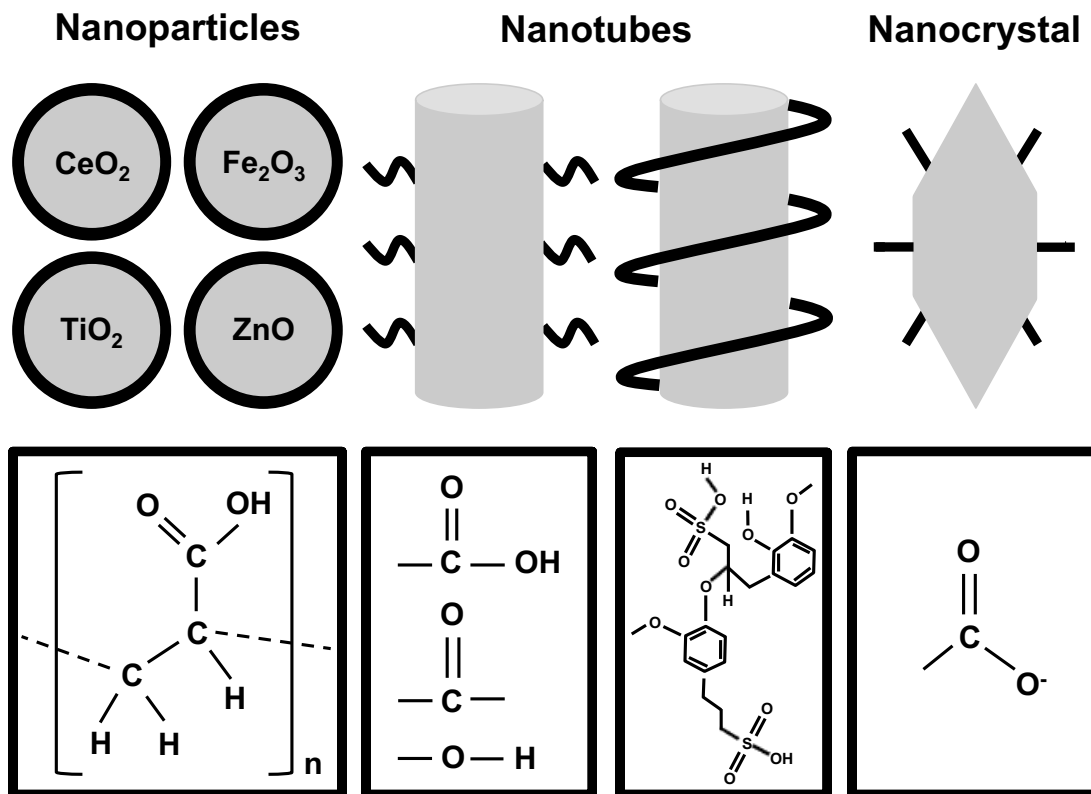


**Figure 1-3. Diagram of the functionalized NMs examined in this thesis.** The surfaces of spherical  $\text{CeO}_2$ ,  $\text{Fe}_2\text{O}_3$ ,  $\text{TiO}_2$  and  $\text{ZnO}$  nanoparticles were coated with poly(acrylic acid) ( $[\text{C}_3\text{H}_4\text{O}_2]_n$ ). Carboxylic acid ( $-\text{COOH}$ ) functional groups and some carbonyl ( $-\text{CO}$ ) and hydroxyl ( $-\text{OH}$ ) groups were covalently bound to the sidewall of a cylinder-like nanotube under acidic conditions or its surface was noncovalently wrapped with lignin sulfonate ( $\text{C}_{20}\text{H}_{26}\text{O}_{10}\text{S}_2$ ). At near-neutral pH, carboxylate ( $-\text{COO}^-$ ) moieties were present on the surface of a rod-like nanocrystal. Black and gray areas indicate surface functionalization and core structure, respectively.

**Table 1-1. General characteristics of the metal oxide- and carbon-based NMs examined in this thesis.**

NM type	Core composition	Surface functionalization	Chemical formula (functionalization)	Shape <sup>a</sup>	Diameter (nm) <sup>a</sup>	Length (nm) <sup>a</sup>	Charge <sup>b</sup>
Nanoparticle	CeO <sub>2</sub>	Poly(acrylic acid)	(C <sub>3</sub> H <sub>4</sub> O <sub>2</sub> ) <sub>n</sub>	Sphere	3-9	–	Negative
	Fe <sub>2</sub> O <sub>3</sub>	Poly(acrylic acid)	(C <sub>3</sub> H <sub>4</sub> O <sub>2</sub> ) <sub>n</sub>	Sphere	3-9	–	Negative
	TiO <sub>2</sub>	–	–	Sphere	35	–	Negative
	TiO <sub>2</sub>	Poly(acrylic acid)	(C <sub>3</sub> H <sub>4</sub> O <sub>2</sub> ) <sub>n</sub>	Sphere	3-9	–	Negative
	ZnO	Poly(acrylic acid)	(C <sub>3</sub> H <sub>4</sub> O <sub>2</sub> ) <sub>n</sub>	Sphere	3-9	–	Negative
Nanotube	SWCNT	–	–	Cylinder-like	10-20	> 2000	–
	SWCNT <sup>c</sup>	Carboxylic acid	-COOH	Cylinder-like	10-20	–	Negative
	SWCNT <sup>d</sup>	Lignin sulfonate	C <sub>20</sub> H <sub>26</sub> O <sub>10</sub> S <sub>2</sub>	Cylinder-like	10-20	> 2000	Negative
Nanocrystal	CNC	Carboxylate	-COO <sup>-</sup>	Rod-like	5.5	128	Negative

<sup>a</sup>Shape, diameter and length as determined by transmission electron microscopy; <sup>b</sup>Charge as determined by dynamic light scattering.

<sup>c</sup>Oxidized at 30, 40, or 50 °C; <sup>d</sup>Wrapped with sodium or ammonium lignin sulfonate; dashed line indicates not applicable or available.

vehicles to reduce harmful nitrogen oxide emissions and convert carbon monoxide to carbon dioxide by releasing or absorbing oxygen in the exhaust system of an internal combustion engine (Dahle and Arai, 2015). Abiotic factors including ionic strength, NOM, and pH have been shown to affect CeO<sub>2</sub> NM toxicity and their stability in natural waters (Van Hoecke et al., 2011). Using concentrations at and well above predicted environmental concentrations (0.0005-80 mg/L), Taylor et al. (2016) demonstrated that ceria NMs were internalized into intracellular vesicles of the unicellular green alga, *Chlamydomonas reinhardtii*, but did not affect their growth at any exposure concentration tested. Manier et al. (2013) reported that non-aged CeO<sub>2</sub> NMs inhibited growth of green microalga (*Pseudokirchneriella subcapitata*; 72 h half maximal effective concentration [EC<sub>50</sub>] = 5.6 mg/L), and suggested that both direct physical effects and indirect membrane damage due to oxidative stress mediated the inhibitory mode of action. After exposing adult zebrafish (*Danio rerio*) to CeO<sub>2</sub> NMs (0.5 mg/L) via the water column (as opposed to oral dose by incorporation into feed pellets) for 7 d, Johnston et al. (2010) noted significant uptake of cerium only in the livers of exposed fishes.

### **1.5.2 Iron oxide nanomaterials**

Due to their unique biochemical, catalytic and magnetic properties, iron oxide NMs like hematite ( $\alpha$ -Fe<sub>2</sub>O<sub>3</sub>) are often employed in the biomedical field as carriers for targeted drug delivery, as contrast agents for magnetic resonance imaging (approved by the US Food and Drug Administration in 1996), and for induced hyperthermia cancer treatments (Valdiglesias et al., 2016). Iron oxide NMs are

typically composed of a ferri- ( $\text{Fe}^{3+}$ ) or ferro ( $\text{Fe}^{2+}$ ) crystalline core and a surface coating that stabilizes the material, prevents agglomeration and enhances biocompatibility (Valdiglesias et al., 2016). However, despite the rapidly growing number of clinical applications and mammalian toxicology studies involving of iron oxide NMs (Valdiglesias et al., 2016), information regarding their potential toxicity to aquatic organisms is limited. Zhu et al. (2012) associated iron oxide NM-mediated toxicity in zebrafish with both metal ion release and ROS generation. The latter study showed that  $\text{Fe}_2\text{O}_3$  NMs ( $\geq 10$  mg/L) induced lethality, hatching delay, and malformations including tissue ulceration, pericardial edema and tail curvature (Zhu et al., 2012). Using transmission electron microscopy and scanning transmission X-ray microscopy, Kwon et al. (2014) observed several incidences of malformation (e.g. irregularly shaped microvilli, protrusion of epithelial cells, and dilatation of intracellular spaces) in the digestive tract of  $\alpha\text{-Fe}_2\text{O}_3$  and magnetite ( $\text{Fe}_3\text{O}_4$ ) NM exposed *Daphnia magna* after 48 h.

### **1.5.3 Titanium dioxide nanomaterials**

Nano- $\text{TiO}_2$  is a white pigment commonly added to a variety of food and personal care products including candies, chewing gums, deodorants, powdered donuts, shampoos and conditioners, shaving crèmes, sunscreens, and toothpastes (Weir et al., 2012).  $\text{TiO}_2$  NMs are wide band-gap semiconductors with photocatalytic properties and have thus been extensively studied for the purposes of environmental remediation (Hoffmann et al., 1995; Ijadpanah-Saravy et al., 2014; Lee and Choi, 2002), particularly air purification, bacterial disinfection and water treatment (Pelaez

et al., 2012). The photocatalytic properties of TiO<sub>2</sub> NMs have also been exploited for self-cleaning and anti-fogging applications (Shi et al., 2013). Two major crystal structures of TiO<sub>2</sub>, anatase and rutile, define their surface reactivity (Watanabe et al., 1999). The band gap energies of anatase (3.2 eV /  $\lambda \leq 387$  nm) and rutile (3.0 eV /  $\lambda \leq 413$  nm) (Lin et al., 2006) crystalline forms of TiO<sub>2</sub> NMs that govern their photoreactivity may also induce or predict phototoxicity (Ma et al., 2012). The phototoxicity of TiO<sub>2</sub> NMs to *Daphnia magna* and Japanese medaka (*Oryzias latipes*) has been shown to increase by several orders of magnitude in the presence of artificial sunlight (Ma et al., 2012). Alterations in thiobarbituric acid reactive substances and total glutathione levels were reported during a 14-d exposure of TiO<sub>2</sub> NMs ( $\leq 1$  mg/L) to trout (Federici et al., 2007). After a 14 d semi-static exposure to 1 mg/L TiO<sub>2</sub> NPs, mature adult female zebrafish produced significantly fewer viable embryos by the end of the 21 d post exposure recovery period (Ramsden et al., 2013). Few nanotoxicological studies have investigated whether the photoreactivity of TiO<sub>2</sub> NMs may increase the risk associated with their release into the environment (Bar-Ilan et al., 2013; 2012; Ma et al., 2012). Even fewer have explored the role of surface coatings on TiO<sub>2</sub> NM phototoxicity (Pan et al., 2009; Yin et al., 2010). Furthermore, literature regarding the *in vivo* phototoxicity of polymer-coated TiO<sub>2</sub> NMs does not exist.

#### **1.5.4 Zinc oxide nanomaterials**

Nano-ZnO is a dispersible metal oxide NM currently used in a variety of commercial and consumer products including batteries, ceramics, electronics, glasses,

industrial coatings, paints, and personal care products like cosmetics and sunscreens due to their unique antimicrobial, catalytic, optoelectronic, reflective, and UV absorption properties (Ma et al., 2013; Schultz et al., 2014). Analogous to TiO<sub>2</sub> NMs, ZnO NMs are also photocatalysts that generate ROS when photon energy from UV irradiation is equal to or greater than their band gap energy ( $3.37 \text{ eV} / \lambda \leq 368 \text{ nm}$ ); which is integral to their effectiveness in environmental remediation of pollutants and in water disinfection (Ma et al., 2013; Masoumbaigi et al., 2015). The formation of ROS by ZnO NMs and their dissolution to free zinc ions are considered to be the two primary modes of action for toxicity (Ma et al., 2013). Many nanotoxicological studies have shown that uncoated ZnO NMs are highly toxic (in the low mg/L range) to a variety of aquatic organisms (Aruoja et al., 2009; Blinova et al., 2010; Zhu et al., 2008). Zhao et al. (2013b) reported a strong correlation ( $R^2 = 0.90$ ) between ROS production by ZnO NMs and DNA damage in 144-hour post fertilization zebrafish larvae, and clearly demonstrated that exposure to both ZnO NMs ( $\leq 100 \text{ mg/L}$ ) and dissolved zinc ions altered the activities of the abovementioned antioxidant defense-related enzymes (see section 1.3.5). Both Aruoja et al. (2009) and Franklin et al. (2007) indicated that toxicity of ZnO NMs to the freshwater microalgae (*Pseudokirchneriella subcapitata*) was solely attributed to ionic metal. Furthermore, ZnO NMs (10 and 100 mg/L) have been shown to completely inhibit hatch of zebrafish embryos and this effect was most likely caused by the interaction between NMs and the zebrafish hatching enzyme (see section 1.6.1) (Ong et al., 2014b), thus compromising its activity (Lin et al., 2011).

### **1.5.5 Single-walled carbon nanotubes**

First discovered by Iijima and Ichihashi (Iijima and Ichihashi, 1993), carbon nanotubes (CNTs) have been described as elongated cylindrical-shaped structures with unique chemical, electronic and physical properties (Liang and Chen, 2010) that make them suitable for a broad range of applications including architecture, electronics and optics (Zhao and Liu, 2012). CNTs are poorly dispersible in water and will likely exist at the air/water interface, depending on the degree of physical mixing that occurs in the water column (Handy et al., 2008a). Currently, no method exists to quantify CNTs in natural waters (Nowack and Bucheli, 2007). The rolling of a single layer of graphene forms SWCNTs whereas multi-walled CNTs consist of multiple graphene layers (Zhao and Liu, 2012). Although an exact mechanism of SWCNT toxicity has yet to be elucidated, nanotoxicologists have proposed that noted toxicity was attributed to both direct physical irritation and indirect occlusion of biological tissues like gills (Smith et al., 2007), ROS production, lipid peroxidation (Alarifi et al., 2014), and/or trace metal impurities (e.g. catalysts) that originate from production processes (Cheng et al., 2007; Colvin, 2003). Embryonic zebrafish embryos are protected from SWCNT agglomerates because most are too large to pass through the pore canals of the chorion (see section 1.6.1) (Cheng et al., 2007). Carboxylated SWCNT dispersions have been shown to generate ROS including hydroxyl radicals, singlet oxygen and superoxide anions in the presence of artificial sunlight (Chen and Jafvert, 2010). However, amorphous carbon and metallic catalysts may have contributed to ROS generation by these colloidal dispersions (Chen and Jafvert, 2010).

### 1.5.6 Cellulose nanocrystals

Biocompatible and biodegradable cellulosic NMs can be produced from many different renewable resources including algae, bacteria and plants at low cost (Roman, 2015). Due to their high water absorption capacity, mechanical strength and stiffness, cellulose-based NMs are becoming increasingly attractive for use as drug delivery vehicles, in polymer nanocomposites, and for wound dressings (Roman, 2015). Although several excellent reviews covering the use of CNCs in biomedical applications and their toxic effects on human health are available (Jorfi and Foster, 2015; Lin and Dufresne, 2014; Roman, 2015; Roman et al., 2009), to my knowledge, only one comprehensive toxicological assessment involving aquatic organisms exists (Kovacs et al., 2010). The latter study evaluated the effects of different concentrations ( $\leq 6000$  mg/L) of CNCs on rainbow trout (*Oncorhynchus mykiss*) hepatocytes and nine aquatic species (*Ceriodaphnia dubia*, *Danio rerio*, *Daphnia magna*, *Hydra attenuate*, *Oncorhynchus mykiss*, *Pimephales promelas*, *Pseudokirchneriella subcapitata*, *Thamnocephalus platyurus*, and *Vibrio fischeri*) using multiple endpoints (cytotoxicity, development, growth, lethality, morphology, reproduction, etc.) for up to 10 d and found the material to have low toxicity (Kovacs et al., 2010). However, toxicity screening rather than toxicity mechanism appeared to be the major focus of this study.

## 1.6 *IN VIVO* AND *IN VITRO* FISH MODELS

Fish are the oldest and most diverse living class of vertebrates (Powers, 1989). Numerous characteristics make fish an excellent experimental model for studies in aquatic toxicology, developmental biology, and environmental science (Powers, 1989). Many fish species can be easily raised and bred under laboratory conditions at a much lower cost than amphibian, avian, mammalian, or reptilian animal models (Powers, 1989). Mammals and fishes share many developmental pathways, organ systems, and physiological mechanisms (Crollius and Weissenbach, 2005), making cross-species comparisons possible. For example, the basic features of gill and gut epithelium that line the external surface and internal body cavities of a fish are similar to other vertebrates (e.g. rodents) (Handy et al., 2008a). In recent years, there has been a movement toward using cultured fish cells in toxicity testing for cost, ethical and logistic reasons, and to minimize the number of animals needed for research and toxicology studies (Bury et al., 2014). Although fish models cannot replace traditional mammalian systems for answering certain types of scientific questions, they can provide a more acceptable alternative for nanotoxicity testing (Powers, 1989). Zebrafish and rainbow trout were selected as *in vivo* and *in vitro* fish model systems, respectively. Details regarding channel catfish (*Ictalurus punctatus*) cell lines have been described elsewhere (Ede, 2015).

### **1.6.1 Zebrafish embryo**

Wild-type zebrafish are commonly used in nanotoxicology studies due to their well-understood biology and acceptance by regulatory authorities as a model aquatic organism (Ma et al., 2013). The zebrafish is a member of the family Cyprinidae and is native to India and Pakistan. Zebrafish offer several advantages for toxicity testing over other mammalian model systems (e.g. primates, rabbits, rodents, etc.) including economical husbandry requirements, high fecundity, low cost, short breeding cycle, small size, transparent embryos (Dai et al., 2014; Hill et al., 2005), and considerable genome sequence homology to humans (Howe et al., 2013). However, non-native (to Canada) zebrafish have low detection sensitivity and experiments require a large sample size, making statistical analysis cumbersome (Dai et al., 2014).

The zebrafish chorion, mainly composed of glycoproteins, acts as a physical and chemical barrier to shield developing zebrafish from noxious external environmental conditions (Bonsignorio et al., 1996) and is the first biological membrane to interact with NMs upon exposure (Cheng et al., 2007). The chorion has two distinct membranes, the outer chorion dotted with protuberances and the inner vitelline membrane containing numerous pore canals (Bai et al., 2010) that may be permeable to NMs. Alternatively, NMs could adsorb to the surface of the chorion (Lin et al., 2011) and block pore canals, thereby creating hypoxic conditions for the embryo (Cheng et al., 2007). Lee et al. (2007) demonstrated that some NMs passively diffused into and out of the embryo through pore canals, while others got stuck, aggregated with incoming particles and consequently clogged the pores of the chorion. Lin et al. (2011) reported an increase in metal ion concentration inside the

chorion following 1 and 24 h exposures to different metal oxide NMs and results suggested that uptake was time-dependent. At time of hatch (48-72 h) (Kimmel et al., 1995), a zinc metalloprotease is released from a hatching gland located on the anterior surface of the yolk sac that functions to partially digest the inner vitelline membrane of the chorion (Sano et al., 2008). Contractile movements of the zebrafish can then rupture the softened chorion allowing the animal to emerge (Sano et al., 2008). Will NMs traverse the chorion and adsorb to the developing zebrafish within the chorion? The answer to this research question is revealed in **Chapter 2**. I hypothesize that most NMs will adsorb to the outer surface of the chorion and some will passively diffuse through the chorion because pores are  $\sim 170 \text{ nm}^2$  in size (Cheng et al., 2007).

### **1.6.2 Rainbow trout gill epithelial cell line**

The fish gill is a complex, multifunctional tissue made up of a variety of different cells types including pavement, mitochondrial-rich and mucous cells, and is the major site of acid-base regulation, gas exchange, metabolic waste excretion, and osmoregulation (Bury et al., 2014; Evans et al., 2005). Since water must continuously flow over the gills, they are one of the primary target organs and uptake sites of aqueous contaminants like NMs (Bury et al., 2014; Handy et al., 2008a). Certain NMs are expected to adsorb onto gill surfaces and be taken up by epithelial cells via endocytosis rather than by membrane transporters or by passive diffusion through cell membranes (Handy et al., 2008a). Permanent gill cell lines (cells that have been passaged multiple times *in vitro*) are utilized in toxicological studies due to their ease of manipulation, high reproducibility, low maintenance, and amenability to culture in

both complete and simplified media (Kühnel et al., 2009; Lee et al., 2009). In theory, cell lines can be cultured indefinitely without deterioration and are thus termed immortal (Bury et al., 2014). The permanent, epithelial cell line, RTgill-W1, derived from primary cell cultures of adult rainbow trout (Walbaum) gills (Bols et al., 1994) was used in my studies. Lee et al. (2009) reported the presence of mucous-secreting goblet-like and mitochondria-rich cells in the RTgill-W1 cell line. In addition, Bols et al. (1994) observed nuclei, mitochondria, lysosomes, and intermediate filaments in RTgill-W1 cells.

## **1.7 THESIS GOALS**

The primary objectives of my thesis were to (1) develop simple and reproducible *in vivo* and *in vitro* methods for NM toxicity testing that could be employed by fellow nanotoxicologists, industry, risk assessors, and regulators, (2) determine whether physicochemical properties including surface functionalization and environmental factors like UV light modulate NM toxicity, (3) assess the toxicological effects of several functionalized metal oxide and carbon-based NMs at multiple levels of biological organization, and (4) elucidate the mechanisms underlying noted toxicity as well as NM uptake by fish embryos and cells. Although four discrete data chapters follow, the abovementioned thesis goals are neither chapter-specific nor are they listed in any particular order and as such there will be some overlap between research chapters. Instead, chapters are arranged in ascending order according to the degree of mechanistic insight into the effects of NMs in fishes.

## CHAPTER 2

### Physicochemical characteristics of polymer-coated metal oxide nanoparticles and their toxicological effects on zebrafish (*Danio rerio*) development

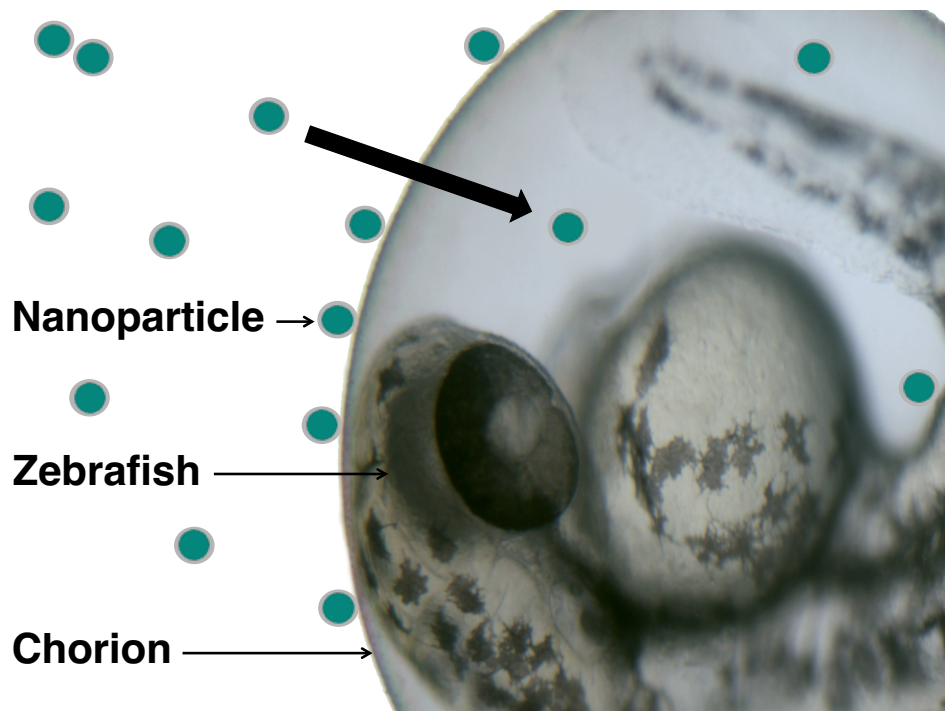


Figure 2-1. Graphical abstract.

Felix, L.C., Ortega, V.A., Ede, J.D., Goss, G.G., 2013. Physicochemical characteristics of polymer-coated metal oxide nanoparticles and their toxicological effects on zebrafish (*Danio rerio*) development. *Environmental Science and Technology* 47(12), 6589–6596. doi: 10.1021/es401403p.

## 2.1 INTRODUCTION

The novel properties imparted by particles at the nanoscale have challenged environmental risk assessment procedures, which traditionally evaluate contaminants based on their bulk-scale properties (Gajewicz et al., 2012). Nanoparticles (NPs) have at least one facet less than 100 nm (Lead and Wilkinson, 2006), and their physicochemical properties can be manipulated via surface functionalization, making them more suitable than their bulk counterparts for specific applications (Neouze and Schubert, 2008). Manipulating physicochemical properties of NPs with a polymer coating can improve their solubility in various solvents and change the permeability of their encapsulating material to prevent or allow the release of core substances (Meier, 2000). The polymer-coated metal oxide (MeO) NPs tested in this study are proposed for use as micronutrients in agriculture while the polymer coating alone (nanocapsule) is currently utilized as a nano-sized carrier for herbicide and insecticide formulations. This will improve the efficiency of herbicide application by increasing plant tissue uptake and by decreasing the required dosage of active substances (Pérez-de-Luque and Rubiales, 2009). These NPs may be present in the environment at high concentrations as a consequence of their direct agricultural application; therefore, it is important to characterize NPs under a variety of environmentally realistic conditions (Handy et al., 2008b) and determine if the polymer coating mediates or mitigates the toxicity of the active substances.

The physicochemical properties of NPs are determined in part by ionic strength, natural organic matter, pH, and solar radiation (Handy et al., 2008b; Keller

et al., 2010; Ma et al., 2012; Sauer and Meier, 2001), all fundamental and variable components of aquatic environments. Baalousha et al. (2008) demonstrated that pH changes the solubility and stability of iron oxide NPs and that the percentage of total iron in the dissolved phase increased with decreasing pH. The polymer coat can also be used to improve NP stability in suspension (Anderson et al., 2011) and prevent dissolution of free metal ions from the NP core (Stebounova et al., 2011), factors that previous ecotoxicological studies suggest contribute to their toxicity (Bai et al., 2010; Yang et al., 2012). It should be noted that an increased stability provided by the polymer coating could increase the residence time of NPs in suspension (Baalousha et al., 2008) and therefore bioavailability to aquatic organisms (Keller et al., 2010).

Toxicity studies using surfactants and uncoated MeO NPs have shown a range of toxic effects to fish. Chen et al. (2011) demonstrated that poly (acrylic acid) (PAA) as a surfactant is less toxic to Japanese medaka (*Oryzias latipes*) larvae than sodium dodecyl sulfate and observed no significant mortality of larvae exposed to < 25 mg/L iron oxide suspensions. In contrast, low concentrations of titanium dioxide (TiO<sub>2</sub>) NPs have been shown to cause respiratory pathologies in rainbow trout (*Oncorhynchus mykiss*) (Federici et al., 2007) and zinc oxide (ZnO) NPs have been reported to induce mortality and developmental impairments in zebrafish (*Danio rerio*) (Bai et al., 2010). Finally, Van Hoecke et al. (2009) observed that high concentrations ( $\leq 200$  mg/L) of cerium oxide (CeO<sub>2</sub>) NPs were not acutely toxic to zebrafish embryos.

Zebrafish are commonly used as a high-throughput animal model in acute toxicity studies. Mature adults are easily bred to produce large quantities of embryos

that are sensitive to low doses of environmental contamination (Hill et al., 2005). Zebrafish embryos are small and develop rapidly thereby minimizing NP use, and their transparent chorion allows for observation of developmental malformations. Moreover, the chorion has pore canals  $\sim 170$  nm<sup>2</sup> in size (Cheng et al., 2007) that may be permeable to NPs. Alternatively, NPs could adsorb to the surface of the chorion and block pore canals, thereby reducing gas exchange (Bai et al., 2010).

Our study examined the physicochemical characteristics and toxicological effects of aqueous polymer-coated MeO NPs including TiO<sub>2</sub>, ZnO, Fe<sub>2</sub>O<sub>3</sub>, and CeO<sub>2</sub> on early-stage zebrafish. We have developed a method for determining MeO NP dissolution as well as a zebrafish embryo toxicity assay that is optimized for nanomaterial testing by measuring a variety of endpoints. We have also investigated whether specific NPs can traverse the chorion of developing embryos. As a paired control, we tested the polymer coating alone without a MeO NP core to determine if it mediates or mitigates the toxicity of the NPs.

## **2.2 MATERIALS AND METHODS**

### **2.2.1 Synthesis of polymer-coated nanoparticles**

Vive Nano (vn) Inc. (now Vive Crop Protection Inc.; Toronto, Canada) manufactured the polymer-coated MeO NPs used in this study including priority Organisation for Economic Co-operation and Development (OECD) materials TiO<sub>2</sub>, ZnO, Fe<sub>2</sub>O<sub>3</sub> and CeO<sub>2</sub> (OECD, 2010). The polymer coating consisted of PAA, a high

molecular weight anionic polyelectrolyte, which increased the stability and thus dispersibility of the NPs in aqueous suspension by minimizing interaction between particles (Anderson et al., 2011). The NP template was synthesized via interaction between oppositely charged polymer chains and counterions (Pham et al., 2010), i.e., inorganic Ti, Zn, Fe, and Ce salts, resulting in condensed orb-like structures of negative charge, 3-9 nm in size. These structures were then stabilized by cross-linking polymer chains either chemically or through ionizing radiation in order to maintain their integrity in suspension. Finally, redox and precipitation reactions were used to convert the counterions encapsulated within the cross-linked coating to inorganic NPs (**Figure S2-1**) (Goh et al., 2009). To produce the nanocapsules (vnCAP), NaCl counterions were used to collapse the polymer prior to the cross-linking step and then Na<sup>+</sup> was removed via diafiltration to form hollow shell structures void of a metal oxide core. The vnCAP may not be hollow structures per se; rather, they are likely a flexible globular matrix of polymer, 3-9 nm in size. Stock suspensions (10,000 mg/L) were dispersed in deionized water and stored at 4 °C in the absence of light.

### **2.2.2 Physicochemical characterization of polymer-coated nanoparticles**

Physicochemical characteristics of MeO NPs, analyzed by the manufacturer, included shape, size, pH, total metal, purity, and trace metal composition. NP shape and size were confirmed using transmission electron microscopy (TEM, FEI Tecnai-20). To determine trace metal content, formulations in powder form were weighed, acidified with HNO<sub>3</sub>, and then measured using an inductively coupled plasma optical emission spectrometer (ICP-OES, Varian Vista-Pro CCD

Simultaneous) equipped with an autosampler (Varian SPS 3). ICP-OES was coupled with Total Organic Carbon (TOC-VCPH Shimadzu analyzer) oxidative combustion-infrared analysis equipped with an autosampler (ASI-V) and solid sample module (SSM-5000A). Our research group conducted all other analyses.

To characterize NP aggregation in 10, 50, 100, and 200 mg/L test suspensions over time, we used dynamic light scattering (DLS; Zetasizer Nano Series, Malvern) in 173° backscatter mode to measure mean hydrodynamic diameter, polydispersity index, and zeta potential at 0, 24, 48, and 72 h. NP test suspensions were prepared with dechlorinated tap water (DTW; pH: 7.5-7.6, conductivity:  $175 \pm 10$   $\mu$ S/cm, temperature:  $28 \pm 1$  °C, dissolved oxygen: 7.02 mg/L, total hardness: 160 mg/L as CaCO<sub>3</sub>, salinity: 0.1 ppt). All samples remained static and were covered with Parafilm between measurements. All measurements were repeated three times. The oxidation state of vnFe<sub>2</sub>O<sub>3</sub> was confirmed by the Department of Chemistry, University of Alberta, using an X-ray photoelectron spectrometer (Kratos Axis Ultra; data not shown).

### **2.2.3 Polymer-coated metal oxide nanoparticle dissolution**

We conducted dissolution experiments to calculate the concentration of free metal ions present in NP stock suspensions and to determine the maximum concentration of metal ions released from the NPs over a 72 h dialysis period. For both experiments, Slide-A-Lyzer dialysis cassettes (~1 nm; 2000 molecular weight cut-off; Pierce) were injected in triplicate with either 0.5 mL of the 10,000 mg/L NP stock suspension (vnTiO<sub>2</sub>, vnZnO, vnFe<sub>2</sub>O<sub>3</sub>, vnCeO<sub>2</sub>, and vnCAP) or with ultra pure

water (resistance 18.3 k $\Omega$ ) for controls. Prior to starting the experiments, each beaker was bathed in 1% HNO<sub>3</sub> overnight and rinsed thoroughly with ultra pure water.

The concentration of free metal ions present in the stock suspensions was determined by adding the cassettes to beakers containing 250 mL (500 fold dilution) of ultra pure water and placed on stir plates, with constant slow rotation, over a 30-min dialysis period to ensure equilibration. Cassettes were then transferred to another beaker containing fresh ultra pure water for a 72 h dialysis to distinguish between free metal ions in the stock suspension (0-0.5 h) and metal ions released from the NP core (0.5-72 h). During the experimental period, the beakers were covered to limit light exposure, evaporation, and production of reactive oxygen species. Duplicate water samples were collected from each beaker at 0, 0.5, 12, 24, 36, 48, and 72 h and analyzed for core metals, Ti<sup>4+</sup>, Zn<sup>2+</sup>, Fe<sup>3+</sup>, and Ce<sup>4+</sup>, by inductively coupled plasma mass spectroscopy (ICP-MS; Perkin Elmer, Elan 6000).

In a separate experiment to mimic entry of pH soluble metals into an acidic aquatic environment, vnZnO stock suspensions were pH-adjusted from 8.95 to 7.00 and 5.50 using 1M HCl (pH meter, Accumet Research, AR15). For example, pH 5.5 was used to represent vnZnO dissolution in lakes of Alberta and the Canadian Shield (Prepas, 1990). Yu et al. (2011) reported that the physicochemical properties of nano ZnO were strongly influenced by pH and that dissolved Zn<sup>2+</sup> was toxic to zebrafish.

#### **2.2.4 Rearing facility and embryo production**

Adult zebrafish were housed in 30 L tanks circulated with a continuous flow of system conditioned river water (pH: 7.7-7.8; conductivity: 1350  $\pm$  100  $\mu$ S/cm;

temperature:  $28 \pm 1$  °C; dissolved oxygen: 6.85 mg/L; total hardness: 100 mg/L as CaCO<sub>3</sub>; salinity: 0.5 ppt) held in the fish rearing facility at the University of Alberta. Zebrafish (wild type strain AB or wild type strain AB/TB) aged 6 to 18 months were fed live brine shrimp (*Artemia salina*; INVE Aquaculture Nutrition) twice daily and trout chow (O.S.I Marine Lab Inc.) as required. Hatching boxes were set up (2 males: 1 female breeding ratio) and acclimated overnight. Viable embryos were collected 1-2 h after the initial onset of the light cycle (14 h light: 10 h dark photoperiod). All embryos were examined under a dissecting microscope to ensure NP exposure started during late cleavage or early blastula stages (2-3 hours post fertilization, hpf), allowing for slight developmental asynchrony (Kimmel et al., 1995).

### **2.2.5 Zebrafish embryo toxicity assay**

Polymer-coated MeO NP stock suspensions were stirred (1200 revolutions per minute) for 30 min and diluted with filtered (0.45 µm SFCA Bottle-Top) and autoclaved DTW without dispersants. Zebrafish embryos were rinsed three times with DTW and placed in 6-well plates (30 embryos/well). Embryos were then exposed to 5 mL of each NP suspension (vnTiO<sub>2</sub>, vnZnO, vnCAP, vnFe<sub>2</sub>O<sub>3</sub>, or vnCeO<sub>2</sub>) at varying concentrations (1, 10, 50, 100, 200, 400, 800, 1200, 1600, and 2000 mg/L) and DTW as a paired control for 72 h. Each NP test suspension was mixed by vortex for 20 s before being added to the well. The plates remained static, i.e., suspensions were not refreshed during the acute experiments and were incubated at  $28 \pm 1$  °C. Dead embryos, identified by a white precipitate within the chorion, and larvae, identified by the absence of a heartbeat (Ali et al., 2011), were recorded and removed

from each well at 24, 48 and 72 hpf. Only experiments with  $\geq 80\%$  survival in the control well were used in analyses.

Pilot acute toxicity tests showed that exposure to 200 mg vnFe<sub>2</sub>O<sub>3</sub>/L caused the highest percent mortality (23.7%) and morphological impairment (32.5%) compared to all other NPs, though not significantly different from DTW control (ANOVA,  $p > 0.05$ ). Therefore, embryos were exposed to 1, 10, 50, 100, and 200 mg vnFe<sub>2</sub>O<sub>3</sub>/L prepared from an aliquot of the stock suspension that was dialyzed for 4 h with beaker transfers at 0.5, 1, 2 and 3 h. The results of this experiment were compared to exposures using vnFe<sub>2</sub>O<sub>3</sub> that had not been dialyzed to determine if free metal released from the NPs had an effect on survival.

We also calculated the total amount of free metal present in 200 mg/L of each NP type using the results from our dissolution experiment and exposed zebrafish to these free metal solutions. The free metal exposures served as controls for the acute toxicity assays. Each experiment ( $n = 180$  animals) was repeated at least 5 times. All chemicals, except bulk TiO<sub>2</sub> (Cristal Global), were purchased from Sigma-Aldrich.

### **2.2.6 Lethal and sublethal endpoints**

Percent survival was measured at 24, 48 and 72 hpf. Lethal concentration 50 (LC50) values were calculated to determine the toxicological limits for these materials using the same exposure method as described above. Body length of 72 hpf larvae exposed to 200 mg/L of each NP type was measured using an inverted microscope (Zeiss Axio Observer A1) connected to AxioVs40 software (v. 4.7.2). Length of 6 randomly selected larvae per treatment was measured and the experiment

was repeated at least 3 times. Percent hatch of zebrafish embryos was measured at 72 hpf using a dissecting microscope, and preliminary data showed inhibition only in those exposed to  $\geq 800$  mg vnCAP/L. We noted that the pH of the vnCAP stock suspension was acidic; measuring pH 3.0 while the other NPs had higher pH values (**Table S2-1**). The pH of the vnCAP test exposures ranged from 4.0 to 5.5 (**Table S2-2**), suggesting that hatch may be affected by either the properties of the vnCAP, the pH of the suspension, or a combination of both the vnCAP and the low pH conditions. To test these factors, percent hatch was measured in embryos exposed to 400, 800, 1200, 1600 and 2000 mg vnCAP/L that was either diluted directly from the stock suspension or diluted and then pH-adjusted to 7.5 with 10 mM NaOH (**Table S2-2**). DTW was used as a paired control either at pH 7.5 or was pH-adjusted to 4.0 with 10 mM HCl (**Table S2-2**).

### **2.2.7 Nanoparticle interaction with zebrafish embryo**

To determine if the NPs were traversing the chorion and interacting with the animal, we exposed embryos to 200 mg vnCeO<sub>2</sub>/L or DTW as a paired control for 48 h. We used vnCeO<sub>2</sub> NPs because background levels of Ce in biological tissue are very low compared to Fe or Zn. Embryos were rinsed twice with DTW, dechorionated, and the chorion and animal were separated and dried at 100 °C for 2 h. The dry samples were acid digested with concentrated HNO<sub>3</sub> overnight at 4 °C. Samples were centrifuged at 13,000 relative centrifugal force for 30 s, and the supernatant was diluted 25-fold with double deionized water. ICP-MS analysis was used to quantify the amount of Ce<sup>4+</sup> in control and treatment samples. The amount of

$Ce^{4+}$  per chorion and animal was calculated and compared to the total amount of  $Ce^{4+}$  in the exposure suspension. This experiment was performed on 6 embryos.

To visually support the above experiment and verify that NPs and not free ions were traversing the chorion, we exposed embryos to either 200 mg/L vnCAP containing the fluorescent dye Nile red (vnCAP-NR) or DTW for 24 h using the same method described above. In addition, several embryos were carefully placed directly under the membrane of a Slide-A-Lyzer cassette containing 200 mg/L vnCAP-NR to confirm that noted fluorescence was attributed to NP interaction rather than to free dye leached from the particles. Embryos were anaesthetized with 10 mg/L tricaine methanesulfonate (TMS) for 15 min, rinsed thrice with phosphate buffered saline (PBS), and fixed in 4% paraformaldehyde at 4 °C for 12 h. Embryos were mounted in 1% low melting temperature agarose (BioWhittaker Molecular Applications), covered in a 70% glycerol/PBS solution to prevent desiccation, and imaged using a laser scanning confocal microscope (Zeiss LSM 710 AxioObserver, Carl Zeiss Microscopy, Jena, Germany) with a 10× objective. NPs were excited with a solid-state laser excitation line of 561 nm and observed through 586-649 nm emission bandpass filters. Images were rendered using ZEN 2011 lite (Carl Zeiss Microscopy, Jena, Germany).

After each experiment, all 72 hpf larvae were euthanized with a high dose of TMS and NP exposure suspensions discarded using proper waste disposal methods designated by the Environmental Services Division, University of Alberta.

### 2.2.8 Statistical analysis

All data are presented as mean  $\pm$  standard error of the mean (SEM). SigmaPlot 11.0 for Windows (Systat Software Inc.) and GraphPad Prism 6 (v. 6.0h, GraphPad Software Inc.) were used to perform statistical analyses and to make graphs, respectively. A one-way analysis of variance (ANOVA) with a Dunnett's post hoc test was used to identify significant differences between control and treatment groups for all experiments. An unpaired Student's t-test was used to identify significant differences between vnCAP and pH-adjusted vnCAP treatments. The U.S. Environmental Protection Agency Probit Analysis Program (v. 1.5) and SigmaPlot were used to generate LC50 values, 95% confidence intervals, and regression equations for each NP suspension. The significance level was set at  $p < 0.05$ .

## 2.3 RESULTS AND DISCUSSION

### 2.3.1 Physicochemical characterization of polymer-coated nanoparticles

Characterizing the physicochemical properties of polymer-coated MeO NPs is a fundamental step in order to predict their transport and fate in the environment. Physicochemical characteristics measured by the manufacturer including TEM images (**Figure S2-2**) and trace metal content (**Table S2-3**) are described in **Appendix I**. DLS measurements of each NP suspension over time suggested a variable size distribution of aggregated particles that were negatively charged when measured with DTW (**Figures S2-3–S2-5**). The hydrodynamic diameters of vnFe<sub>2</sub>O<sub>3</sub>

and vnCeO<sub>2</sub> in suspension were similar between 10 and 200 mg/L, indicating that these particles were stable colloids in our test media over the 72 h test period (**Figure S2-3d, e**) while vnCAP were relatively stable over time with the exception of the highest concentration (200 mg/L) where some aggregation was noted (**Figure S2-3c**). However, for vnTiO<sub>2</sub> (**Figure S2-3a**) and vnZnO (**Figure S2-3b**), variable mean sizes were noted both initially and over time. vnTiO<sub>2</sub> tended to have reduced aggregation over time at each concentration, likely due to sedimentation of larger aggregates while vnZnO showed an initial increase in mean size followed again by a reduction, likely due to sedimentation and removal from the sampling mean.

The polydispersity index is an indicator of the relative size distribution of particles in suspension (Miglietta et al., 2009). Size distribution profiles indicated that vnTiO<sub>2</sub> were very polydisperse (> 0.7) overtime while those for vnZnO and vnCAP showed mid-range polydispersity (0.08-0.7). Profiles for vnFe<sub>2</sub>O<sub>3</sub> and vnCeO<sub>2</sub> suggested that these particles were nearly monodispersed (0.05-0.08) and monodispersed (0-0.05), respectively (**Figure S2-4**).

Zeta potential is a measure of surface charge and can be used to determine particle stability in suspension (White et al., 2007). Each NP suspension (pH ~7.6) was negatively charged, ranging from -21.1 mV (vnZnO) to -9.3 mV (vnFe<sub>2</sub>O<sub>3</sub>) (**Figure S2-5**). The small variability in zeta potential between NP types may have been attributed to charge shielding effects caused by the sharing of metal core ions with the PAA coating, and this may account for different degrees of aggregation as displayed by the particles.

### 2.3.2 Polymer-coated nanoparticle dissolution

Nanotoxicologists often misinterpret results as solely a NP effect when it is possible that toxicity may have been caused by free metal ions released from the NP core. Free metal from unreacted synthesis reagents or released from unstable metal cores is typically present in MeO NP stock suspensions. Dissolved metal was present in vnTiO<sub>2</sub> (16.44 ± 12.99 mg/L), vnFe<sub>2</sub>O<sub>3</sub> (0.85 ± 1.12 mg/L) and vnCeO<sub>2</sub> (14.87 ± 7.54 mg/L) stock suspensions, which could potentially contribute to toxicity and would need to be appropriately controlled. A small amount of free Zn was present in the vnCAP stock suspension (0.08 ± 0.50 mg/L). The variation in free metal concentrations between each NP type was a function of the synthesis procedure and highlights the importance of initial characterization prior to experimentation to determine the appropriate controls. The percentage of primary dialyzed free metal ions, Ti<sup>4+</sup> (1.067%), Zn<sup>2+</sup> (0.005%), Fe<sup>3+</sup> (0.167%), and Ce<sup>4+</sup> (0.736%) (**Figure 2-2**), was negligible when compared to the total primary metal composition of the respective vnTiO<sub>2</sub> (25.7%), vnCAP (18.0%), vnFe<sub>2</sub>O<sub>3</sub> (21.0%), and vnCeO<sub>2</sub> (24.8%) stock suspensions. Despite these low percentages, the concentration of free metal ions must be considered prior to conducting nanotoxicological studies, as a free metal effect may be misinterpreted as a NP effect or vice versa.

We also measured the dissolution characteristics of each NP over a 72 h period. Following the 30-min removal of free metal ions by dialysis, very little metal ions were released from the metal core of the NP over 72 h in all NP suspensions tested (data not shown; ANOVA,  $p > 0.05$ ). The relative amount of metal released from the NP core remained consistently low or below the detection limit (DL),

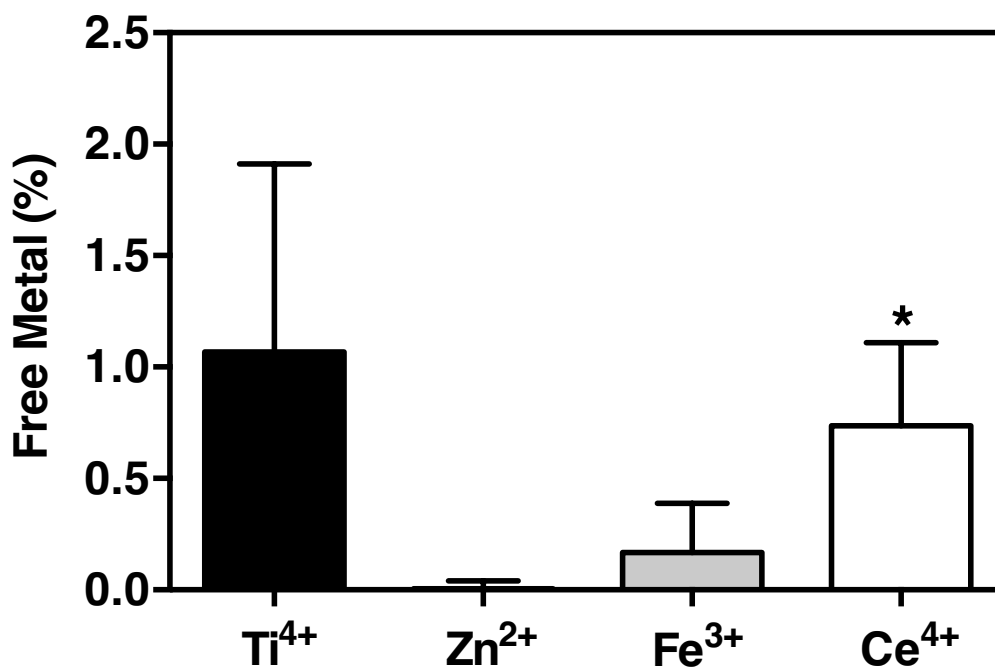


**Figure 2-2. Dissolution of polymer-coated NPs.** Percent free metal ion (Ti<sup>4+</sup>, Zn<sup>2+</sup>, Fe<sup>3+</sup>, and Ce<sup>4+</sup>) released after 0.5 h dialysis, relative to total metal, in respective NP stock suspensions (vnTiO<sub>2</sub>, vnCAP, vnFe<sub>2</sub>O<sub>3</sub>, vnCeO<sub>2</sub>). ICP-MS detection limits: Ti (0.09 µg/L), Zn (0.08 µg/L), Fe (3.7 µg/L) and Ce (0.03 µg/L). Values are mean ± SEM. An asterisk (\*) represents a significant difference (ANOVA, Dunnett's *p* < 0.05).

suggesting that the free metal in each stock suspension was removed by initial dialysis and that each particle type was stable and not dissolving overtime in our test media. The relative amount of free metal released from the NP core in vnTiO<sub>2</sub> (< 1.5 µg/L), vnCAP (< 2.0 µg/L), vnFe<sub>2</sub>O<sub>3</sub> (< DL), and vnCeO<sub>2</sub> (< 0.4 µg/L) diluents were nominal compared to the free metal ions released after 30 min of dialysis (data not shown; ANOVA,  $p > 0.05$ ). These results agree with findings of Dergunov et al. (2010) who observed structural stability of polymer nanocapsules over a 240-d period. Overall, the release of free metal from each NP stock suspension remained low over the experimental period and we suggest that the polymer coating contributed to the stability of the NPs in suspension.

The stability of MeO NPs can be altered by several components of aquatic environments including ionic strength (Petosa et al., 2012), pH, and natural organic matter (Baalousha et al., 2008). Franklin et al. (2007) observed rapid dissolution of uncoated ZnO NPs at pH 7.6 followed by equilibration of dissolved Zn metal after 72 h. Based on Franklin et al. (2007) findings, we used vnZnO to investigate the effects of different pHs on PAA-coated MeO NPs in aquatic environments. The stability of vnZnO decreased slightly with decreasing pH (8.95 to 5.50) as indicated by the increased concentration of free Zn<sup>2+</sup> (3.40 mg/L) when dialyzed at pH 5.50 after 30 min (data not shown). The vnZnO stock suspension at pH 7.00 and 5.50 had 0.002% and 0.232% Zn<sup>2+</sup>, respectively (**Figure 2-3a**).

Following 72 h of dialysis, there was more Zn<sup>2+</sup> released from vnZnO at pH 5.5 (**Figure 2-3b**), which was likely attributed to dissociation of the carboxylic

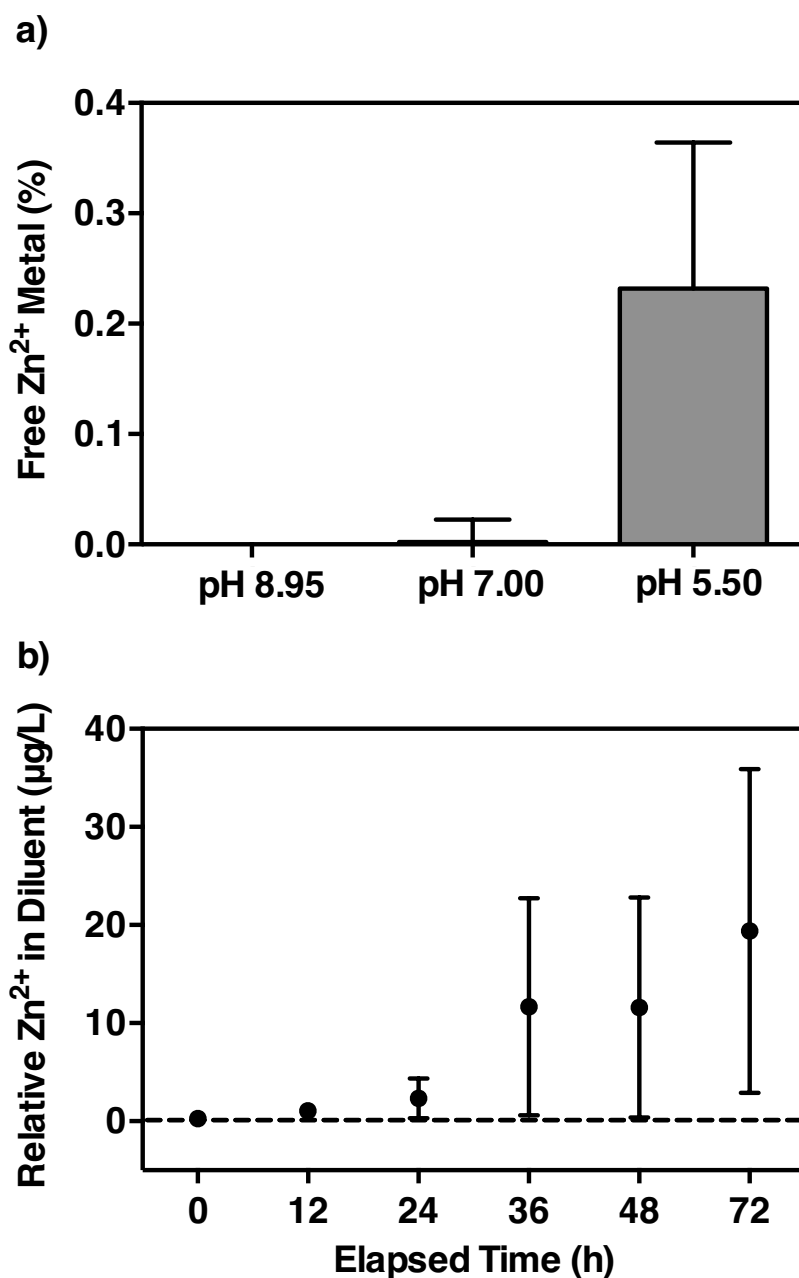


**Figure 2-3. pH-dependent dissolution of polymer-coated ZnO NPs.** a) Percent free Zn<sup>2+</sup> metal ion released, relative to control, after 0.5 h dialysis at pH 8.95, 7.00, and 5.50 from pH-adjusted vnZnO stock suspension (10,000 mg/L) (n = 3). Note that free Zn<sup>2+</sup> at pH 8.95 was below the ICP-MS detection limit (0.08 µg/L; dashed line). b) Concentration of Zn<sup>2+</sup> (µg/L), relative to control, released into diluent from pH 5.50-adjusted vnZnO stock suspension between 0.5 and 72 h dialysis (n = 3). Values are mean ± SEM (ANOVA, Dunnett's, *p* > 0.05).

functional groups of the polymer matrix, increased permeability of the PAA coating (Sauer and Meier, 2001), and thus increased etching of the metal core itself (Meulenkamp, 1998). Despite the effect of pH on NP stability, only a small portion of  $Zn^{2+}$  (0.019 mg/L), relative to the total amount of Zn metal in the stock suspension (1800 mg/L), was released from the NP over 72 h (**Figure 2-3b**). Compared to the DTW control, the concentration of  $Zn^{2+}$  in the diluent at pH 7.00 was below the ICP-MS DL (data not shown; ANOVA,  $p > 0.05$ ) while at pH 8.95 was  $< 1.0 \mu\text{g/L}$  (data not shown; ANOVA,  $p > 0.05$ ). The pH of natural waters may alter the dissolution of MeO NPs and free metal may catalyze undesirable reactions.

### **2.3.3 Lethality tests on zebrafish embryos and post-hatch larvae**

Uncoated MeO NPs have been previously shown to cause toxicity in fish (Bai et al., 2010; Federici et al., 2007; Zhu et al., 2008). Interestingly, cumulative 72 h survival of zebrafish embryos and newly hatched larvae exposed to  $\leq 200 \text{ mg/L}$  of  $\text{vnTiO}_2$ ,  $\text{vnZnO}$ ,  $\text{vnCAP}$ ,  $\text{vnFe}_2\text{O}_3$ , dialyzed  $\text{vnFe}_2\text{O}_3$ , and  $\text{vnCeO}_2$  showed no effects and were not significantly different from the controls (**Figure 2-4**). The paired free metal controls also had no effect on survival (**Figure S2-6**) or hatch (data not shown). Biesinger and Christensen (1972) exposed *Daphnia magna* to Fe and Zn metal ions in the presence of food and calculated a 48 h LC50 values of 9.6 mg/L and 0.28 mg/L, respectively, which were higher than the concentrations of Fe (0.85 mg/L representing  $\text{vnFe}_2\text{O}_3$ ) and Zn (0.03 mg/L representing  $\text{vnZnO}$  at pH 7.00 and 0.08 mg/L representing  $\text{vnCAP}$ ) tested in this study.

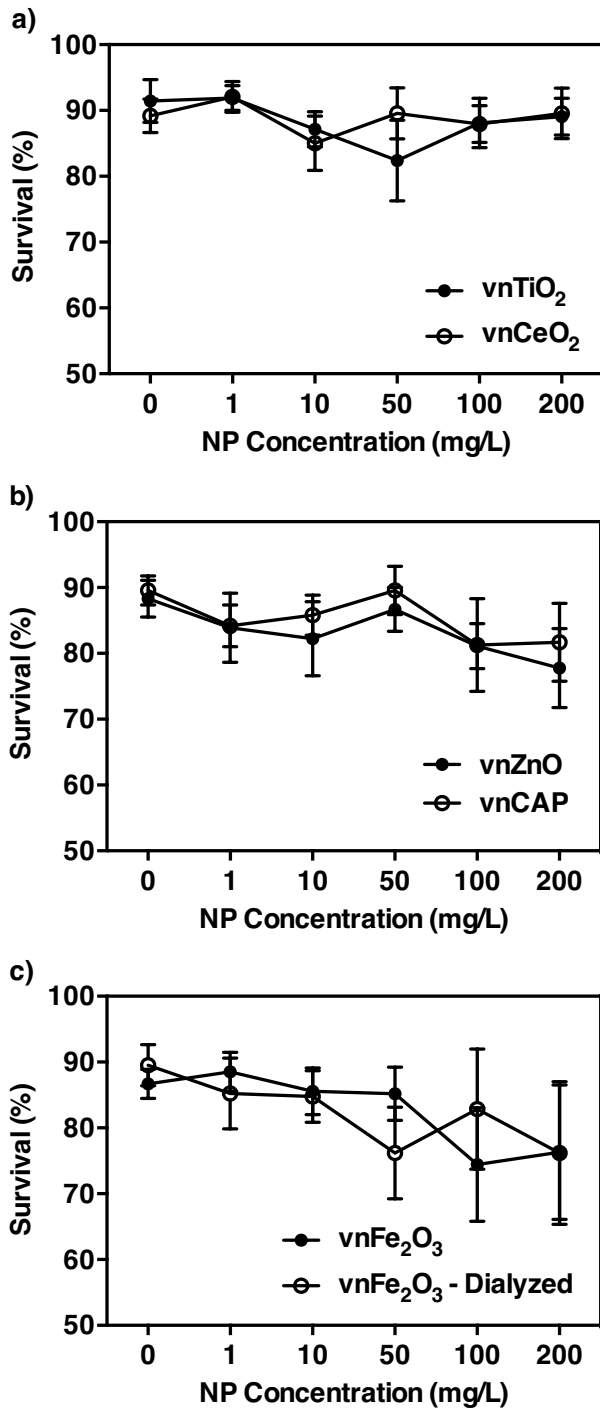


**Figure 2-4. Cumulative percent survival of NP exposed zebrafish.** Embryos (1-2 hpf) were exposed to 1, 10, 50, 100, or 200 mg/L of a) vnTiO<sub>2</sub> (n = 7), vnCeO<sub>2</sub> (n = 8), b) vnZnO (n = 6), vnCAP (n = 8), c) vnFe<sub>2</sub>O<sub>3</sub> (n = 9) or dialyzed vnFe<sub>2</sub>O<sub>3</sub> (n = 7) for 72 h. Each n represents 6-well plate replicate consisting of 180 embryos. Values are mean ± SEM (ANOVA, Dunnett's, *p* > 0.05).

To generate usable data for construction of LC50 curves, embryos were exposed to high concentrations that might be expected during environmental spills. The LC50 values generated for vnTiO<sub>2</sub> (> 2000 mg/L), vnZnO (1589.04 mg/L), vnCAP (1234.86 mg/L), vnFe<sub>2</sub>O<sub>3</sub> (> 2000 mg/L) and vnCeO<sub>2</sub> (>2000 mg/L) confirmed our prediction that acute toxicity will only occur at high NP concentrations that might be present in the environment (**Table S2-4**). Our findings agree with Chen et al. (2011) who calculated a LC50 value of 1323 ± 10.2 mg/L for medaka larvae exposed to a PAA stabilizer similar to the polymer used to coat the surfaces of the MeO NPs used in this study. The polymer-coated vnZnO were substantially less toxic than the uncoated ZnO NPs examined by Zhu et al. (2008) who calculated a 96 h LC50 value of 1.79 mg/L. Given this information, we suggest that the PAA coating reduced the toxicity of these NPs by minimizing the release of free metal.

#### **2.3.4 Sublethal effects on zebrafish**

Neither the NPs nor the free metal controls had a significant effect on 72 hpf larval body length (**Figure S2-7**) or hatching success (data not shown). Total hatching inhibition was observed but only in embryos exposed to ≥ 800 mg vnCAP/L (**Figure 2-5**). This was an unexpected result considering that each NP type was encapsulated by the same PAA coating. However, we noted that the pH of the vnCAP stock suspension was lower (3.0) than the pH of vnTiO<sub>2</sub> (7.0), vnZnO (8.9), vnFe<sub>2</sub>O<sub>3</sub> (9.6), and vnCeO<sub>2</sub> (8.9) stock suspensions (**Table S2-1**). Percent hatch was significantly inhibited by vnCAP (≥ 800 mg/L; ANOVA, *p* < 0.05) compared to the DTW control and pH-adjusted vnCAP (≥ 800 mg/L; t-test, *p* < 0.05) exposed

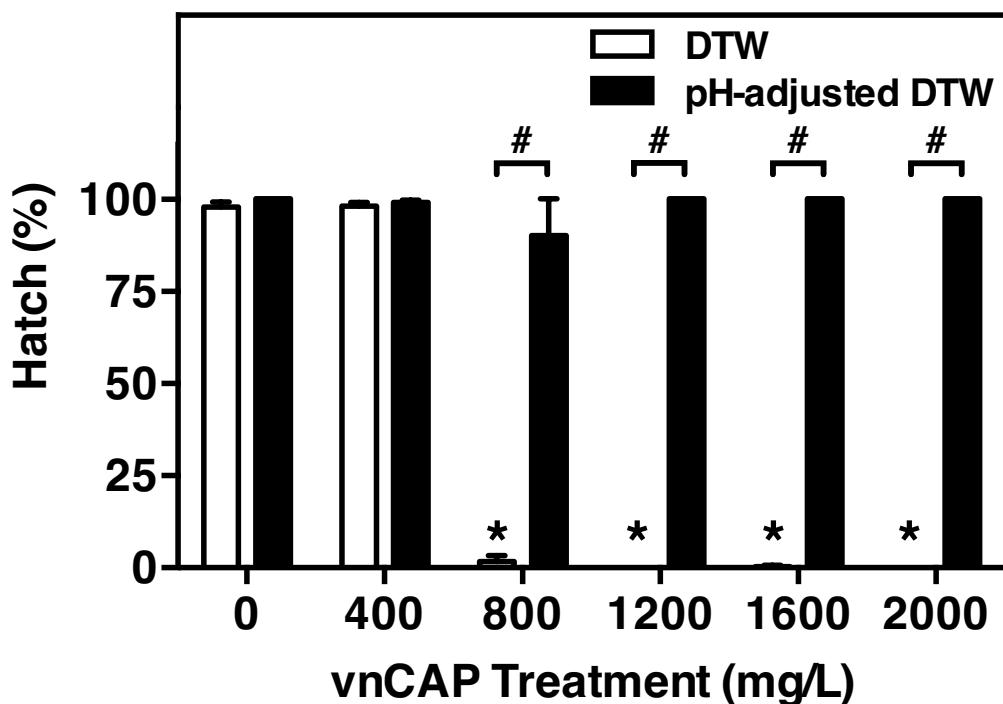


**Figure 2-5. Percent hatch of MeO NP exposed zebrafish.** Embryos were exposed to 400, 800, 1200, 1600, or 2000 mg vnCAP/L for 72 h. White bars represent vnCAP treatments prepared with DTW (pH ~ 4.0; n = 10). Black bars represent vnCAP treatments prepared with pH-adjusted DTW (pH ~7.5; n = 10). Each n represents a 6-well plate replicate consisting of 180 embryos. Values are mean  $\pm$  SEM. An asterisk (\*) represents significant difference compared to control (ANOVA, Dunnett's,  $p < 0.05$ ). A number sign (#) represents significant difference between treatment groups (t-test,  $p < 0.05$ ).

embryos (**Figure 2-5**). Importantly, embryos exposed to pH-adjusted DTW (4.0) did not show inhibition of hatch suggesting that pH was not the only contributing factor. The noted effects may also have been mediated via charge-charge interactions between vnCAP and the organism. DLS results showed that at pH 7.5, vnCAP (10,000 mg/L) were more negative (zeta potential: -36.3 mV) than at pH 4.0 (zeta potential: -20.1 mV). As the pH of the test suspension decreased, the net charge zeta potential of the polymer became less negative due to charge shielding by the H<sup>+</sup>. Tortiglione et al. (2009) found that NP uptake could be controlled by manipulating surface charge and that only positively charged NPs were internalized by hydra (*Hydra vulgaris*) under acidic conditions.

Recent literature also demonstrated that NPs bind to and alter enzyme function by changing the conformational structure of the protein (MacCormack et al., 2012). This may be a mechanism by which zebrafish hatch was impaired in our study. Prior to hatch, the embryo releases hatching enzymes that weaken the chorionic structure (Sano et al., 2008), and these enzymes have been compromised via nano-bio interactions (Bai et al., 2010; Ong et al., 2014b; Zhao et al., 2013a). However, hatching enzymes are secreted from glands located on the epidermis of the yolk sac (Kim et al., 2006); therefore, the NP must first traverse the chorion.

### **2.3.5 Nanoparticle interaction with zebrafish embryo**

We have investigated whether the chorion of a zebrafish embryo allows NPs to passively traverse its porous membrane or if it acts as a protective barrier to limit interaction between the NP surface and the animal. Lee et al. (2007) found Ag NPs

(5-46 nm) passively diffused into embryos via chorion pore canals. Some Ag NPs stayed in the chorion pore canals for 0.1 to 15 s while others got stuck, aggregated with incoming particles, and clogged the pores. Browning et al. (2009) reported similar results with Au NPs ( $11.6 \pm 0.9$  nm) and suggested that viscosity gradients exist between the chorion pore canals and the inner mass of embryos. Our findings indicate that  $37.79 \pm 2.65\%$  of the total  $\text{Ce}^{4+}$  (38.73 mg/L) was adsorbed to the chorion after 48 h (**Figure 2-6**) and  $0.07 \pm 0.01\%$  was associated with each animal, which suggested that  $\text{vnCeO}_2$  traversed the chorion.

To further test this hypothesis, we examined the presence or absence of vnCAP-NR fluorescence by laser scanning confocal microscopy (**Figure 2-7**). While there was no apparent autofluorescence in control embryos or fluorescence of embryos located beneath the cassette membrane (data not shown), vnCAP-NR labelled embryos showed staining on both the surface of the chorion and on the exterior of the animal (**Figure 2-7e**). Fluorescently labelled vnCAP were concentrated on the yolk sac; however, this is not apparent in the images due to the chosen plane of focus. We could not distinguish whether there was uptake across the external surface of the animal, but research is ongoing to investigate this further (see **Chapter 5**). Although NP-induced toxicity was not observed, our quantitative and qualitative data clearly show that specific NPs can traverse the chorion.

This study demonstrates the importance of characterizing the physicochemical properties of MeO NPs including polymer coating or other surface functionalization. Importantly, we measured the free metal present in both NP stock suspensions and the

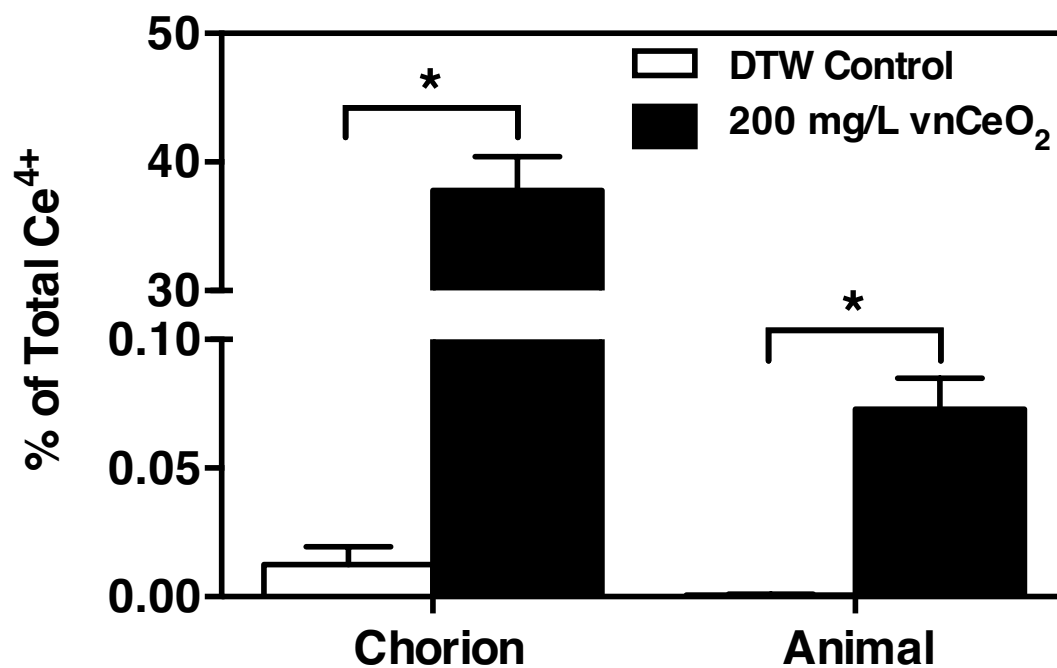


**Figure 2-6. Sorption of CeO<sub>2</sub> NPs to zebrafish embryos.** Total percent Ce<sup>4+</sup> adsorbed to the chorion (n = 6) and present sorbed to the animal (n = 6) following a 48 h exposure to 200 mg vnCeO<sub>2</sub>/L or DTW as paired control. Each n represents 10 randomly selected embryos. Note that the concentration of Ce<sup>4+</sup> in control embryos was below the ICP-MS detection limit (0.03 µg/L). Values are mean ± SEM. An asterisk (\*) represents significant difference in treatment compared to controls (ANOVA, Dunnett's, *p* < 0.05).

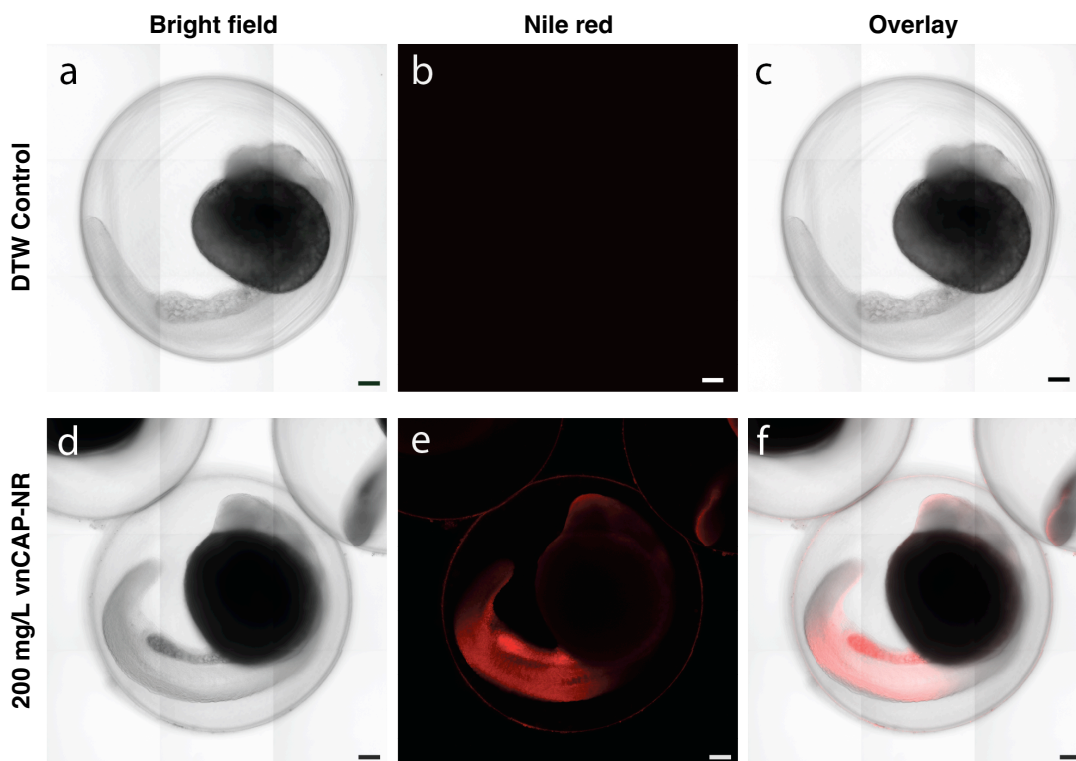


**Figure 2-7. Sorption of vnCAP-NR to zebrafish embryos.** (a, d) Bright field, (b, e) vnCAP-NR fluorescence ( $\lambda = 561 \text{ nm}$ ), and (c, f) overlay laser scanning confocal micrographs of 24 hpf zebrafish embryos exposed to DTW control (top) or 200 mg/L vnCAP-NR (bottom). Scale bars are 100  $\mu\text{m}$ .

metal released from the NPs to ensure an accurate understanding of the test conditions. We observed no apparent toxicity of these NPs on zebrafish development, partially due to the embryonic chorion and/or the NP core–polymer shell structure. However, laboratory conditions do not fully represent the complex variables present in aquatic ecosystems. Therefore, it is important to investigate these NPs under environmentally realistic conditions and with different animal species to develop sensitivity distributions at multiple levels of biological organization including physiological, cellular, and molecular. It is also important to determine the long-term effects of low concentrations of these NPs since their physicochemical characteristics and toxic properties may change as the NPs age or degrade in the environment (Handy et al., 2008b). This research has directly contributed to the ongoing hazard assessment of NPs, which is necessary to improve standards for nanotoxicity testing and to establish environmental safety and regulatory guidelines.

## CHAPTER 3

### **Physicochemical properties of functionalized carbon-based nanomaterials and their toxicity to fishes**

Felix, L.C., Ede, J.D., Snell, D.A., Oliveira, T.M., Martinez-Rubi, Y., Simard, B., Luong, J.H.T., Goss, G.G., 2016. Physicochemical properties of functionalized carbon-based nanomaterials and their toxicity to fishes. *Carbon* 104, 78–89. doi: 10.1016/j.carbon.2016.03.041.

### 3.1 INTRODUCTION

Nanotechnology is used in many applications from imaging and targeted drug delivery for the detection and treatment of diseases (Thakare et al., 2015) to strong and lightweight composite materials (Sur, 2012). Of the 1827 nanotechnology-based consumer products currently available on the market, 43 products were identified to contain either carbon nanotubes (CNTs) or cellulose nanomaterials (NMs) (Vance et al., 2015). The median worldwide production and use of CNTs was estimated to be 300 tons/year (Piccinno et al., 2012) while the volume of cellulose NMs produced in the USA is projected to reach several million metric tons annually (Cowie et al., 2014).

The increasing usage of CNTs will lead to their inevitable release into the environment, either from manufacturing facilities or through disposal and aging of consumer products (Nowack et al., 2013). Gottschalk et al. (2009) predicted that  $1 \times 10^{-9}$  mg/L CNTs will be present in USA surface waters while Mueller and Nowack (2008) made a similar estimate ( $5 \times 10^{-7}$  mg/L) for water in Switzerland. Due to their unique physical and chemical properties, single-walled carbon nanotubes (SWCNTs) have been proposed for use in a variety of applications including nanoelectronic devices, drug delivery vehicles, and biosensors (Liang and Chen, 2010; Smart et al., 2006). Characteristics such as high tensile strength, thermal stability and aspect ratio make SWCNTs an excellent reinforcing material for polymeric composites (Spitalsky et al., 2010). However, SWCNTs are also non-biodegradable and poorly dispersible in most organic and inorganic solvents (Vardharajula et al., 2012), and the presence

of metal impurities may confound toxicity evaluations (Isobe et al., 2006). Furthermore, the toxic effects observed could be attributed to the SWCNTs themselves, to the trace metal contaminants (Colvin, 2003), or to some combination of both (Ge et al., 2012).

Cellulose nanocrystals (CNCs) are produced from a myriad of renewable resources such as higher plants (trees), animals, and bacteria (Habibi et al., 2010). Their projected low cost (Habibi et al., 2010) has prompted the pilot production of CNCs in Canada and the USA (Boluk and Danumah, 2014) for use in a variety of products and applications. Biodegradable and absorbent properties make CNCs a suitable candidate for a variety of applications including plastic packaging, disposal diapers, and other environmentally friendly polymer composites (Cowie et al., 2014). CNCs are one of the most sought-after materials for enzyme immobilization (Mahmoud et al., 2009) and tissue engineering applications due to their hydrophilicity, mechanical strength, and ease of chemical modification (Eichhorn et al., 2010).

The SWCNTs and CNCs tested in this study have similar architectures and are primarily carbon based, but have distinctly different surface functionalities. We investigated the toxicological consequences of carboxylic acid functionalization on SWCNTs as this surface modification is increasingly being utilized to tune the hydrophobicity or hydrophilicity of NMs (Leung et al., 2011) and facilitate covalent binding of target biomolecules (Male et al., 2012) or provide active sites for enzyme immobilization (Mahmoud et al., 2009). Non-covalently wrapping lignin around the surface of CNTs can reduce the van der Waals interactions between the individual

tubes (Star et al., 2001) and minimize aggregation. Lignin is a waste byproduct of pulp and paper manufacturing (Garcia-Valls and Hatton, 2003). We examined the potential toxicity of lignin-wrapped SWCNTs as proposed use of this phenolic polymer as a surfactant will be to reduce waste while simultaneously generating increased revenue for the industry (Garcia-Valls and Hatton, 2003). Since functionalized NMs are expected to widen the range of products and applications, it is important to determine whether or not surface functionality plays a role in NM toxicity by evaluating effects on fish health at multiple levels of biological organization.

Zebrafish (*Danio rerio*) embryos are one of the most common *in vivo* model systems for high-throughput toxicity screening of chemicals because of their small size, rapid development, high fecundity (Hill et al., 2005), and sequenced genome with considerable homology to humans (Howe et al., 2013). Channel catfish (*Ictalurus punctatus*) are increasingly being utilized in cell-based toxicological evaluations, as they are one of the few economically important teleost species with viable *in vitro* culture systems (Bengtén et al., 2006). The availability of several cell lines allows us to examine *in vitro* the effect of NM exposure on teleost cells and provide a more comprehensive evaluation of NM toxicity (Zhao et al., 2013a).

We have examined the physicochemical properties of SWCNTs with three degrees of carboxylic acid functionalization, two types of lignin-wrapped SWCNTs, as well as nonfunctionalized SWCNTs. We have investigated the potential toxicological effects of these NMs during early stages of zebrafish development by measuring survival, hatching success, and alteration in gene expression. We have also

characterized carboxylated CNCs and assessed their effects both *in vivo* using zebrafish and *in vitro* using three channel catfish cell lines.

## **3.2 EXPERIMENTAL**

### **3.2.1 Nanomaterial production and functionalization**

The National Research Council of Canada (NRC) manufactured the NMs tested in this study including the priority Organisation for Economic Co-operation and Development (OECD) material: SWCNTs and chemically modified SWCNTs (OECD, 2010). Details regarding SWCNT production can be found elsewhere (Kim et al., 2007; 2009). Briefly, nonfunctionalized SWCNTs (NF-SWCNTs) were produced by evaporation of carbon black (Elftex-12, Cabot Co.) and bimetallic catalyst (Ni-Y<sub>2</sub>O<sub>3</sub> / 2-0.5 mole %) mixtures using induction thermal plasma technology. NF-SWCNTs were oxidized with a mixture of HNO<sub>3</sub> and H<sub>2</sub>SO<sub>4</sub> for 2 h at 30 °C (COOH-30-SWCNTs), 40 °C (COOH-40-SWCNTs), or 50 °C (COOH-50-SWCNTs), yielding ultra-short bundles with mostly carboxylic acid groups and some hydroxyl and carbonyl groups covalently bound to their sidewalls (**Figure S3-1**); the number and position of these groups is determined by oxidation time and temperature (Yu et al., 2008). Carboxylic acids typically have a pKa value of  $\sim 4 \pm 0.5$  and these surface functionalities become ionized and exist primarily as carboxylate anions (-COO<sup>-</sup>) in near-neutral water (pH 7) (Maag, 2007). NF-SWCNTs were also non-covalently wrapped with sodium lignin sulfonate (SLS-SWCNTs) or with

ammonium lignin sulfonate (ALS-SWCNTs) by direct mixing (1:2, SWCNTs: lignin). SLS and ALS solutions were used as controls.

Details regarding CNC production have been published elsewhere (Leung et al., 2011). Briefly, highly crystalline carboxylated CNCs (COO<sup>-</sup>-CNCs) were produced by ammonium persulfate (APS) treatment of microcrystalline cellulose (MCC; Avicel PH-101, 50  $\mu\text{m}$  particles). To yield high-quality CNCs, a mixture of APS and MCC was heated, repeatedly centrifuged (12,000 revolutions per minute [rpm]; 22,100 relative centrifugal force; 10 min), washed with deionized water and lyophilized. The material was neutralized to pH 7 (with NaOH) before lyophilization, thereby converting carboxylic acid groups to their carboxylate form, making the dispersion of 0.1 g powder in 100 mL double-distilled water (ddH<sub>2</sub>O) easier. All stock suspensions were stored in the dark at room temperature.

### **3.2.2 Preparation of nanomaterial test suspensions**

SWCNT and CNC stock suspensions were stirred at 600 rpm for 30 min, placed in a sonication bath (50 / 60 Hz, 117 V, 1 A, Branson 2200, Branson Ultrasonics Corporation, CT, USA) for 5 min and then serially diluted to 1, 10, 50, 100 or 200 mg/L with filtered (0.45  $\mu\text{m}$  pore size, cellulose acetate membrane bottle-top filter, Corning) and autoclaved dechlorinated tap water (DTW; pH: 7.4, conductivity:  $168.5 \pm 0.5$   $\mu\text{S}/\text{cm}$ , temperature:  $28.5 \pm 1$   $^{\circ}\text{C}$ , dissolved oxygen:  $7.5 \pm 0.5$  mg/L, general hardness: 175 mg/L as CaCO<sub>3</sub>, salinity: 0 ppt) without dispersants. Test suspensions were sonicated on ice for  $3 \times 20$  s with a 20 s pause in between, to reduce the likelihood of mechanically-induced damage (Lu et al., 1996), using a

Sonifier Cell Disrupter model SLPe probe sonicator (150 W, 50% amplitude, Branson Ultrasonics Corporation, CT, USA) and then mixed by vortex (Fisher Vortex Genie 2, Fisher Scientific) for 20 s to ensure a homogeneous dispersion of materials immediately before aliquoting the samples for further analyses.

### **3.2.3 Physicochemical characterization of nanomaterials**

Sizes of NF-SWCNT bundles were analyzed by field emission transmission electron microscopy (FETEM; JEOL JEM-2100F). Low voltage TEM (LVTEM) images of COO<sup>-</sup>-CNCs were obtained using the procedure described by Leung et al. (2011). We used dynamic light scattering (DLS; Zetasizer Nano Series, Malvern Instruments Ltd.) in 173° backscatter mode (Zetasizer software, v. 7.01) to characterize the size and charge of NM agglomerates in 10 and 50 mg/L test suspensions at 28.5 °C. Mean z-average hydrodynamic diameter, polydispersity index and zeta ( $\zeta$ ) potential were measured by DLS at 0, 24, 48 and 72 h, and pH was measured with an electrode connected to a pH meter (Accumet Basic, AB15, Fisher Scientific) at 0 h. Air bubbles were moved from the electrodes of the universal dip cell (ZEN1002) to avoid interference with  $\zeta$  potential measurements. All samples remained static and were covered with Parafilm between daily measurements.

To measure the dispersion of CNTs in water, each 1000 mg/L oxidized SWCNT stock suspension (COOH-30-SWCNTs, COOH-40-SWCNTs, and COOH-50-SWCNTs) remained static for three weeks; the suspensions were collected (i.e. separated from any sediment on the bottom of the flask) and were subsequently filtered (0.2  $\mu$ m pore size, polycarbonate membrane filter, Sterlitech) to determine the

fraction still in suspension. After filtration, the solid residue was recovered, dried at 150 °C for 24 h in a vacuum oven, and weighed using an analytical balance (AX205 Mettler Toledo, readability 0.1 mg).

To determine the maximum concentration of trace metal contaminants present in our exposure suspensions, DTW and 200 mg/L NF-SWCNT, SLS-SWCNT, and SLS test suspensions were filtered (0.22 µm pore size, mixed cellulose esters membrane Millex-GS Syringe Filter Unit, EMD Millipore), acidified with two drops of concentrated HNO<sub>3</sub> (70%, ACS reagent grade, Sigma-Aldrich) and kept in the dark at room temperature until analysis with inductively coupled plasma mass spectrometry (ICP-MS; Thermo-Finnigan iCAP Qc, California, USA). Certified reference material (SLRS-5; NRC, Ottawa, CA) for each element was measured multiple times alongside each sample. Metal concentrations were the average of three runs and measured against calibration standard solutions (Spex CertiPrep, New Jersey, USA). A flame atomic absorption spectrometer (FAAS; SpectrAA 880, Varian Australia Pty Ltd., Victoria, AUS) was used to measure Na concentration in 200 mg/L SLS. Samples were compared to known external reference (Ultra Scientific QC1-702, Rhode Island, USA) and calibration (SCP Science, Quebec, CA) standards.

To determine if the filter (0.22 µm pore size, mixed cellulose esters membrane Millex-GS Syringe Filter Unit, EMD Millipore) effectively removed SWCNTs from the sample, we used an Ultrospec 3000 UV/Visible spectrophotometer. Spectral scans (200-800 nm) of 50 mg/L NF-SWCNTs and SLS-SWCNTs gave the expected profiles for CNTs (**Figure S3-2ab**); however, we were unable to identify a distinct peak (i.e. the wavelength of maximum absorbance) due to the limited absorbance

range (-3.00-3.00 a.u.) of the spectrophotometer. Smith et al. (2007) found a distinct peak at 260 nm for SWCNTs in sodium dodecyl sulfate; therefore, percent transmittance of 0.005, 0.05, 0.5, 5 and 50 mg/L NF-SWCNTs and SLS-SWCNTs were measured at this particular wavelength (**Figure S3-2cd**).

Lastly, we determined the concentration of ammonia ( $\text{NH}_4^+/\text{NH}_3$ ) present in 5 mg/L filtered ALS-SWCNTs using the salicylate method (Verdouw et al., 1978). Briefly, 40  $\mu\text{L}$  sodium salicylate (50%; Sigma-Aldrich), sodium nitroprusside dihydrate (0.02%; Sigma-Aldrich) and equal parts fresh 7.4% sodium hypochlorite and tri-sodium citrate dihydrate (EMD Millipore) in 0.1 N NaOH (BDH) were added to each well of a clear, flat-bottom 96-well microtest plate (Sarstedt, Nümbrecht, Germany) containing 160  $\mu\text{L}$  of samples or standards. Ammonium chloride ( $\text{NH}_4\text{Cl}$ ; Fisher Scientific) standards (0, 20, 40, 60, 80 and 100  $\mu\text{M}$ ) were spiked with 5 mg/L filtered SLS-SWCNTs to control for nanotube absorbance. The plate was incubated in the dark at room temperature for 1 h and absorbance was read at 525 nm using a VERSAmax tunable microplate reader equipped with SoftMax Pro 5.2 software (Molecular Devices, Sunnyvale, CA, USA).

#### **3.2.4 Zebrafish holding facility and collection of viable embryos**

Adult zebrafish (wild type strain AB or AB/TB) aged 6 to 18 months were housed in 30 L tanks filled with DTW (pH: 7.4, conductivity: 1260  $\mu\text{S}/\text{cm}$ , temperature:  $28.5 \pm 1$  °C, dissolved oxygen: 6.9 mg/L, general hardness: 100 mg/L as  $\text{CaCO}_3$ , salinity: 0.6 ppt) treated by a RiOs 100 water purification system held in the Biological Sciences Building at the University of Alberta. One male and two female

zebrafish were placed in a hatching box and acclimated overnight. Fertilized embryos were collected the next day after spawning was triggered by the start of the light cycle (14 h light: 10 h dark photoperiod).

### **3.2.5 Cell culture**

Channel catfish B-cell lines, 3B11 and 1G8, and T-cell line, 28S.3, were cultured in filter sterilized (0.22  $\mu\text{m}$  pore size, cellulose acetate membrane bottle-top filter, Corning) AL media (1:1, AIM V medium: L-15 medium, Gibco) containing 3% catfish serum, 0.5 g sodium bicarbonate (Sigma), 0.05 M 2-mercaptoethanol, 100 units/mL penicillin (Gibco), and 100  $\mu\text{g}/\text{mL}$  streptomycin (Gibco) at 27 °C and 5%  $\text{CO}_2$  in 25  $\text{cm}^2$  cell culture flasks (Corning). Cells were grown for 3-5 days or until  $\geq 80\%$  confluence was reached before being passed into a new flask.

### **3.2.6 Whole-animal effects of nanomaterial exposure to zebrafish**

Acute (72 h) toxicity assays were conducted in accordance with an OECD guideline (OECD, 2012c) optimized by our research group for testing NMs (Felix et al., 2013). Viable embryos (1-2 hours post fertilization, hpf) were combined, rinsed thrice with DTW, and then randomly distributed into six-well plates (Sarstedt, Nümbrecht, Germany; 30 embryos/well). Embryos were exposed to varying concentrations (1, 10, 50, 100 or 200 mg/L) of nine different treatments (NF-SWCNTs, COOH-30-SWCNTs, COOH-40-SWCNTs, COOH-50-SWCNTs,  $\text{COO}^-$ -CNCs, SLS-SWCNTs, SLS, ALS-SWCNTs, or ALS), as well as a paired

DTW control. Embryos were also exposed to filtered NF-SWCNT test suspensions, and to varying concentrations (0.10, 1.02, 5.10, 10.02 or 20.40 mg/L) of  $\text{NH}_4\text{Cl}$ , which served as trace metal and  $\text{NH}_4^+/\text{NH}_3$  controls, respectively. Six-well plates containing exposed zebrafish were incubated at  $28.5 \pm 1$  °C for 72 h.

Survival and hatching success of zebrafish were recorded at 24, 48, 52, 56 and 72 hpf. Zebrafish were considered dead and removed from each well if they lacked movement, a heartbeat, and transparent tissues (Ali et al., 2011). Only plates with  $\geq 80\%$  survival in the DTW control well were analyzed. Adsorption of 1, 10 and 50 mg/L NF-SWCNTs to the chorion of 24 and 48 hpf embryos and to the 72 hpf larvae was imaged using a dissecting microscope (Zeiss Axio Observer A1) connected to a camera (AxioVs40 software, v. 4.7.2). Each experiment was performed on groups of 30 embryos and repeated at least 7 times.

### **3.2.7 Cellular effects of nanomaterial exposure to channel catfish cells**

Channel catfish 3B11, 1G8, and 28S.3 cells were counted and seeded into a 96-well round-bottom plate (Becton Dickinson) at a density of 20,000 cells/well in AL3 culture media. Cells were exposed to 1, 10, 50, 100 or 200 mg/L  $\text{COO}^-$ -CNCs for 6, 12, 24 or 48 h at 27 °C and 5%  $\text{CO}_2$ . Cell viability was analyzed by flow cytometry (Beckman Coulter Cell Lab Quanta SC flow cytometer, Cell Lab Quanta SC MPL Analysis software, v. 1.0). Following  $\text{COO}^-$ -CNC exposure, cells were stained with propidium iodide (PI, 100  $\mu\text{g}/\text{mL}$ ) and populations of 3B11, 1G8, or 28S.3 cells were gated and the FL2 filter was utilized to measure PI staining to separate viable from non-viable cells. Since PI is membrane impermeant, this

fluorescent dye was used to detect necrotic cells in CNC-treated populations. The percentage of viable cells in culture was calculated from the number of cells within the whole population gate that concurrently exhibited low levels of PI fluorescence. The experiment was replicated 4 times.

### **3.2.8 Molecular effects of nanomaterial exposure to zebrafish**

Immediately following exposure to 100 or 200 mg/L NF-SWCNTs, COOH-50-SWCNTs, SLS-SWCNTs, or COO<sup>-</sup>-CNCs, five 72 hpf larvae for each treatment were randomly selected and washed twice with ddH<sub>2</sub>O. Total RNA was isolated from whole larvae using the MasterPure RNA Purification Kit (Epicentre Biotechnologies; MCR85102). Briefly, recombinant DNase I (Ambion) and 10X Reaction Buffer with MgCl<sub>2</sub> (ThermoFisher Scientific) were added to each sample immediately prior to a 30 min incubation period at 37 °C. The reaction was terminated with 50 mM ethylenediaminetetraacetic acid and samples were stored in nuclease-free water (non-DEPC treated, Ambion) containing SUPERase-In RNase Inhibitor at 4 °C overnight. RNA purity was measured using a NanoDrop spectrophotometer (ND-1000, v. 3.8.1) and then first strand cDNA was made from select samples (260/280 and 260/230 ratios ~ 2 ± 0.2 a.u.; > 200 ng/mL) using the RevertAid First Strand cDNA Synthesis Kit (Thermo Scientific; K1622). This experiment was performed on groups of 5 fish and repeated 4 times.

Gene-specific primers (Integrated DNA Technologies, Iowa, USA) for zebrafish *elongation factor 1 alpha (ef1a)*, *hypoxia-inducible factor 1 alpha subunit b (hif1ab)*, *alpha-tocopherol transport protein ( $\alpha$ -ttp)*, *glutamate-cysteine ligase*

*catalytic subunit (gclc)*, and *heat shock protein 70 kDa (hsp70)* were designed using National Center for Biotechnology Information (NCBI) Primer-BLAST software and specificity validated using BLAST. See section 3.3.4 for further discussion of selected genes. Genes of interest (*hif1ab*,  *$\alpha$ -ttp*, *gclc*, and *hsp70*) were normalized to *ef1a* and measured using quantitative polymerase chain reaction (qPCR; SDS v. 1.4, Applied Biosystems 7500 Fast Real-Time PCR System) in combination with the double stranded DNA-specific dye SYBR Green I (Molecular Biology Service Unit, University of Alberta). Prior to qPCR, all primer sets were screened using polymerase chain reaction and agarose gel electrophoresis (**Figure S3-3**). Relative quantification of the expression level of each transcript in each sample was calculated using the  $2^{-\Delta\Delta C_t}$  method (Livak and Schmittgen, 2001). Reaction conditions were as follows: 95 °C for 2 min (annealing) followed by 40 cycles of 95 °C for 15 s and 60 °C for 1 min (elongation), and a denaturation stage of 95 °C for 15 s, 60 °C for 1 min, 95 °C for 15 s, and 60 °C for 15 s. Information on the primers is listed in **Table S3-1**.

### **3.2.9 Statistical analysis**

Prism 6 for Mac OS X (v. 6.0h; GraphPad Software Inc.) was used for graphing and statistical analyses. An unpaired Student's t-test and one-way analysis of variance (ANOVA) with a Dunnett's post hoc test or with a Tukey's multiple comparisons test were used as indicated. Data are presented as mean  $\pm$  standard error of the mean (SEM). The fiducial level of significance was set at  $p < 0.05$ .

### 3.3 RESULTS AND DISCUSSION

#### 3.3.1 Physicochemical characteristics of functionalized nanomaterials

Interactions between NMs and biological systems are modulated by size, shape, charge, and surface functionality; therefore, comprehensive examination of these physicochemical properties is essential as they have implications for toxicity (Verma and Stellacci, 2010). Internalization of NMs into cells, for example, largely depends on NM size and aspect ratio where toxicity can be attributed to their ability to interact with or enter biological systems (Ede et al., 2015; Shang et al., 2014). Kostarelos et al. (2007) demonstrated that functionalized multi-walled carbon nanotubes and SWCNTs ( $\leq 20$  mg/L) can pass through the plasma membrane and enter the cytoplasm of a variety of mammalian and prokaryotic cells. FETEM images suggest that the diameter of the cylindrical-shaped NF-SWCNT bundles ranged between 10 and 20 nm (**Figure S3-4a**). Most bundles extended a couple of micrometers in length; however, amorphous carbon particles entangled with the well-ordered SWCNT bundles hindered our ability to measure exact length. LVTEM images indicated that the average cross-section dimensions of the dried, rod-like COO<sup>-</sup>-CNCs were  $128 \pm 38$  nm by  $5.5 \pm 1.5$  nm (**Figure S3-4b**) and the particles were uniform in size with amorphous cellulose segments removed.

Most NMs including CNTs form agglomerates in water (Murdock et al., 2008) and require energy or dispersants to break them apart (Kühnel and Nickel, 2014). Mean hydrodynamic diameters of oxidized SWCNTs (10 and 50 mg/L) at 0 h suggest that the length of the bundles became shorter with increasing oxidative

temperature (**Figure 3-1a, b**). Similarly, Price et al. (2009) demonstrated that SWCNTs oxidized at 65 °C were shorter and more water-dispersible due to increased carboxylic acid group functionalization compared to those oxidized at 30 °C. Thus, these properties can be tuned by changing the reaction temperature. Oxidized SWCNT agglomerates ranged between  $2458.00 \pm 62.18$  nm and  $10,165.00 \pm 2287.78$  nm while SLS-SWCNT and ALS-SWCNT bundles were  $\leq 323.23 \pm 2.60$  nm in size over 72 h. CNCs are dispersible in water and form stable colloidal suspensions (Boluk and Danumah, 2014). Hydrodynamic diameter profiles for  $\text{COO}^-$ -CNCs suggest that the test suspensions were stable over time. Size distribution profiles for all NM suspensions tested indicate midrange (0.08-0.70) or high ( $> 0.70$ ) polydispersity (**Figure 3-1c, d**). Though NM size strongly influences cellular uptake, intracellular localization and cytotoxicity, surface functionality affects other important NM characteristics including colloidal stability and dispersibility with implications for NM toxicity (Shang et al., 2014; Verma and Stellacci, 2010).

All NMs used in this study were negatively charged at near neutral pH (7.29-7.43; **Figure 3-1e, f**). Positively charged NMs have a high affinity for negatively charged cell membranes due to electrostatic interaction (Honary and Zahir, 2013). Conversely, negatively charged NMs adsorb at the cationic binding sites on the cell surface and form clusters because of their repulsive interactions with the negatively charged membrane (Honary and Zahir, 2013). The  $\zeta$  potentials of our oxidized SWCNTs and  $\text{COO}^-$ -CNCs fell between  $-8.39 \pm 0.61$  mV and  $-16.87 \pm 0.22$  mV. The negative  $\zeta$  potential of CNCs creates repulsive Coulombic interactions between the rod-like particles and reduces agglomeration (Roman, 2015). Chen and

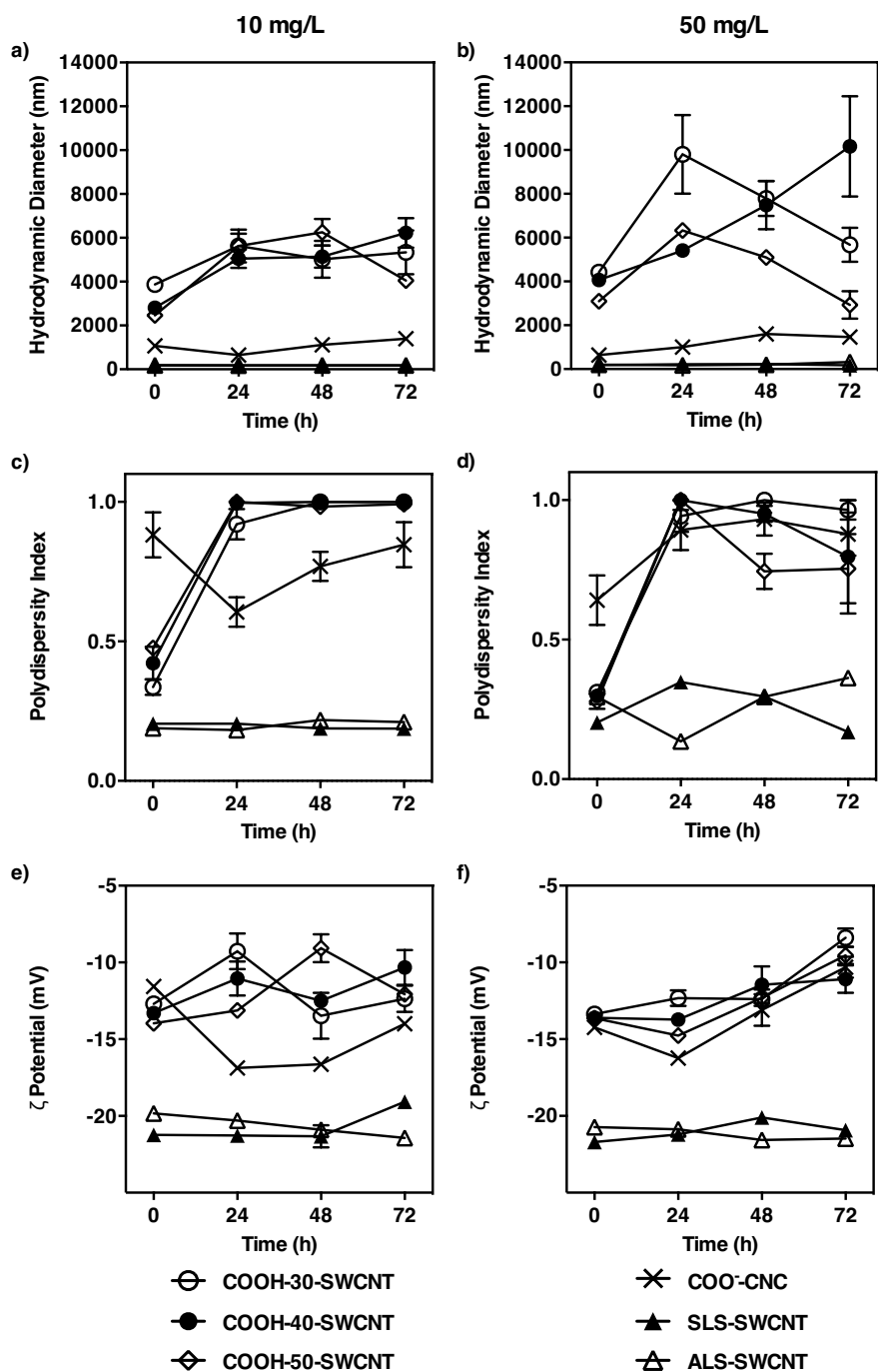


**Figure 3-1. Physicochemical properties of functionalized SWCNT and CNC test suspensions over time.** Time-dependent changes in mean (a, b) hydrodynamic diameter (nm), (c, d) polydispersity index, and (e, f)  $\zeta$  potential (mV) of 10 and 50 mg/L COOH-30-SWCNT (pH 7.43), COOH-40-SWCNT (pH 7.41), COOH-50-SWCNT (pH 7.29), COO<sup>-</sup>-CNC (pH 7.41), SLS-SWCNT (pH 7.41), and ALS-SWCNT (pH 7.40) test suspensions in DTW (pH 7.40) at 0, 24, 48 and 72 h. Sample values are the average of three replicates and are presented as mean  $\pm$  SEM.

Jafvert (2010) reported a  $\zeta$  potential of -52.00 mV for 10 mg/L carboxylated SWCNTs suspended in water (pH 6.56) and Kovacs et al. (2010) reported a  $\zeta$  potential of -32.60 mV for 1000 mg/L CNCs also suspended in water (pH 7.30). The  $\zeta$  potentials of SLS-SWCNTs and ALS-SWCNTs ranged between  $-21.70 \pm 0.17$  mV and  $-19.07 \pm 0.22$  mV, in agreement with White et al. (2007) who measured a  $\zeta$  potential of -23.60 mV for surfactant-wrapped SWCNTs. Measurements of 1 mg/L NM test suspensions were highly variable and considered below DLS detection limits (data not shown). Characterization of  $\geq 100$  mg/L oxidized SWCNTs and COO<sup>-</sup>-CNCs in ddH<sub>2</sub>O at 0 h have been reported elsewhere (Ede, 2015). Reproducible DLS measurements of COOH-30-SWCNTs, COOH-40-SWCNTs, COOH-50-SWCNTs, COO<sup>-</sup>-CNCs, SLS-SWCNTs, and ALS-SWCNTs in AL3 media were not possible. Cell culture medium typically contains biomolecules and small molecules including proteins, antibodies, salts/ions, vitamins, and lipids that scatter light and interact with NMs, leading to an inaccurate characterization of NMs in suspension (Baolog et al., 2015).

Though NF-SWCNT test suspensions were not characterized by DLS due to their poor dispersibility in water (Rai et al., 2007), a significant improvement in these properties is achieved after functionalization. In agreement with Price et al. (2009), the dispersibility of COOH-30-SWCNT, COOH-40-SWCNT, and COOH-50-SWCNT stock suspensions was 677, 591, and 800 mg/L, respectively. Poor dispersibility stems from the hydrophobic nature of the graphitic sidewalls, coupled with strong van der Waals interactions between tubes causing them to form aggregate bundles (Cirillo et al., 2014).

As-produced SWCNT stock suspensions typically contain impurities such as graphitic debris, catalyst particles, and amorphous carbon (Liang and Chen, 2010), as well as metal released from dispersed and settled CNTs (Petersen et al., 2015). A dilution prepared from a well-dispersed stock suspension to achieve the desired concentration would have a different CNT:metal-ion ratio than a separate stock suspension made at the same concentration (Petersen et al., 2015). Filtered NF-SWCNT, SLS-SWCNT, and SLS test suspensions contained a variety of trace metals, as expected (**Figure 3-2**). Interestingly, most of the metals detected in 200 mg/L SLS-SWCNT samples were present at concentrations significantly higher than those detected in NF-SWCNTs, SLS, and the DTW control, as indicated by the different letters. We suspect that SLS acted as a chelating agent of the metals present in the samples (Garcia-Valls and Hatton, 2003). All metals detected in DTW, except Na, were present at concentrations  $< 0.10$  mg/L. There was more Na present in SLS-SWCNTs ( $44.25 \pm 0.22$  mg/L) compared to SLS ( $23.89 \pm 0.11$  mg/L; **Figure 3-2a**), likely due to batch reproducibility or carry-over from sample preparation. The transition metals, Ni and Y, were added directly to function as catalysts since they play a critical role in breaking down amorphous carbon to produce high-quality SWCNTs at large scales (Kim et al., 2007). Interestingly, concentrations of Ni and Y in SLS-SWCNTs were significantly higher compared to NF-SWCNTs, SLS, and DTW (**Figure 3-2b**). Other metals were detected at concentrations  $< 0.50$  mg/L and these included Cu, Fe, Ba, Mn, Cd, Cr, Rb, Co, Sb, Pb, and V (**Figure 3-2c-f**). These metals were likely introduced into the SLS-SWCNT samples during production processes including sonication, centrifugation, and

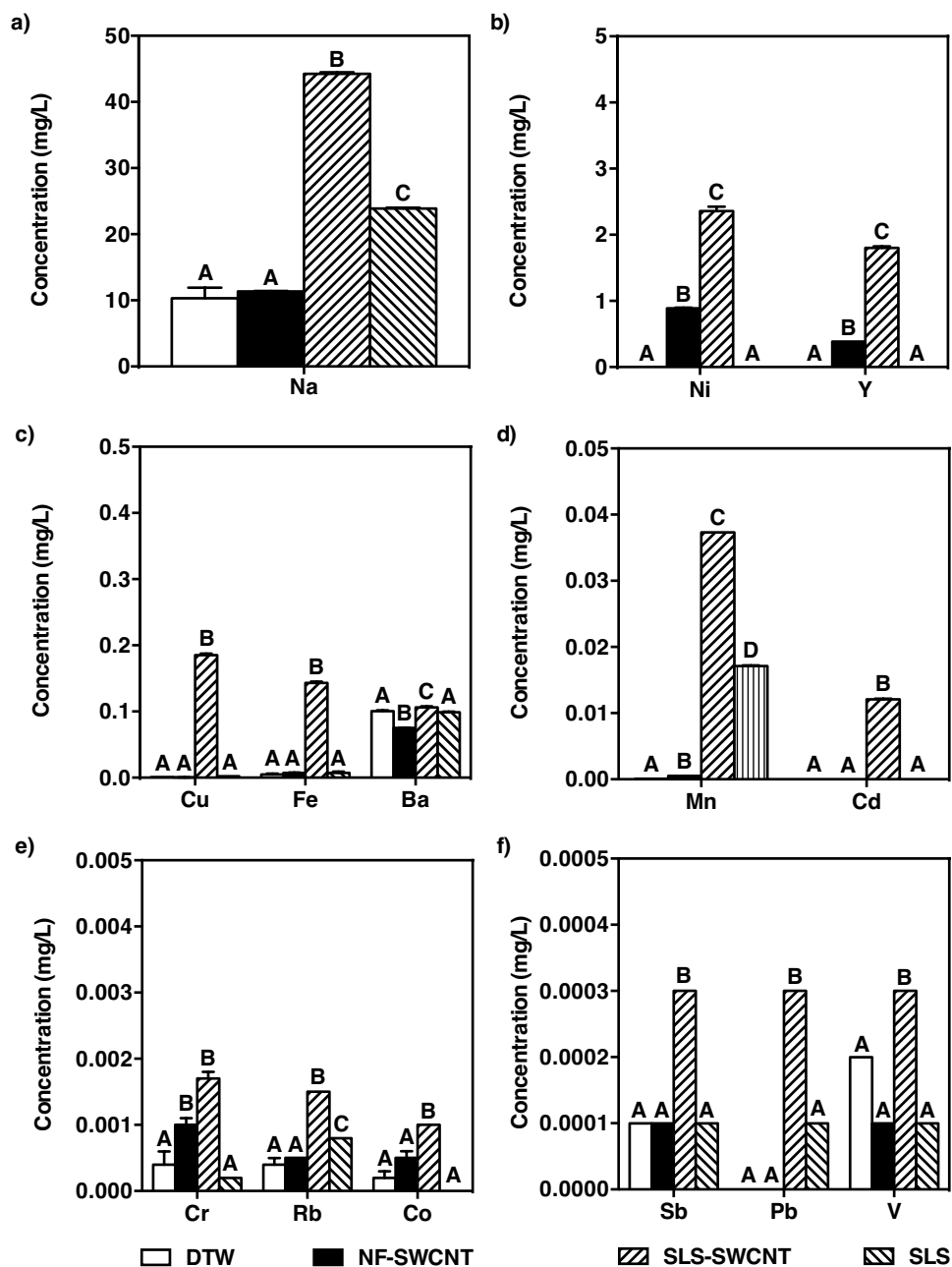


**Figure 3-2. Trace metals present SWCNT and SLS test suspensions.** NF-SWCNT, SLS-SWCNT, and SLS test suspensions were diluted to 200 mg/L with DTW, filtered and then acidified prior to ICP-MS or FAAS analyses. Trace metals detected included (a) Na, (b) Ni, Y, (c) Cu, Fe, Ba, (d) Mn, Cd, (e) Cr, Rb, Co, (f) Sb, Pb, and V. Most of the metals detected have several oxidation states; therefore, these notations have been omitted for clarity. Metal concentration (mg/L) indicated on the y-axis is 1/10<sup>th</sup> of the previous panel. Sample values are the average of three replicates and are presented as mean  $\pm$  SEM. Means with different letters are significantly different (ANOVA, Tukey's,  $p < 0.05$ ).

isolation, and were higher in the SLS-SWCNT preparations because lignin acts as a chelating agent, complexing with divalent transition metals (Garcia-Valls and Hatton, 2003). Total metals present in the NF-SWCNT filtrate served as trace metal controls and  $\text{NH}_4\text{Cl}$  was added to a separate set of controls to account for the contribution of  $\text{NH}_4^+/\text{NH}_3$  to any noted toxicity. These controls were performed for our whole-animal endpoints only. Filtering with a 0.22  $\mu\text{m}$  filter effectively removed the NF-SWCNTs from the sample (**Figure S3-2c**) while SLS-SWCNTs were not completely removed even after two passes through the 0.22  $\mu\text{m}$  filter (**Figure S3-2d**), suggesting that SLS-SWCNT test suspensions were more monodispersed compared to NF-SWCNTs. In neutral water (pH 7), ammonia predominantly exists as  $\text{NH}_4^+$  with a small proportion (1%) occurring as  $\text{NH}_3$ ; the latter form being toxic to fish (Eddy and Handy, 2012). When measured against a blank containing 5 mg/L filtered SLS-SWCNTs, 5 mg/L ALS-SWCNTs was found to contain  $0.51 \pm 0.03$  mg/L  $\text{NH}_4^+/\text{NH}_3$  (**Figure S3-5**). Therefore, 1, 10, 50, 100 and 200 mg/L ALS-SWCNT test suspensions were assumed to contain 0.10, 1.02, 5.10, 10.20 and 20.40 mg/L  $\text{NH}_4^+/\text{NH}_3$ , respectively. Overall, the above findings indicate that surface functionality affects the physicochemical properties of SWCNTs in suspension and predicts reduced aggregation. Decreased agglomerate size would increase surface area for interactions leading to an increase in adsorption of SWCNTs or free metal ions to biological membranes potentially causing deleterious effects (Nel et al., 2009).

### 3.3.2 Whole-animal effects

To investigate acute NM toxicity, embryos were exposed to higher concentrations than might normally be present in the environment. Acute toxicity based on 72 h lethal concentration 50 (LC50) values could not be determined for all materials because more than 50% of the population survived exposure to even the highest concentration tested (**Figure 3-3**). Cumulative 72 h survival of larvae exposed to  $\leq 200$  mg/L NF-SWCNTs, filtered NF-SWCNTs, oxidized SWCNTs, and COO<sup>-</sup>-CNCs was not significantly different from the DTW control (**Figure 3-3a, b**). While there were also no significant differences between NF-SWCNTs and filtered NF-SWCNTs or between SWCNTs oxidized at different temperatures, survival of zebrafish exposed to 100 mg/L COOH-50-SWCNTs ( $80.00 \pm 3.20\%$ ) was significantly lower compared to those exposed to the same concentration of NF-SWCNTs ( $92.12 \pm 1.92\%$ ; ANOVA, Tukey's,  $p < 0.05$ ). Kovacs et al. (2010) reported an LC50 value of  $> 6000$  mg/L for 120 hpf zebrafish larvae exposed to CNCs and our results support their findings. Interestingly, while 200 mg/L SLS-SWCNTs significantly decreased total survival to  $70.00 \pm 5.90\%$  and differed significantly from 200 mg/L NF-SWCNT and SLS exposures (ANOVA, Dunnett's, Tukey's,  $p < 0.05$ ), NF-SWCNTs, SLS, ALS-SWCNTs, ALS, and NH<sub>4</sub>Cl had no effect compared to the DTW control (**Figure 3-3c, d**; ANOVA, Dunnett's,  $p > 0.05$ ). This data suggests that the core NM, surface functionality, and trace metal impurities exhibited a combined effect.

Any alteration in the developmental processes of an organism will have serious negative consequences, especially in species that reach maturity quickly or in

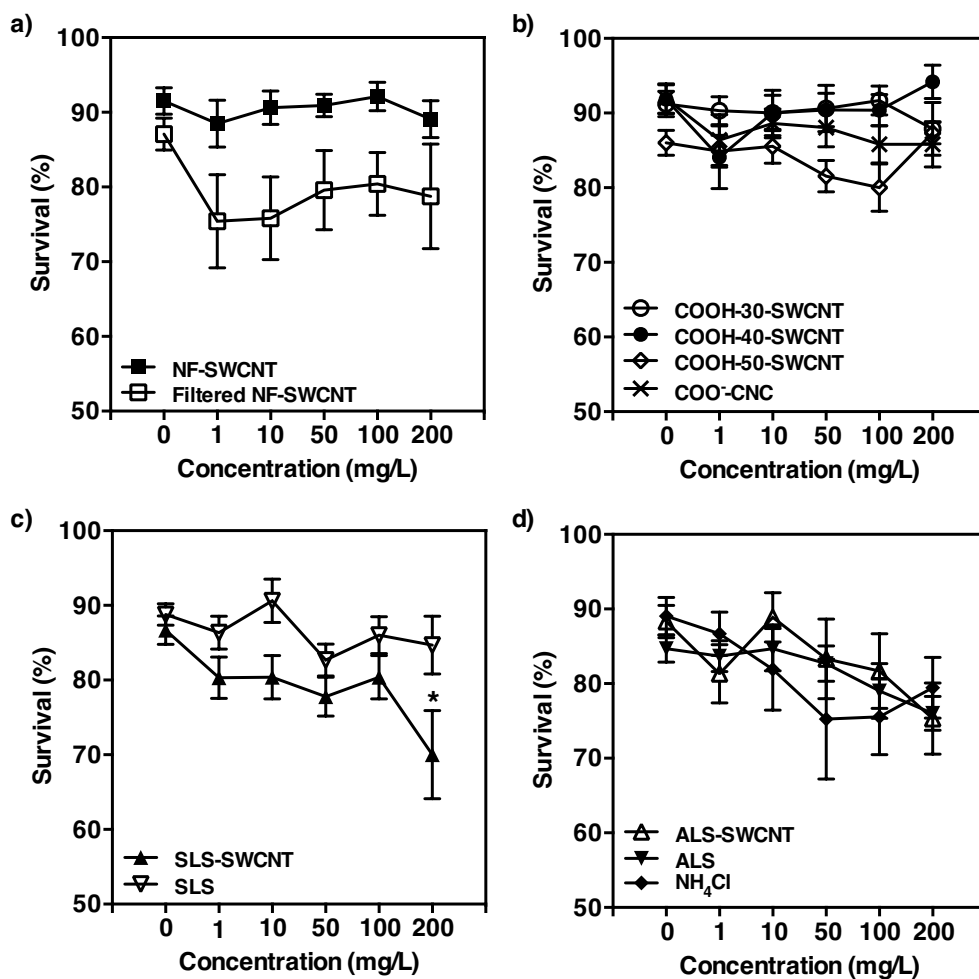


**Figure 3-3. Cumulative percent survival of zebrafish exposed to SWCNT and CNC test suspensions.** Zebrafish embryos were exposed to 0, 1, 10, 50, 100 or 200 mg/L (a) NF-SWCNT (n = 11), filtered NF-SWCNT (n = 8), (b) COOH-30-SWCNT (n = 11), COOH-40-SWCNT (n = 9), COOH-50-SWCNT (n = 15), COO<sup>-</sup>-CNC (n = 12), (c) SLS-SWCNT (n = 10), SLS (n = 11), (d) ALS-SWCNT (n = 10), ALS (n = 10), or NH<sub>4</sub>Cl (n = 7) test suspensions for 72 h from 1 to 2 hpf. Each n represents a 6-well plate with 30 embryos/well. Values are mean ± SEM. An asterisk (\*) indicates significant difference compared to the DTW control (ANOVA, Dunnett's, *p* < 0.05).

cases where the reproduction period coincides with specific environmental cues (Cheng et al., 2007). Contrary to the findings of Cheng et al. (2007), NF-SWCNTs did not induce a significant hatching delay in embryos at the time points tested (**Figure 3-4a**). We did, however, observe accelerated hatching in embryos exposed to 200 mg/L COOH-30-SWCNTs, COOH-40-SWCNTs, and COOH-50-SWCNTs at 48 hpf, and the same effect was observed in 52 and 56 hpf embryos exposed to COOH-30-SWCNTs and COOH-50-SWCNTs (**Figure 3-4b**; unpaired Student's t-test,  $p < 0.05$ ). There were also significant differences between NF-SWCNT and COOH-30-SWCNT exposed embryos at 48 hpf and between 48 and 56 hpf embryos exposed to NF-SWCNTs and COOH-50-SWCNTs (ANOVA, Tukey's,  $p < 0.05$ ). Chen et al. (2016) demonstrated that a 48 h exposure to 100 mg/L graphene oxide completely covered the surface of the zebrafish chorion and created a hypoxic microenvironment in embryos. Similar observations were made for 24 and 48 hpf embryos exposed to  $\leq 50$  mg/L NF-SWCNTs (**Figure S3-6**); embryos were not visible at concentrations  $\geq 50$  mg/L due to the opacity of the exposure suspensions. Though oxygen concentration was not measured in this study, we suspect that mild hypoxia caused by an inadequate exchange of ambient oxygen across the chorionic membrane (to satisfy aerobic metabolic requirements of the developing embryo) induced premature hatch (Wu, 2009). Rainbow trout (*Salmo gairdneri*) embryos have also been shown to hatch earlier in response to hypoxia (Latham and Just, 1989).

Aquatic organisms become more susceptible to mortality by predation when hatching time is altered (Ong et al., 2014b). Exposure to SLS induced a hatching delay that differed significantly from SLS-SWCNTs at 52 hpf, but was similar to the

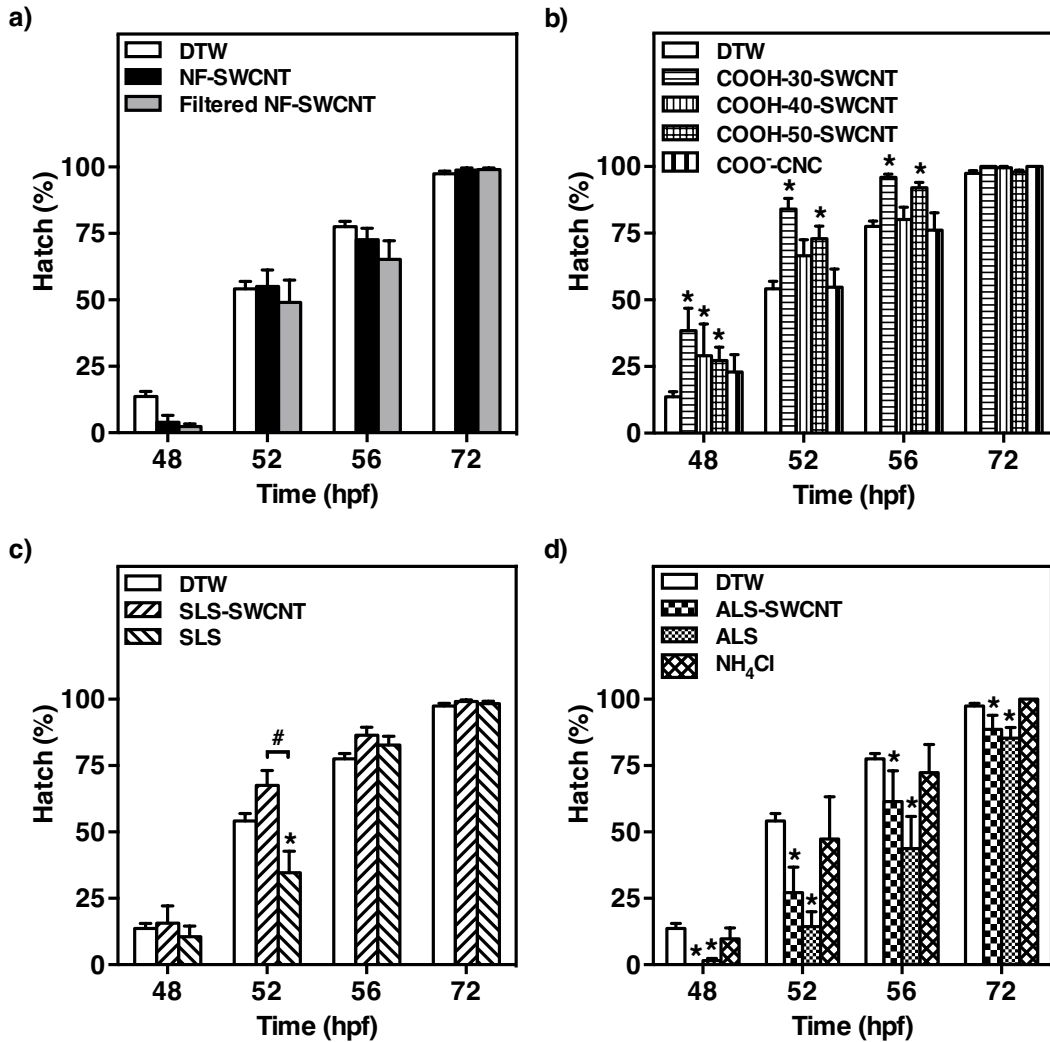


**Figure 3-4. Percent hatch of zebrafish exposed to SWCNT and CNC test suspensions.** Zebrafish embryos were exposed to DTW or 200 mg/L (a) NF-SWCNT (n = 11), filtered NF-SWCNT (n = 8), (b) COOH-30-SWCNT (n = 11), COOH-40-SWCNT (n = 9), COOH-50-SWCNT (n = 15), COO<sup>-</sup>-CNC (n = 12), (c) SLS-SWCNT (n = 10), SLS (n = 11), (d) ALS-SWCNT (n = 10), ALS (n = 10), or NH<sub>4</sub>Cl (n = 7) test suspensions for 72 h from 1 to 2 hpf. Hatching success was recorded at 48, 52, 56 and 72 hpf. Each n represents a 6-well plate consisting of 30 embryos/well. Values are mean ± SEM. DTW controls for all treatments were combined. An asterisk (\*) indicates significant difference compared to the DTW control (unpaired Student's t-test). A number sign (#) indicates significant difference between treatment groups (ANOVA, Tukey's, *p* < 0.05).

DTW control 4 h later (**Figure 3-4c**). Similarly, ALS-SWCNTs and ALS delayed hatch at all time points tested (**Figure 3-4d**). Although Cheng et al. (2007) suggested that hypoxia resulting from exposure to SWCNTs was responsible for a delayed hatching response in zebrafish, hypoxia is known to actually accelerate hatching in fish embryos (Latham and Just, 1989) so this is unlikely the cause of the delayed hatching noted in either study. Metals including Cu, Ni, Pb, and Co were shown to delay hatching in zebrafish (*Brachydanio rerio*) embryos (Dave and Xiu, 1991). Our findings show that SLS-SWCNTs have significantly increased concentrations of these metals in suspension (**Figure 3-2**). However, given that both trace metal controls and the NF-SWCNTs did not show delayed hatch (**Figure 3-4a**), it is unlikely that metals are the proximal cause of the hatching delay. Hatching in fish embryos occurs with release of Zn metalloprotease hatching enzymes that are secreted from hatching gland cells (Bai et al., 2010) located on the pericardium (on the yolk sac ventral to the head) (Kimmel et al., 1995). We have previously suggested that hatching retardation might be due to interference with the function of the proteolytic hatching enzymes (Ong et al., 2014b). Ong et al. (2014b) reported a strong correlation ( $R^2 = 0.76$ ) between nanoparticles (NPs) that delayed or inhibited zebrafish hatch and those that inhibited hatching protease activity. For this to happen, the NM must be able to traverse the chorion and enter the chorionic fluid. The chorionic membrane of zebrafish is known to possess a regular pattern of pores of  $\sim 170 \text{ nm}^2$  in size (Cheng et al., 2007) and given the mean hydrodynamic diameter of 10 mg/L SLS-SWCNTs and ALS-SWCNTs at 72 h was  $172.83 \pm 1.68 \text{ nm}$  and  $180.43 \pm 1.68 \text{ nm}$ , respectively,

interaction between lignin-wrapped SWCNTs and the hatching enzymes likely led to hatching delay.

### 3.3.3 Cellular effects

CNCs have become an attractive carbon-based NM alternative for biomedical applications (Male et al., 2012). We have investigated the cytotoxic response of channel catfish B and T cells to different concentrations of water-dispersible COO<sup>-</sup>-CNCs. Zhao et al. (2013a) noted a correlation between the sublethal effects resulting from hydroxyapatite NP exposure to zebrafish embryos and catfish cell lines (3B11 and 28S.3); therefore, we chose 3B11, 1G8, and 28S.3 cell lines to determine whether the effects observed *in vivo* were similar to the effects noted in vertebrate *in vitro* systems. *In vitro* COO<sup>-</sup>-CNC exposures did not affect cell viability, except at the highest nominal concentrations examined (**Figure 3-5**). The two channel catfish B-cell lines tested, 3B11 and 1G8, had high viability even at the highest concentrations tested (**Figure 3-5a, b**) demonstrating good biocompatibility. After a 48 h exposure to 200 mg/L COO<sup>-</sup>-CNCs, 79.85 ± 2.98% of 3B11 cells and 78.81 ± 1.96% of 1G8 cells remained viable (**Figure 3-5a, b**). Significant declines in viability were only noted for 1G8 cells exposed to 100 and 200 mg/L COO<sup>-</sup>-CNCs for 48 h (**Figure 3-5b**). Similarly, the T-cell line examined, 28S.3, had high viability following COO<sup>-</sup>-CNC exposure (**Figure 3-5c**). After a 48 h exposure to 200 mg/L COO<sup>-</sup>-CNCs, 28S.3 had 83.18 ± 2.41% viable cells in culture and was the only concentration and time point with significant declines in viability (**Figure 3-5c**). In agreement with our findings, Catalan et al. (2014) observed low levels of toxicity

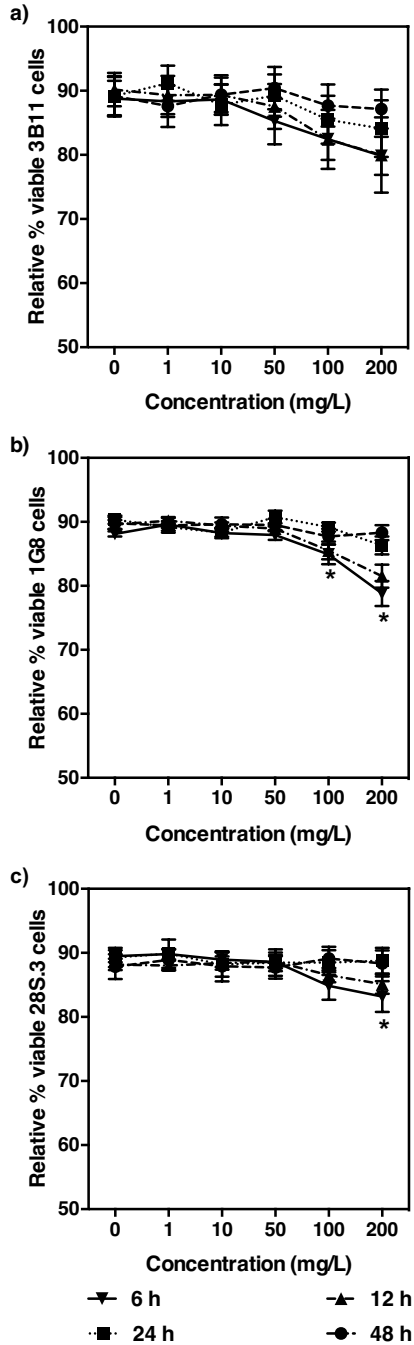


**Figure 3-5. The viability of channel catfish cell lines after *in vitro* CNC exposure.** (a) 3B11, (b) 1G8, and (c) 28S.3 cell lines were exposed to 0, 1, 10, 50, 100 or 200 mg/L COO<sup>-</sup>-CNCs for 6, 12, 24 or 48 h (n = 4). Each n represents a 96-well plate consisting of 20,000 cells/well. Viability was assessed using flow cytometry with PI as a marker for cell death. Values are mean  $\pm$  SEM. An asterisk (\*) indicates significant difference compared to the AL3 media control (ANOVA, Dunnett's,  $p < 0.05$ ).

following 2, 24 and 48 h CNC exposures to BEAS 2B cells with significant reductions in cell viability noted around 100 mg/L. Male et al. (2012) examined the cellular effects of CNC exposure to *Spodoptera frugiperda* Sf9 insect cells and Chinese hamster lung fibroblast V79 cells and found the material to have low cytotoxicity. Together, these results suggest low cytotoxicity and high biocompatibility of COO<sup>-</sup>-CNCs *in vitro*. A detailed assessment of nonfunctionalized and oxidized SWCNT cytotoxicity has been described elsewhere (Ede, 2015). Results found a concentration-dependent decline in channel catfish cell viability following a 48 h exposure to 0.25, 0.5, 1, 5, 10, 25 or 50 mg/L NF-SWCNT, COOH-30-SWCNT, COOH-40-SWCNT or COOH-50-SWCNT suspensions with 3B11 and 1G8 cells having similar, and significantly greater, declines in viability compared to 28S.3 cells. Using human dermal fibroblasts, Sayes et al. (2006) reported a negative correlation between the degree of sidewall functionalization and SWCNT cytotoxicity *in vitro*, and that sidewall functionalized SWCNTs were less cytotoxic than surfactant stabilized SWCNT suspensions. However, it should be noted that CNTs can adsorb essential micronutrients like folate from cell culture media; therefore, significant declines in cell viability may be attributed to this secondary effect and not to the nanotubes directly (Guo et al., 2008).

#### **3.3.4 Molecular effects**

Nutrient, gas and waste exchange may be impeded by SWCNT aggregation on the chorion (Cheng et al., 2007). Agglomerates on the chorionic surface may interfere with oxygen exchange by creating a larger diffusion distance and cause hypoxic

conditions for the embryo (Cheng et al., 2007). Hypoxia-inducible factors regulate the transcription of genes in response to decreased oxygen availability in the environment (Rojas et al., 2007). Expression of the *hif1ab* gene was not altered by acute exposure to 100 or 200 mg/L NF-SWCNTs, COOH-50-SWCNTs, SLS-SWCNTs, or COO<sup>-</sup>-CNCs likely because the surface of the chorion was not completely covered by NM agglomerates (**Figure 3-6a**). The *hif1ab* zebrafish gene was selected based on our observation that NF-SWCNTs ( $\leq 50$  mg/L) adsorb to or settle on the chorion of 24 and 48 hpf embryos and to 72 hpf larvae (**Figure S3-6**). A similar adsorption pattern was observed during oxidized SWCNT exposures but not with lignin-wrapped SWCNT exposures (data not shown); the latter NMs were visually more monodispersed. In previous work (Felix et al., 2013), our research group has shown that fluorescent polymer NPs adsorb to the chorion and to the developing zebrafish within the chorion, but we could not differentiate between NPs adsorbed to the fish from those that may have been internalized by the fish. Wang et al. (2015) found a concentration-dependent accumulation of both dialyzed pristine and carboxylated Pluronic F-108 surfactant suspended SWCNTs in 120 hpf zebrafish and noted reduced accumulation of carboxylated SWCNTs compared to pristine SWCNTs. These differential interactions of NMs provide evidence that the nano-bio interface can be tuned for specific applications.

Usenko et al. (2008) utilized microarrays to demonstrate that  *$\alpha$ -ttp*, *gclc*, and *hsp70* were significantly upregulated over 2-fold in 36 and 48 hpf embryos exposed to 0.2 mg/L C<sub>60</sub>, a carbon-based NM. The  *$\alpha$ -ttp* functions to maintain plasma

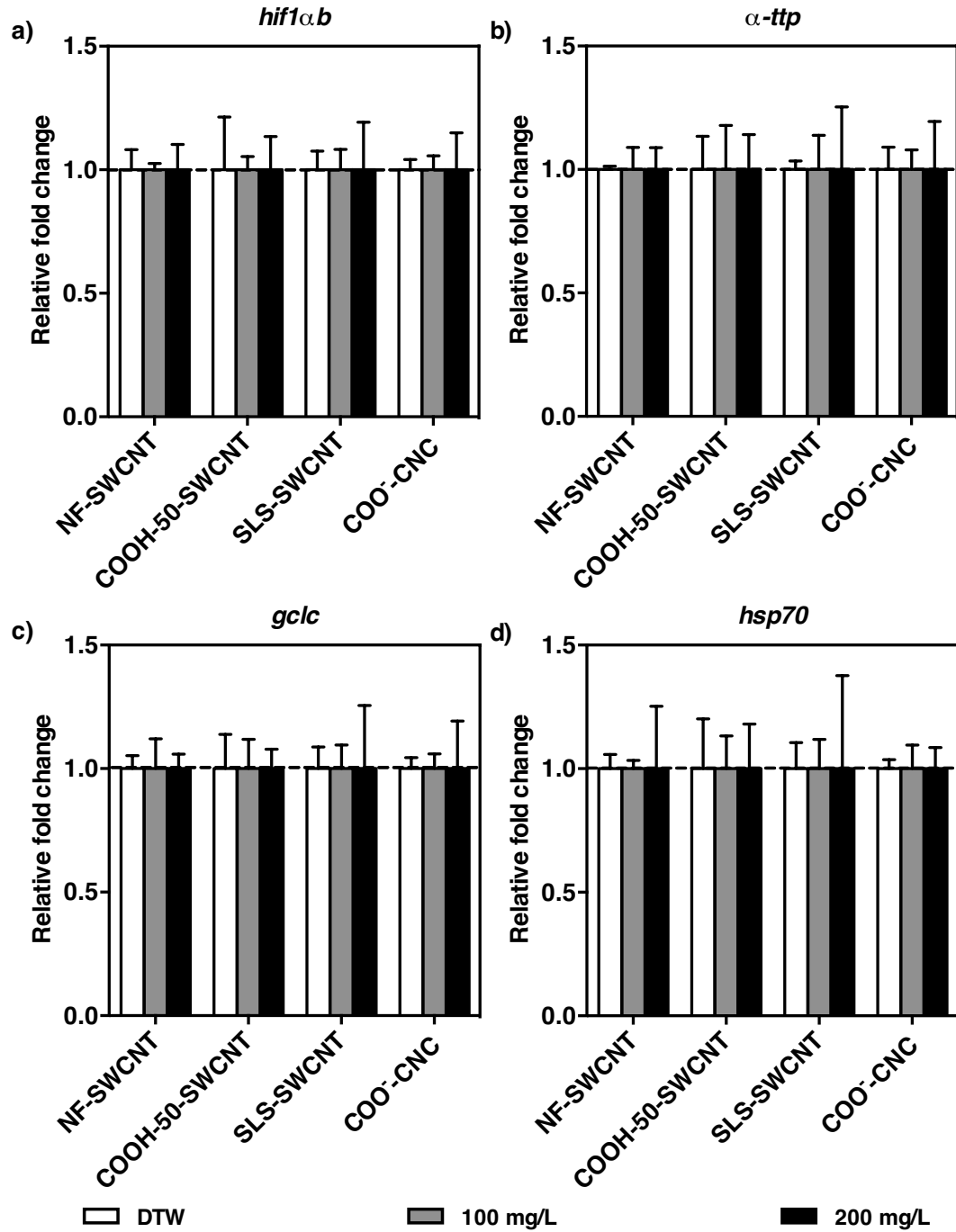


**Figure 3-6. Changes in gene expression patterns following exposure to SWCNT and CNC test suspensions.** Relative fold change of (a) *hif1 $\alpha$ .b*, (b)  *$\alpha$ -ttp*, (c) *gclc*, and (d) *hsp70*, relative to *ef1 $\alpha$* , in zebrafish larvae exposed to 0 (DTW), 100 or 200 mg/L NF-SWCNT (n = 4), COOH-50-SWCNT (n = 4), SLS-SWCNT (n = 4), or COO-CNC (n = 4) test suspensions for 72 h from 1 to 2 hpf. Data are relative to unexposed DTW control larvae (dotted line; n = 4). Each n represents five pooled 72 hpf zebrafish larvae. Values are mean  $\pm$  SEM (ANOVA, Dunnett's,  $p > 0.05$ ).

levels of the antioxidant vitamin E in zebrafish embryos and its amino acid sequence is homologous to the human protein (Miller et al., 2012). Similarly, transcription of the *gclc* gene is induced by reactive oxygen species (ROS) and by different xenobiotics (Kimura et al., 2009). Carboxylated SWCNTs have been reported to produce ROS under artificial sunlight and in water (Chen and Jafvert, 2010). *hsp70* is often utilized as a biomarker due to its response to various environmental stressors including xenobiotics (Carnevali and Maradonna, 2003). All NMs had no effect on the expression of  *$\alpha$ -ttp*, *gclc*, and *hsp70* genes (**Figure 3-6b-d**). There were also no significant differences in gene expression patterns between NF-SWCNT, COOH-50-SWCNT, and SLS-SWCNT-exposed larvae (ANOVA, Tukey's,  $p > 0.05$ ). Though Usenko et al. (2008) reported changes in the expression patterns of  *$\alpha$ -ttp*, *gclc*, and *hsp70*, they used shorter exposures (36 and 48 hpf) and a much lower concentration (0.2 mg/L) of a different type of carbon-based NM ( $C_{60}$ ) than those tested in this study making direct comparison difficult. We chose to examine the molecular effects of 100 and 200 mg/L NM exposures because whole-animal and cellular effects were observed only at these high concentrations. We chose 72 hpf because this time point marks the end of embryogenesis (Kimmel et al., 1995). Endogenous control gene *efl $\alpha$*  was selected based on findings of McCurley and Callard (2008) and was also found to be stable across treatment groups (**Figure S3-7**).

### 3.4 CONCLUSIONS

We have examined the physicochemical properties of seven different types of NMs (NF-SWCNTs, COOH-30-SWCNTs, COOH-40-SWCNTs, COOH-50-

SWCNTs, COO<sup>-</sup>-CNCs, SLS-SWCNTs, and ALS-SWCNTs) and we have assessed their lethal and sublethal effects. Since surface properties affect NM agglomeration in suspension and size of the NM influences its interaction with living organisms, we cannot say with certainty that surface functionality affects SWCNT toxicity directly or that surface functionality can be used for predicting the toxicity of other CNTs like multi-walled carbon nanotubes or NMs in general. However, our results show that surface functionality plays a key role in noted biological effects resulting from SWCNT exposure and that SWCNTs and CNCs will produce adverse effects but only at high concentrations ( $\geq 100$  mg/L) that may be encountered in the environment. High concentrations of COO<sup>-</sup>-CNCs had a minimal effect at the cellular level but not at whole-animal and molecular levels, indicating that there was little correlation between *in vivo* and *in vitro* studies. Furthermore, despite the relatively low acute toxicity of COO<sup>-</sup>-CNCs, the presence of cellular responses indicate that this material is not entirely benign. Functionalized SWCNTs were associated with decreased survival and delays in zebrafish hatching that are likely attributable to direct interaction between hatching enzymes and the lignin-wrapped SWCNTs, although this remains to be directly demonstrated. Further research examining lower concentrations over longer time periods is needed to identify the molecular responses to functionalized carbon-based NMs. Since surface functionality clearly affects the characteristics of some NMs and results in differential responses, the development of new toxicological profiles are essential for safe use of functionalized NMs in commercial, consumer, and industrial applications.

## CHAPTER 4

### Poly (acrylic acid) polymer coating mitigates hydroxyl radical-mediated effects of titanium dioxide nanoparticles in developing zebrafish (*Danio rerio*)

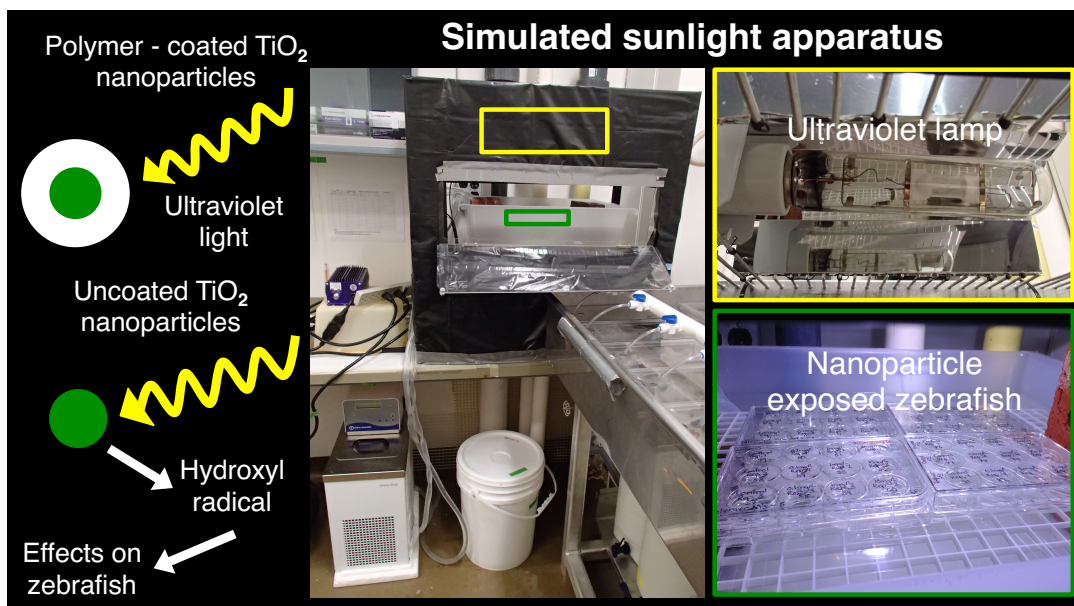


Figure 4-1. Graphical abstract.

Felix, L.C., Folkerts, E.J., He, Y., Goss, G.G. Poly (acrylic acid) polymer coating mitigates hydroxyl radical-mediated effects of titanium dioxide nanoparticles in developing zebrafish (*Danio rerio*). To be submitted.

## 4.1 INTRODUCTION

Human and environmental risks will accrue from the ever-growing production of engineered nanoparticles (NPs) for use in various products and applications (Malysheva et al., 2015). NPs may be unintentionally released into the aquatic environment via effluent from wastewater treatment plants and industries or purposely liberated through groundwater remediation efforts (Dhar Dwivedi et al., 2015). Mounting evidence supporting NP-induced adverse effects on aquatic organisms has raised concerns regarding whether current nanotoxicity testing methods should represent realistic exposure scenarios and environmental conditions (Scown et al., 2010). However, most researchers have investigated NP toxicity in the laboratory under controlled conditions (Wagner et al., 2014).

Engineered titanium dioxide (TiO<sub>2</sub>) NPs have been exploited for use in a wide range of applications, from food and personal care products (Weir et al., 2012), to self-cleaning surfaces and environmental remediation measures (Pelaez et al., 2012). Sunscreens and moisturizers contain TiO<sub>2</sub> NPs because of their intrinsic ultraviolet (UV)-absorbing properties and small size that render lotions transparent (Meißner et al., 2014). In addition to UV attenuation, TiO<sub>2</sub> NPs exhibit antimicrobial properties (Pelaez et al., 2012) and are considered strong oxidizing agents that can degrade organic contaminants (Mahlambi et al., 2015). TiO<sub>2</sub> NPs are considered wide band-gap semiconductors (Li et al., 2015a). When sufficient energy is obtained from sources like natural sunlight, TiO<sub>2</sub> NPs absorb photons and generate electron-hole pairs that react with water and oxygen in the environment to produce reactive oxygen

species (ROS) (Bar-Ilan et al., 2012; Ma et al., 2012) including hydrogen peroxides ( $\text{H}_2\text{O}_2$ ), hydroxyl radicals ( $\bullet\text{OH}$ ), and superoxide anions ( $\text{O}_2^-$ ) (Cerutti, 1985). Although endogenous cellular production of ROS is a biologically important function in several aerobic cellular metabolic processes (Weydert and Cullen, 2009), excessive concentrations of ROS may overwhelm the antioxidant defense system resulting in lipid peroxidation and DNA damage in cells (Riley, 1994). Antioxidant enzymes including catalase (Cat), glutathione peroxidase, and superoxide dismutase (Sod) have evolved to prevent or repair injurious ROS-mediated effects (Riley, 1994).

Surface coatings may be utilized to mitigate the deleterious effects associated with redox reactions at the  $\text{TiO}_2$  NP surface without reducing their photocatalytic efficacy (Priestly et al., 2014; Smijs and Pavel, 2011). Coatings can capture free radicals or hinder their formation, thereby minimizing photocatalytic activity by preventing interactions between the  $\text{TiO}_2$  NP surface, water and oxygen (Smijs and Pavel, 2011). However, only a few studies have focused on photoreactivity of  $\text{TiO}_2$  NPs and the potential hazard associated with their release into aquatic environments (Bar-Ilan et al., 2013; 2012; Li et al., 2015b; Ma et al., 2012). Even fewer have explored the role of surface coating in determining NP phototoxicity (Pan et al., 2009; Yin et al., 2010). Here,  $\text{TiO}_2$  NPs with and without a poly (acrylic acid)(PAA) coating, as well as the PAA coating alone, were characterized and investigated for their  $\text{OH}\bullet$  production capabilities. Early-stage zebrafish (*Danio rerio*) were co-exposed to these NPs and UV light or ambient fluorescent laboratory lighting, and endpoints including survival, hatching success, malformation, thiobarbituric acid reactive substances (TBARS), Cat activity, total glutathione (TG) level, Sod activity,

as well as modulation of antioxidant-related gene expression were measured. We suggest that toxicity induced by uncoated TiO<sub>2</sub> NPs is enhanced by UV illumination while the PAA polymer coating mitigates these •OH-mediated effects. Simulated natural conditions including sunlight activation should be considered by nanotoxicologists who seek to accurately assess the potential hazard associated with release of uncoated and polymer-coated TiO<sub>2</sub> NPs into aquatic environments.

## **4.2 MATERIALS AND METHODS**

Procedures are described only briefly here. Refer to **Appendix II** for further details.

### **4.2.1 Nanoparticle sources and preparation of suspensions**

Aeroxide TiO<sub>2</sub> P25 NPs (CAS No. 13463-67-7; average particle size: 25.1 ± 8.2 nm; Brauner-Emmett-Teller specific surface area: 51.1 m<sup>2</sup>/g; 86% anatase, 14% rutile) in powder form were purchased from Evonik Industries (Essen, Germany). PAA-coated TiO<sub>2</sub> NPs in powder form and aqueous PAA NPs without a metal core in pure water were donated by Vive Crop Protection Inc. (Toronto, CA). These particles are referred to as uncoated TiO<sub>2</sub> NPs, polymer-coated TiO<sub>2</sub> NPs and polymer NPs, respectively. Details regarding polymer-coated TiO<sub>2</sub> NP, and polymer NP synthesis are reported in a previously published study (Felix et al., 2013).

Uncoated and polymer-coated TiO<sub>2</sub> NP stock suspensions (1000 mg/L) were prepared by dispersing bulk powder in double-distilled water (ddH<sub>2</sub>O) followed by

bath sonication (50 / 60 Hz, 117 V, 1 A, Branson 2200, Branson Ultrasonics Corporation, CT, USA) for 1 h. Polymer NP stock suspension was stirred at 600 revolutions per minute (rpm) for 1 h before being diluted 1:10 with ddH<sub>2</sub>O (1000 mg/L). All NP stock suspensions were stored in the dark at 4 °C. Immediately prior to use, each NP stock suspension was probe sonicated (Sonifier Cell Disrupter model SLPe, 150 W, 50% amplitude, Branson Ultrasonics Corporation, CT, USA) on ice (5 min), mixed by vortex (30 s), and then serially diluted to 0.1, 1, or 10 mg/L with filtered (0.45 µm pore size, cellulose acetate membrane bottle-top filter, Corning) and autoclaved dechlorinated tap water (DTW; pH: 7.4, conductivity: 168.5 ± 0.5 µS/cm, temperature: 28.5 ± 1 °C, dissolved oxygen: 7.5 ± 0.5 mg/L, general hardness: 175 mg/L as CaCO<sub>3</sub>, salinity: 0 ppt) without dispersants. All dilutions were probe sonicated (3 × 20 s with a 20 s pause in between) and then mixed by vortex (30 s) immediately before conducting further analyses.

#### **4.2.2 Production of hydroxyl radicals by nanoparticles**

A modified version of the method described by Biaglow et al. (1997) was used to determine whether the NPs tested in this study generate OH• in water. Briefly, 10 mL of 0.1, 1, or 10 mg/L uncoated TiO<sub>2</sub> NP, polymer-coated TiO<sub>2</sub> NP, and polymer NP suspensions were split into individual wells of two separate polystyrene 12-well plates (Corning). A 2-deoxy-D-ribose (2-DR) stock solution (400 mM) in ddH<sub>2</sub>O was mixed by vortex (1 min) and placed in a sonication bath (5 min). Immediately prior to incubation, 50 µL of 2-DR stock solution was added to each well containing either DTW or NP suspension, making a final concentration of

4 mM. One 12-well plate was incubated under UV light (UVA: 2.78 W/m<sup>2</sup>, UVB: 1.70 W/m<sup>2</sup>) for 30 min while the other plate was incubated under laboratory lighting. After incubation, aliquots were removed and subsequently analyzed for TBARS using the procedure described below.

#### **4.2.3 Coexposure of zebrafish embryos to nanoparticles and simulated sunlight**

Viable 24-hour post fertilization (hpf) zebrafish embryos were randomly distributed into 12-well plates (20 embryos/well) and exposed to 5 mL of 0.1, 1, or 10 mg/L uncoated TiO<sub>2</sub> NPs, polymer-coated TiO<sub>2</sub> NPs, or polymer NP suspensions. Embryos in DTW alone served as paired controls. Plates were incubated at 28.5 °C under laboratory lighting until UV illumination 24 h later, starting at 52 hpf. Half of the NP exposed embryos were placed 17 cm below a UV lamp in a container of water regulated by a digital refrigerated bath (Isotemp 3016D, Fisher Scientific) and illuminated for 8 h/d for 5 subsequent days while the other half were incubated under laboratory lighting. All NP exposure suspensions were renewed every 48 h (74 and 122 hpf) during the experimental period. At the end of the exposure period, 168 hpf zebrafish larvae from each well were transferred to an Eppendorf tube, rinsed thrice with DTW, snap frozen in liquid nitrogen without liquid, and stored at -80 °C until further analyses. A detailed schematic of the experimental design is shown in **Figure S4-1**.

#### **4.2.4 Survival, hatching success, and malformation**

Survival of embryos and larvae were recorded immediately before and after the 8 h illumination period at 48, 60, 72, 84, 96, 108, 120, 132, 144, 156, and 168 hpf while hatching success of embryos was recorded at 48, 60, 72, and 84 hpf. Zebrafish considered dead were removed from each well if movement, heartbeat or transparent tissues were not apparent (Ali et al., 2011). Malformations including bent spine (bs), pericardial edema (pe), and yolk sac edema (yse; **Figure S4-2**) were recorded and imaged at 144 hpf using a dissecting microscope (Zeiss Axio Observer A1) connected to a camera (AxioVs40 software, v. 4.7.2). Only plate replicates with  $\geq 80\%$  survival in the DTW control well throughout the experimental period were used in analyses. Each experiment ( $n = 80$  embryos) was repeated at least 4 times.

#### **4.2.5 Thiobarbituric acid reactive substances assay**

TBARS in 168 hpf larvae was measured using a procedure adapted from Janero (1990). Briefly, tissue pooled from 4-9 larvae was homogenized in 300  $\mu\text{L}$  phosphate buffer (pH 7.5) for 30 s, centrifuged at 1000 relative centrifugal force (RCF) for 1 min, and 130  $\mu\text{L}$  supernatant transferred to an Eppendorf tube on ice. The supernatant was diluted with phosphate buffer (1:4 dilution) and treated with 32.5  $\mu\text{L}$  butylated hydroxytoluene (1 mmol/L) and 162.5  $\mu\text{L}$  50% trichloroacetic acid. Samples were centrifuged (13,000 RCF; 2 min) and 120  $\mu\text{L}$  supernatant was added in triplicate to a black-walled, clear-bottom 96-well microplate (Greiner Cellstar, Frickenhausen, Germany) containing 75  $\mu\text{L}$  1.3% thiobarbituric acid (TBA) dissolved in 0.3% NaOH (BDH). Samples and 0-25  $\mu\text{mol/L}$  1,1,3,3-tetraethoxypropane (TEP)

standards (Sigma) were incubated for 1 h at 80 °C before fluorescence excitation (531 nm) and emission (572 nm) readings were recorded using a microplate reader (1420 Multilabel Counter, VICTOR 3 V, PerkinElmer, MA, USA) equipped with Wallac 1420 software (v. 3.0). This experiment was repeated at least 4 times, and each experimental condition was repeated in triplicate wells in each experiment.

#### **4.2.6 Catalase, total glutathione, superoxide dismutase, and protein assays**

For all assays, 168 hpf zebrafish (11-20 larvae/sample) were homogenized (20 s) in the appropriate buffer for the assay, centrifuged (14,000 rpm; 10 min; 4 °C), and supernatant transferred to an Eppendorf tube on ice. The supernatant was then diluted 1:10 with 1× reaction buffer (pH 7.5) for the Cat assay and diluted 1:4 with isotonic sucrose buffer (pH 7.8) for TG, Sod, and protein assays. All assay measurements were carried out with a SpectraMax M2 microplate reader equipped with SoftMax Pro software (v. 5.4, Molecular Devices, CA, USA). Sample absorbance was read at 560, 412, 450, and 562 nm for Cat, TG, Sod, and protein assays, respectively.

Cat activity was measured using the Amplex Red Catalase Assay Kit (Molecular Probes; A22180) according to manufacturer's recommendations. TG levels were determined using a procedure adapted from Baker et al (1990) and Griffith (1980). Briefly, 20 µL diluted supernatants and glutathione disulfide (GSSG) standards (0 - 40 µmol/L) in sucrose buffer were added in triplicate to a clear, flat-bottom 96-well microtest plate (Sarstedt, Nümbrecht, Germany) on ice. Then, 140 µL mastermix containing 0.714 mmol/L 5,5'-dithiobis(2-nitrobenzoic acid),

0.1 M potassium phosphate buffer (pH 7.5), and 0.357 U/mL glutathione reductase from baker's yeast (*Saccharomyces cerevisiae*) was added to each well. Finally, 40  $\mu$ L  $\beta$ -nicotinamide adenine dinucleotide 2'-phosphate reduced tetrasodium salt in phosphate buffer was added to initiate the reaction. Chemicals used in the TG assay were purchased from Sigma-Aldrich. Sod activity was measured using the SOD determination kit (Sigma-Aldrich; 19160) according to manufacturer's specifications. All samples were normalized to total protein present in the corresponding supernatant, as determined by the Pierce BCA Protein Assay Kit (Thermo Scientific, Product No. 23225) according to manufacturer's instructions. These experiments were replicated three times and each tissue sample was run in triplicate.

#### **4.2.7 Gene expression profiles**

Total RNA was isolated from five 168 hpf larvae previously exposed to various concentrations (0, 0.1, 1, or 10 mg/L) of each treatment (uncoated TiO<sub>2</sub> NPs, polymer-coated TiO<sub>2</sub> NPs, or polymer NPs) using the MasterPure RNA Purification Kit (Epicentre Biotechnologies; MCR85102). Briefly, recombinant DNase I (Ambion) and 10X Reaction Buffer with MgCl<sub>2</sub> (ThermoFisher Scientific) were added to each sample immediately prior to a 30 min incubation period at 37 °C. The reaction was terminated with 50 mM ethylenediaminetetraacetic acid and samples were stored in nuclease-free water (non-DEPC treated, Ambion) containing SUPERase-In RNase Inhibitor at 4 °C overnight. RNA quality (260/280 and 260/230 ratios  $\sim 2 \pm 0.2$  a.u.;  $> 200$  ng/mL) was checked the next day using a NanoDrop spectrophotometer (ND-1000, v. 3.8.1), and subsampled to perform first strand cDNA

synthesis using the RevertAid First Strand cDNA Synthesis Kit (Thermo Scientific; K1622). Gene-specific primers (Integrated DNA Technologies, Iowa, USA) for zebrafish *elongation factor 1 alpha (ef1a)*, *cat*, *glutathione peroxidase 1a (gpx1a)*, and *superoxide dismutase 2 (sod2)* were designed using National Center for Biotechnology Information (NCBI) Primer-BLAST software and specificity validated using BLAST. Genes of interest (*cat*, *gpx1a*, and *sod2*) were normalized to *ef1a* and measured using quantitative polymerase chain reaction (qPCR; SDS v. 1.4, Applied Biosystems 7500 Fast Real-Time PCR System) in combination with the double stranded DNA-specific dye SYBR Green I (Molecular Biology Service Unit, University of Alberta). Prior to qPCR, all primer sets were screened using polymerase chain reaction and agarose gel electrophoresis (**Figure S4-3**). Relative quantification of the expression level of each transcript in each sample was calculated using the  $2^{-\Delta\Delta C_t}$  method (Livak and Schmittgen, 2001). Reaction conditions were as follows: 95 °C for 2 min (annealing) followed by 40 cycles of 95 °C for 15 s and 60 °C for 1 min (elongation), and a denaturation stage of 95 °C for 15 s, 60 °C for 1 min, 95 °C for 15 s, and 60 °C for 15 s. This experiment was replicated three times. Primer information is listed in **Table S4-1**.

#### **4.2.8 Statistical analysis**

GraphPad Prism 6 (v. 6.0h, GraphPad Software Inc.) was used for statistical analysis and to create graphs. A one- or two-way analysis of variance (ANOVA) with a Dunnett's multiple comparisons test was used to compare illuminated and non-illuminated treatment groups to their respective controls. An unpaired Student's

t-test was employed to identify differences between illuminated and non-illuminated groups. A two-way ANOVA with a Tukey's test was used to determine the stability of *eflα* across treatment groups. All data are presented as mean ± standard error of the mean (SEM). The fiducial level of significance was set at  $p < 0.05$ .

## 4.3 RESULTS AND DISCUSSION

Refer to **Appendix III** for physicochemical characteristics of the NPs used in this study (**Figures S4-4 and S4-5**).

### 4.3.1 Hydroxyl radical generation

While fluorescent lamps used to illuminate laboratories can emit very low doses of UV radiation (Safari et al., 2015), these levels are considerably lower than the local average radiation flux of natural sunlight that ranges between 3.5 W/m<sup>2</sup> in December to 15.1 W/m<sup>2</sup> in July (Sadler, 1992). By adapting the 2-DR method (Biaglow et al., 1997) for measuring UV-induced OH• formation, we have demonstrated that the NP suspensions used in our study directly generate OH• in the presence of UV light only (**Figure 4-2**). The addition of 2-DR to a suspension containing NP generated OH• resulted in 2-DR degradation, yielding TBA-malondialdehyde adducts (pink chromogens) that were quantified colorimetrically (Gutteridge and Halliwell, 1988). We have demonstrated that OH• generation by uncoated TiO<sub>2</sub> NPs was both concentration- and UV light-dependent

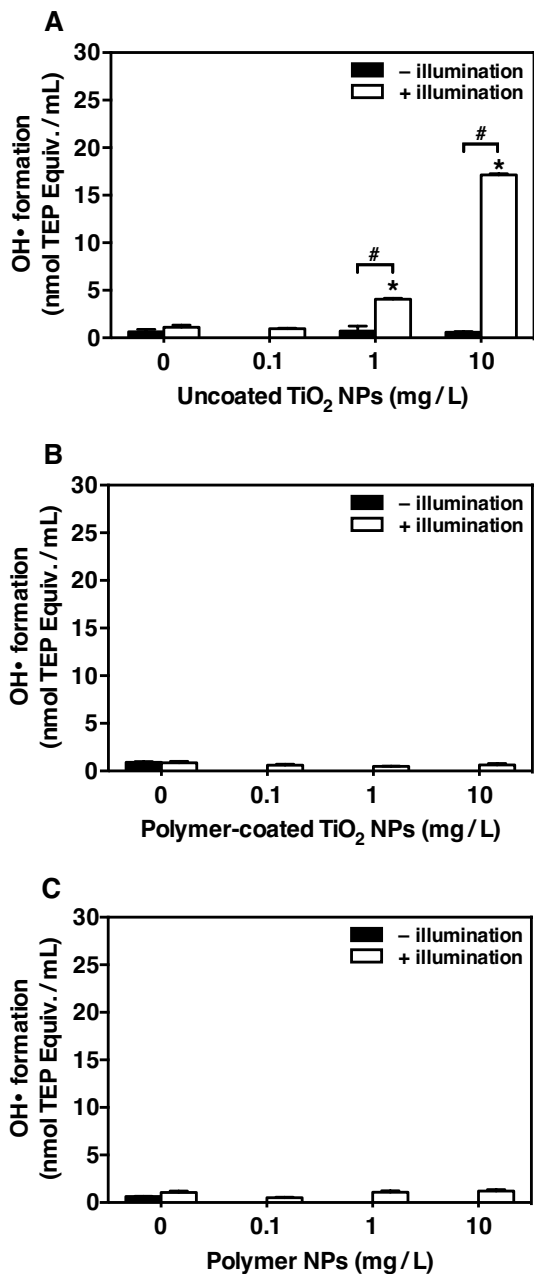


**Figure 4-2. Generation of OH• by NPs.** (A) Uncoated TiO<sub>2</sub> NPs, (B) polymer-coated TiO<sub>2</sub> NPs, and (C) polymer NPs diluted to 0.1, 1, or 10 mg/L with DTW in the absence (–) and presence (+) of illumination. Each NP suspension containing 4 mM 2-DR was incubated for 30 min under UV light or laboratory lighting, and analyzed for TBARS, expressed as nmol TEP equivalent/mL NP suspension (n = 3). For these experiments, each n represents one well of a 4-well plate. An asterisk (\*) indicates significant difference compared to the DTW control (two-way ANOVA, Dunnett’s, *p* < 0.05). A number sign (#) indicates significance between illuminated and non-illuminated groups (unpaired t-test, *p* < 0.05). Values are mean ± SEM.

(**Figure 4-2A**). The amount of OH• produced by 1 ( $4.05 \pm 0.11$  nmol TEP Equiv./mL) and 10 ( $17.15 \pm 0.11$  nmol TEP Equiv./mL) mg/L uncoated TiO<sub>2</sub> NPs after 30 min incubation under UV light were higher than the DTW control ( $1.10 \pm 0.24$  nmol TEP Equiv./mL) and differed significantly from non-illuminated groups (**Figure 4-2A**). This effect was not evident with polymer-coated TiO<sub>2</sub> and polymer NPs regardless of illumination (**Figure 4-2B, C**). Polymer-coated TiO<sub>2</sub> and polymer NPs did not generate significant amounts of OH• in water ( $\leq 1.22 \pm 0.14$  nmol TEP Equiv. / mL; **Figure 4-2B, C**). Although we cannot be certain that OH• were the only type of ROS produced by uncoated TiO<sub>2</sub> NPs, the 2-DR assay was designed specifically for the quantitation of this free radical. Other nanomaterials like carboxylated single-walled carbon nanotubes (Chen and Jafvert, 2010) and zinc oxide NPs (Jassby et al., 2012) have also been shown to produce OH• in water. Using fluorescent probes, Bar-Ilan et al. (2012) demonstrated ROS production in both the uncoated TiO<sub>2</sub> NP exposure suspension alone and in developing zebrafish co-exposed to NPs and UV light. However, the potential for mitigation of ROS-mediated damage by polymer-coated TiO<sub>2</sub> NPs has not been investigated previously. We hypothesized that uncoated TiO<sub>2</sub> NPs are phototoxic under artificial sunlight as measured by a variety of endpoints and that polymer coatings act to mitigate these effects.

#### **4.3.2 Whole-animal effects**

Since the yolk sac of a zebrafish larva is completely absorbed by  $\sim 6.9 \pm 0.5$  d (Jardine and Litvak, 2003), we chose a 7 d experimental period to eliminate NP ingestion as a variable while we investigated endpoints resulting from NP exposure,

in the presence or absence of UV light. Moreover, since Bar-Ilan et al. (2013) reported a significance increase in lethality of zebrafish co-exposed to  $\leq 10$  mg/L TiO<sub>2</sub> NPs and UV light at 8 d and thereafter, a 7 d exposure period would examine early events in the biological responses. No significant reduction in zebrafish survival or increased incidence of malformation under the experimental conditions by 7d was noted (**Figures S4-6 and S4-7**). Uncoated TiO<sub>2</sub> NPs (0.1 mg/L) significantly delayed hatch in 60, 72, and 84 hpf embryos in the presence of UV illumination and hatch of 60 hpf embryos ( $47.64 \pm 10.56\%$ ) was lower compared to those exposed under laboratory lighting ( $87.74 \pm 5.52\%$ ; **Figure 4-3A, B**). However, polymer-coated TiO<sub>2</sub> NPs had no effect on hatching success under either lighting condition (**Figure 4-3C, D**) while 1 mg/L polymer NPs caused a very slight but significant hatching delay in UV irradiated 84 hpf embryos ( $98.27 \pm 1.14\%$ ) compared to DTW control ( $100.00 \pm 0.00\%$ ; **Figure 4-3E, F**). Using Japanese medaka (*Oryzias latipes*), Ma et al. (2012) reported that uncoated TiO<sub>2</sub> NP and UV light co-exposures enhanced phototoxicity by almost 100 times compared to laboratory lighting. Won et al. (2014) demonstrated that increased mortality and reduced hatching rate of copepods (*Paracyclopsina nana*) was the result of UV-induced ROS production. In agreement with our findings, Zhu et al. (2008) reported no effect on survival of zebrafish exposed to uncoated TiO<sub>2</sub> NPs at concentrations up to 500 mg/L over 96 h and Felix et al. (2013) showed no toxic effects on zebrafish exposed to  $\leq 200$  mg/L polymer-coated TiO<sub>2</sub> NPs and polymer NPs over a 72 h period under laboratory lighting. Hatching retardation in zebrafish has been attributed to interference with the function of zinc metalloprotease hatching enzymes (Ong et al., 2014b). It is possible that UV-mediated OH•

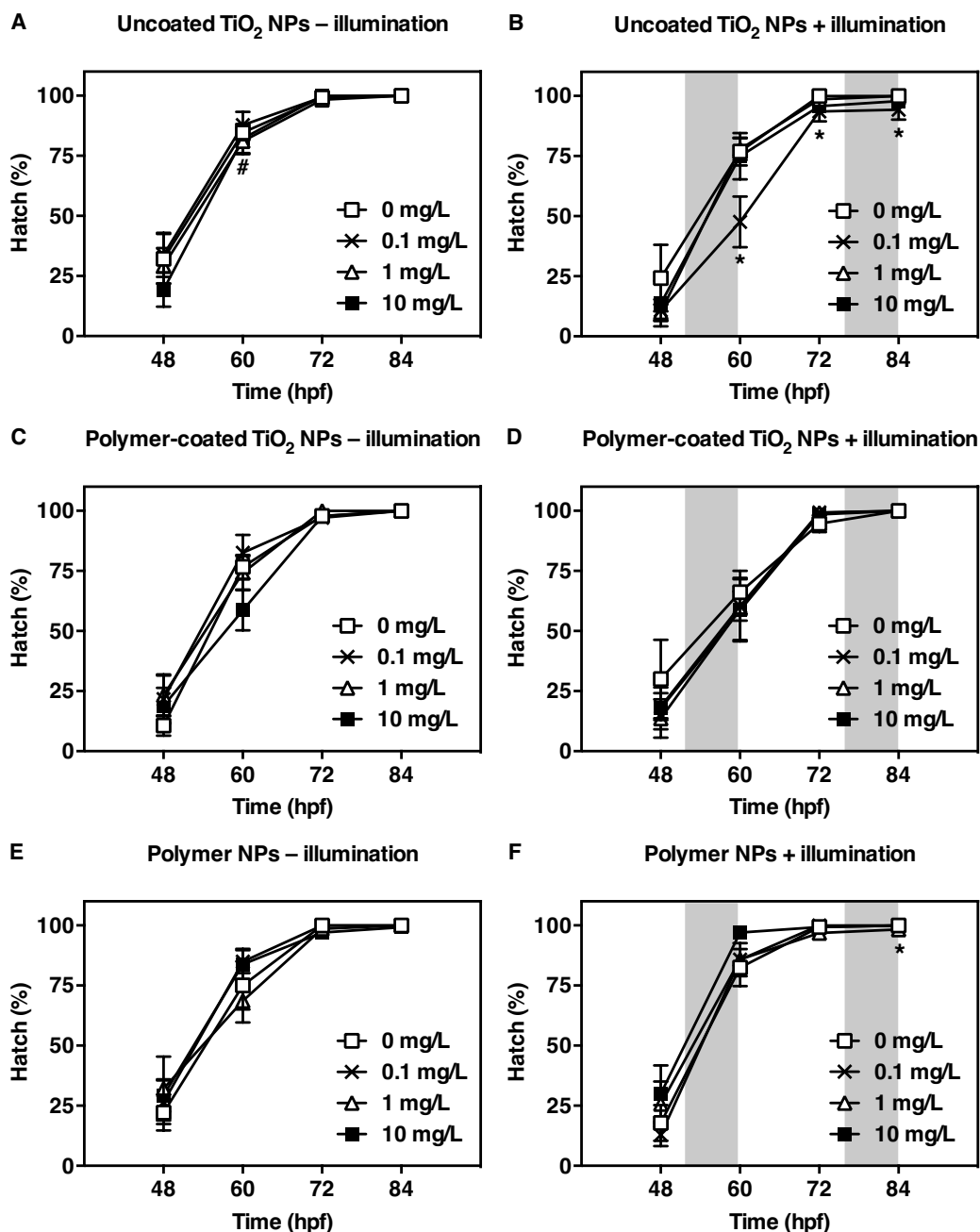


**Figure 4-3. Percent hatch of zebrafish exposed to NPs in the absence (–) or presence (+) of illumination.** Zebrafish were exposed to 0 (DTW), 0.1, 1 or 10 mg/L (A, B) uncoated TiO<sub>2</sub> NPs, (C, D) polymer-coated TiO<sub>2</sub> NPs, or (E, F) polymer NPs (n = 7) for 6 d from 24 hpf. Half of the NP exposed zebrafish were illuminated for 8 h / d for 5 subsequent days, as indicated by the gray bars. The other half was kept under ambient fluorescent lighting. Each n represents 4-well plate replicate consisting of 80 embryos (20 embryos/well). An asterisk (\*) indicates significant difference compared to the DTW control (two-way ANOVA, Dunnett's, *p* < 0.05). A number sign (#) indicates significance between illuminated and non-illuminated groups (unpaired t-test, *p* < 0.05). Values are mean ± SEM.

production directly damaged the hatching enzyme thereby reducing enzyme function, although this remains to be investigated.

### 4.3.3 Tissue and biochemical effects

Oxidative damage occurs when ROS oxidize lipids, adversely affecting the integrity and function of cell membranes (Kong and Lin, 2010). Lipid peroxidation, measured by TBARS, was observed in 168 hpf larvae co-exposed to 0.1, 1, or 10 mg/L uncoated TiO<sub>2</sub> NPs and UV light; the highest and lowest NP concentrations tested differed significantly from non-illuminated groups (**Figure 4-4A**). Furthermore, exposure to 1 and 10 mg/L uncoated TiO<sub>2</sub> NPs in the absence of UV illumination significantly increased lipid peroxidation by  $1.54 \pm 0.14$ - and  $1.74 \pm 0.11$ -fold, respectively (**Figure 4-4A**). Polymer-coated TiO<sub>2</sub> NPs (1 and 10 mg/L) also induced lipid peroxidation in the presence and absence of illumination but to a lesser extent than uncoated TiO<sub>2</sub> NPs (**Figure 4-4B**). Polymer-coated TiO<sub>2</sub> NPs still produced a TBARS response when our 2-DR method for OH• generation did not detect any increase during UV activation (**Figure 4-2**). These results suggest that polymer-coated TiO<sub>2</sub> NPs also produced a small amount of OH• but the 2-DR assay may not have been sensitive enough to discern low levels of UV light-mediated OH• production by these NPs. No peroxidative tissue damage was observed in larvae exposed to polymer NPs in the presence or absence of UV illumination (**Figure 4-4C**). Overall, these findings imply that tissue damage was both NP concentration- and UV light-dependent and that the polymer coating partially mitigated these effects.

Cellular biochemical functions are known to generate certain ROS (H<sub>2</sub>O<sub>2</sub>, O<sub>2</sub><sup>-</sup>,

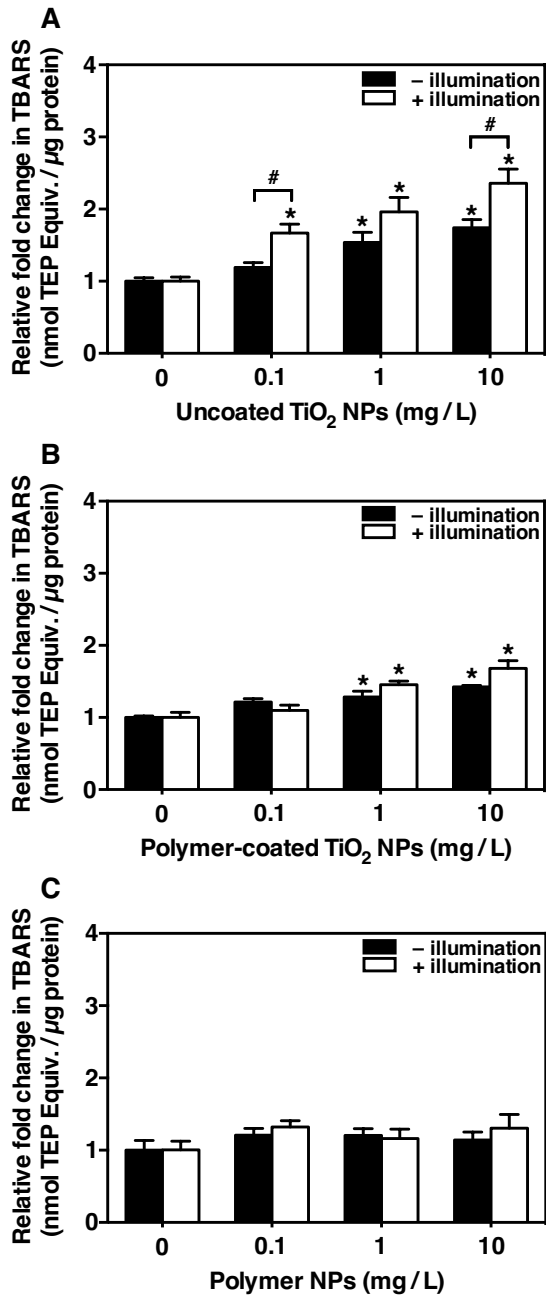


**Figure 4-4. Lipid peroxidation in zebrafish larvae.** Relative fold change of TBARS expressed as nmol TEP equivalent/ $\mu\text{g}$  protein. Zebrafish larvae were exposed to 0 (DTW), 0.1, 1 or 10 mg/L of (A) uncoated TiO<sub>2</sub> NPs, (B) polymer-coated TiO<sub>2</sub> NPs, or (C) polymer NPs in the absence (–) or presence (+) of illumination for 6 d from 24 hpf ( $n = 4$ ). For these experiments,  $n$  represents 4-9 randomly pooled 168 hpf zebrafish larvae per treatment. An asterisk (\*) indicates significant difference compared to the DTW control (two-way ANOVA, Dunnett's,  $p < 0.05$ ). A number sign (#) indicates significance between illuminated and non-illuminated groups (unpaired t-test,  $p < 0.05$ ). Values are mean  $\pm$  SEM.

etc.) and their concentrations are normally well regulated by the antioxidant defense system (Weydert and Cullen, 2009). For example, the antioxidant enzymes Cat and peroxidase protect oxygen-metabolizing cells from oxidative damage by converting  $H_2O_2$  into water and/or molecular oxygen, whereas Sod catalyzes the dismutation of  $O_2^-$  into  $H_2O_2$  and molecular oxygen (Weydert and Cullen, 2009). It is known that  $H_2O_2$ , not detoxified by Cat or peroxidase, can be converted to  $OH^\bullet$  by the Fenton reaction and this free radical may be further reduced to water upon oxidation of glutathione through the action of glutathione peroxidase (Yuan et al., 2012). In the presence of UV light, 10 mg/L uncoated  $TiO_2$  NPs significantly increased Cat activity in 168 hpf larvae compared to DTW control (**Figure 4-5A**). Raised TG levels were observed in UV irradiated larvae exposed to 0.1, 1, and 10 mg/L uncoated  $TiO_2$  NPs compared to DTW control and non-illuminated groups (**Figure 4-5B**). Uncoated  $TiO_2$  NPs had no effect on Sod activity in larvae incubated under UV light or laboratory lighting (**Figure 4-5C**). Fewer effects were noted with polymer-coated  $TiO_2$  NPs, which had no effect on Cat or Sod activities but increased TG levels in UV irradiated larvae exposed to the lowest concentration tested (**Figure 4-5D-F**). While co-exposure to 0.1 and 1 mg/L polymer NPs and UV light enhanced Cat activity, these particles did not affect TG levels or Sod activity under either lighting condition (**Figure 4-5G-I**). Interestingly, Cat activity was markedly reduced by UV exposure (**Figure 4-5A, D, G**) likely due to irrevocable oxidative damage of the enzyme (Pigeolet et al., 1990) by  $OH^\bullet$ -dependent oxidation of the protein potentially leading to peptide bond cleavage, reactive carbonyl group formation, and/or structural modification (Stadtman and Levine, 2003). Differences in the susceptibility of

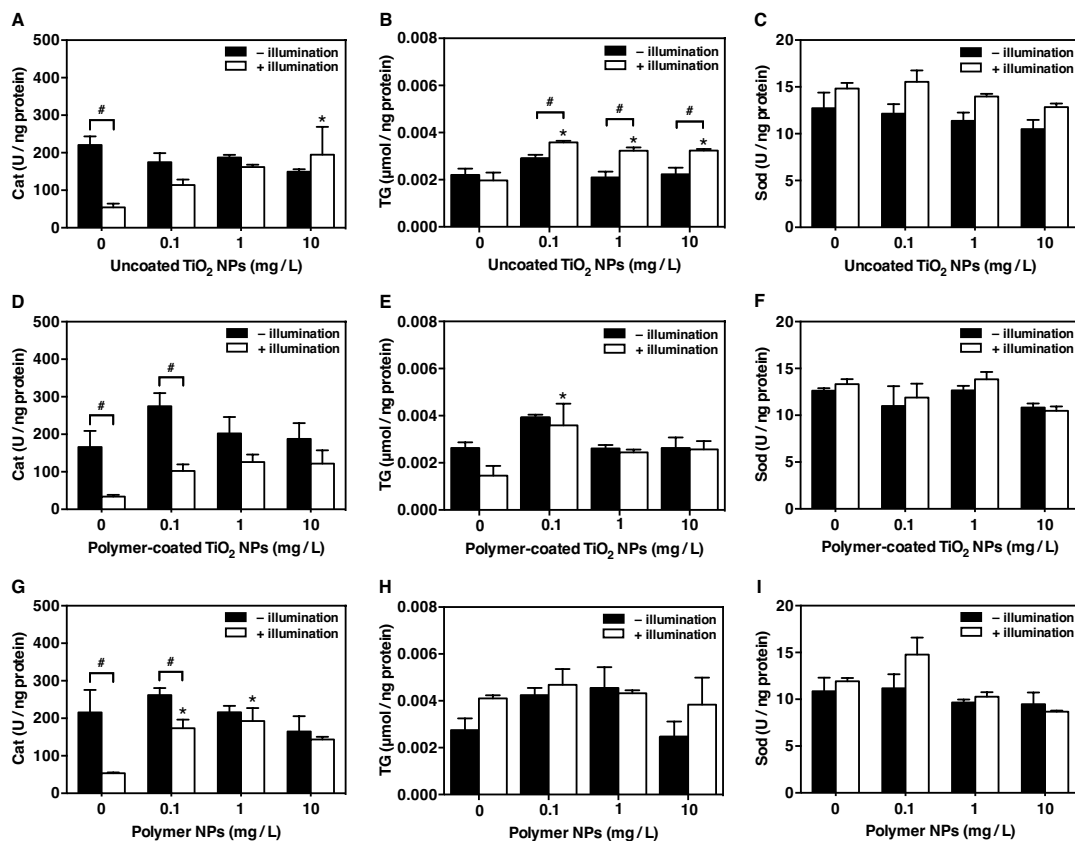


**Figure 4-5. Cat activity, TG level, and Sod activity in co-exposed zebrafish larvae.** Embryos were exposed to 0 (DTW), 0.1, 1 or 10 mg/L of (A, B, C) uncoated  $\text{TiO}_2$  NPs, (D, E, F) polymer-coated  $\text{TiO}_2$  NPs, and (G, H, I) polymer NPs in the absence (-) and presence (+) of UV illumination for 6 d from 24 hpf ( $n = 3$ ). For these experiments,  $n$  represents 11-20 randomly pooled 168 hpf larvae per treatment. An asterisk (\*) indicates significant difference compared to the DTW control (two-way ANOVA, Dunnett's,  $p < 0.05$ ). A number sign (#) indicates significance between illuminated and non-illuminated groups (unpaired t-test,  $p < 0.05$ ). Values are mean  $\pm$  SEM.

macromolecules to ROS damage may explain why TG and Sod were not affected in the same manner (Stadtman and Levine, 2003). We are aware of the potential for NP interference with biochemical assays (Ong et al., 2014a) and took great care to accurately identify those assays potentially affected by our NPs and to eliminate inaccurate interpretation of the results. These steps included multiple washes to remove surface bound NPs from the larvae, absorbance measurements, and demonstration of the effect of NPs on assay function (**Figures S4-8 and S4-9**).

#### **4.3.4 Molecular effects**

In agreement with our biochemical assay findings, 0.1 mg/L uncoated TiO<sub>2</sub> NP and UV light co-exposure significantly upregulated *gpx1a* expression by 1.59-fold in 168 hpf zebrafish larvae but had no effect on either *cat* or *sod2* gene expression (**Figure 4-6A-C**). Though not significantly different from DTW control, *sod2* expression was slightly higher in UV irradiated larvae exposed to 0.1 and 1 mg/L uncoated TiO<sub>2</sub> NPs compared to those incubated under laboratory lighting (**Figure 4-6C**). Polymer-coated TiO<sub>2</sub> and polymer NPs did not alter gene expression in either illuminated or non-illuminated groups (**Figure 4-6D-I**). Endogenous control gene *ef1a* was chosen based on findings of McCurley and Callard (2008) and was found to be stably expressed under all experimental conditions (**Figure S4-10**). Overall, our findings indicate that UV light can trigger •OH-mediated lipid peroxidation, modulate antioxidant enzyme activity and alter gene expression, potentially leading to delayed development in zebrafish.

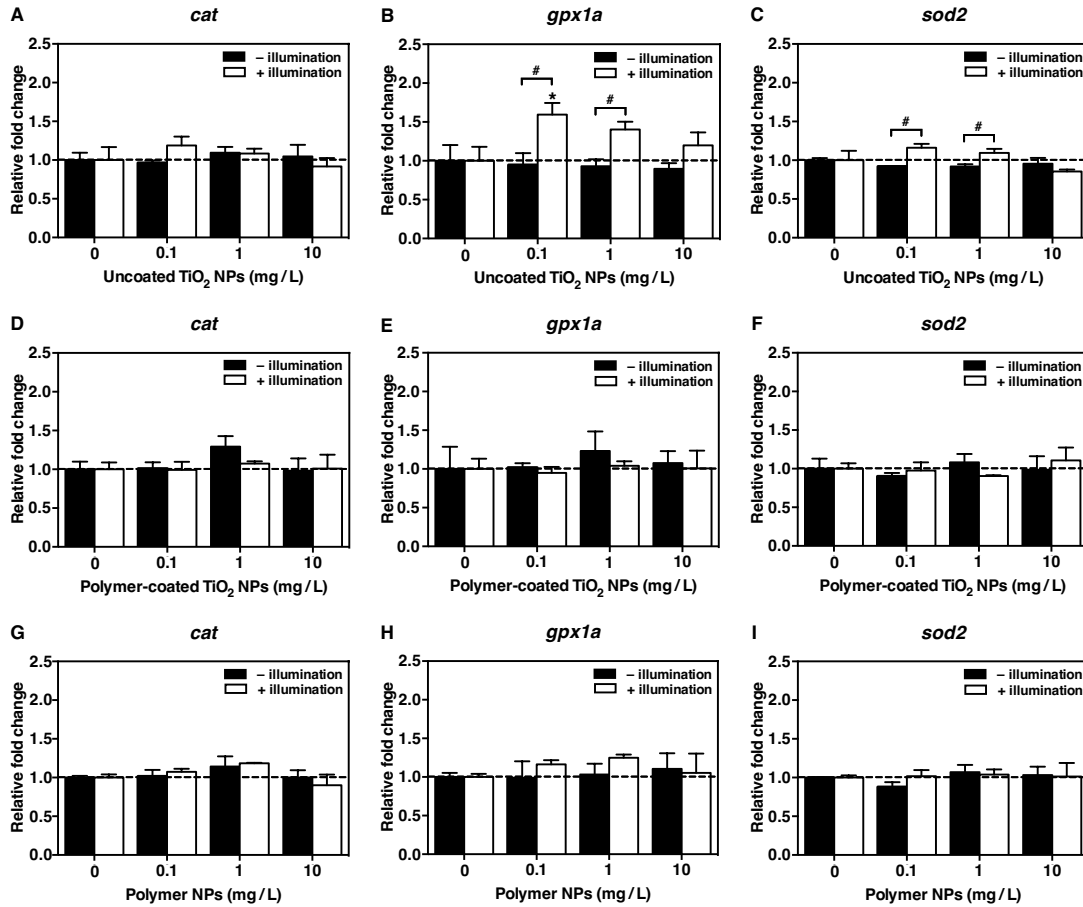


**Figure 4-6. Changes in zebrafish gene expression patterns following NP and UV light co-exposure.** Relative fold change of (A, D, G) *cat*, (B, E, H) *gpx1a*, and (C, F, I) *sod2*, relative to *ef1a*, in zebrafish larvae exposed to 0 (DTW), 0.1, 1 or 10 mg/L uncoated TiO<sub>2</sub> NPs (n = 3), polymer-coated TiO<sub>2</sub> NPs (n = 3), or polymer NPs (n = 3) in the absence (–) or presence (+) of illumination for 6 d from 24 hpf. Data are relative to unexposed DTW control larvae (dotted line; n = 3). Each n represents five randomly pooled 168 hpf zebrafish larvae per treatment. An asterisk (\*) indicates significant difference compared to the DTW control (two-way ANOVA, Dunnett’s,  $p < 0.05$ ). A number sign (#) indicates significance between illuminated and non-illuminated groups (unpaired t-test,  $p < 0.05$ ). Values are mean  $\pm$  SEM.

To our knowledge, no reports on the *in vivo* effects of polymer coating on TiO<sub>2</sub> NP phototoxicity exist. Our experimental results emphasize the importance of surface coatings when predicting the phototoxicity of TiO<sub>2</sub> NPs in the environment. In the present study, we have demonstrated that 1 and 10 mg/L uncoated TiO<sub>2</sub> NPs generated OH• in the presence of UV light, which was the likely mode of action involved in noted sublethal effects. We expect that OH• produced by 0.1 mg/L uncoated TiO<sub>2</sub> NPs and by all concentrations of polymer-coated TiO<sub>2</sub> NPs tested were below detection limits of our modified 2-DR assay. While 0.1 mg/L uncoated TiO<sub>2</sub> NPs delayed hatch, enhanced lipid peroxidation, increased TG levels and upregulated the expression of the *gpx1a* zebrafish gene, polymer-coated TiO<sub>2</sub> NPs caused fewer effects. Additionally, lipid peroxidation was slightly lower in larvae exposed to 1 and 10 mg/L polymer-coated TiO<sub>2</sub> NPs compared to uncoated TiO<sub>2</sub> NP exposures. We suggest that the polymer coating mitigated •OH-mediated effects in developing zebrafish. Failure to consider the effect of solar radiation in ecotoxicological studies could lead to a severe underestimation of the risk associated with release of TiO<sub>2</sub> NPs into aquatic environments and the potential for these NPs to harm fish. Further research is needed to investigate the role of polymer coating in determining TiO<sub>2</sub> NP phototoxicity, and development of new and more accurate endpoints for nanotoxicity testing is essential.

## CHAPTER 5

### **Cellular uptake and intracellular localization of poly (acrylic acid) nanoparticles in a rainbow trout (*Oncorhynchus mykiss*) gill epithelial cell line**

Felix, L.C., Ortega, V.A., Goss, G.G. Cellular uptake and intracellular localization of poly (acrylic acid) nanoparticles in a rainbow trout (*Oncorhynchus mykiss*) gill epithelial cell line. To be submitted.

## 5.1 INTRODUCTION

Nanotechnology is increasingly playing a vital role in agriculture, creating innovative solutions for pest management and providing new tools for crop protection by replacing conventional methods that adversely affect the environment or by providing more targeted delivery of insecticide and fungicide formulations. Engineered nanoparticles (NPs) are increasingly being used in agricultural applications as micronutrients for crops and carriers for insecticides to improve crop yields and to mitigate adverse environmental effects (Liu and Lal, 2015; Xu et al., 2014). However, direct application of NP-enabled micronutrient and insecticide formulations on crops increases the likelihood of runoff into surface water, groundwater contamination, and exposure to non-target aquatic organisms including fish (Khatri and Tyagi, 2015). The gill is the primary target organ for NP uptake in fish and endocytosis at the gill cell surface is a potential mechanism by which NPs are likely to be internalized into the animal (Handy et al., 2008). Endocytosis is an energy-dependent process used by cells to take in select extracellular macromolecules including proteins, viruses, and even NPs that are impermeable to the plasma membrane (Shang et al., 2014). While the endocytotic pathways involved in NP uptake have been extensively studied using mammalian cell models (Firdessa et al., 2014; Kuhn et al., 2014; Monti et al., 2015; Sokolova et al., 2013), only a few studies have examined the internalization of NPs by fish cells (Farkas et al., 2011; Kühnel et al., 2009) and the mechanisms by which this occurs were not investigated. We have examined the role of clathrin-mediated endocytosis (CME), caveolae-mediated

endocytosis (CavME), and macropinocytosis (MP) in the internalization of NPs by fish gill epithelial cells and some aspects of these pathways are summarized below.

CME is the best-characterized and understood endocytotic pathway (Khalil et al., 2006). The interaction between a membrane receptor and ligand initiates clathrin-coated pit formation where cytosolic coat proteins, the main assembly unit being clathrin, polymerize into a polygonal lattice with the help of adaptor proteins (Khalil et al., 2006). The mechanochemical guanosine triphosphatase (GTPase) dynamin then catalyzes the scission of the invaginated pit forming a clathrin-coated vesicle (~ 100-150 nm in size) that entraps the receptor-ligand complex (Conner and Schmid, 2003; Khalil et al., 2006; Kou et al., 2013). Once the clathrin coat is shed, the vesicle releases its cargo into an early endosome where the ligand and receptor are sorted and routed to their appropriate subcellular destinations (Andersen and Moestrup, 2014). For example, iron-loaded transferrin (Tf) bound to the Tf receptor is recycled back to the plasma membrane, whereas low-density lipoprotein particles dissociate from their receptor within a late endosome and the particles eventually fuse with an acidic lysosome where they are degraded (Khalil et al., 2006; Kou et al., 2013). The CME pathway is blocked by chlorpromazine (CPZ) which inhibits clathrin assembly-disassembly, GTPases, and receptor recycling back to the cell surface (Wang et al., 1993; Zhang and Monteiro-Riviere, 2009).

Unlike CME, CavME follows a non-acidic and non-digestive route where ligands are delivered to the Golgi apparatus, endoplasmic reticulum and/or nucleus in vesicles that have a neutral pH thus avoiding lysosomal degradation (Khalil et al., 2006; Kou et al., 2013). Caveolae are small (~ 50-60 nm in diameter) flask-shaped,

flat, tubular or detached vesicular invaginations of the plasma membrane enriched in lipids including cholesterol, glycosphingolipids and the coat protein, caveolin (Conner and Schmid, 2003; Khalil et al., 2006; Kou et al., 2013). The caveolae pinch off from the plasma membrane, aided by dynamin, and form caveolar vesicles that rely on actin and microtubules for intracellular transport and later fusion into caveosomes (Kou et al., 2013). Caveolae have been implicated in the internalization of viruses including simian virus 40, as well as bacterial toxins including cholera toxin (Khalil et al., 2006). Cholera toxin B subunit (CTb) binds to the glycosphingolipid GM1 predominantly associated with lipid rafts and caveolae, a subset of membrane rafts (Patel and Insel, 2009). Binding of a ligand such as simian virus 40 to its ganglioside receptor GM1 triggers a tyrosine kinase-based signaling cascade that disrupts the actin cytoskeleton and recruits dynamin to the endocytotic site where it is engulfed along with caveolin (Magaldi et al., 2012; Nabi and Le, 2003). Genistein (GN) is a tyrosine kinases inhibitor (Akiyama et al., 2001) that blocks the disruption of the actin network and the recruitment of dynamin, both necessary for uptake via the CavME pathway (Nabi and Le, 2003).

Cells utilize the non-specific, growth-factor induced, actin-dependent MP pathway to engulf both biological fluids, membrane, and particles ( $\leq 5 \mu\text{m}$  in size) from the external environment (Conner and Schmid, 2003; Khalil et al., 2006; Mercer and Helenius, 2009; Oh and Park, 2014). The MP pathway is typically stimulated by growth factors that trigger the activation of a receptor tyrosine kinase-signalling cascade, inducing changes in the actin cytoskeleton to form plasma membrane ruffles (Mercer and Helenius, 2009). Lamellipodia-like membrane ruffles disconnect from

the plasma membrane and form fluid-filled vacuoles called macropinosomes (Kou et al., 2013; Mercer and Helenius, 2009). Dextrans (Dex) are polysaccharides produced by certain bacteria (e.g. *Leuconostoc mesenteroides*) when grown on sucrose-based medium (Santos et al., 2000) and are known to be taken up via the MP pathway (Li et al., 2015). Wortmannin (WN) blocks the action of phosphoinositide 3-kinase (Araki et al., 1996) necessary for plasma membrane ruffle formation and macropinosome closure (Mercer and Helenius, 2009). The NPs used in this study could potentially exploit any of the abovementioned endocytosis pathways to enter cells due to their small size.

We have investigated the uptake mechanisms and fate of 3-9 nm poly (acrylic acid) (PAA) NPs using the permanent, epithelial cell line, RTgill-W1, derived from primary cell cultures of rainbow trout (*Oncorhynchus mykiss*, Walbaum) gills (Bols et al., 1994). The NPs used in this study act as nano-sized carriers for the insecticide bifenthrin, the fungicide azoxystrobin, or both insecticide and fungicide combined. These novel NP-containing products were designed to lower the active ingredient load by increasing penetration through plant tissues, reducing mobility in soil, and providing a delayed release of insecticide and fungicide formulations (Pérez-de-Luque and Rubiales, 2009). However, encapsulating known toxicants into NPs may also increase the uptake of these nanocomposites across gills since they are the primary sites of xenobiotic exchange between the fish and the aquatic environment (Stott et al., 2015). Thus, our primary study objectives were to first determine whether CME, CavME and MP uptake pathways were present in RTgill-W1 cells,

then examine the mechanisms by which NPs could enter these cells, and finally investigate the intracellular fate of NPs within cells.

## **5.2 METHODS**

### **5.2.1 Nanoparticle synthesis, stock preparation, and characterization**

Vive Crop Protection Inc. (Toronto, Canada) donated the NPs used in this study. Briefly, 19.8 g PAA nanocapsules, synthesized using a procedure described elsewhere (Felix et al., 2013), and 0.2 g Nile red (NR; excitation/emission wavelengths [Ex/Em] = 552/636 nm) were dispersed in methanol, causing an association between the polymer NPs and the fluorescent lipophilic dye, and then spray dried. NR-loaded NPs (herein referred to as NPs), in powder form, were suspended in dimethyl sulfoxide (DMSO) and stored at 4 °C in the dark. The NP stock suspension (1000 µg/mL) was mixed by vortex (Fisher Vortex Genie 2, Fisher Scientific) for 5 s and bath sonicated (50 / 60 Hz, 117 V, 1 A, Branson 2200, Branson Ultrasonics Corporation, CT, USA) for 5 min to ensure a homogenous dispersion of particles immediately prior to conducting further analyses.

Dynamic light scattering (DLS; Zetasizer Nano Series, Malvern Instruments Ltd.) in 173° backscatter mode (Zetasizer software, v. 7.01) was used to characterize the size and charge of 10 and 25 µg/mL NP agglomerates in both double-distilled water (ddH<sub>2</sub>O) and cell culture medium. Mean z-average hydrodynamic diameter, polydispersity index, and zeta (ζ) potential were measured by DLS at 0 and 1 h after

NP addition while pH measurements were made using a calibrated digital pH meter (Accumet Basic AB15, Fisher Scientific).

### **5.2.2 Fluorescent biomarkers, transport inhibitors, and organelle stains**

Biomolecules known to selectively enter cells via a specific endocytotic pathway were used as positive controls for this study. Tf from human serum, fluorescein conjugate (Tf-FL; Ex/Em = 494/518 nm; T2871, Molecular Probes), dissolved in 1× phosphate buffered saline (PBS; 2.7 mM KCl, 1.5 mM KH<sub>2</sub>PO<sub>4</sub>, 136.9 mM NaCl, 15.2 mM Na<sub>2</sub>HPO<sub>4</sub>, pH 7.0) containing 1% NaN<sub>3</sub> (Sigma) and diluted to a final concentration of 120.0 µg/mL in 1X PBS, was used as a specific marker for CME. It is well known that Tf enters cells via CME (McMahon and Boucrot, 2011), and thus its uptake should be affected by treatment with CPZ, a specific inhibitor of this endocytotic pathway (Wang et al., 1993). Therefore, Tf-FL was used as a positive control both to confirm the presence of CME in RTgill-W1 cells and to determine the efficacy of CPZ in inhibiting this particular pathway. CTb, fluorescein isothiocyanate conjugate (CTb-FITC; Ex/Em = 495/525 nm; C1655, Sigma), a positive marker of CavME, was reconstituted in ddH<sub>2</sub>O and added to 1X PBS to make a final concentration of 1.0 µg/mL. To measure MP, 10 kDa Dex, fluorescein conjugate (Dex-FL; Ex/Em = 494/521 nm; D1820, Molecular Probes) was prepared in 1X PBS and used at a concentration of 500.0 µg/mL in 1X PBS. Fluorescently labelled CTb and Dex have been used as probes to identify CavME and MP pathways, respectively (Li et al., 2015; Patel and Insel, 2009). For this reason, we used these fluorescent markers as positive controls to confirm the presence and

inhibition of CavME and MP pathways upon treatment with GN and WN, respectively. All fluorescent biomarker stock solutions were gently mixed by vortex for 5 s and centrifuged at 12,000 g (relative centrifugal force) for 5 min (Tf-FL and Dex-FL) or spun down at 400 g for 10 s (CTb-FITC) immediately prior to use.

Inhibition of CME was tested with 10.0  $\mu\text{g}/\text{mL}$  CPZ (C8138, Sigma). CavME inhibition was achieved by adding 54.0  $\mu\text{g}/\text{mL}$  GN (E1147, Biomol) and 0.2  $\mu\text{g}/\text{mL}$  WN (W1628, Sigma) solution was used as a specific marker for MP. All transport inhibitors were prepared in DMSO, mixed by vortex for 10 s, and centrifuged at 14,000 g for 10 s prior to dilution in cell culture medium.

Mounting media containing either 1.0  $\mu\text{g}/\text{mL}$  4',6-diamidino-2-phenylindole (DAPI; Ex/Em = 358/461 nm; Cross Cancer Institute, Alberta, Canada) or Hoechst 33342 (Ex/Em = 361/486 nm; 62249, Thermo Scientific) prepared in ddH<sub>2</sub>O and diluted to a final concentration of 1.0  $\mu\text{g}/\text{mL}$  in cell culture medium, were used to stain the nuclei (blue) of fixed and living cells, respectively. CellMask Deep Red (CMDR; Ex/Em = 649/666 nm; C10046, Molecular Probes), dissolved in DMSO and diluted to 5.0  $\mu\text{g}/\text{mL}$  with 1X PBS, was used to stain the plasma membranes (magenta) of fixed cells. The acidotropic dye LysoTracker Yellow-HCK-123 (LTY; Absorption/Em = 465/535 nm; L12491, Molecular Probes), dissolved in DMSO and added to cell culture medium to make a final concentration of 0.1  $\mu\text{g}/\text{mL}$ , was used to label lysosomes in live cells (Chazotte, 2011).

Stock solutions were stored at 4 (Tf-FL, CTb-FITC, DAPI, and LTY) or -20 (Dex-FL, CPZ, GN, WN, and CMDR) °C and protected from light. Concentrations and incubation times for NPs, fluorescent biomarkers, inhibitors, and organelle stains

were individually optimized. **Figure 1-1** summarizes the endocytotic pathways potentially utilized by RTgill-W1 cells to internalize the fluorescent biomarkers, inhibitors, NPs, and organelle stains used in this study.

### **5.2.3 Cell culture and seeding of cells**

The RTgill-W1 cell line was cultivated in filter sterilized (0.22  $\mu\text{m}$  pore size, cellulose acetate membrane bottle-top filter, Corning) L-15 medium (Leibovitz; Sigma) supplemented with 10% fetal bovine serum (FBS; heat inactivated, Sigma) and 1% penicillin/streptomycin (HyClone) and grown in a 75  $\text{cm}^2$  tissue culture-treated flask with a non-vented cap (Sarstedt). Cells were maintained at room temperature ( $\sim 21$   $^{\circ}\text{C}$ ) in the dark and grown for 7-10 d or until  $\geq 80\%$  confluence was reached. Confluent cells were washed once with filter sterilized 1X PBS and detached by trypsin containing 0.05% ethylenediaminetetraacetic acid (trypsin/EDTA; Gibco). Cells were counted using a hemocytometer and seeded at a density of  $7.5 \times 10^5$  cells / well in a final volume of 1.5 mL L-15 medium in a 6-well tissue culture-treated plate (Corning) or at a density of  $1 \times 10^5$  cells / well in a final volume of 0.2 mL L-15 medium in a chambered coverslip ( $\mu$ -slide 8-well, ibiTreat, ibidi GmbH, Munich, Germany). For fixed cell imaging, cells were grown on a poly-d-lysine-coated coverslip (12 mm diameter, 1.5 thickness, Neuvitro Corporation, Vancouver, Canada) placed into each well of a 6-well plate. Each well of a chambered coverslip was pre-coated with poly-l-lysine solution (Sigma) for 30 min, washed thrice with ddH<sub>2</sub>O, and allowed to dry for 24 h. The next day, each well was washed once with 95% ethanol, twice with 1X PBS, and once with L-15 medium before adding the cells. Plates or

chambered coverslips were sealed with Parafilm and cells were grown for 72 h at room temperature in the dark, yielding  $\sim 1.08 \times 10^5$  cells / mL immediately prior to exposure.

#### **5.2.4 Efficacy of endocytosis inhibitors**

Fluorescent biomarkers were used to determine whether CME, CavME, and MP pathways were present in RTgill-W1 cells, and to measure the effectiveness of CPZ, GN, and WN in inhibiting these pathways, respectively. At 72 h (see section 5.2.3), confluent adherent cells in 6-well plates were washed twice with 1X PBS containing 0.05% bovine serum albumin (1X PBS/BSA; Sigma) and once with 1X PBS; plates were covered with tinfoil, placed on a rocking platform (VWR Scientific Products), and rocked at a gentle speed for 1 min between each wash. All subsequent washes were carried out in the manner described above. Cells were then pre-incubated with CPZ, GN, or WN for 30 min at room temperature. Cells in L-15 medium or DMSO alone served as negative and vehicle controls for this study, respectively; the DMSO control was prepared and applied in the same manner and volume as the inhibitor working solutions. Cells pre-incubated with DMSO and incubated with a biomolecule served as a positive control for this study. At 30 min, cells were washed and the corresponding well of cells was incubated with Tf-FL, CTb-FITC, or Dex-FL for an additional 30 min at room temperature. Plates for this study and subsequent experiments were sealed with Parafilm and covered with tinfoil during incubation periods. This experiment was replicated thrice per treatment.

### **5.2.5 Nanoparticle uptake and inhibition of endocytotic pathways**

Confluent adherent cells in a 6-well plate were washed as above, and pre-incubated with CPZ, GN, or WN in L-15 medium for 30 min at room temperature. Ice-cold L-15 medium was added to a separate well and kept at 2 °C served as a negative control for endocytosis (temperature-related inhibition of endocytosis). At 30 min, NPs were added directly to appropriate wells at a final concentration of 25 µg/mL and incubated at room temperature or 2 °C for 1 h protected from light. In addition to the negative 2 °C control, cells in L-15 medium or DMSO alone served as unexposed and vehicle controls for this study; the DMSO control was added to the corresponding well in the same manner as the NP stock suspension. Cells incubated with NPs alone served as a positive control for this study. This experiment was repeated four times independently.

### **5.2.6 Flow cytometry analysis of uptake in live cells**

Following the incubation periods (see sections 5.2.4 and 5.2.5), cells were washed and incubated with 0.5 mL trypsin/EDTA for up to 5 min and detached by mechanical separation. The suspended cells were added to an Eppendorf tube containing 1 mL 1X PBS/BSA on ice and then pelleted by centrifugation (400 g, 7 min, 2 °C). After the supernatant was decanted, the cell pellet was suspended in 0.4 mL 1X PBS and disrupted prior to analysis by flow cytometry. The uptake of biomolecules or NPs into RTgill-W1 cells was measured using a Beckman Coulter Cell Lab Quanta SC flow cytometer (fluorescence parameter) and data was analyzed with Cell Lab Quanta SC MPL Analysis software (v. 1.0). Cells were gated and the

FL1 or FL2 filter was utilized to measure biomarker or NP fluorescence. All fluorescent biomarkers were excited with a 488 nm argon laser and emission was observed through a 525/40 band-pass filter (FL1). The same laser excited the NPs but emission was observed through a 575/30 nm band-pass filter (FL2). The percentage of cell fluorescence was calculated from the number of cells within the whole population gate that exhibited biomarker or NP fluorescence. Five thousand total events were acquired for each measurement.

### **5.2.7 Laser scanning confocal microscopy of fixed and live cells**

Following the 1 h incubation period (see section 5.2.5), cells were thrice washed and their plasma membranes stained with CMDR for 10 min in the dark, with the exception of the L-15 medium control. Using carboxylated polystyrene NPs, dos Santos et al. (2011) demonstrated that three washes were sufficient to ensure NP removal from the outer cell membrane and that remaining cell fluorescence after washing was attributed to NPs within the cell. After 10 min, the cells on coverslips were washed and fixed at room temperature in the dark for 20 min with 4% paraformaldehyde, followed by washing with 1X PBS and mounted on glass slides using mounting medium containing DAPI. The glass slides were dried overnight on a flat surface in the dark at room temperature and imaged the next day.

To determine whether NPs co-localize with lysosomes, confluent adherent cells in chambered coverslips (see section 5.2.3) were washed as above and incubated with 10  $\mu\text{g/mL}$  NPs for 1 h. At 1h, cells were washed and their nuclei and lysosomal compartments stained with Hoechst 33342 and LTY for 2 h. At 2 h, live cells were

washed and imaged immediately because LTY is non-fixable (Van der Velden et al., 2013) and was observed to have a short retention time (< 30 min).

Both fixed and live cells were imaged using a laser scanning confocal microscope (LSCM, LSM 710, Zeiss AxioObserver, Carl Zeiss Microscopy, Jena, Germany) with a Plan-Apochromat 40×/1.30 numerical aperture oil objective. DAPI and Hoechst 33342 were excited with a 405 nm diode laser and emissions were recorded with a band-pass filter of 454/44 nm (blue). For LTY detection, the stain was excited with a 488 nm argon laser and its emission was collected with a band-pass filter of 523/30 nm (green). NP and CMDR fluorescence were imaged at 561 nm (solid-state laser) and 633 nm (HeNe laser) and emissions were captured with 600/38 nm (red) and 695/45 nm (magenta) band-pass filters, respectively. Multi-color images were taken with the pinhole set to 1 airy unit, digitized at Nyquist sampling rate and analyzed using ZEN 2011 lite Edition software (Carl Zeiss Microscopy, Jena, Germany). Three-dimensional z-stack images were surface or spot rendered and then animated using Imaris software (v. 7.0, Bitplane, Zurich, Switzerland) to visualize intracellular NP localization while co-localization of NPs (red spheres) and lysosomes (green spheres) were quantified using ImageJ 1.49 software (Rasband, 2012). The gain and offset for the different channels of LSCM were kept constant for each experiment to allow qualitative comparison of the cell fluorescence intensities.

### **5.2.8 Statistical analysis**

Prism 6 for Mac OS X (v. 6.0h; GraphPad Software Inc.) was used for graphing and statistical analyses. Significance relative to control was determined

using a one-way analysis of variance (ANOVA) with a Dunnett's post hoc test. Results are reported as the percentage of uptake normalized to cells treated with fluorescent biomarkers or NPs in the absence of inhibitors at room temperature such that the level of uptake in these positive controls was set to 100%. Uptake was calculated by dividing the fluorescence of cells treated with fluorescent biomarkers or NPs in the presence of inhibitors by that of cells treated with fluorescent biomarkers or NPs alone at room temperature. Data are reported as mean  $\pm$  standard error of the mean (SEM) of 3-4 independent replicates. The threshold for significance was set at  $p < 0.05$ .

## **5.3 RESULTS**

### **5.3.1 Physicochemical properties of nanoparticle suspensions**

Physicochemical characteristics of NPs suspended in either ddH<sub>2</sub>O or L-15 medium over time are reported in **Table 5-1**. Results showed that water-dispersed NP suspensions were more aggregated (hydrodynamic diameter  $\leq 1373.0 \pm 494.8$  nm), polydisperse (polydispersity index  $\leq 0.8 \pm 0.2$ ), negatively charged ( $\zeta$  potential  $\leq -24.1 \pm 1.2$  mV), acidic (pH  $\leq 5.4 \pm 0.1$ ), and less stable over time compared to NPs suspended in cell culture medium (hydrodynamic diameter  $\leq 99.9 \pm 25.1$  nm;

**Table 5-1. Physicochemical characteristics of NP suspensions.** Time-dependent changes in hydrodynamic diameter (nm), polydispersity index,  $\zeta$  potential (mV), and pH of 10 and 25  $\mu\text{g/mL}$  NPs suspended in either ddH<sub>2</sub>O or L-15 medium. Data are presented as mean  $\pm$  SEM.

Concentration ( $\mu\text{g/mL}$ )	Solvent	Time (h)	Hydrodynamic diameter (nm)	Polydispersity index	$\zeta$ potential (mV)	pH
10	ddH <sub>2</sub> O	0	937.4 $\pm$ 310.8	0.7 $\pm$ 0.2	-13.8 $\pm$ 1.6	5.4 $\pm$ 0.1
		1	445.4 $\pm$ 169.6	0.5 $\pm$ 0.1	-11.8 $\pm$ 1.0	5.2 $\pm$ 0.1
	L-15 medium	0	15.7 $\pm$ 0.1	0.3 $\pm$ 0.0	-8.1 $\pm$ 1.2	7.3 $\pm$ 0.0
		1	15.9 $\pm$ 0.2	0.3 $\pm$ 0.0	-8.1 $\pm$ 0.6	7.3 $\pm$ 0.1
25	ddH <sub>2</sub> O	0	1373.0 $\pm$ 494.8	0.8 $\pm$ 0.2	-24.1 $\pm$ 1.2	4.9 $\pm$ 0.0
		1	355.4 $\pm$ 58.7	0.5 $\pm$ 0.1	-18.5 $\pm$ 0.8	4.7 $\pm$ 0.1
	L-15 medium	0	99.9 $\pm$ 25.1	0.2 $\pm$ 0.0	-10.7 $\pm$ 0.2	7.1 $\pm$ 0.1
		1	98.3 $\pm$ 6.0	0.2 $\pm$ 0.1	-10.8 $\pm$ 0.5	7.2 $\pm$ 0.1

polydispersity index  $\leq 0.3 \pm 0.0$ ;  $\zeta$  potential  $\leq -10.8 \pm 0.5$  mV; pH  $\leq 7.3 \pm 0.1$ ;  
**Table 5-1).**

### **5.3.2 Uptake and intracellular localization of nanoparticles**

The significant reduction of biomolecule association by CPZ, GN and WN indicated that CME, CavME, and MP pathways are present in RTgill-W1 cells and confirmed the applied inhibition protocol. Inhibitors CPZ, GN and WN significantly reduced cellular association of Tf-FL ( $48.6 \pm 0.8\%$ ), CTb-FITC ( $78.8 \pm 6.2\%$ ) and Dex-FL ( $61.4 \pm 7.3\%$ ), respectively, relative to positive control cells (**Figure 5-1**). Fluorescence of cells incubated with L-15 medium or DMSO alone were also significantly lower than the positive control ( $< 21.4 \pm 3.3\%$ ; **Figure 5-1**).

While treatment with CPZ significantly reduced NP association to  $68.6 \pm 6.8\%$  of NP-treated cells, GN and WN had no statistically significant effect but reduced NP association to  $84.3 \pm 9.2\%$  and  $73.1 \pm 12.8\%$ , respectively (**Figure 5-2**). Negligible fluorescence was observed in negative control cells ( $< 1.6 \pm 0.4\%$ ) and NP uptake was significantly reduced to  $36.1 \pm 5.8\%$  of NP treated cells when the temperature was lowered to  $2^\circ\text{C}$  (**Figure 5-2**). LSCM images support the above findings (**Figure 5-3 and 5-4**). When compared to cells incubated with NPs alone (**Figure 5-3A-D**), fluorescence intensities of cells concomitantly treated with NPs and inhibitors, except GN, were visually lower (**Figure 5-3E-P**). In addition, no cell fluorescence was observed with either L-15 medium or with solvent controls (**Figure 5-4A-H**) and minimal NR staining was noted with cells exposed to NPs at  $2^\circ\text{C}$  (**Figure 5-4I-L**).

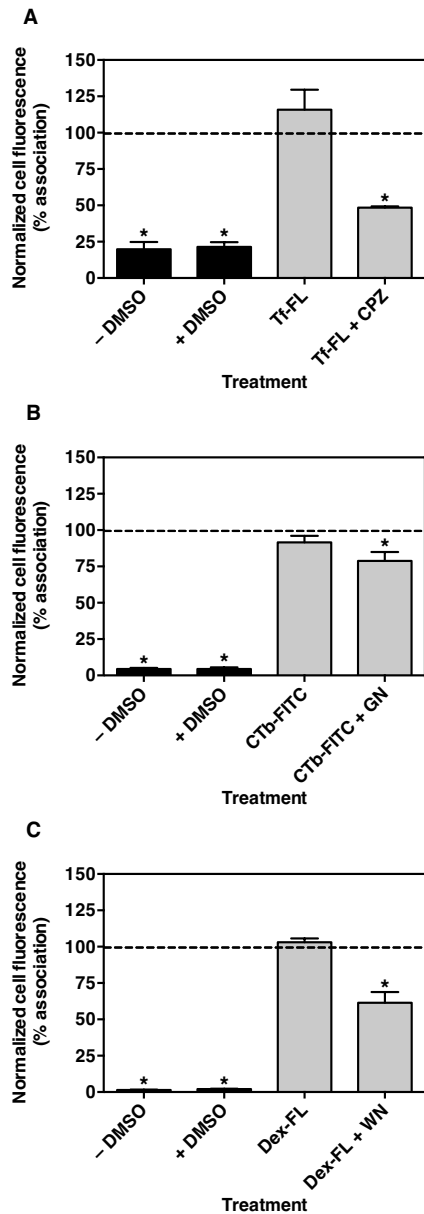


**Figure 5-1. Effects of pharmacological inhibitors on the association of fluorescently labelled biomolecules with RTgill-W1 cells.** Cells were pre-treated with (A) CPZ, (B) GN, or (C) WN for 30 min, treated with (A) Tf-FL, (B) CTb-FITC, or (C) Dex-FL, respectively, for 30 min in the absence of the inhibitor, and analyzed by flow cytometry. Cells incubated with L-15 medium alone (–DMSO), L-15 medium and DMSO (+ DMSO), or fluorescent biomarker alone served as the medium, solvent, and positive controls, respectively. Results are reported as the percentage of association relative to cells treated with DMSO and fluorescent biomarker (dotted line). Data are presented as mean  $\pm$  SEM of three independent experiments. The asterisk (\*) indicates significant difference compared to cells treated with DMSO and fluorescent biomarker (ANOVA, Dunnett,  $p < 0.05$ ).

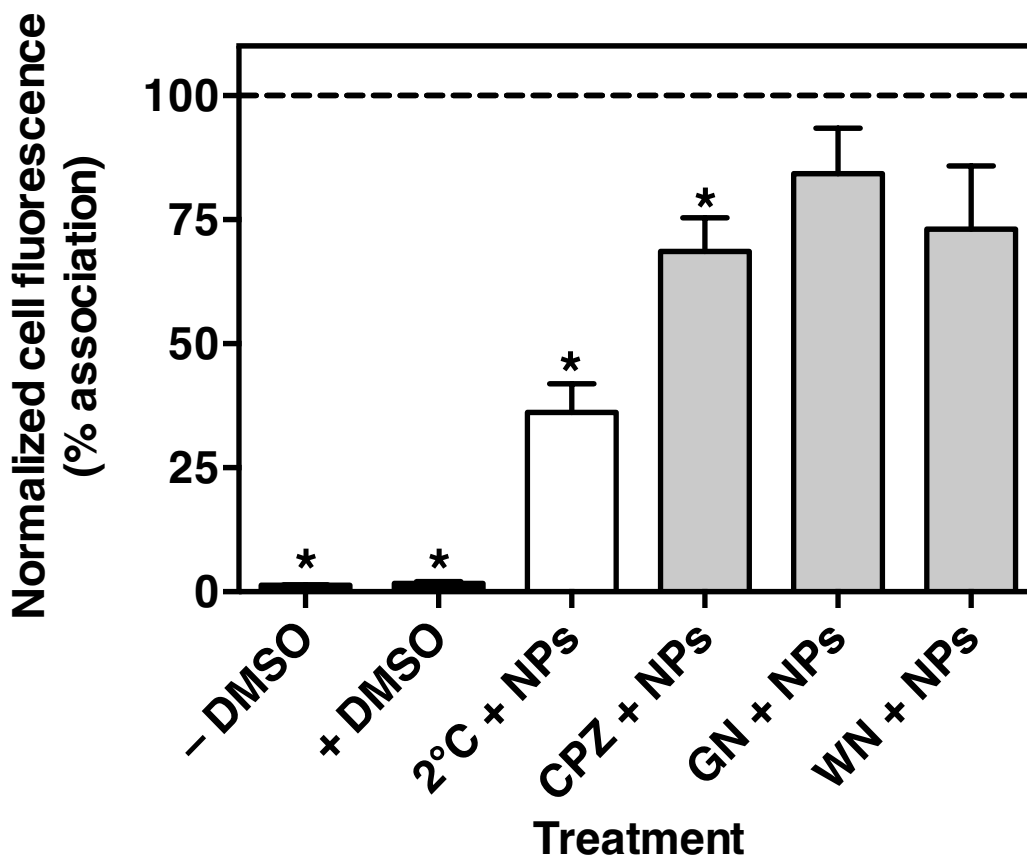


**Figure 5-2. Effect of endocytosis inhibitors on the association of 3-9 nm NPs with RTgill-W1 cells.** Cells were pre-incubated with CPZ, GN, or WN for 30 min, incubated with 25  $\mu\text{g}/\text{mL}$  NPs for 1 h in the presence of the inhibitor, and analyzed by flow cytometry. Cells incubated with L-15 medium alone (– DMSO), L-15 medium and DMSO (+ DMSO), or NPs at 2 °C (2°C + NPs) which served as the medium, solvent, and temperature controls, respectively. Results are reported as the percentage of association relative to NP treated cells without inhibitors at room temperature (dotted line). Data are presented as mean  $\pm$  SEM of four independent experiments. An asterisk (\*) indicates significant difference compared to cells treated with NPs at room temperature (ANOVA, Dunnett,  $p < 0.05$ ).

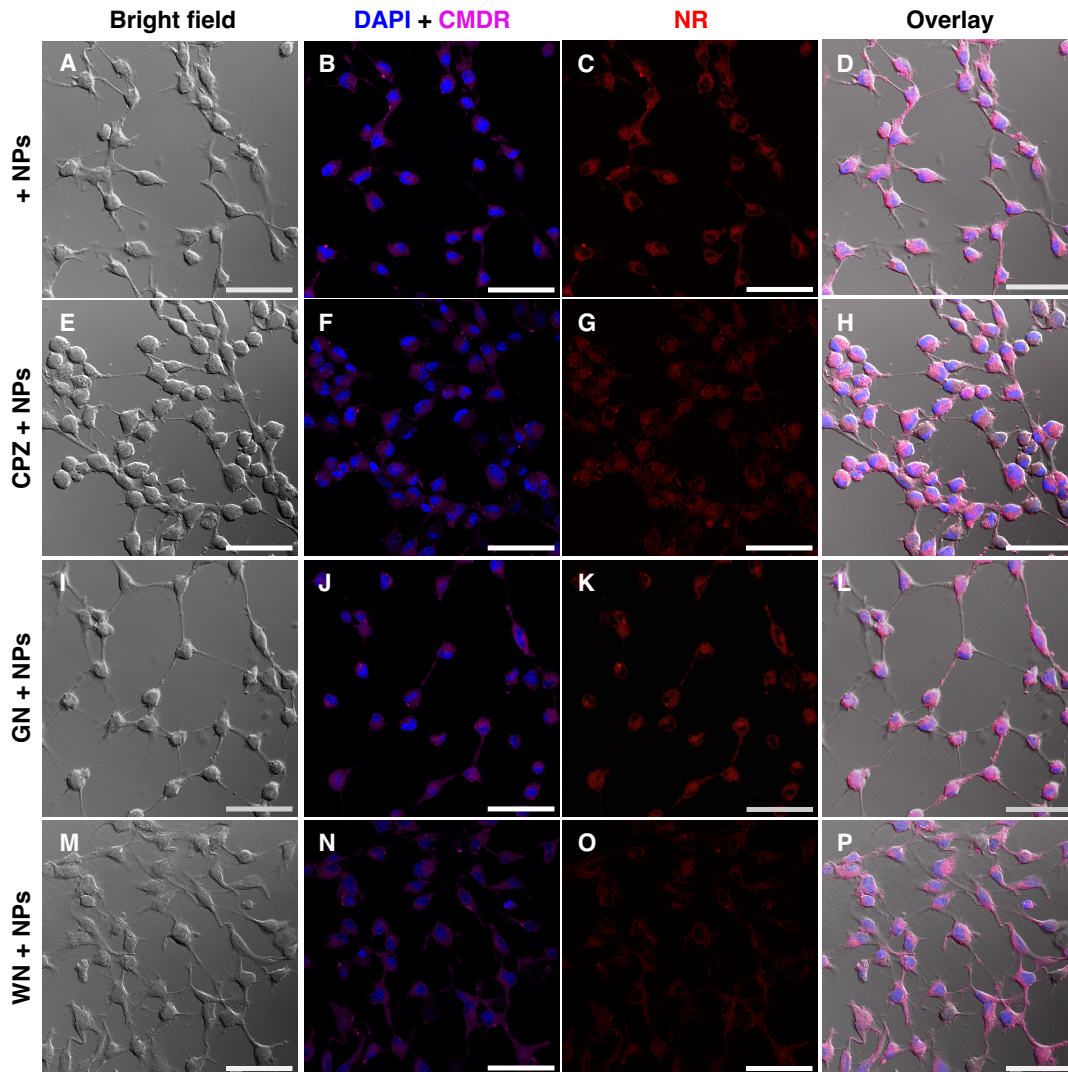


**Figure 5-3. LSCM images revealed NP association with RTgill-W1 cells.** (A, E, I, M) Representative bright field micrographs after differential interference contrast, (B, F, J, N) DAPI, CMDR, and (C, G, K, O) NR fluorescence micrographs, as well as (D, H, L, P) overlay micrographs of RTgill-W1 cells. (A–D) Untreated cells in the presence (+) of 25  $\mu\text{g}/\text{mL}$  NPs. (E–H) CPZ, (I–L) GN, and (M–P) WN-treated cells in the presence of NPs. The blue fluorescence of DAPI and the magenta fluorescence of CMDR were used respectively as probes for cell nucleus and plasma membrane. Scale bars are 50  $\mu\text{m}$ .

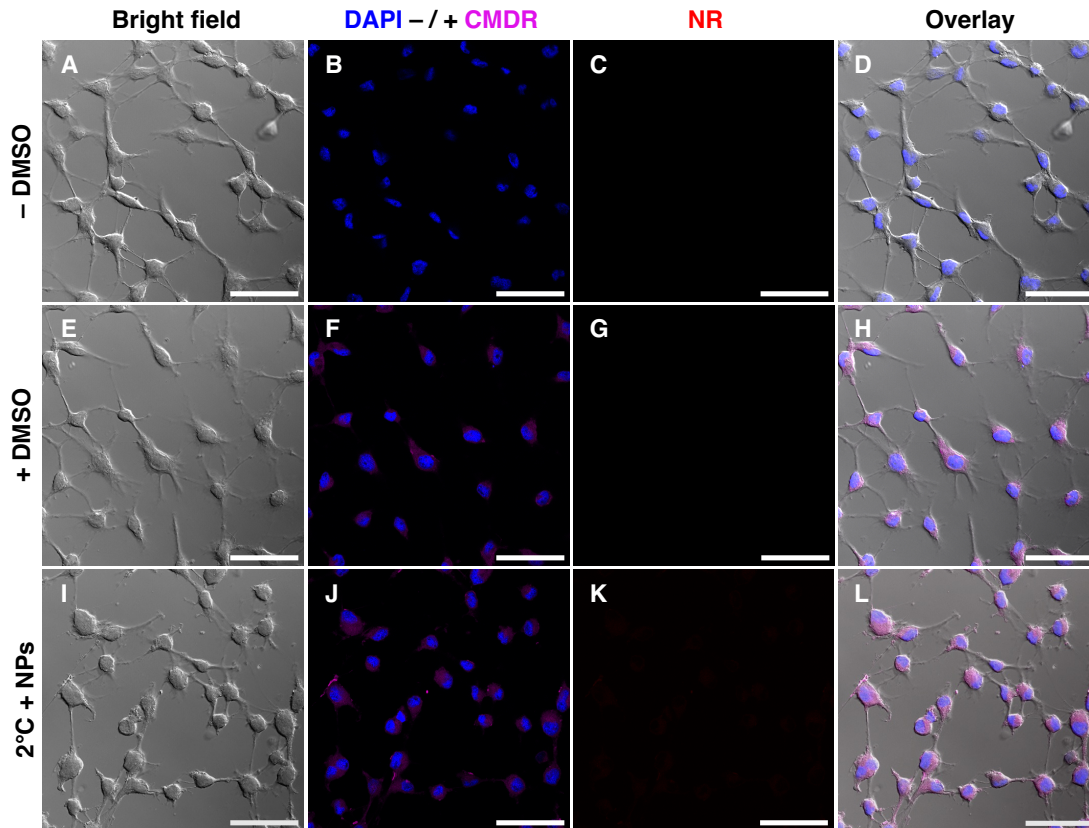


**Figure 5-4. LSCM images of negative control cells.** (A, E, I) Representative bright field micrographs after differential interference contrast, (B, F, J) DAPI, CMDR, and (C, G, K) NR fluorescence micrographs, as well as (D, H, L) overlay micrographs of RTgill-W1 cells. (A–D) Cells incubated in L-15 medium alone (– DMSO) without CMDR stain. (E–H) DMSO treated cells (+ DMSO) stained with CMDR. (I–L) Cells incubated at 2 °C in the presence of NPs and stained with CMDR. The blue fluorescence of DAPI and the magenta fluorescence of CMDR were used as probes for cell nucleus and plasma membrane, respectively. Scale bars are 50  $\mu$ m.

Three-dimensional LSCM images show globules of NR fluorescence within cells (**Figure 5-5**) and indicate that many NPs were associated with lysosomal compartments (**Figure 5-6 and 5-7**). Of the 56 NPs (red spheres) and 43 lysosomes (green spheres) discernable in **Figure 5-7**, 29% of NPs co-localized with the lysosomal marker at 3 h post-exposure to NPs.

## 5.4 DISCUSSION

In the present study, we have demonstrated that fluorescent PAA NPs utilized the CME pathway to enter RTgill-W1 cells and became localized within lysosomal compartments. Physicochemical properties including size and surface charge are known to govern the entry of NPs into cells (Kou et al., 2013). According to the supplier, the spherical NPs used in this study were 3-9 nm in size and loaded with NR, which was physically absorbed by the polymer creating strong fluorescent signals with little photo bleaching. Although our DLS measurements suggested that L-15 medium improved the stability of the NPs over time, aggregate sizes were much larger in cell culture medium ( $99.9 \pm 25.1$  nm) and in ddH<sub>2</sub>O ( $\leq 1373.0 \pm 494.8$  nm) compared to the size range reported by the manufacturer. Furthermore, NP aggregates were more polydisperse in ddH<sub>2</sub>O ( $\leq 0.8 \pm 0.2$ ) than in cell culture medium ( $\leq 0.3 \pm 0.0$ ). Schultz et al. (2012) demonstrated that  $\sim 54.5$  nm citrate-capped Ag NPs impeded sodium uptake in gills of juvenile rainbow trout, and suggested that noted effects were NP-specific rather than dissolution-based. Similar to our results, Kühnel et al. (2009) showed that FBS prevented the agglomeration of tungsten carbide NPs

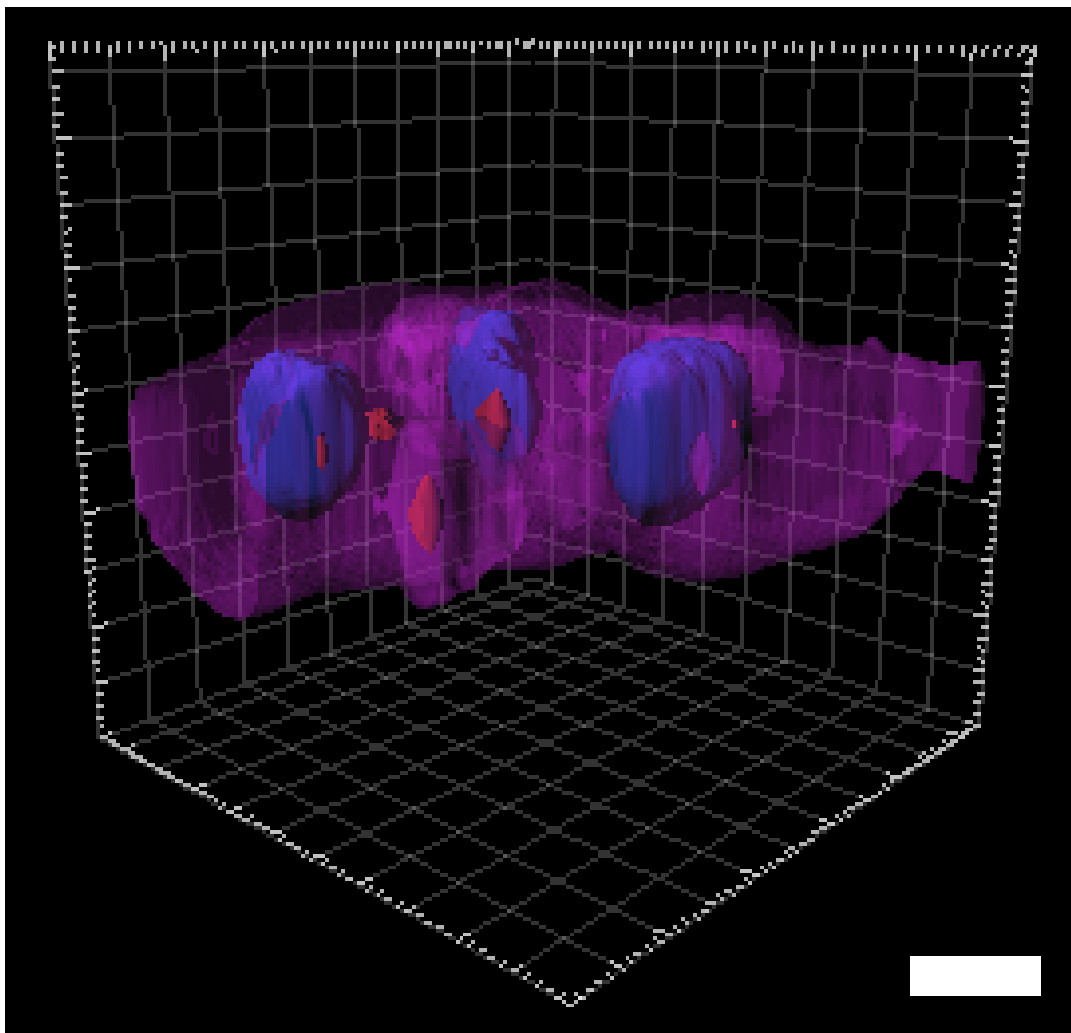


**Figure 5-5. Three-dimensional rendering of RTgill-W1 cells following a 1 h exposure to 25  $\mu\text{g}/\text{mL}$  NPs (red). Nuclei were stained blue with DAPI and the plasma membrane was stained magenta with CMDR (70% transparent surface). Scale bar is 10  $\mu\text{m}$ .**

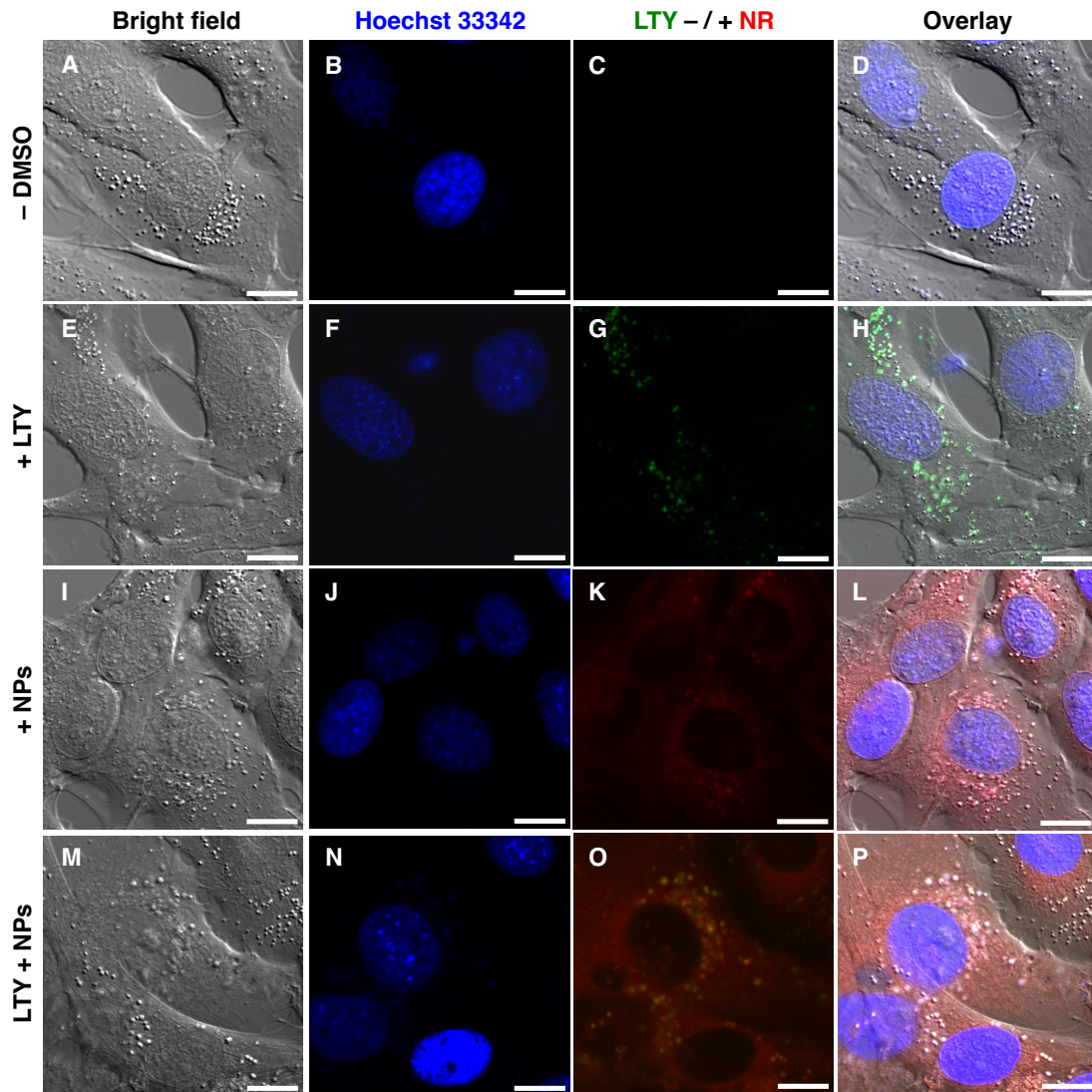


**Figure 5-6. Association of NPs with lysosomes of RTgill-W1 cells.** (A, E, I, M) Representative bright field micrographs after differential interference contrast, (B, F, J, N) Hoechst 33342, (C, G, K, O) LTY, and NR fluorescence micrographs, as well as (D, H, L, P) overlay micrographs of RTgill-W1 cells. Treatments are as follows: (A–D) Cells incubated in L-15 medium alone (– DMSO), (E–H) cells stained with (+) LTY, (I–L) cells following a 1 h incubation with 10  $\mu\text{g}/\text{mL}$  NPs, and (M–P) cells with LTY and NPs combined. Yellow spots indicate NPs close to (co-localized with) lysosomes. Scale bars are 10  $\mu\text{m}$ .

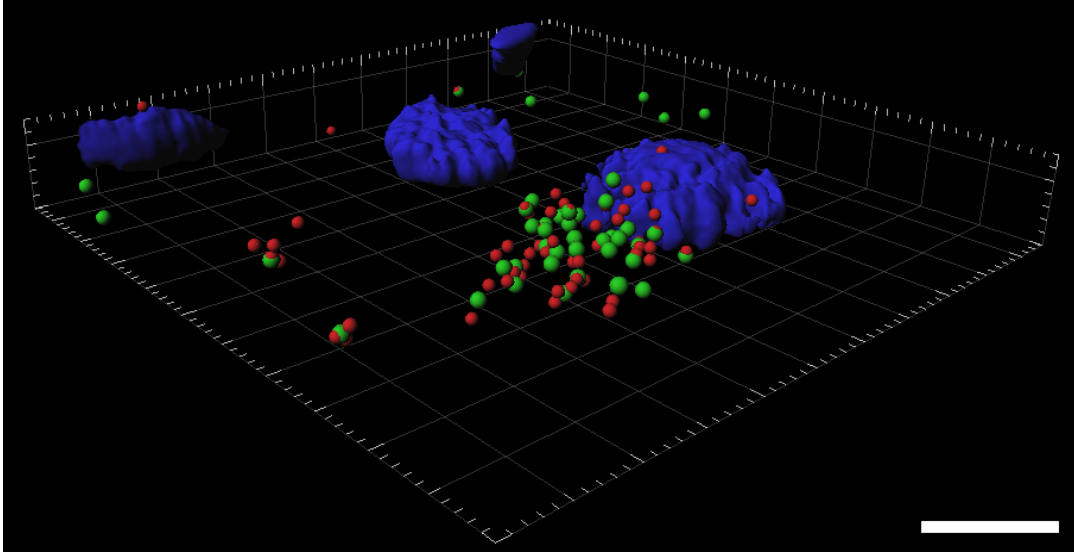


**Figure 5-7. Three-dimensional rendering of RTgill-W1 cells following coexposure to 10  $\mu\text{g}/\text{mL}$  NPs (red spheres) and LTY (green spheres). Nuclei were stained blue with Hoechst 33342. Scale bar is 10  $\mu\text{m}$ .**

suspended in L-15 medium due to the electrosteric stabilization of serum proteins, and noted rapid agglomeration of NPs in serum-free media over a 30 min observation period. Conversely, Monti et al. (2015) observed increased agglomeration of polystyrene NPs in cell culture medium supplemented with 2% FBS compared to serum-free media and suggested that NP agglomeration and adsorption of serum proteins to the NP surface need to be considered in uptake studies. It is noteworthy that cell culture media normally contains biomolecules including proteins and lipids, as well as other small molecules such as salts, that adsorb to the NP surface forming a biomolecular corona, which have been found hinder the accurate characterization of certain NPs in exposure suspensions (Baolog et al., 2015; Monopoli et al., 2012). Positively charged NPs bind to negatively charged cell membranes due to electrostatic interactions while negatively charged NPs, like those used in our study, cluster around cationic sites of the proteins in cell membranes due to repulsive interactions (Kou et al., 2013). The  $\zeta$  potential of the NPs dispersed in L-15 medium was less negative ( $\leq -10.8 \pm 0.5$  mV) compared to those suspended in ddH<sub>2</sub>O ( $\leq -24.1 \pm 1.2$  mV), and we suspect that this effect may have been attributed to the cloaking ability of the biomolecular corona (Baolog et al., 2015; Monopoli et al., 2012; Schultz et al., 2014). Moreover, serum proteins also adds buffering capacity to the cell culture medium (Jung et al., 2012), which explains the lower more acidic pH of the water-dispersed NP suspensions ( $\leq 5.4 \pm 0.1$ ) compared to the near-neutral pH of the NPs dispersed in L-15 medium ( $\text{pH} \leq 7.3 \pm 0.1$ ).

The endocytosis inhibitors CPZ, GN and WN significantly reduced uptake of the positive control biomolecules, indicating that CME, CavME and MP pathways

were present in RTgill-W1 cells and that NPs exploited these pathways to enter cells. We observed a significant reduction of both Tf-FL and NP uptake in the presence of CPZ, suggesting that the CME was the primary uptake pathway for 3-9 nm NPs in RTgill-W1 cells. Similarly, dos Santos et al. (2011) demonstrated that Alexa fluor 488 labelled Tf was strongly inhibited by CPZ in human cervix epithelium HeLa, human glial astrocytoma 1321N1, and human lung epithelium A549 cells, and noted a size-dependent inhibition of carboxylated polystyrene NP uptake by CPZ using the 1321N1 cell line, where stronger inhibitory effects were observed for larger particles. The latter study reported no significant reduction in cell viability after a 2 h exposure to CPZ. Interestingly, Firdessa et al. (2014) showed that while CPZ effectively blocked the uptake of Alexa fluor 488 labelled Tf, WN and other endocytosis inhibitors had a lesser effect or even increased the uptake of Tf in 293T kidney epithelial cells. These results suggest that Tf is specifically internalized via the CME pathway. Although NP uptake was inhibited by CPZ, implicating the involvement of CME, it should be noted that CPZ also inhibit GTPases, which regulates MP and other internalization pathways (Conner and Schmid, 2003; Vercauteren et al., 2009). Therefore, CPZ cannot be regarded as a specific inhibitor of the CME pathway and may have also contributed to decreased NP uptake by preventing internalization through the GTPase-mediated MP pathway.

We observed a significant but low inhibition of CTb-FITC and Dex-FL by GN and WN, respectively, but a non-significant reduction for NPs, indicating that these pathways can be effectively blocked in RTgill-W1 cells. Using human lung epithelium A549 cells, dos Santos et al. (2011) reported that the internalization of

Alexa fluor 488 labelled CTb was not significantly inhibited by GN and also suggested that this finding was likely attributable to the poor specificity of CTb for the CavME pathway. Using the macrophage-like J774A.1 cell line, Fernando et al. (2010) showed that  $18 \pm 5$  nm poly[(9,9-dioctylfluorenyl-2,7-diyl)-co-(1,4-benzo-{2,1',3}-thiadazole)] conjugated polymer NPs co-localize with Texas Red Dex and found that uptake of these NPs was inhibited by WN, both findings implicated MP as the primary uptake mechanism for NPs; no significant cytotoxic effects were observed.

In mammalian cells cultured at 37 °C, endocytosis, and other energy-dependent pathways can be inhibited by lowering the temperature to 4 °C (Firdessa et al., 2014; Jiao et al., 2009). To further verify that NPs were internalized via an active transport process (as opposed to passive transport), cells were incubated in parallel at room temperature (normal cell culture conditions) and at 2 °C. Incubation with NPs at 2 °C resulted in a strong inhibition of endocytosis, as expected. The critical thermal minima for rainbow trout is 2 °C; typically determined by steadily decreasing the temperature of the water until fish movements become disorganized and/or neutral buoyancy is lost (Currie et al., 1998). Since NP uptake was not completely inhibited at 2 °C, we suspect that some energy-dependent transport processes remained active in RTgill-W1 cells because of the low critical temperature tolerances for rainbow trout survival (Molony, 2001). Low temperatures also inhibit exocytosis (Mori et al., 2000); therefore, we concluded that NP uptake was effectively reduced when active transport processes were disrupted.

Two-dimensional LSCM images complement our abovementioned findings while three-dimensional computer-rendered images of cells stained with CMDR indicated that NPs were present in the cytoplasm and accumulated in intracellular vesicles. Using a combination of transmission electron microscopy (TEM) and energy dispersive X-ray spectroscopy, Farkas et al. (2011) observed both small groups of polyvinylpyrrolidone-coated silver NPs in vesicles as well as individual particles in the cytoplasm of rainbow trout gill cell monolayers, and our results support their findings. Similarly, Kühnel et al. (2009) observed both individual and agglomerated tungsten carbide NPs in the cytoplasm of RTgill-W1 cells. Moreover, Greulich et al. (2011) demonstrated that polyvinylpyrrolidone-coated silver NPs were located within endo-lysosomal structures and in the perinuclear region of human mesenchymal stem cells. It is believed that NPs can escape the endosomal-lysosomal pathway and exhibit perinuclear localization due to the 'proton sponge' effect (Kou et al., 2013). This hypothesis states that polycations become protonated in acidic cellular compartments, which causes an influx of chloride ions and water leading to lysosomal swelling and rupture (Boussif et al., 1995).

To visualize NP co-localization with lysosomes, cells treated with both 10 µg/mL NPs and LTY were imaged in two- and three-dimensions using LSCM. It is clear from the images that NPs end up in intracellular organelles, many of them lysosomes, similar to several other NP-cell systems (Bramini et al., 2014; Greulich et al., 2011; Rejman et al., 2004). All pathways except CavME are affiliated with lysosomes (Kou et al., 2013). The fate of macropinosomes in the MP pathway is cell type-specific (Kou et al., 2013). In macrophages, for example, macropinosomes fuse

with lysosomes, whereas in human A431 cells, macropinosomes are trafficked back to the cell membrane and release their cargo to the extracellular fluid (Kou et al., 2013). Fluorescent polystyrene NPs have been shown to co-localize with the endosomal marker FM4-64FX and with the endosome/lysosome marker lysosensor blue within bone marrow derived macrophages (Firdessa et al., 2014). Using TEM, Bols et al. (1994) confirmed the presence of lysosomes in RTgill-W1 cells. We also observed lysosomes in RTgill-W1 cells and found that many NPs were associated with these acidic compartments, which further confirms the involvement of the CME pathway in NP uptake. It is noteworthy that our quantification does not account for the possibility that several NPs or agglomerates may have been identified as a single red sphere due to the limited resolution of the LSCM. It is likely that most of the remaining NPs were in early endosomal CME pathways that were not yet acidified. Alternatively, the NPs that did not appear co-localized may be either in the cytoplasm itself or potentially associated with compartments resulting from other uptake pathways. Following a 10 min exposure, 100 nm carboxylated polystyrene NPs have been shown to accumulate in the lysosomes of human brain capillary microvascular endothelial hCMEC/D3 cells and remained present in these acidic vesicles 24 and 48 h after the initial exposure (Bramini et al., 2014). A NP entering the CME pathway will be subjected to a drop in pH as it transitions from clathrin-coated vesicles (pH 7.0) to early endosomes (pH 6.5), and will experience an even further reduction in pH as it transitions from late endosomes (pH 6.0) to lysosomes (pH 4.5-5.0) (Khalil et al., 2006; Mindell, 2012). The acid hydrolases present in lysosomes may have degraded the NPs used in this study (Luzio et al., 2007); however, this remains

to be demonstrated. The lowered pH may trigger the release of active ingredients encapsulated within the NPs and induce cytotoxicity (Zhang et al., 2016).

## **5.5 CONCLUSIONS**

Our results clearly show that NP uptake by RTgill-W1 cells was mediated through energy-dependent CME endocytosis and the propensity of NPs to accumulate in lysosomes makes them a suitable candidate for targeted drug delivery applications. Since many pharmacological inhibitors are non-specific, we recommend using several drugs that inhibit the same endocytotic pathway to validate the findings of future mechanistic studies. Moreover, the fate and effects of NPs within subcellular organelles including the nucleus, mitochondria, Golgi apparatus, and endoplasmic reticulum remain to be investigated. The probability that live RTgill-W1 cells secreted NPs through exocytosis under normal physiological temperature cannot be ignored and warrants further investigation (Sakhtianchi et al., 2013). Further research examining the endocytosis and exocytosis mechanisms is essential to improve the safe application of NP-based insecticides and/or fungicides. Understanding the mechanisms by which NPs interact with cells could provide new insights into the design of NPs for targeted delivery of the active ingredients in insecticide and/or fungicide formulations and could lead to new and more sustainable approaches to pest management in agricultural systems.

## **CHAPTER 6**

### **Conclusions and future directions**

## 6.1 CONCLUSIONS AND FUTURE DIRECTIONS

Developing fish are highly sensitive and vulnerable to toxicants and may provide advanced warning of their potential hazard upon release into the aquatic environment (Powers, 1989). Widespread production and use of functionalized nanomaterials (NMs) mean that they will inevitably contaminate aquatic ecosystems and interact with fishes (Mitrano et al., 2015). My doctoral thesis examined the physicochemical characteristics of functionalized NMs and their effects at multiple levels of biological organization using *in vivo* and *in vitro* fish model systems. The experiments presented in this thesis focused on addressing the four main goals outlined in the introduction: To (1) develop simple and reproducible *in vivo* and *in vitro* methods for NM toxicity testing that could be employed by fellow nanotoxicologists, industry, risk assessors, and regulators, (2) determine whether physicochemical properties including surface functionalization and environmental factors like ultraviolet (UV) light modulate NM toxicity, (3) assess the toxicological effects of several functionalized metal oxide and carbon-based NMs at multiple levels of biological organization, and (4) elucidate the mechanisms underlying noted toxicity as well as NM uptake by fish embryos and cells. My original contribution to knowledge with respect to the abovementioned goals is highlighted below. Specifically, I will draw general conclusions by relating the data presented in **Chapters 2-5** to the specific research questions and hypotheses set out in the introduction, provide several recommendations for future research, and finally, discuss my outlook toward the fields of nanotechnology and nanotoxicology.

### 6.1.1 General conclusions

To accurately assess the potential hazard associated with engineered NMs, reliable toxicity screening methods are needed to determine how their physicochemical properties relate to differential biological or ecological responses (Oberdörster et al., 2005a). *In vivo* (whole-animal) assays should supplement *in vitro* (cellular and molecular) tests to better understand the biological effects of NMs and to complement research findings (Oberdörster et al., 2005a). I have developed several *in vivo* and *in vitro* methods for nanotoxicity testing during my graduate studies. Briefly, I played a key role in the implementation of a novel approach for the precise measurement of metal oxide NM dissolution over time via membrane dialysis (see **Chapter 2**), formulated techniques to visualize and measure NM adsorption to zebrafish (*Danio rerio*) embryos (see **Chapter 2**), perfected a zebrafish embryo-larval toxicity assay to examine the acute toxicity of metal oxide and carbon-based NMs at whole-animal, biochemical and molecular levels of biological organization (see **Chapters 2 and 3**), rigorously designed and built an apparatus that closely simulated natural sunlight to investigate the effect of UV radiation on metal oxide NM phototoxicity (see **Chapter 4**), and devised quantitative and qualitative methods for determining specific endocytosis mechanisms involved in the uptake of NMs and their subsequent fate within adherent gill epithelial cells (see **Chapter 5**). Some of my colleagues have utilized the simulated sunlight apparatus for their studies and my interesting findings have prompted the potential purchase of a humidity- temperature- and UV light controlled chamber for future work. By

establishing simple and reproducible *in vivo* and *in vitro* methods designed to assist nanotoxicologists in their accurate assessment of the responses of fishes to many different types of NMs, I was able to fulfill the first goal of my thesis and make considerable contributions to and fill some important information gaps in the multidisciplinary field of aquatic nanotoxicology.

All NMs used in my research were negatively charged and had either different cores with the same surface coating (see **Chapter 2**) or had different surface functionalizations with identical core structures (see **Chapter 3**). I predicted that size, agglomeration, and surface charge modulates NM toxicity because surface area and reactivity increase with decreasing particle size (see section 1.3.1) (Pietroiusti et al., 2014). Without making proper comparisons between bulk materials or NMs with different charges (i.e. neutral, no charge, or positive) and the NMs used in my studies, I was unable to determine how these properties affect NM toxicity directly. I did, however, attempt to link the characteristics of the NMs tested with certain aspects of toxicity. My research emphasizes the importance of characterizing the physicochemical properties of NMs before, during and after administration or exposure and in the context of toxicity screening tests (i.e. under the same exposure conditions) (Oberdörster et al., 2005a; Schultz et al., 2014). I have learned, however, that NM toxicity does not solely depend on individual or a combination of properties intrinsic to the material itself. Various extrinsic abiotic environmental factors including ionic strength, natural organic matter, pH, sunlight, and temperature can also modulate NM toxicity. In **Chapter 2**, the free metal present in both NM stock suspensions and dissolved metal released from the NMs over 72 h was measured to

better understand pH-dependent dissolution properties. At near-neutral pH, very little ionic metal was released initially (i.e. at 30 min) and remained consistently low over the experimental period for all NM suspensions tested, suggesting that the polymer coating contributed to the stability of the NMs in suspension; this finding supports my original hypothesis stated in the introduction (see section 1.3.2). A negative correlation between pH and free metal release was also noted. In **Chapter 3**, a variety of trace metals were detected in both functionalized and nonfunctionalized single-walled carbon nanotube (SWCNT) suspensions. The highest metal concentrations were measured in lignin-wrapped SWCNT suspensions, which suggested that lignin acted as a chelating agent (Garcia-Valls and Hatton, 2003). It is well known that surface properties like charge affect NM agglomeration in suspension (Bantz et al., 2014) and size of the NM influences its interaction with living systems (Shang et al., 2014). Therefore, I cannot say with certainty that surface functionality affected SWCNT toxicity directly or that chemical moieties can be used to predict the toxicity of NMs in general. However, my findings suggested that surface functional groups played a key role in noted biological effects resulting from acute SWCNT exposure. Furthermore, I reported that while uncoated metal oxide NM and UV light co-exposures delayed zebrafish hatch and altered the expression of an antioxidant defense-related gene, these effects were not observed in zebrafish concomitantly exposed to polymer-coated metal oxide NMs and UV light. Lipid peroxidation was also less severe in larvae exposed to polymer-coated NMs compared to their uncoated counterparts. These findings verify my initial hypothesis (see section 1.3.5) and imply that the polymer coating mitigates UV-mediated effects

in developing zebrafish because it inhibits the formation of reactive oxygen species (ROS) by preventing the direct contact between the NM surface, oxygen, and water (Smijs and Pavel, 2011). The abovementioned findings clearly show that both surface functionalization and UV radiation modulate NM toxicity, which answers my research question, supports my hypothesis (see section 1.3.3), and accomplishes the second goal of my thesis.

To achieve the third goal of my thesis, I sought to examine whole-animal effects resulting from acute exposure to high concentrations of metal oxide NMs under controlled laboratory conditions (see **Chapter 2**), then I used different fish species to investigate lethal and sublethal effects at organismal, cellular, and molecular levels of biological organization caused by acute exposure to high concentrations of carbon-based NMs under laboratory conditions (see **Chapter 3**), and finally, I explored the whole-animal, biochemical, and molecular level effects attributed to lower concentrations of metal oxide NMs over a longer exposure period under more environmentally realistic laboratory conditions (see **Chapter 4**). Both functionalized and nonfunctionalized metal oxide and carbon-based NMs were found to have low toxicity at all concentrations tested and levels of biological organization examined. No apparent acute toxicity of polymer-coated metal oxide NMs under laboratory conditions was observed in **Chapter 2**, partially due to the protective zebrafish chorion and polymer coating. Under similar exposure conditions, carbon-based NMs generated adverse effects but only at concentrations higher than might normally be present in the environment (see **Chapter 3**). Neither NM nor paired free metal control exposures induced significant toxicity in zebrafish;

therefore, NM-specific effects could not be distinguished from dissolution-based effects (see section 1.3.2). Different functionalized SWCNTs both delayed and accelerated zebrafish hatch, and these developmental impairments were likely attributed to the direct interaction of individual NMs or small agglomerates with zebrafish hatching enzymes and slight hypoxia resulting from partial coverage of the chorion by adsorbed NMs, respectively. High concentrations of polymer NMs were also shown to completely inhibit zebrafish hatch, and I suggested that low pH ( $\leq$  pH 5.5) might explain this effect. For example, an optimum pH between 8.0 and 8.5 was reported for the hatching enzyme of the mummichog (*Fundulus heteroclitus*) (DiMichele et al., 1981). However, nanotoxicity tests conducted in the laboratory under controlled conditions do not fully represent the complexity of the environment. As discussed previously (see section 1.3.5 and **Chapter 4**), fluorescent lamps emit very little to no UV radiation (Safari et al., 2015), yet nano-sized wide band-gap semiconductors are known to generate harmful ROS in the presence of UV light. Failure to consider this mode of action could severely underestimate the potential risk associated with the release of photoreactive NMs into the aquatic environment.

Although I was unable to identify the precise molecular mechanism underlying SWCNT toxicity, microarray technologies that attempt to corroborate global gene expression profiles of SWCNT-exposed cells or tissues with biological responses may be useful in this regard (Zhao and Liu, 2012). Using this technique, Usenko et al. (2008) identified several key stress response genes in zebrafish embryos that were altered by fullerene C<sub>60</sub> (a type of carbon-based NM) exposure. Furthermore, an anoxic environment created via nitrogen bubbling (Ong et al. 2014b)

or exposure to H<sub>2</sub>O<sub>2</sub> may induce changes in *hif1ab* and *gclc* zebrafish gene expression, respectively. As predicted (see section 1.6.1), most negatively charged NMs adsorbed to the outermost membrane of embryonic zebrafish while some NMs passively diffused through pore canals and sorbed to the external surface of the developing fish within the chorion (see **Chapter 2**). However, the NMs bound to the external larval surface could not be distinguished from those that may have been taken up by the animal using *in vivo* methods. Therefore, a rainbow trout (*Oncorhynchus mykiss*) gill epithelial cell line was used in **Chapter 5** as an *in vitro* model to augment the abovementioned study with a mechanistic investigation of the cellular uptake of NMs and their subsequent intracellular fate. My results clearly show that NM uptake was significantly impeded by low temperature and by the drug chlorpromazine (CPZ), which suggested that certain NMs were actively internalized via clathrin-mediated endocytosis (CME). However, NM uptake was not abolished by treatment with any of the pharmacological inhibitors, which indicates that either multiple endocytosis pathways were involved, that the drugs induced nonspecific effects, or that the drugs used were not completely effective at the concentrations tested. Co-localization studies showed that NMs were trafficked to lysosomal compartments, which confirmed that CME was the dominant operative mechanism involved in the uptake of NMs by fish gill cells. These findings confirm my hypothesis (see section 1.2.2.1) and clearly demonstrated that certain NMs can traverse both acellular (i.e. the chorion) and cellular membranes due to their unique nanoscale properties. In addition, I have demonstrated that uncoated metal oxide NMs generate ROS in the presence of UV light only, which was a likely mode of action

underlying noted sublethal effects (see **Chapter 4**). I found that active and passive transport processes played a role in NM uptake by cells and embryos, respectively and that photocatalytic properties govern the phototoxicity of certain nanoscale semiconductors, which has allowed me to obtain my fourth thesis goal. The abovementioned studies have enhanced my understanding of complex nano-bio interactions and the results obtained both *in vivo* and *in vitro* imply a risk for aquatic organisms. Overall, my research has directly contributed to ongoing hazard assessment for NMs and facilitated the development of nanotoxicity tests and environmental safety and regulatory guidelines.

### **6.1.2 Recommendations for future research**

While this thesis provides valuable information regarding the intrinsic physicochemical properties and extrinsic environmental factors that modulate engineered NM toxicity, further research is needed to ensure their safe use and disposal. Several knowledge gaps regarding the potential hazard of NMs need to be addressed in order for risk assessors to accurately predict their potential impact on the environment. To meet these needs, I recommend that nanotoxicologists (1) move away from controlled mechanistic-oriented laboratory studies toward those that explore more complex, environmentally realistic matrices and exposure scenarios, (2) investigate whether polymer coating or other surface functionalizations lessen the severity of UV-mediated effects of different types of nanoscale semiconductors at the cellular level, (3) utilize several pharmacological inhibitors and intracellular biomarkers to accurately identify cellular uptake mechanisms and to visualize the fate

of NMs within cells, respectively, and (4) explore the absorption, distribution, metabolism, and excretion of functionalized NMs using fish model systems to determine clearance rates and potential sites of toxicity after systemic exposure.

#### ***6.1.2.1 Evaluate nanomaterial toxicity under environmentally realistic conditions***

Despite substantial recent progress in the field of nanotoxicology (Petersen et al., 2015; Selck et al., 2016), there is still a gap in knowledge in relation to the interactions between the environment and NMs, particularly their behaviour, bioavailability, effects, and fate (Schultz et al., 2014). Therefore, future nanotoxicology studies should attempt to address the potential effects resulting from a combination of chronic exposure and modelled or predicted environmental concentrations, and employ more environmentally realistic exposure scenarios. According to Amara's law, "we tend to overestimate the effect of a technology in the short run and underestimate the effect in the long run (Amara, 1972)." It is important to study lower concentrations over longer time periods because the physicochemical characteristics and toxic potential of NMs may change as they age or transform in the environment (Mitrano et al., 2015). Until reliable real-time detection techniques and monitoring instruments become available to accurately quantify engineered NMs in the environment, nanotoxicologists should examine NM concentrations below, at and above modelled or predicted environmental concentrations to facilitate risk assessments (Oberdörster et al., 2005a). Moreover, I recommend that natural waters obtained from local sources that contain natural organic matter should be used instead of synthetic or pristine media to disperse NMs for aquatic nanotoxicity studies.

### ***6.1.2.2 Assess functionalized nanomaterial phototoxicity at the cellular level***

The role of the surface coating in determining NM phototoxicity warrants further study. Other NMs including cerium oxide, iron oxide, zinc oxide and SWCNTs also exhibit photocatalytic properties (Alarifi et al., 2014; Dahle and Arai, 2015; Ma et al., 2013; Valdiglesias et al., 2016). The polymer-coated and uncoated forms of these NMs are available and could thus be used as models to close this gap in knowledge. Given the insufficient amount of information provided in the literature, reports that address UV-mediated toxicity of functionalized NMs under solar radiation at the cellular level are needed (Ma et al., 2013). Excessive ROS production can induce adverse cellular effects including the inability to proliferate and death (Riley, 1994) or facilitate NM accumulation and uptake into cells (Xie et al., 2011). Therefore, it would be interesting to examine UV-mediated cytotoxicity, time-dependent intracellular accumulation, and uptake in metal oxide NM exposed cells. Following cellular internalization, certain metal oxide NMs can induce cytotoxic effects via a Fenton reaction (Cortajarena et al., 2014). For example, iron oxide NMs taken up by cells may degrade within lysosomes and then free ferrous ions could traverse the mitochondrial membrane and react with hydrogen peroxide and oxygen produced therein and form ferric ions and highly reactive and damaging hydroxyl radicals (Cortajarena et al., 2014). Cell death could easily be quantified in NM and UV light coexposed cell populations using membrane-impermeable dyes such as propidium iodide to differentiate viable from non-viable cells using flow cytometry (Schultz et al., 2014). Furthermore, lipid peroxidation and DNA strand

breakage could be measured using thiobarbituric acid reactive substances (Janero, 1990) and DNA precipitation assays (Olive, 1988), respectively.

### ***6.1.2.3 Examine cellular uptake and fate of nanomaterials by several approaches***

A common misconception among researchers is that an endocytosis inhibitor possesses an absolute specificity toward the pathway of interest (Ivanov, 2008). Since many endocytosis inhibitors are known to induce nonspecific effects and undesirable modes of action (Dutta and Donaldson, 2013), I recommend using more than one type of drug that has the same function to verify the results of future mechanistic-oriented studies. For example, chloroquine, monensin or dynasore could be used alongside CPZ to inhibit CME (Dutta and Donaldson, 2013). However, dynasore may affect the actin cytoskeleton (Dutta and Donaldson, 2013) and reorganization of these filaments may disrupt uptake processes, leading to an erroneous interpretation of results (dos Santos et al., 2011). Therefore, a cytoskeletal stain like fluorescein phalloidin should be used in conjunction with the inhibitor dynasore to assess possible structural damage. Among different methods of CavME inhibition, filipin and nystatin produce the fewest nonspecific effects (Ivanov, 2008). These antibiotics disrupt the structure and function of cholesterol-rich membrane domains and decreasing the drug concentration can minimize potential side effects like membrane permeabilization (Ivanov, 2008). Although phosphoinositide 3-kinase inhibitors like wortmannin are widely employed to inhibit MP, they can effectively block uptake of ligands involved in CME and CavME pathways (Ivanov, 2008). It would also be interesting to determine whether some combination of endocytosis inhibitors would completely

abolish NM uptake. According to the proton-sponge hypothesis, NMs could potentially escape from lysosomes (Boussif et al., 1995). Therefore, the fate of NMs within other intracellular compartments including the endoplasmic reticulum, Golgi apparatus and mitochondria should be subsequently investigated using molecular probes such as BODIPY FL glibenclamide, CellLight Golgi-GFP, and MitoTracker Green FM, respectively.

#### ***6.1.2.4 Explore the toxicokinetics of functionalized nanomaterials using fish***

Detailed toxicokinetics studies that include absorption, distribution, metabolism and excretion of NMs through different exposure routes into fish are essential. After systematic administration *in vivo*, functionalized NMs are transported more efficiently throughout the human body compared to their nonfunctionalized counterparts, which has implications for targeted delivery of therapeutic agents (Subbiah et al., 2010). Indeed, this remains to be demonstrated in fish species and pharmacokinetic profiles for fish are lacking. Since the gill is a major site for metabolic waste excretion (Bury et al., 2014), cellular exocytosis of functionalized NMs from cells cannot be ignored and warrants further investigation. Endocytosis or the inward movement of plasma membrane vesicles was a major focus of my thesis; therefore, exocytosis or the trafficking of vesicles in the opposite direction to the cytomembrane should be addressed in future studies (Ivanov, 2008). By measuring fluorescence intensity over time, retention time or recovery from exposure to fluorescently labelled NMs could be elucidated to determine how long it takes for NMs to be cleared from the system. Improved knowledge of the mechanisms by

which NMs enter and exit cells could lead to new insights into the design of targeted delivery systems. The polymer NMs used in **Chapters 2 and 5** serve as carriers for systemic insecticide (bifenthrin) and/or fungicide (azoxystrobin) formulations in agriculture; however, the potential cytotoxicity of these nanocomposites remains to be investigated. Finally, continued multidisciplinary collaborations between nanotoxicologists and researchers from different fields including chemistry, engineering, and physics are strongly recommended. Taken together, new unconventional approaches to nanotoxicity testing are essential to accurately assess the potential hazard of functionalized NMs and to safely use these unique nanoscale materials in commercial, consumer, and industrial applications.

### **6.1.3 Outlook**

The interrelated fields of nanotechnology and nanotoxicology have progressed throughout my PhD and over the past decade. The Organisation for Economic Co-operation and Development Chemicals Committee Working Party on Manufactured Nanomaterials was established in 2006 to advise on issues related to the human health and environmental safety of engineered NMs and to ensure that hazard, exposure, and risk assessments are of the highest-quality. In 2011, the European Commission for Standardization recommended that NMs should be defined as “a natural, incidental or manufactured material containing particles, in an unbound state or as an aggregate or as an agglomerate and where, for 50% or more of the particles in the number size distribution, one or more external dimensions is in the size range 1-100 nm (European Commission, 2011).” Although this was an important

step in the right direction and many believe that a strict definition is needed to ensure that nanotechnology is safety integrated into society, some argue that NMs should not be defined (Maynard, 2011). The mineral Libby vermiculite, for example, contains harmful asbestiform fibres, but, for many years, it was left unregulated because it did not fit the definition of asbestos (Maynard, 2011). In 2013, the European Commission announced new cosmetics regulations that require engineered NMs and their physicochemical characteristics to be listed on product labels (European Commission, 2013). A few guidelines and guidance documents related to nanotoxicity testing have emerged in recent years (OECD, 2012b; 2012a; SCENIHR, 2009) and more are expected to become publically available by the end of this year (Rasmussen et al., 2016). Nanotoxicologists have begun to collaborate with scientists and engineers from all fields, modify their approaches to nanotoxicity testing, and think beyond conventional toxicology paradigms. More concerted and coordinated efforts are needed to close the gap between the development of nanotechnology-based applications and toxicological testing of nanoscale materials. Nanotechnology has the potential to build on the great progress already made and I am excited to see the impact that it will have on human health and the environment over the next decade.

## WORKS CITED

- Akiyama, T., Ishida, J., Nakagawa, S., Ogawara, H., Watanabe, S.-i., Itoh, N., et al., 1987. Genistein, a specific inhibitor of tyrosine-specific protein kinases. *The Journal of Biological Chemistry* 262(12), 5592–5595.
- Alarifi, S., Ali, D., Verma, A., Almajhdi, F.N., Al-Qahtani, A.A., 2014. Single-walled carbon nanotubes induce cytotoxicity and DNA damage via reactive oxygen species in human hepatocarcinoma cells. *In Vitro Cellular & Developmental Biology-Animal* 50, 714–722. doi: 10.1007/s11626-014-9760-3.
- Ali, S., van Mil, H.G.J., Richardson, M.K., 2011. Large-scale assessment of the zebrafish embryo as a possible predictive model in toxicity testing. *PLoS ONE* 6(6), e21076. doi: 10.1371/journal.pone.0021076.
- Amara, R., 1972. A framework for national science policy analysis (Report). Institute for the future, Menlo Park, California. OCLC 4484161.
- Andersen, C.B.F., Moestrup, S.K., 2014. How calcium makes endocytic receptors attractive. *Trends in Biochemical Sciences* 39(2), 82–90. doi: 10.1016/j.tibs.2013.12.003.
- Anderson, D., Dinglasan, A., Loukine, N., 2011. Producing nanoparticles using nanoscale polymer templates. U.S. Patent 7,967,890.
- Araki, N., Johnson, M.T., Swanson, J.A., 1996. A role for phosphoinositide 3-kinase in the completion of macropinocytosis and phagocytosis by macrophages. *The Journal of Cell Biology* 135(5), 1249–1260. doi: 10.1083/jcb.135.5.1249.
- Aruoja, V., Dubourguier, H.-C., Kasemets, K., Kahru, A., 2009. Toxicity of

- nanoparticles of CuO, ZnO and TiO<sub>2</sub> to microalgae *Pseudokirchneriella subcapitata*. *Science of the Total Environment* 407, 1461–1468. doi: 10.1016/j.scitotenv.2008.10.053.
- Baalousha, M., Manciuola, A., Cumberland, S., Kendell, K., Lead, J.R., 2008. Aggregation and surface properties of iron oxide nanoparticles: Influence of pH and natural organic matter. *Environmental Toxicology and Chemistry* 27(9), 1875–1882. doi: 10.1897/07-559.1.
- Bai, W., Zhang, Z., Tian, W., He, X., Ma, Y., Zhao, Y., et al., 2010. Toxicity of zinc oxide nanoparticles to zebrafish embryo: A physicochemical study of toxicity mechanism. *Journal of Nanoparticle Research* 12, 1645–1654. doi: 10.1007/s11051-009-9740-9.
- Baker, M.A., Cerniglia, G.J., Zaman, A., 1990. Microtiter plate assay for the measurement of glutathione and glutathione disulfide in large numbers of biological samples. *Analytical Biochemistry* 190, 360–365. doi: 10.1016/0003-2697(90)90208-Q.
- Balbus, J.M., Maynard, A.D., Colvin, V.L., Castranova, V., Daston, G.P., Denison, R.A., et al., 2007. Meeting report: Hazard assessment for nanoparticles—Report from an interdisciplinary workshop. *Environmental Health Perspectives* 115(11), 1654–1659. doi: 10.1289/ehp.10327.
- Bantz, C., Koshkina, O., Lang, T., Galla, H.-J., Kirkpatrick, C.J., Stauber, R.H., et al., 2014. The surface properties of nanoparticles determine the agglomeration state and the size of the particles under physiological conditions. *Beilstein Journal of Nanotechnology* 5, 1774–1786. doi: 10.3762/bjnano.5.188.

- Baolog, S., Rodriguez-Lorenzo, L., Monnier, C.A., Obiols-Rabasa, M., Rothen-Rutishauser, B., Schurtenberger, P., et al., 2015. Characterizing nanoparticles in complex biological media and physiological fluids with depolarized dynamic light scattering. *Nanoscale* 7, 5991–5997. doi:10.1039/c4nr06538g.
- Bar-Ilan, O., Chuang, C.C., Schwahn, D.J., Yang, S., Joshi, S., Pedersen, J.A., et al., 2013. TiO<sub>2</sub> nanoparticle exposure and illumination during zebrafish development: Mortality at parts per billion concentrations. *Environmental Science and Technology* 47, 4726–4733. doi: 10.1021/es304514r.
- Bar-Ilan, O., Louis, K.M., Yang, S.P., Pedersen, J.A., Hamers, R.J., Peterson, R.E., et al., 2012. Titanium dioxide nanoparticles produce phototoxicity in the developing zebrafish. *Nanotoxicology* 6(6), 670–679. doi: 10.3109/17435390.2011.604438.
- Baun, A., Hartmann, N.B., Grieger, K., Kusk, K.O., 2008. Ecotoxicity of engineered nanoparticles to aquatic invertebrates: A brief review and recommendations for future toxicity testing. *Ecotoxicology* 17, 387–395. doi: 10.1007/s10646-008-0208-y.
- BCC Research, 2014. Nanotechnology: A realistic market assessment. A BBC Research Nanotechnology Report (NANO31F), pp. 1–268.
- Behra, R., Sigg, L., Clift, M.J.D., Herzog, F., Minghetti, M., Johnston, B., et al., 2013. Bioavailability of silver nanoparticles and ions: from a chemical and biochemical perspective. *Journal of the Royal Society Interface* 10, 20130396. doi: 10.1098/rsif.2013.0396.
- Bengtén, E., Clem, L.W., Miller, N.W., Warr, G.W., Wilson, M., 2006. Channel catfish immunoglobulins: Repertoire and expression. *Developmental &*

- Comparative Immunology 30, 77–92. doi:10.1016/j.dci.2005.06.016.
- Biaglow, J.E., Manevich, Y., Uckun, F., Held, K.D., 1997. Quantitation of hydroxyl radicals produced by radiation and copper-linked oxidation of ascorbate by 2-deoxy-D-ribose method. *Free Radical Biological & Medicine* 22(7), 1129–1138. doi: 10.1016/S0891-5849(96)00527-8.
- Biesinger, K.E., Christensen, G.M., 1972. Effects of various metals on survival, growth, reproduction, and metabolism of *Daphnia magna*. *Journal of the Fisheries Research Board of Canada* 29(12), 1691–1700. doi: 10.1139/f72-269.
- Blinova, I., Ivask, A., Heinlaan, M., Mortimer, M., Kahru, A., 2010. Ecotoxicity of nanoparticles of CuO and ZnO in natural water. *Environmental Pollution* 158, 41–47. doi: 10.1016/j.envpol.2009.08.017.
- Bols, N.C., Barlian, A., Chirino-Trejo, M., Caldwell, S.J., Goegan, P., Lee, L.L.E.J., 1994. Development of a cell line from primary cultures of rainbow trout, *Oncorhynchus mykiss* (Walbaum), gills. *Journal of Fish Diseases* 17, 601–311. doi: 10.1111/j.1365-2761.1994.tb00258.x.
- Boluk, Y., Danumah, C., 2014. Analysis of cellulose nanocrystal rod lengths by dynamic light scattering and electron microscopy. *Journal of Nanoparticle Research* 16, 2174. doi: 10.1007/s11051-013-2174-4.
- Bolyard, S.C., Reinhart, D.R., Santra, S., 2013. Behavior of engineered nanoparticles in landfill leachate. *Environmental Science and Technology* 14, 8114–8122. doi: 10.1021/es305175e.
- Bonsignorio, D., Perego, L., Del Gaicco, L., Cotelli, F., 1996. Structure and macromolecular composition of the zebrafish egg chorion. *Zygote* 4, 101–108.

doi: 10.1017/S0967199400002975.

- Boussif, O., Lezoualc'h, F., Zanta, M.A., Mergyn, M.D., Scherman, D., Demeneix, B., et al., 1995. A versatile vector for gene and oligonucleotide transfer into cells in culture and *in vivo*: Polyethylenimine. *Proceedings of the National Academy of Sciences* 92, 7297–7301. doi: 10.1073/pnas.92.16.7297.
- Bramini, M., Ye, D., Hallerbach, A., Raghnaill, M.N., Salvati, A., Åberg, C., et al., 2014. Imaging approach to mechanistic study of nanoparticle interactions with the blood–brain barrier. *ACS Nano* 8(5), 4304–4312. doi:10.1021/nn5018523.
- Browning, L.M., Lee, K.J., Huang, T., Nallathamby, P.D., Lowman, J.E., Xu, X.-H.N., 2009. Random walk of single gold nanoparticles in zebrafish embryos leading to stochastic toxic effects on embryonic developments. *Nanoscale* 1, 138–152. doi:10.1039/b9nr00053d.
- Brunner, D., Frank, J., Appl, H., Schöffl, H., Pfaller, W., Gstraunthaler, G., 2010. Serum-free cell culture: The serum-free media interactive online database. *ALTEX* 27, 53–62.
- Bury, N.R., Schnell, S., Hogstrand, C., 2014. Gill cell culture systems as models for aquatic environmental monitoring. *The Journal of Experimental Biology* 217, 639–650. doi: 10.1242/jeb.095430.
- Byrne, H., Ahluwalia, A., Boraschi, D., Fadeel, B., Gehr, P., 2013. The bio-nano-interface in predicting nanoparticle fate and behaviour in living organisms: Towards grouping and categorising nanomaterials and ensuring nanosafety by design. *BioNanoMaterials* 14, 195–216. doi: 10.1515/bnm-2013-0011.
- Carnevali, O., Maradonna, F., 2003. Exposure to xenobiotic compounds: looking for

- new biomarkers. *General and Comparative Endocrinology* 131, 203–209. doi: 10.1016/S0016-6480(03)00105-9.
- Castaño, A., Gómez-Lechón, A. J., 2005. Comparisob of basal cytotoxicity data between mammalian and fish cell lines: A literature survey. *Toxicology in Vitro* 19, 695–705. doi: doi:10.1016/j.tiv.2005.04.002.
- Catalán, J., Ilves, M., Järventaus, H., Hannukainen, K.-S., Kontturi, E., Vanhala, E., et al., 2014. Genotoxic and immunotoxic effects of cellulose nanocrystals *in vitro*. *Environmental and Molecular Mutagenesis* 56(2), 171–182. doi: 10.1002/em.21913.
- Canadian Environmental Protection Act (CEPA), 2015. CEPA 1999 section 71 Notice with respect to certain nanomaterials in Canadian commerce. *Canada Gazette Part I* 149(30), 1939–2136.
- Cerutti, P.A., 1985. Prooxidant states and tumor promotion. *Science* 227(4685), 375–381. doi: 10.1126/science.2981433.
- Charron, R.A., Fenwick, J.C., Lean, D.R.S., Moon, T.W., 2000. Ultraviolet-B radiation effects on antioxidant status and survival in the zebrafish, *Brachydanio rerio*. *Photochemistry and Photobiology* 72(3), 327–333. doi: 10.1562/0031-8655(2000)0720327UBREOA2.0.CO2.
- Chazotte, B., 2011. Labeling lysosomes in live cells with LysoTracker. *Cold Spring Harbor Protocols*, 210–212. doi: 10.1101/pdb.prot5571.
- Chen, C.-Y., Jafvert, C.T., 2010. Photoreactivity of carboxylated single-walled carbon nanotubes in sunlight: Reactive oxygen species production in water. *Environmental Science and Technology* 44, 6674–6679. doi:10.1021/es101073p.

- Chen, P.-J., Su, C.-H., Tseng, C.-Y., Tan, S.-W., Cheng, C.-H., 2011. Toxicity assessments of nanoscale zerovalent iron and its oxidation products in medaka (*Oryzias latipes*) fish. *Marine Pollution Bulletin* 63(5-12), 339–346. doi: 10.1016/j.marpolbul.2011.02.045.
- Chen, Y., Hu, Y., Sun, J., Zhou, Q., 2016. Specific nanotoxicity of graphene oxide during zebrafish embryogenesis 1, 45–52. doi: 10.3109/17435390.2015.1005032.
- Cheng, J., Flahaut, E., Cheng, S.H., 2007. Effect of carbon nanotubes on developing zebrafish (*Danio rerio*) embryos. *Environmental Toxicology and Chemistry* 26(4), 708–716. doi: 10.1897/06-272R.1.
- Cirillo, G., Hampel, S., Spizzirri, U.G., Parisi, O.I., Picci, N., Iemma, F., 2014. Carbon nanotubes hybrid hydrogels in drug delivery: A perspective review. *BioMed Research International* 2014(825017), 1–17. doi: 10.1155/2014/825017.
- Colvin, V.L., 2003. The potential environmental impact of engineered nanomaterials. *Nature Biotechnology* 21(10), 1166–1170. doi: 10.1038/nbt875.
- Conner, S.D., Schmid, S.L., 2003. Regulated portals of entry into the cell. *Nature* 422, 37–44. doi: 10.1038/nature01451.
- Cortajarena, A.L., Ortega, D., Ocampo, S.M., Gonzalez-García, A., Couleaud, P., Miranda, R., et al., 2014. Engineering iron oxide nanoparticles for clinical settings. *Nanobiomedicine* 1, 1–20. doi:10.5772/58841.
- Cowie, J., Bilek, E.M., Wegner, T.H., Shatkin, J.A., 2014. Market projections of cellulose nanomaterial-enabled products – Part 2: Volume estimates. *Tappi Journal* 13(6), 57–69.
- Crollius, H.R., Weissenbach, J., 2005. Fish genomics and biology. *Genome Research*

- 15, 1675–1682. doi: 10.1101/gr.3735805.
- Currie, R.J., Bennett, W.A., Beitinger, T.L., 1998. Critical thermal minima and maxima of three freshwater game-fish species acclimated to constant temperatures. *Environmental Biology of Fishes* 51, 187–200. doi: 10.1023/A:1007447417546.
- Dahle, J.T., Arai, Y., 2015. Environmental geochemistry of cerium: Applications and toxicology of cerium oxide nanoparticles. *International Journal of Environmental Research and Public Health* 12, 1253–1278. doi: 10.3390/ijerph120201253.
- Dai, Y.-J., Jia, Y.-F., Chen, N., Bian, W.-P., Li, Q.-K., Ma, Y.-B., et al., 2014. Zebrafish as a model system to study toxicology. *Environmental Toxicology and Chemistry* 33(1), 11–17. doi: 10.1002/etc.2406.
- Dave, G., 1991. Toxicity of mercury, copper, nickel, lead, and cobalt to embryos and larvae of zebrafish, *Brachydanio rerio*. *Archive of Environmental Contamination and Toxicology* 21, 126–134. doi: 10.1007/BF01055567.
- Dergunov, S.A., Kesterson, K., Li, W., Wang, Z., Pinkhassik, E., 2010. Synthesis, characterization, and long-term stability of hollow polymer nanocapsules with nanometer-thin walls. *Macromolecules* 43(18), 7785–7792. doi: 10.1021/ma1012418.
- Derjaguin, B., Landau, L., 1941. Theory of the stability of strongly charged lyophobic sols and of the adhesion of strongly charged particles in solutions of electrolytes. *Acta Physicochimica URSS* 14, 633–662.
- Dhar Dwivedi, A., Dubey, S.P., Sillanpää, M., Kwon, Y.-N., Lee, C., Varma, R.S., 2015. Fate of engineered nanoparticles: Implications in the environment.

- Coordination Chemistry Reviews 287, 64–78. doi: 10.1016/j.ccr.2014.12.014.
- DiMichele, L., Taylor, M.H., Singleton, R.Jr., 1981. The hatching enzyme of *Fundulus heteroclitus*. The Journal of Experimental Zoology 216(1), 133–140. doi: 10.1002/jez.1402160114.
- Donaldson, K., Stone, V., Tran, C.L., Kreyling, W., Borm, P.J.A., 2004. Nanotoxicology. Occupational and Environmental Medicine 61, 727–728. doi: 10.1136/oem.2004.013243.
- dos Santos, T., Varela, J., Lynch, I., Salvati, A., Dawson, K.A., 2011. Effects of transport inhibitors on the cellular uptake of carboxylated polystyrene nanoparticles in different cell lines. PLoS ONE 6(9), e24438. doi:10.1371/journal.pone.0024438.
- Dutta, D., Donaldson, J.G., 2013. Search for inhibitors of endocytosis. Cellular Logistics 2(4), 203–208. doi: 10.4161/cl.23967.
- Ebrahimi, M., Taherianfard, M., 2011. The effects of heavy metals exposure on reproductive systems of cyprinid fish from Kor River. Iranian Journal of Fisheries Sciences 10(1), 13–24.
- Eddy, F.B., Handy, R.D., Eds., 2012. Ecological and Environmental Physiology of Fishes, first ed., Oxford University Press.
- Ede, J.D., 2015. Immunotoxicology of high aspect ratio nanomaterials. University of Alberta, Edmonton, AB, CA. PhD thesis.
- Ede, J.D., Ortega, V.A., Boyle, D., Beingessner, R.L., Hemraz, U.D., Fenniri, H., et al., 2015. Rosette nanotubes alter IgE-mediated degranulation in the rat basophilic leukemia (RBL)-2H3 cell line. Toxicological Sciences 148(1), 108–

120. doi: 10.1093/toxsci/kfv166.
- Eichhorn, S.J., Dufresne, A., Aranguren, M., Marcovich, N.E., Capadona, J.R., Rowan, S.J., et al., 2010. Review: current international research into cellulose nanofibres and nanocomposites. *Journal of Material Science* 45, 1–33. doi: 10.1007/s10853-009-3874-0.
- Engqvist-Goldstein, Å.E.Y., Drubin, D.G., 2003. Actin assembly and endocytosis: From yeast to mammals. *Annual Review of Cell and Developmental Biology* 19, 287–332. doi:10.1146/annurev.cellbio.19.111401.093127.
- European Commission, 2013. Commission implementing decision on guidelines on annex I to regulation (EC) no 1223/2009 of the European Parliament and of the council on cosmetic products. *Official Journal of the European Union*, L. 83–105.
- European Commission, 2011. Commission recommendation of 18 October 2011 on the definition of nanomaterial (text with EEA relevance). *Official Journal of the European Union*, L. 275, 38–40.
- Evans, D.H., Piermarini, P.M., Choe, K.P., 2005. The multifunctional fish gill: Dominant site of gas exchange, osmoregulation, acid-base regulation, and excretion of nitrogenous waste. *Physiological Reviews* 85, 97–177. doi: 10.1152/physrev.00050.2003.
- Faille, D., El-Assaad, F., Mitchell, A.J., Alessi, M.-C., Chimini, G., Fusai, T., et al., 2012. Endocytosis and intracellular processing of platelet microparticles by brain endothelial cells. *Journal of Cellular and Molecular Medicine* 16(8), 1731–1738. doi: 10.1111/j.1582-4934.2011.01434.x.
- Farkas, A., Salánki, J., Specziár, A., 2002. Relation between growth and the heavy

- metal concentration in organs of ream *Abramis brama* L. populating lake Balaton. *Archives of Environmental Contamination and Toxicology* 43, 236–243. doi: 10.1007/s00244-002-1123-5.
- Farkas, J., Christian, P., Gallego-Urrea, J.A., Roos, N., Hassellöv, M., Tollefsen, K.E., et al., 2011. Uptake and effects of manufactured silver nanoparticles in rainbow trout (*Oncorhynchus mykiss*) gill cells. *Aquatic Toxicology* 117–125. doi: 10.1016/j.aquatox.2010.09.010.
- Federici, G., Shaw, B.J., Handy, R.D., 2007. Toxicity of titanium dioxide nanoparticles to rainbow trout (*Oncorhynchus mykiss*): Gill injury, oxidative stress, and other physiological effects. *Aquatic Toxicology* 84, 415–430. doi: 10.1016/j.aquatox.2007.07.009.
- Felix, L.C., Ortega, V.A., Ede, J.D., Goss, G.G., 2013. Physicochemical characteristics of polymer-coated metal-oxide nanoparticles and their toxicological effects on zebrafish (*Danio rerio*) development. *Environmental Science and Technology* 47, 6589–6596. doi: 10.1021/es401403p.
- Fernando, L.P., Kandel, P.K., Yu, J., McNeill, J., Ackroyd, P.C., Christensen, K.A., 2010. Mechanism of cellular uptake of highly fluorescent conjugated polymer nanoparticles. *Biomacromolecules* 11, 2675–2682. doi: 10.1021/bm1007103.
- Feynman, R.P., 1959. There is plenty of room at the bottom. *American Physical Society* 1–7.
- Firdessa, R., Oelschlaeger, T.A., Moll, H., 2014. Identification of multiple cellular uptake pathways of polystyrene nanoparticles and factors affecting the uptake: Relevance for drug delivery systems. *European Journal of Cell Biology* 93, 323–

337. doi: 10.1016/j.ejcb.2014.08.001.
- Franklin, N.M., Rogers, N.J., Apte, S.C., Batley, G.E., Gadd, G.E., Casey, P.S., 2007. Comparative toxicity of nanoparticulate ZnO, bulk ZnO, and ZnCl<sub>2</sub> to a freshwater microalga (*Pseudokirchneriella subcapitata*): The importance of particle solubility. *Environmental Science and Technology* 41, 8484–8490. doi: 10.1021/es071445r.
- Fujimoto, T., Kogo, H., Nomura, R., Une, T., 2000. Isoforms of caveolin-1 and caveolar structure. *Journal of Cell Science* 113, 3509–3517.
- Gajewicz, A., Rasulev, B., Dinadayalane, T.C., Urbaszek, P., Puzyn, T., Leszczynska, D., et al., 2012. Advancing risk assessment of engineered nanomaterials: Application of computational approaches. *Advanced Drug Delivery Reviews* 64, 1663–1693. doi: 10.1016/j.addr.2012.05.014.
- Gallud, A., Fadeel, B., 2015. Keeping it small: towards a molecular definition of nanotoxicology. *European Journal of Nanomedicine* 7(3), 143–151. doi: 10.1515/ejnm-2015-0020.
- Garcia-Valls, R., Hatton, T.A., 2003. Metal ion complexation with lignin derivatives. *Chemical Engineering Journal* 94, 99–105. doi: 10.1016/S1385-8947(03)00007.
- Ge, C., Li, Y., Yin, J.-J., Liu, Y., Wang, L., Zhao, Y., et al., 2012. The contributions of metal impurities and tube structure to the toxicity of carbon nanotube materials. *NPG Asia Materials* 4, e32. doi: 10.1038/am.2012.60.
- Georgescu, B., Georgescu, C., Dărăban, S., Bouaru, A., Pașcalau, S., 2011. Heavy metals acting as endocrine disrupters. *Scientific Papers: Animal Science and Biotechnologies* 42(2), 89–93.

- Ghosh, S., Mashayekhi, H., Bhowmik, P., Xing, B., 2010. Colloidal stability of Al<sub>2</sub>O<sub>3</sub> nanoparticles as affected by coating of structurally different humic acids. *Langmuir* 26(2), 873–879. doi: 10.1021/la902327q.
- Goh, C.M., Dinglasan, J.D., Goh, J.B., Loo, R., Veletanlie, E., 2009. Composite nanoparticles, nanoparticles and methods for producing same. U.S. Patent 7,534,490.
- Gottschalk, F., Nowack, B., 2011. The release of engineered nanomaterials to the environment. *Journal of Environmental Monitoring* 13, 1145–1155. doi: 10.1039/c0em00547a.
- Gottschalk, F., Sonderer, T., Scholz, R.W., Nowack, B., 2010. Possibilities and limitations of modeling environmental exposure to engineered nanomaterials by probabilistic material flow analysis. *Environmental Toxicology and Chemistry* 29(5), 1036–1048. doi: 10.1002/etc.135.
- Gottschalk, F., Sonderer, T., Scholz, R.W., Nowack, B., 2009. Modeled environmental concentrations of engineered nanomaterials (TiO<sub>2</sub>, ZnO, Ag, CNT, fullerenes) for different regions. *Environmental Science and Technology* 43, 9216–9222. doi: 10.1021/es9015553.
- Gottschalk, F., Sun, T., Nowack, B., 2013. Environmental concentrations of engineered nanomaterials: Review of modeling and analytical studies. *Environmental Pollution* 181, 287–300. doi: 10.1016/j.envpol.2013.06.003.
- Govind, P., Madhuri, S., 2014. Heavy metals causing toxicity in animals and fishes. *Research Journal of Animal, Veterinary and Fishery Sciences* 2(2), 17–23.
- Greulich, C., Diendorf, J., Simon, T., Eggeler, G., Epple, M., Köller, M., 2011.

- Uptake and intracellular distribution of silver nanoparticles in human mesenchymal stem cells. *Acta Biomaterialia* 7, 347–354. doi: 10.1016/j.actbio.2010.08.003.
- Griffith, O.W., 1980. Determination of glutathione and glutathione disulfide using glutathione reductase and 2-vinylpyridi. *Analytical Biochemistry* 106, 207–212. doi: 10.1016/0003-2697(80)90139-6.
- Grillo, R., Rosa, A.H., Fraceto, L.F., 2015. Engineered nanoparticles and organic matter: a review of the state-of-the-art. *Chemosphere* 119, 608–619. doi: 10.1016/j.chemosphere.2014.07.049.
- Guo, L., Von Dem Bussche, A., Buechner, M., Yan, A., Kane, A.B., Hurt, R.H., 2008. Adsorption of essential micronutrients by carbon nanotubes and the implications for nanotoxicity testing. *Small* 4(6), 721–727. doi: 10.1002/sml.200700754.
- Gutteridge, J.M.C., 1995. Lipid peroxidation and antioxidants as biomarkers of tissue damage. *Clinical Chemistry* 41(12), 1819–1828.
- Gutteridge, J.M.C., Halliwell, B., 1988. The deoxyribose assay: an assay both for “free” hydroxyl radical and for site-specific hydroxyl radical production. *Biochemical Journal* 253(3), 932–933.
- Habibi, Y., Lucia, L.A., Rojas, O.J., 2010. Cellulose nanocrystals: Chemistry, self-assembly, and applications. *Chemical Reviews* 110, 3479–3500. doi: 10.1021/cr900339w.
- Hampton, J.A., Lantz, R.C., Goldblatt, P.J., Lauren, D.J., Hinton, D.E., 1988. Functional units in rainbow trout (*Salmo gairdneri*, Richardson) liver: II. The

- biliary system. *The Anatomical Record* 221, 619–634.
- Handy, R.D., Henry, T.B., Scown, T.M., Johnston, B.D., Tyler, C.R., 2008. Manufactured nanoparticles: their uptake and effects on fish—a mechanistic analysis. *Ecotoxicology* 17, 396–409. doi: 10.1007/s10646-008-0205-1.
- Handy, R.D., von der Kammer, F., Lead, J.R., Hassellöv, M., Owen, R., Crane, M., 2008b. The ecotoxicology and chemistry of manufactured nanoparticles. *Ecotoxicology* 17, 287–314. doi: 10.1007/s10646-008-0199-8.
- Hao, L., Chen, L., Hao, J., Zhong, N., 2013. Bioaccumulation and sub-acute toxicity of zinc oxide nanoparticles in juvenile carp (*Cyprinus carpio*): A comparative study with its bulkcounterparts. *Ecotoxicology and Environmental Safety* 91, 52–60. doi: 10.1016/j.ecoenv.2013.01.007.
- Hill, A.J., Teraoka, H., Heideman, W., Peterson, R.E., 2005. Zebrafish as a model vertebrate for investigating chemical toxicity. *Toxicological Sciences* 86(1), 6–19. doi: 10.1093/toxsci/kfi110.
- Hoffmann, M.R., Martin, S.T., Choi, W., Bahnemann, D.W., 1995. Environmental applications of semiconductor photocatalysis. *Chemical Reviews* 95, 69–96.
- Honary, S., Zahir, F., 2013. Effect of zeta potential on the properties of nano-drug delivery systems - A review (Part 1). *Tropical Journal of Pharmaceutical Research* 12(2), 255–264. doi: 10.4314/tjpr.v12i2.19.
- Howe, K., Clark, M.D., Torroja, C.F., Torrance, J., Berthelot, C., Muffato, M., et al., 2013. The zebrafish reference genome sequence and its relationship to the human genome. *Nature* 496, 498–503. doi:10.1038/nature12111.
- Iijima, S., Ichihashi, T., 1993. Single-shell carbon nanotubes of 1-nm diameter.

- Nature 363, 603–605. doi: 10.1038/363603a0.
- Ijadpanah-Saravy, H., Safari, M., Darban-Khodadadi, A., Razaei, A., 2014. Synthesis of titanium dioxide nanoparticles for photocatalytic degradation of cyanide in wastewater. *Analytical Letters* 47(10), 1772–1782. doi: 10.1080/00032719.2014.880170.
- International Organization for Standardization, 2015. *Nanotechnologies - Vocabulary - Part 2: Nano-objects*, ISO/TS 80004-2:2015(en). <https://www.iso.org/obp/ui/#iso:std:iso:ts:80004:-2:ed-1:v1:en> (accessed 25.04.16).
- Iqbal, M., Purkait, T.K., Goss, G.G., Bolton, J.R., El-Din, M.G., Veinot, J.G.C., 2016. Application of engineered Si nanoparticles in light-induced advanced oxidation remediation of a water-borne model contaminant. *ACS Nano*. doi: 10.1021/acsnano.6b01619.
- Isobe, H., Tanaka, T., Maeda, R., Noiri, E., Solin, N., Yudasaka, M., et al., 2006. Preparation, purification, characterization, and cytotoxicity assessment of water-soluble, transition-metal-free carbon nanotube aggregates. *Angewandte Chemie International Edition* 45, 6676–6680. doi: 10.1002/anie.200601718.
- Ivanov, A.I., 2008. Pharmacological inhibition of endocytic pathways: is it specific enough to be useful? In: Ivanov, A.I. (Ed.), *Exocytosis and Endocytosis. Methods in Molecular Biology* 440, Human Press, pp. 15–33. doi: 10.1007/978-1-59745-178-9\_2.
- Janero, D.R., 1990. Malondialdehyde and thiobarbituric acid-reactivity as diagnostic indices of lipid peroxidation and peroxidative tissue injury. *Free Radical Biology*

- & Medicine 9, 515–540. doi: [http://dx.doi.org/10.1016/0891-5849\(90\)90131-2](http://dx.doi.org/10.1016/0891-5849(90)90131-2).
- Jardine, D., Litvak, M.K., 2003. Direct yolk sac volume manipulation of zebrafish embryos and the relationship between offspring size and yolk sac volume. *Journal of Fish Biology* 63, 388–397. doi: [10.1046/j.1095-8649.2003.00161.x](https://doi.org/10.1046/j.1095-8649.2003.00161.x).
- Jassby, D., Budarz, F.J., Wiesner, M.R., 2012. Impact of aggregate size and structure on the photocatalytic properties of TiO<sub>2</sub> and ZnO nanoparticles. *Environmental Science and Technology* 46, 6934–6941. doi: [10.1021/es202009h](https://doi.org/10.1021/es202009h).
- Jiang, J., Oberdörster, G., Biswas, P., 2009. Characterization of size, surface charge, and agglomeration state of nanoparticle dispersions for toxicological studies. *Journal of Nanoparticle Research* 11, 77–89. doi: [10.1007/s11051-008-9446-4](https://doi.org/10.1007/s11051-008-9446-4).
- Jiao, C.-Y., Delaroche, D., Burlina, F., Alves, I.D., Chassaing, G., Sagan, S., 2009. Translocation and endocytosis for cell-penetrating peptide internalization. *The Journal of Biological Chemistry* 284(49), 33957–33965. doi: [10.1074/jbc.M109.056309](https://doi.org/10.1074/jbc.M109.056309).
- Johnston, B.D., Scown, T.M., Moger, J., Cumberland, S.A., Baalousha, M., Linge, K., et al., 2010. Bioavailability of nanoscale metal oxides TiO<sub>2</sub>, CeO<sub>2</sub>, and ZnO to fish. *Environmental Science and Technology* 44, 1144–1151. doi: [10.1021/es901971a](https://doi.org/10.1021/es901971a).
- Jorfi, M., Foster, E.J., 2015. Recent advances in nanocellulose for biomedical applications. *Journal of Applied Polymer Science* 132, 41719. doi: [10.1002/app.41719](https://doi.org/10.1002/app.41719).
- Jung, S., Panchalingam, K.M., Rosenberg, L., Behie, L.A., 2012. *Ex vivo* expansion of human mesenchymal stem cells in defined serum-free media. *Stem Cells*

- International 2012(123030), 1–21. doi: 10.1155/2012/123030.
- Keller, A.A., Wang, H., Zhou, D., Lenihan, H.S., Cherr, G., Cardinale, B.J., et al., 2010. Stability and aggregation of metal oxide nanoparticles in natural aqueous matrices. *Environmental Science and Technology* 44(6), 1962–1967. doi: 10.1021/es902987d.
- Kelly, S.A., Havrilla, C.M., Brady, T.D., Abramp, K.H., Levin, E.D., 1998. Oxidative stress in toxicology: Established mammalian and emerging piscine model systems. *Environmental Health Perspectives* 106(7), 375–384. doi: 10.1289/ehp.98106375.
- Khalil, I.A., Kogure, K., Akita, H., Harashima, H., 2006. Uptake pathways and subsequent intracellular trafficking in nonviral gene delivery. *Pharmacological Reviews* 58, 32–45. doi: 10.1124/pr.58.1.8.
- Khan, M.M., Adil, S.F., Al-Mayouf, A., 2015. Metal oxides as photocatalysts. *Journal of Saudi Chemical Society* 19, 462–464. doi: 10.1016/j.jscs.2015.04.003.
- Khatri, N., Tyagi, S., 2015. Influences of natural and anthropogenic factors on surface and groundwater quality in rural and urban areas. *Frontiers in Life Science* 8(1), 23–39. doi: 10.1080/21553769.2014.933716.
- Kim, D.-H., Hwang, C.N., Sun, Y., Lee, S.H., Kim, B., Nelson, B.J., 2006. Mechanical analysis of chorion softening in prehatching stages of zebrafish embryos. *IEEE Transactions on Nanobioscience* 5(2), 89–94. doi: 10.1109/TNB.2006.875054.
- Kim, K.S., Cota-Sanchez, G., Kingston, C.T., Imris, M., Simard, B., Soucy, G., 2007. Large-scale production of single-walled carbon nanotubes by induction thermal plasma. *Journal of Physics D: Applied Physics* 40, 2375–2387. doi:

10.1088/0022-3727/40/8/S17.

- Kim, K.S., Imris, M., Shahverdi, A., Alinejad, Y., Soucy, G., 2009. Single-walled carbon nanotubes prepared by large-scale induction thermal plasma process: Synthesis, characterization, and purification. *The Journal of Physical Chemistry C* 113, 4340–4348. doi: 10.1021/jp810096k.
- Kimmel, C.B., Ballard, W.W., Kimmel, S.R., Ullmann, B., Schilling, T.F., 1995. Stages of embryonic development of the zebrafish. *Developmental Dynamics* 203, 253–310.
- Kimura, T., Kawasaki, Y., Okumura, F., Sone, T., Natsuki, R., Isobe, M., 2009. Ethanol-induced expression of glutamate–cysteine ligase catalytic subunit gene is mediated by NF- $\kappa$ B. *Toxicology Letters* 185(2), 110–115. doi: 10.1016/j.toxlet.2008.12.006.
- Kong, Q., Lin, C.-L.G., 2010. Oxidative damage to RNA: Mechanisms, consequences, and diseases. *Cellular and Molecular Life Sciences* 67(11), 1817–1829. doi: 10.1007/s00018-010-0277-y.
- Kostarelos, K., Lacerda, L., Pastorin, G., Wu, W., Wieckowski, S., Luangsivilay, J., et al., 2007. Cellular uptake of functionalized carbon nanotubes is independent of functional group and cell type. *Nature Nanotechnology* 2, 108–113. doi: 10.1038/nnano.2006.209.
- Kou, L., Sun, J., Zhai, Y., He, Z., 2013. The endocytosis and intracellular fate of nanomedicines: Implication for rational design. *Asian Journal of Pharmaceutical Sciences* 8, 1–10. doi: 10.1016/j.ajps.2013.07.001.
- Kovacs, T., Naish, V., O'Connor, B., Blaise, C., Gagné, F., Hall, L., et al., 2010. An

- ecotoxicological characterization of nanocrystalline cellulose (NCC).  
Nanotoxicology 4(3), 255–270. doi: 10.3109/17435391003628713.
- Kroll, A., Pillukat, M.H., Hahn, D., Schnekenburger, J., 2012. Interference of engineered nanoparticles with *in vitro* toxicity assays. Archives of Toxicology 86, 1123–1136. doi: 10.1007/s00204-012-0837-z.
- Krug, H.F., 2014. Nanosafety research-are we on the right track? Angewandte Chemie International Edition 53, 12304–12319. doi: 10.1002/anie.201403367.
- Kuhn, D.A., Vanhecke, D., Michen, B., Blank, F., Gehr, P., Petri-Fink, A., et al., 2014. Different endocytotic uptake mechanisms for nanoparticles in epithelial cells and macrophages. Beilstein Journal of Nanotechnology 5, 1625–1636. doi: 10.3762/bjnano.5.174.
- Kumar, A., Jee, M., 2013. Nanotechnology: A review of applications and issues. International Journal of Innovative Technology and Exploring Engineering 3(4), 89–92.
- Kühnel, D., Busch, W., Meißner, T., Springer, A., Potthoff, A., Richter, V., et al., 2009. Agglomeration of tungsten carbide nanoparticles in exposure medium does not prevent uptake and toxicity toward a rainbow trout gill cell line. Aquatic Toxicology 93, 91–99. doi: 10.1016/j.aquatox.2009.04.003.
- Kühnel, D., Nickel, C., 2014. The OECD expert meeting on ecotoxicology and environmental fate – Towards the development of improved OECD guidelines for the testing of nanomaterials. Science of the Total Environment 472, 347–353. doi: 10.1016/j.scitotenv.2013.11.055.
- Kwon, D., Nho, H.W., Yoon, T.H., 2014. X-ray and electron microscopy studies on

- the biodistribution and biomodification of iron oxide nanoparticles in *Daphnia magna*. *Colloids and Surfaces B: Biointerfaces* 122, 384–389. doi: 10.1016/j.colsurfb.2014.07.016.
- Landfester, K., Ostafin, A., 2008. Enhancing effectiveness of nanoparticles and nanoreactor in human (stem) cells—understanding and influencing the uptake of nanostructured materials in (stem) cells. In: Landfester, K., Ostafin, A. (Eds.), *Nanoreactor Engineering for Life Sciences and Medicine*, Artech House, pp. 251–262.
- Latham, K.E., Just, J.J., 1989. Oxygen availability provides a signal for hatching in the rainbow trout (*Salmo gairdneri*) embryo. *Canadian Journal of Fisheries and Aquatic Sciences* 46, 55–58.
- Lead, J.R., Wilkinson, K.J., 2006. Aquatic colloids and nanoparticles: Current knowledge and future trends. *Environmental Chemistry* 3(3), 159–171. doi: 10.1071/EN06025.
- Lee, H., Choi, W., 2002. Photocatalytic oxidation of arsenite in TiO<sub>2</sub> suspension: Kinetics and mechanisms. *Environmental Science and Technology* 36(17), 3872–3878. doi: 10.1021/es0158197.
- Lee, K.J., Nallathamby, P.D., Browning, L.M., Osgood, C.J., Xu, X.-H.N., 2007. *In vivo* imaging of transport and biocompatibility of single silver nanoparticles in early development of zebrafish embryos. *ACS Nano* 1(2), 133–143. doi: 10.1021/nn700048y.
- Lee, L.E.J., Dayeh, V.R., Schirmer, K., Bols, N.C., 2009. Applications and potential uses of fish gill cell lines: examples with RTgill-W1. *In Vitro Cellular &*

- Developmental Biology - Animal 45, 127–134. doi: 10.1007/s11626-008-9173-2.
- Leung, A.C.W., Hrapovic, S., Lam, E., Liu, Y., Male, K.B., Mahmoud, K.A., et al., 2011. Characteristics and properties of carboxylated cellulose nanocrystals prepared from a novel one-step procedure. *Small* 7(3), 302–305. doi: 10.1002/sml.201001715.
- Li, L., Wan, T., Wan, M., Liu, B., Cheng, R., Zhang, R., 2015a. The effect of the size of fluorescent dextran on its endocytic pathway. *Cell Biology International* 39, 531–539. doi: 10.1002/cbin.10424.
- Li, M., Al-Jamal, K.T., Kostarelos, K., Reineke, J., 2010. Physiologically based pharmacokinetic modeling of nanoparticles. *ACS Nano* 4(11), 6303–6317. doi: 10.1021/nn1018818.
- Li, S., Erickson, R.J., Wallis, L.K., Diamond, S.A., Hoff, D.J., 2015b. Modeling TiO<sub>2</sub> nanoparticle phototoxicity: The importance of chemical concentration, ultraviolet radiation intensity, and time. *Environmental Pollution* 205, 327–332. doi: 10.1016/j.envpol.2015.06.020.
- Li, X., Schirmer, K., Bernard, L., Sigg, L., Pillai, S., Behra, R., 2015c. Silver nanoparticle toxicity and association with the alga *Euglena gracilis*. *Environmental Science: Nano* 2, 594–602. doi: 10.1039/C5EN00093A.
- Liang, F., Chen, B., 2010. A review on biomedical applications of single-walled carbon nanotubes 17(1), 10–24.
- Lin, H., Huang, C.P., Li, W., Ni, C., Ismat Shah, S., Tseng, Y.-H., 2006. Size dependency of nanocrystalline TiO<sub>2</sub> on its optical property and photocatalytic reactivity exemplified by 2-chlorophenol. *Applied Catalysis B: Environmental*

- 68, 1–11. doi: 10.1016/j.apcatb.2006.07.018.
- Lin, N., Dufresne, A., 2014. Nanocellulose in biomedicine: Current status and future prospect. *European Polymer Journal* 59, 302–325. doi: 10.1016/j.eurpolymj.2014.07.025.
- Lin, S., Zhao, Y., Xia, T., Meng, H., Ji, Z., Liu, R., et al., 2011. High content screening in zebrafish speeds up hazard ranking of transition metal oxide nanoparticles. *ACS Nano* 5(9), 7284–7295. doi: 10.1021/nn202116p.
- Livak, K. J., Schmittgen, T. D., 2001. Analysis of relative gene expression data using real-time quantitative PCR and the  $2^{-\Delta\Delta C_t}$  method. *Methods* 25, 402–408. doi: 10.1006/meth.2001.1262.
- Liu, A.P., Aguet, F., Danuser, G., Schmid, S.L., 2010. Local clustering of transferrin receptors promotes clathrin-coated pit initiation. *The Journal of Cell Biology* 191(7), 1381–1393. doi:10.1007/978-1-59745-513-8\_17.
- Liu, J., Hurt, R.H., 2010. Ion release kinetics and particle persistence in aqueous nano-silver colloids. *Environmental Science and Technology* 44, 2169–2175. doi: 10.1021/es9035557.
- Liu, R., Lal, R., 2015. Potentials of engineered nanoparticles as fertilizers for increasing agronomic productions. *Science of the Total Environment* 514, 131–139. doi: 10.1016/j.scitotenv.2015.01.104.
- Lu, K.L., Lago, R.M., Chen, Y.K., Green, M.L.H., Harris, P.J.F., Tsang, S.C., 1996. Mechanical damage of carbon nanotubes by ultrasound. *Carbon* 34, 814–816. doi:10.1016/0008-6223(96)89470-X.
- Luzio, J.P., Pryor, P.R., Bright, N.A., 2007. Lysosomes: fusion and function. *Nature*

- Reviews Molecular Cell Biology 8, 622–632. doi: 10.1038/nrm2217.
- Ma, H., Brennan, A., Diamond, S.A., 2012. Phototoxicity of TiO<sub>2</sub> nanoparticles under solar radiation to two aquatic species: *Daphnia magna* and Japanese medaka. Environmental Toxicology and Chemistry 31(7), 1621–1629. doi: 10.1002/etc.1858.
- Ma, H., Williams, P.L., Diamond, S.A., 2013. Ecotoxicity of manufactured ZnO nanoparticles - A review. Environmental Pollution 172, 76–85. doi: 10.1016/j.envpol.2012.08.011.
- Maag, H., 2007. Prodrugs of carboxylic acids. In: Biotechnology: Pharmaceutical Aspects V, Springer-Verlag New York, pp. 703–729. doi: 10.1007/978-0-387-49785-3\_20.
- MacCormack, T.J., Clark, R.J., Dang, M.K.M., Ma, G., Kelly, J.A., Veinot, J.G.C., et al., 2012. Inhibition of enzyme activity by nanomaterials: potential mechanisms and implications for nanotoxicity testing. Nanotoxicology 6(5), 514–525. doi: 10.3109/17435390.2011.587904.
- Magaldi, T.G., Buch, M.H.C., Murata, H., Erickson, K.D., Neu, U., Garcea, R.L., et al., 2012. Mutations in the GM1 binding site of simian virus 40 VP1 alter receptor usage and cell tropism. Journal of Virology 86(13), 7028–7042. doi: 10.1128/JVI.00371-12.
- Mahlambi, M.M., Ngila, C.J., Mamba, B.B., 2015. Recent developments in environmental photocatalytic degradation of organic pollutants: The case of titanium dioxide nanoparticles – A Review. Journal of Nanomaterials 2015(790173), 1–29. doi: 10.1155/2015/790173.

- Mahmoud, K.A., Male, K.B., Hrapovic, S., Luong, J.H.T., 2009. Cellulose nanocrystal/gold nanoparticle composite as a matrix for enzyme immobilization. *ACS Applied Materials Interfaces* 1(7), 1383–1386. doi: 10.1021/am900331d.
- Male, K.B., Leung, A.C.W., Montes, J., Kamen, A., Luong, J.H.T., 2012. Probing inhibitory effects of nanocrystalline cellulose: inhibition versus surface charge. *Nanoscale* 4(4), 1373–1379. doi: 10.1039/c2nr11886f.
- Malysheva, A., Lombi, E., Voelcker, N.H., 2015. Bridging the divide between human and environmental nanotoxicology. *Nature Nanotechnology* 10, 835–844. doi: 10.1038/nnano.2015.224.
- Manier, N., Bado-Nilles, A., Delalain, P., Aguerre-Chariol, O., Pandard, P., 2013. Ecotoxicity of non-aged and aged CeO<sub>2</sub> nanomaterials towards freshwater microalgae. *Environmental Pollution* 180, 63–70. doi: 10.1016/j.envpol.2013.04.040.
- Masoumbaigi, H., Rezaee, A., Hosseini, H., Hashemi, S., 2015. Water disinfection by zinc oxide nanoparticle prepared with solution combustion method. *Desalination and Water Treatment* 56(9), 2376–2381. doi: 10.1080/19443994.2014.961556.
- Maynard, A.D., 2011. Don't define nanomaterials. *Nature* 475, 31. doi: 10.1038/475031a.
- McCurley, A.T., Callard, G.V., 2008. Characterization of housekeeping genes in zebrafish: male-female differences and effects of tissue type, developmental stage and chemical treatment. *BMC Molecular Biology* 9, 102. doi: 10.1186/1471-2199-9-102.
- McMahon, H.T., Boucrot, E., 2011. Molecular mechanism and physiological

- functions of clathrin-mediated endocytosis. *Nature Reviews Molecular Cell Biology* 12, 517–533. doi: 10.1038/nrm3151.
- Meier, W., 2000. Polymer nanocapsules. *Chemical Society Reviews* 29, 295–303. doi: 10.1039/a809106d.
- Meißner, T., Oelschlägel, K., Potthoff, A., 2014. Implications of the stability behavior of zinc oxide nanoparticles for toxicological studies. *International Nano Letters* 4, 116. doi: 10.1007/s40089-014-0116-5.
- Meng, L., Fu, C., Lu, Q., 2009. Advanced technology for functionalization of carbon nanotubes. *Progress in Natural Science* 19, 801–810. doi: 10.1016/j.pnsc.2008.08.011.
- Mercer, J., Helenius, A., 2009. Virus entry by macropinocytosis. *Nature Cell Biology* 11(5), 510–520. doi: 10.1146/annurev-biochem-060208-104626.
- Merdzan, V., Domingos, R.F., Monteiro, C.E., Hadioui, M., Wilkinson, K.J., 2014. The effects of different coatings on zinc oxide nanoparticles and their influence on dissolution and bioaccumulation by the green alga, *C. reinhardtii*. *Science of the Total Environment*, 488-489, 316–324. doi: 10.1016/j.scitotenv.2014.04.094.
- Meulenkamp, E.A., 1998. Size dependence of the dissolution of ZnO nanoparticles. *The Journal of Physical Chemistry B* 102(40), 7764–7769. doi: 10.1021/jp982305u.
- Miao, A.-J., Zhang, X.-Y., Luo, Z., Chen, C.-S., Chin, W.-C., Santschi, P.H., et al., 2010. Zinc oxide-engineered nanoparticles: Dissolution and toxicity to marine phytoplankton. *Environmental Toxicology and Chemistry* 29(12), 2814–2822. doi: 10.1002/etc.340.

- Miglietta, M.L., Rametta, G., Di Francia, G., 2009. Characterization of carbon based nanoparticles dispersion in aqueous solution using dynamic light scattering technique. *Macromolecular Symposium* 286, 95–100. doi: 10.1002/masy.200951212.
- Miller, G.W., Ulatowski, L., Labut, E.M., Lebold, K.M., Manor, D., Atkinson, J., et al., 2012. The  $\alpha$ -tocopherol transfer protein is essential for vertebrate embryogenesis. *PLoS ONE* 7(10), e47402. doi: 10.1371/journal.pone.0047402.s006.
- Mindell, J.A., 2012. Lysosomal acidification mechanisms. *Annual Review of Physiology* 74, 69–86. doi: 10.1146/annurev-physiol-012110-142317.
- Mitrano, D.M., Motellier, S., Clavaguera, S., Nowack, B., 2015. Review of nanomaterial aging and transformations through the life cycle of nano-enhanced products. *Environment International* 77, 132–147. doi: 10.1016/j.envint.2015.01.013.
- Molony, B., 2001. Environmental requirements and tolerances of rainbow trout (*Oncorhynchus mykiss*) and brown trout (*Salmo trutta*) with special reference to western australia: a review. *Fisheries Research Report No. 130* 1–28.
- Monopoli, M.P., Åberg, C., Salvati, A., Dawson, K.A., 2012. Biomolecular coronas provide the biological identity of nanosized materials. *Nature Nanotechnology* 7, 779–786. doi: 10.1038/nnano.2012.207.
- Monti, D.M., Guarnieri, D., Napolitano, G., Piccoli, R., Netti, P., Fusco, S., et al., 2015. Biocompatibility, uptake and endocytosis pathways of polystyrene nanoparticles in primary human renal epithelial cells. *Journal of Biotechnology*

- 193, 3–10. doi: 10.1016/j.jbiotec.2014.11.004.
- Mori, S., Saino, T., Satoh, Y.I., 2000. Effect of low temperatures on compound 48/80-induced intracellular  $\text{Ca}^{2+}$  changes and exocytosis of rat peritoneal mast cells. *Archives of Histology and Cytology* 63(3), 261–270.
- Mueller, N.C., Nowack, B., 2008. Exposure modeling of engineered nanoparticles in the environment. *Environmental Science and Technology* 42, 4447–4453. doi: 10.1021/es7029637.
- Murdock, R.C., Braydich-Stolle, L., Schrand, A.M., Schlager, J.J., Hussain, S.M., 2008. Characterization of nanomaterial dispersion in solution prior to *in vitro* exposure using dynamic light scattering technique. *Toxicological Sciences* 101(2), 239–253. doi:10.1093/toxsci/kfm240.
- Nabi, I.R., Le, P.U., 2003. Caveolae/raft-dependent endocytosis. *The Journal of Cell Biology* 161(4), 673–677. doi: 10.1083/jcb.200302028.
- Nel, A.E., Mädler, L., Velegol, D., Xia, T., Hoek, E.M.V., Somasundaran, P., et al., 2009. Understanding biophysicochemical interactions at the nano-bio interface. *Nature Materials* 8, 543–557. doi: 10.1038/nmat2442.
- Neouze, M.-A., Schubert, U., 2008. Surface modification and functionalization of metal and metal oxide nanoparticles by organic ligands. *Chemical Monthly* 139, 183–195. doi: 10.1007/s00706-007-0775-2.
- Ngarize, S., Makuch, K.E., Pereira, R., 2012. The regulation of nanotechnologies. In: Makuch, K.E., Pereira, R. (Eds.), *Environmental and Energy Law*, John Wiley & Sons, Inc.
- Nowack, B., Bucheli, T.D., 2007. Occurrence, behavior and effects of nanoparticles

- in the environment. *Environmental Pollution* 150, 5–22. doi:  
10.1016/j.envpol.2007.06.006.
- Nowack, B., David, R.M., Fissan, H., Morris, H., Shatkin, J.A., Stintz, M., et al.,  
2013. Potential release scenarios for carbon nanotubes used in composites.  
*Environment International* 59, 1–11. doi: 10.1016/j.envint.2013.04.003.
- Oberdörster, G., Maynard, A., Donaldson, K., Castranova, V., Fitzpatrick, J.,  
Ausman, K., et al., 2005a. Principles for characterizing the potential human  
health effects from exposure to nanomaterials: elements of a screening strategy.  
*Particle and Fibre Toxicology* 2(8), 1–35. doi: 10.1186/1743-8977-2-8.
- Oberdörster, G., Oberdörster, E., Oberdörster, J., 2005b. Nanotoxicology: An  
emerging discipline evolving from studies of ultrafine particles. *Environmental  
Health Perspectives* 113(7), 823–839. doi: 10.1289/ehp.7339.
- Organisation for Economic Co-operation and Development (OECD), 2012a.  
Important issues on risk assessment of manufactured nanomaterials: Series on the  
Safety of Manufactured Nanomaterials No. 33, ENV/JM/MONO(2012)8;  
[http://www.oecd.org/officialdocuments/publicdisplaydocumentpdf/?cote=env/jm/  
mono\(2012\)8&doclanguage=en](http://www.oecd.org/officialdocuments/publicdisplaydocumentpdf/?cote=env/jm/mono(2012)8&doclanguage=en) (accessed 02.01.2013).
- OECD, 2012b. Guidance on sample preparation and dosimetry for the safety testing  
of manufactured nanomaterials: Series on the safety of manufactured  
nanomaterials No. 36, ENV/JM/MONO(2012)40; [http://www.oecd.org/  
officialdocuments/publicdisplaydocumentpdf/?cote=env/jm/mono\(2012\)40&docl  
anguage=en](http://www.oecd.org/officialdocuments/publicdisplaydocumentpdf/?cote=env/jm/mono(2012)40&doclanguage=en) (accessed 08.11.14).
- OECD, 2012c. OECD guideline for the testing of chemicals: Fish embryo acute

aquatic toxicity test, [http://www.oecd.org/env/ehs/testing/Draft\\_FET\\_TG\\_v9\\_Draft%2011%20Dec%202012\\_CLEAN.pdf](http://www.oecd.org/env/ehs/testing/Draft_FET_TG_v9_Draft%2011%20Dec%202012_CLEAN.pdf) (accessed 15.02.13).

OECD, 2010. List of Manufactured Nanomaterials and List of Endpoints for Phase One of the Sponsorship Programme for the Testing of Manufactured Nanomaterials: Series on the Safety of Manufactured Nanomaterials No. 27, ENV/JM/MONO(2010)46; [http://www.oecd.org/officialdocuments/publicdisplaydocumentpdf/?cote=env/jm/mono\(2010\)46&doclanguage=en](http://www.oecd.org/officialdocuments/publicdisplaydocumentpdf/?cote=env/jm/mono(2010)46&doclanguage=en) (accessed 03.06.12).

Oh, N., Park, J.-H., 2014. Endocytosis and exocytosis of nanoparticles in mammalian cells. *International Journal of Nanomedicine* 9, 51–63. doi: 10.2147/IJN.S26592.

Olive, P.L., 1988. DNA precipitation assay: A rapid and simple method for detecting DNA damage in mammalian cells. *Environmental and Molecular Mutagenesis* 11, 487–495.

Ong, K.J., MacCormack, T.J., Clark, R.J., Ede, J.D., Ortega, V.A., Felix, L.C., et al., 2014a. Widespread nanoparticle-assay interference: Implications for nanotoxicity testing. *PLoS ONE* 9(3), e90650. doi: 10.1371/journal.pone.0090650.

Ong, K.J., Zhao, X., Thistle, M.E., MacCormack, T.J., Clark, R.J., Ma, G., et al., 2014b. Mechanistic insights into the effect of nanoparticles on zebrafish hatch. *Nanotoxicology* 8(2), 295–304. doi: 10.3109/17435390.2013.778345.

Ortega, V.A., Katzenback, B.A., Stafford, J.L., Belosevic, M., Goss, G.G., 2015. Effects of polymer-coated metal oxide nanoparticles on goldfish (*Carassius auratus* L.) neutrophil viability and function. *Nanotoxicology* 9(1), 23–33. doi: 10.3109/17435390.2013.861943.

- Pan, Z., Lee, W., Slutsky, L., Clark, R.A.F., Pernodet, N., Rafailovich, M.H., 2009. Adverse effects of titanium dioxide nanoparticles on human dermal fibroblasts and how to protect cells. *Small* 5(4), 511–520. doi: 10.1002/sml.200800798.
- Patel, H.H., Insel, P.A., 2009. Lipid rafts and caveolae and their role in compartmentation of redox signaling. *Antioxidants and Redox Signaling* 11(6), 1357–1372. doi: 10.1089=ars.2008.2365.
- Patil, S., Sandberg, A., Heckert, E., Self, W., Seal, S., 2007. Protein adsorption and cellular uptake of cerium oxide nanoparticles as a function of zeta potential. *Biomaterials* 28, 4600–4607. doi: 10.1016/j.biomaterials.2007.07.029.
- Pelaez, M., Nolan, N.T., Pillai, S.C., Seery, M.K., Falaras, P., Kontos, A.G., et al., 2012. A review on the visible light active titanium dioxide photocatalysts for environmental applications. *Applied Catalysis B: Environmental* 125, 331–349. doi: 10.1016/j.apcatb.2012.05.036.
- Petersen, E.J., Diamond, S.A., Kennedy, A.J., Goss, G.G., Ho, K., Lead, J., et al., 2015. Adapting OECD aquatic toxicity tests for use with manufactured nanomaterials: Key issues and consensus recommendations. *Environmental Science and Technology* 49, 9532–9547. doi:10.1021/acs.est.5b00997.
- Petersen, E.J., Henry, T.B., Zhao, J.A., MacCuspie, R.I., Kirschling, T.L., Dobrovolskaia, M.A., et al., 2014. Identification and avoidance of potential artifacts and misinterpretations in nanomaterial ecotoxicity measurements. *Environmental Science and Technology* 48, 4226–4246. doi: 10.1021/es4052999.
- Petosa, A.R., Brennan, S.J., Rajput, F., Tufenkji, N., 2012. Transport of two metal oxide nanoparticles in saturated granular porous media: Role of water chemistry

- and particle coating. *Water Research* 46(4), 1273–1285. doi: 10.1016/j.watres.2011.12.033.
- Pérez-de-Luque, A., Rubiales, D., 2009. Nanotechnology for parasitic plant control. *Pest Management Science* 65, 540–545. doi: 10.1002/ps.1732.
- Pham, H., Li, F., Goh, J.B., Dinglasan, J., Anderson, D., 2010. Polymer nanoparticles as formulation agents. *NSTI-Nanotech* 1, 869–871.
- Piccinno, F., Gottschalk, F., Seeger, S., Nowack, B., 2012. Industrial production quantities and uses of ten engineered nanomaterials in Europe and the world. *Journal of Nanoparticle Research* 14, 1109. doi: 10.1007/s11051-012-1109-9.
- Pietrojusti, A., Magrini, A., Campagnolo, L., 2014. Mechanisms of nanomaterial toxicity. In: Njuguna, J., Pielichowski, K., Zhu, H. (Eds.), *Health and Environmental Safety of Nanomaterials: Polymer Nanocomposites and Other Materials Containing Nanoparticles*, Elsevier, pp. 28–43. doi: 10.1533/9780857096678.1.28.
- Pigeolet, E., Corbisier, P., Houbion, A., Lambert, D., Michiels, C., Raes, M., et al., 1990. Glutathione peroxidase, superoxide dismutase, and catalase inactivation by peroxides and oxygen derived free radicals. *Mechanisms of Ageing and Development* 51, 283–297. doi: [http://dx.doi.org/10.1016/0047-6374\(90\)90078](http://dx.doi.org/10.1016/0047-6374(90)90078).
- Pitkänen, M., Kangas, H., Vartiainen, J., 2014. Toxicity and health issues. In: Oksman, K., Mathew, A.P., Bismarck, A., Rojas, O., Sain, M. (Eds.), *Handbook of Green Materials: Processing Technologies, Properties and Applications*. World Scientific, pp. 1–1200.
- Popova, N.V., Deyev, I.E., Petrenko, A.G., 2013. Clathrin-mediated endocytosis and

- adaptor proteins. *Acta Nature* 5(3), 62–73.
- Powers, D.A., 1989. Fish as model systems. *Science* 246, 351–348.
- Prasad, K.N., 2012. Health risks of nonionizing radiation and their prevention and mitigation. In: *Radiation injury prevention and mitigation*. CRC Press, pp. 1-312.
- Prepas, E., 1990. Water quality. In: Mitchell, P., Prepas, E. (Eds.), *Atlas of Alberta Lakes* [Online]. The University of Alberta Press.
- Price, B.K., Lomeda, J.R., Tour, J.M., 2009. Aggressively oxidized ultra-short single-walled carbon nanotubes having oxidized sidewalls. *Chemistry of Materials* 21, 3917–3923. doi: 10.1021/cm9021613.
- Priestly, B.G., Bartholomaeus, A., Drew, R., 2014. Hazards of food contact material: Nanotechnologies and nanomaterials. In: *Reference Module in Food*, from *Encyclopedia of Food Safety*. Academic Press, pp. 444–448.
- Rai, P.K., Parra-Vasquez, A.N.G., Chattopadhyay, J., Pinnick, R.A., Liang, F., Sadana, A.K., et al., 2007. Dispersions of functionalized single-walled carbon nanotubes in strong acids: Solubility and rheology. *Journal of Nanoscience and Nanotechnology* 7(10), 3378–3385. doi:10.1166/jnn.2007.835.
- Ramsden, C. S., Henry, T. B., Handy, R. D., 2013. Sub-lethal effects of titanium dioxide nanoparticles on the physiology and reproduction of zebrafish. *Aquatic Toxicology* 126, 404–413. doi: 10.1016/j.aquatox.2012.08.021.
- Rasband, W.S., 2012. ImageJ. U.S. National Institutes of Health, Bethesda, Maryland, USA, <http://imagej.nih.gov/ij/> (accessed 23.03.16).
- Rasmussen, K., González, M., Kearns, P., Sintes, J.R., Rossi, F., Sayre, P., 2016. Review of achievements of the OECD Working Party on Manufactured

- Nanomaterials' Testing and Assessment Programme. From exploratory testing to test guidelines. *Regulatory Toxicology and Pharmacology* 74, 147–160. doi: 10.1016/j.yrtph.2015.11.004.
- Rawson, D.M., Zhang, T., Kalicharan, D., Jongebloed, W.L., 2000. Field emission scanning electron microscopy and transmission electron microscopy studies of the chorion, plasma membrane and syncytial layers of the gastrula-stage embryo of the zebrafish *Brachydanio rerio*: a consideration of the structural and functional relationships with respect to cryoprotectant penetration. *Aquaculture Research* 31(3), 325–336. doi: 10.1046/j.1365-2109.2000.00401.x.
- Reinsborough, M., Sullivan, G., 2011. The regulation of nano-particles under the european biocidal products directive: Challenges for effective civil society participation. *European Journal of Law and Technology* 2(3), 1–19.
- Rejman, J., Oberle, V., Zuhorn, I.S., Hoekstra, D., 2004. Size-dependent internalization of particles via the pathways of clathrin- and caveolae-mediated endocytosis. *Biochemical Journal* 377, 159–169. doi: 10.1042/bj20031253.
- Riley, P.A., 1994. Free radicals in biology: oxidative stress and the effects of ionizing radiation. *International Journal Radiation Biology* 65(1), 27–33. doi: 10.1080/09553009414550041.
- Rojas, D.A., Perez-Munizaga, D.A., Centanin, L., Antonelli, M., Wappner, P., Allende, M.L., et al., 2007. Cloning of *hif-1 $\alpha$*  and *hif-2 $\alpha$*  and mRNA expression pattern during development in zebrafish. *Gene Expression Patterns* 7, 339–345. doi: 10.1016/j.modgep.2006.08.002.
- Roman, M., 2015. Toxicity of cellulose nanocrystals: A review. *Industrial*

- Biotechnology 11(1), 25–33. doi: 10.1089/ind.2014.0024.
- Roman, M., Dong, S., Hirani, A., Lee, Y.W., 2009. Cellulose nanocrystals for drug delivery. In: ACS Symposium Series. American Chemical Society, Washington, DC, pp. 81–91. doi: 10.1021/bk-2009-1017.ch004.
- Sadler, G.W., 1992. Ultraviolet radiation at Edmonton, Alberta, Canada. Solar Energy 49(1), 13–17. doi: [http://dx.doi.org/10.1016/0038-092X\(92\)90121-P](http://dx.doi.org/10.1016/0038-092X(92)90121-P).
- Safari, S., Dehkordy, S.E., Kazemi, M., Dehghan, H., Mahaki, B., 2015. Ultraviolet radiation emissions and illuminance in different brands of compact fluorescent lamps. International Journal of Photoenergy 2015(504674), 1–6. doi: 10.1155/2015/504674.
- Sakhtianchi, R., Minchin, R.F., Lee, K.-B., Alkilany, A.M., Serpooshan, V., Mahmoudi, M., 2013. Exocytosis of nanoparticles from cells: role in cellular retention and toxicity. Advances in Colloid and Interface Science. 201-202, 18–29. doi: 10.1016/j.cis.2013.10.013.
- Sano, K., Inohaya, K., Kawaguchi, M., Yoshizaki, N., Iuchi, I., Yasumasu, S., 2008. Purification and characterization of zebrafish hatching enzyme - an evolutionary aspect of the mechanism of egg envelope digestion. FEBS Journal 275, 5934–5946. doi: 10.1111/j.1742-4658.2008.06722.x.
- Santos, M., Teixeira, J., Rodrigues, A., 2000. Production of dextransucrase, dextran and fructose from sucrose using *Leuconostoc mesenteroides* NRRL B512(f). Biochemical Engineering Journal 4, 177–188. doi: 10.1016/S1369-703X(99)00047-9.
- Sauer, M., Meier, W., 2001. Responsive nanocapsules. Chemical Communications

55–56. doi: 10.1039/b007118h.

Sayes, C.M., Liang, F., Hudson, J.L., Mendez, J., Guo, W., Beach, J.M., et al., 2006.

Functionalization density dependence of single-walled carbon nanotubes

cytotoxicity *in vitro*. *Toxicology Letters* 161, 135–142. doi:

10.1016/j.toxlet.2005.08.011.

Scientific Committee on Emerging and Newly Identified Health Risks (SCENIHR),

2009. Risk Assessment of Products of Nanotechnologies. European Commission,

pp. 1–71. [http://ec.europa.eu/health/ph\\_risk/committees/04\\_scenihhr/docs/](http://ec.europa.eu/health/ph_risk/committees/04_scenihhr/docs/scenihhr_o_023.pdf)

[scenihhr\\_o\\_023.pdf](http://ec.europa.eu/health/ph_risk/committees/04_scenihhr/docs/scenihhr_o_023.pdf) (accessed 15.04.16).

Schultz, A.G., Boyle, D., Chamot, D., Ong, K.J., Wilkinson, K.J., McGeer, J.C., et

al., 2014. Aquatic toxicity of manufactured nanomaterials: Challenges and

recommendations for future toxicity testing. *Environmental Chemistry* 11, 207–

226. doi: 10.1071/EN13221.

Schultz, A.G., Ong, K.J., MacCormack, T., Ma, G., Veinot, J.G.C., Goss, G.G., 2012.

Silver nanoparticles inhibit sodium uptake in juvenile rainbow trout

(*Oncorhynchus mykiss*). *Environmental Science and Technology* 46, 10295–

10301. doi: 10.1021/es3017717.

Scown, T.M., van Aerle, R., Tyler, C.R., 2010. Review: Do engineered nanoparticles

pose a significant threat to the aquatic environment? *Critical Reviews in*

*Toxicology* 40(7), 653–670. doi: 10.3109/10408444.2010.494174.

Selck, H., Handy, R.D., Fernandes, T.F., Klaine, S.J., Petersen, E.J., 2016.

Nanomaterials in the aquatic environment: A European Union-United States

perspective on the status of ecotoxicity testing, research priorities, and challenges

- ahead. *Environmental Toxicology and Chemistry* 35(5), 1055–1067. doi:  
10.1002/etc.3385.
- Shang, L., Nienhaus, K., Nienhaus, G.U., 2014. Engineered nanoparticles interacting with cells: size matters. *Journal of Nanobiotechnology* 12, 5, 1–11. doi:  
10.1186/1477-3155-12-5.
- Sharma, A., Anghore, D., Awasthi, R., Kosey, S., Jundal, J., Gupta, N., et al., 2015. A review on current carbon nanomaterials and other nanoparticles technology and their applications in biomedicine. *World Journal of Pharmacy and Pharmaceutical Sciences* 4(12), 1088–1113.
- Shi, H., Magaye, R., Catstranova, V., Zhao, J., 2013. Titanium dioxide nanoparticles: a review of current toxicological data. *Particle and Fibre Toxicology* 10, 1–33. doi: 10.1186/1743-8977-10-15.
- Shin, S.W., Song, I.N., Um, S.H., 2015. Role of physicochemical properties in nanoparticle toxicity. *Nanomaterials* 5, 1351–1365. doi: 10.3390/nano5031351.
- Shukla, S.J., Huang, R., Austin, C.P., Xia, M., 2010. The future of toxicity testing: A focus on *in vitro* methods using a quantitative high-throughput screening platform. *Drug Discovery Today* 15(23-24), 997–1007. doi:  
10.1016/j.drudis.2010.07.007.
- Shvedova, A., Pietroiusti, A., Kagan, V., 2016. Nanotoxicology ten years later: Lights and shadows. *Toxicology and Applied Pharmacology* 299, 1–2. doi:  
10.1016/j.taap.2016.02.014.
- Sies, H., 2007. Biological redox systems and oxidative stress. *Cellular and Molecular Life Sciences* 64, 2181–2188. doi: 10.1007/s00018-007-7230-8.

- Singh, J., Michel, D., Chitanda, J.M., Verrall, R.E., Badea, I., 2012. Evaluation of cellular uptake and intracellular trafficking as determining factors of gene expression for amino acid-substituted gemini surfactant-based DNA nanoparticles. *Journal of Nanobiotechnology* 10, 7, 1–14. doi: 10.1186/1477-3155-10-7.
- Singh, R., Tiwari, S., Tawaniya, J., 2013. Review on nanotechnology with several aspects. *International Journal of Research in Computer Engineering and Electronics* 2(3), 1–8. doi: 10.1016/j.yrtph.2008.10.008.
- Smart, S.K., Cassady, A.I., Lu, G.Q., Martin, D.J., 2006. The biocompatibility of carbon nanotubes. *Carbon* 44, 1034–1047. doi: 10.1016/j.carbon.2005.10.011.
- Smijs, T.G., Pavel, S., 2011. Titanium dioxide and zinc oxide nanoparticles in sunscreens: focus on their safety and effectiveness. *Nanotechnology, Science and Applications* 4, 95–112. doi: 10.2147/NSA.S19419.
- Smith, C.J., Shaw, B.J., Handy, R.D., 2007. Toxicity of single walled carbon nanotubes to rainbow trout, (*Oncorhynchus mykiss*): Respiratory toxicity, organ pathologies, and other physiological effects. *Aquatic Toxicology* 82, 94–109. doi: 10.1016/j.aquatox.2007.02.003.
- Sokolova, V., Kozlova, D., Knuschke, T., Buer, J., Westendorf, A.M., Epple, M., 2013. Mechanism of the uptake of cationic and anionic calcium phosphate nanoparticles by cells. *Acta Biomaterialia* 9, 7527–7535. doi: 10.1016/j.actbio.2013.02.034.
- Spitalsky, Z., Tasis, D., Papagelis, K., Galiotis, C., 2010. Carbon nanotube–polymer composites: Chemistry, processing, mechanical and electrical properties. *Progress*

- in *Polymer Science* 35, 357–401. doi: 10.1016/j.progpolymsci.2009.09.003.
- Stadtman, E. R., Levine, R. L., 2003. Free radical-mediated oxidation of free amino acids and amino acid residues in proteins. *Amino Acids* 25, 207–218. doi: 10.1007/s00726-003-0011-2.
- Star, A., Stoddart, J.F., Steuerman, D., Diehl, M., Boukai, A., Wong, E.W., et al., 2001. Preparation and properties of polymer-wrapped single-walled carbon nanotubes. *Angewandte Chemie International Edition* 40(9), 1721–1725. doi: 10.1002/1521-3773(20010504)40:9<1721::AID-ANIE17210>3.0.CO;2-F.
- Stebounova, L.V., Guio, E., Grassian, V.H., 2011. Silver nanoparticles in simulated biological media: a study of aggregation, sedimentation, and dissolution. *Journal of Nanoparticle Research* 13, 233–244. doi: 10.1007/s11051-010-0022-3.
- Stott, L.C., Schnell, S., Hogstrand, C., Owen, S.F., Bury, N.R., 2015. A primary fish gill cell culture model to assess pharmaceutical uptake and efflux: Evidence for passive and facilitated transport. *Aquatic Toxicology* 159, 127–137. doi: 10.1016/j.aquatox.2014.12.007.
- Subbiah, R., Veerapandian, M., Yun, K.S., 2010. Nanoparticles: Functionalization and multifunctional applications in biomedical sciences. *Current Medicinal Chemistry* 17, 4559–4577. doi: 10.2174/092986710794183024.
- Suen, W.-L.L., Chau, Y., 2013. Size-dependent internalisation of folate-decorated nanoparticles via the pathways of clathrin and caveolae-mediated endocytosis in ARPE-19 cells. *Journal of Pharmacy and Pharmacology* 66, 564–573. doi: 10.1111/jphp.12134.
- Sur, U.K., 2012. Graphene: A rising star on the horizon of materials science.

- International Journal of Electrochemistry 2012(237689), 1–12. doi:  
10.1155/2012/237689.
- Taniguchi, N., 1974. On the basic concept of nano-technology. In: Proceedings of the International Conference on Production Engineering, Tokyo, pp. 18–23.
- Taurozzi, J.S., Hackley, V.A., Wiesner, M.R., 2011. Ultrasonic dispersion of nanoparticles for environmental, health and safety assessment – issues and recommendations. *Nanotoxicology* 5(4), 711–729. doi:  
10.3109/17435390.2010.528846.
- Taylor, N.S., Merrifield, R., Williams, T.D., Chipman, K.J., Lead, J.R., Viant, M.R., 2016. Molecular toxicity of cerium oxide nanoparticles to the freshwater alga *Chlamydomonas reinhardtii* is associated with supra-environmental exposure concentrations. *Nanotoxicology* 10(1), 32–41. doi:  
10.3109/17435390.2014.1002868.
- Thakare, V.S., Prendergast, D., Pastorin, G., Jain, S., 2015. Carbon-based nanomaterials for targeted drug delivery and imaging. In: Devarajan, S., Jain, S. (Eds.), *Targeted Drug Delivery: Concepts and Design*, Springer International Publishing, pp. 615e645. doi: 10.1007/978-3-319-11355-5\_19.
- Tortiglione, C., Quarta, A., Malvindi, M.A., Tino, A., Pellegrino, T., 2009. Fluorescent nanocrystals reveal regulated portals of entry into and between the cells of hydra. *PLoS ONE* 4(11), e7698. doi:10.1371/journal.pone.0007698.
- Usenko, C.Y., Harper, S.L., Tanguay, R.L., 2008. Fullerene C<sub>60</sub> exposure elicits an oxidative stress response in embryonic zebrafish. *Toxicology and Applied Pharmacology* 229, 44–55. doi: 10.1016/j.taap.2007.12.030.

- Valdiglesias, V., Fernández-Bertólez, N., Kiliç, G., Costa, C., Costa, S., Fraga, S., et al., 2016. Are iron oxide nanoparticles safe? Current knowledge and future perspectives. *Journal of Trace Elements in Medicine and Biology*. 1–11. doi: 10.1016/j.jtemb.2016.03.017.
- Van der Velden, J.L., Bertoncello, I., McQualter, J.L., 2013. LysoTracker is a marker of differentiated alveolar type II cells. *Respiratory Research* 14, 123, 1–7. doi: 10.1186/1465-9921-14-123.
- Van Hoecke, K., De Schamphelaere, K.A.C., Van der Meeren, P., Smagghe, G., Janssen, C.R., 2011. Aggregation and ecotoxicity of CeO<sub>2</sub> nanoparticles in synthetic and natural waters with variable pH, organic matter concentration and ionic strength. *Environmental Pollution* 159, 970–976. doi: 10.1016/j.envpol.2010.12.010.
- Van Hoecke, K., Quik, J.T.K., Mankiewicz-Boczek, J., Schamphelaere, K.A.C.D., Elsaesser, A., Meeren, P.V.D., et al., 2009. Fate and effects of CeO<sub>2</sub> nanoparticles in aquatic ecotoxicity tests. *Environmental Science and Technology* 43, 4537–4546. doi: 10.1021/es9002444.
- Vance, M.E., Kuiken, T., Vejerano, E.P., McGinnis, S.P., Hochella, M.F.Jr., Rejeski, D., et al., 2015. Nanotechnology in the real world: Redeveloping the nanomaterial consumer products inventory. *Beilstein Journal of Nanotechnology*. 6, 1769–1780. doi: 10.3762/bjnano.6.181.
- Vandamme, T.F., Brobeck, L., 2005. Poly(amidoamine) dendrimers as ophthalmic vehicles for ocular delivery of pilocarpine nitrate and tropicamide. *Journal of Controlled Release* 102, 23–38. doi: 10.1016/j.jconrel.2004.09.015.

- Vardharajula, S., Ali, S.K., Tiwari, P.M., Eroğlu, E., Vig, K., Dennis, V.A., et al., 2012. Functionalized carbon nanotubes: biomedical applications. *International Journal of Nanomedicine* 7, 5361–5374. doi: 10.2147/IJN.S35832.
- Vercauteren, D., Vandenbroucke, R.E., Jones, A.T., Rejman, J., Demeester, J., De Smedt, S.C., et al., 2010. The use of inhibitors to study endocytic pathways of gene carriers: optimization and pitfalls. *Molecular Therapy* 18(3), 561–569. doi: 10.1038/mt.2009.281.
- Verdouw, H., van Echteld, C.J.A., Dekkers, E.M.J., 1978. Ammonia determination based on indophenol formation with sodium salicylate. *Water Research* 12, 399–402. doi: 10.1016/0043-1354(78)90107-0.
- Verma, A., Stellacci, F., 2010. Effect of surface properties on nanoparticle-cell interactions. *Small* 6(1), 12–21. doi: 10.1002/smll.200901158.
- Verwey, E.J.W., Overbeek, J.T.G., 1948. Theory of the stability of lyophobic colloids. Elsevier 1–108.
- Wagner, S., Gondikas, A., Neubauer, E., Hofmann, T., von der Kammer, F., 2014. Spot the difference: Engineered and natural nanoparticles in the environment-Release, behavior, and fate. *Angewandte Chemie International Edition* 53, 12398–12419. doi: 10.1002/anie.201405050.
- Wang, B., He, X., Zhang, Z., Zhao, Y., Feng, W., 2013. Metabolism of nanomaterials *in vivo*: Blood circulation and organ clearance. *Accounts of Chemical Research* 46(3), 761–769. doi: 10.1021/ar2003336.
- Wang, L.-H., Rothberg, K.G., Anderson, R.G.W., 1993. Mis-assembly of clathrin lattices on endosomes reveals a regulatory switch for coated pit formation. *The*

- Journal of Cell Biology 123(5), 1107–1117. doi: 10.1083/jcb.123.5.1107.
- Wang, R.H., Meredith, A.N., Lee, M.Jr., Deutsch, D., Miadzedskaya, L., Braun, E., et al., 2015. Toxicity assessment and bioaccumulation in zebrafish embryos exposed to carbon nanotubes suspended in Pluronic® F-108, 1–11. doi: 10.3109/17435390.2015.1107147.
- Warheit, D.B., Donner, M., 2010. Rationale of genotoxicity testing of nanomaterials: Regulatory requirements and appropriateness of available OECD test guidelines. *Nanotoxicology* 44, 409–413. doi: 10.3109/17435390.2010.485704.
- Watanabe, T., Nakajima, A., Wang, R.H., Minabe, M., Koizumi, S., Fujishima, A., et al., 1999. Photocatalytic activity and photoinduced hydrophilicity of titanium dioxide coated glass. *Thin Solid Films* 351(1-2), 260–263. doi: [http://dx.doi.org/10.1016/S0040-6090\(99\)00205-9](http://dx.doi.org/10.1016/S0040-6090(99)00205-9).
- Weir, A., Westerhoff, P., Fabricius, L., Hristovski, K., von Goetz, N., 2012. Titanium dioxide nanoparticles in food and personal care products. *Environmental Science and Technology* 46(4), 2242–2250. doi: 10.1021/es204168d.
- Westmeier, D., Stauber, R.H., Docter, D., 2016. The concept of bio-corona in modulating the toxicity of engineered nanomaterials (ENM). *Toxicology and Applied Pharmacology* 299, 53–57. doi: 10.1016/j.taap.2015.11.008.
- Weydert, C.J., Cullen, J.J., 2009. Measurement of superoxide dismutase, catalase and glutathione peroxidase in cultured cells and tissue. *Nature Protocols* 5, 51–66. doi: 10.1038/nprot.2009.197.
- White, B., Banerjee, S., O'Brien, S., Turro, N.J., Herman, I.P., 2007. Zeta-potential measurements of surfactant-wrapped individual single-walled carbon nanotubes.

- The Journal of Physical Chemistry C 111(37), 13684–13690. doi:  
10.1021/jp070853e.
- Wiesner, M.R., Lowry, G.V., Jones, K.L., Hochella, M.F.J., Giulio, R.T., Casman, E.,  
et al., 2009. Decreasing uncertainties in assessing environmental exposure, risk,  
and ecological implications of nanomaterials. *Environmental Science and  
Technology* 43(17), 6458–6462. doi: 10.1021/es803621k.
- Wilhelm, C., Billotey, C., Roger, J., Pons, J.N., Bacri, J.C., Gazeau, F., 2003.  
Intracellular uptake of anionic superparamagnetic nanoparticles as a function of  
their surface coating. *Biomaterials* 24(6), 1001–1011. doi:  
[http://dx.doi.org/10.1016/S0142-9612\(02\)00440-4](http://dx.doi.org/10.1016/S0142-9612(02)00440-4).
- Won, E.-J., Lee, Y., Han, J., Hwang, U.-K., Shin, K.-H., Park, H.G., et al., 2014.  
Effects of UV radiation on hatching, lipid peroxidation, and fatty acid  
composition in the copepod *Paracyclops nana*. *Comparative Biochemistry and  
Physiology, Part C* 165, 60–66. doi: 10.1016/j.cbpc.2014.06.001.
- Wörle-Knirsch, J.M., Pulskamp, K., Krug, H.F., 2006. Oops they did it again! Carbon  
nanotubes hoax scientists in viability assays. *Nano Letters* 6(6), 1261–1268. doi:  
10.1021/nl060177c.
- Wu, R.S.S., 2009. Effects of hypoxia on fish reproduction and development. In:  
Richards, J.G., Farrell, A.P., Brauner, C.J. (Eds.), *Fish Physiology: Hypoxia*,  
Academic Press, pp. 79e141.
- Xie, Y., He, Y., Irwin, P.L., Jin, T., Shi, X., 2011. Antibacterial activity and  
mechanism of action of zinc oxide nanoparticles against *Campylobacter jejuni*.  
*Applied and Environmental Microbiology* 77(7), 2325–2331. doi:

10.1128/AEM.02149-10.

- Xu, L., Cao, L.-D., Li, F.-M., Wang, X.-J., Huang, Q.-L., 2014. Utilization of chitosan-lactide copolymer nanoparticles as controlled release pesticide carrier for pyraclostrobin against *colletotrichum gossypii* southw. *Journal of Dispersion Science and Technology* 35(4), 554–550. doi:10.1080/01932691.2013.800455.
- Yang, X., Gondikas, A.P., Marinakos, S.M., Auffan, M., Liu, J., Hsu-Kim, H., et al., 2012. Mechanism of silver nanoparticle toxicity is dependent on dissolved silver and surface coating in *Caenorhabditis elegans*. *Environmental Science and Technology* 46(2), 1119–1127. doi: 10.1021/es202417t.
- Yih, T.C., Moudgil, V.K., 2007. Nanotechnology comes of age to trigger the third industrial revolution. *Nanomedicine: Nanotechnology, Biology, and Medicine* 3(4), 245. doi: 10.1016/j.nano.2007.10.083.
- Yin, H., Casey, P.S., McCall, M.J., 2010. Surface modification of ZnO nanoparticles and their cytotoxicity. *Journal of Nanoscience and Nanotechnology*. 10(11), 7565–7570. doi: 10.1166/jnn.2010.2833.
- Yu, H., Jin, Y., Peng, F., Wang, H., Yang, J., 2008. Kinetically controlled side-wall functionalization of carbon nanotubes by nitric acid oxidation. *The Journal of Physical Chemistry C*. 112(17), 6758–6763. doi: 10.1021/jp711975a.
- Yu, L.-P., Fang, T., Xiong, D.-W., Zhu, W.-T., Sima, X.-F., 2011. Comparative toxicity of nano-ZnO and bulk ZnO suspensions to zebrafish and the effects of sedimentation, OH• production and particle dissolution in distilled water. *Journal of Environmental Monitoring* 13(7), 1975–1982. doi: 10.1039/c1em10197h.
- Yuan, C.-Y., Lee, Y.-J., Hsu, G.-S. W., 2012. Aluminum overload increases oxidative

- stress in four functional brain areas of neonatal rats. *Journal of Biomedical Science* 19:51. doi: 10.1186/1423-0127-19-51.
- Zhang, L.W., Monteiro-Riviere, N.A., 2009. Mechanisms of quantum dot nanoparticle cellular uptake. *Toxicological Sciences* 110(1), 138–155. doi:10.1093/toxsci/kfp087.
- Zhang, W., Dong, D., Li, P., Wang, D., Mu, H., Niu, H., et al., 2016. Novel pH-sensitive polysialic acid based polymeric micelles for triggered intracellular release of hydrophobic drug. *Carbohydrate Polymers* 139, 75–81. doi: 10.1016/j.carbpol.2015.12.041.
- Zhao, X., Liu, R., 2012. Recent progress and perspectives on the toxicity of carbon nanotubes at organism, organ, cell, and biomacromolecule levels. *Environment International* 40, 244–255. doi: 10.1016/j.envint.2011.12.003.
- Zhao, X., Ong, K.J., Ede, J.D., Stafford, J.L., Ng, K.W., Goss, G.G., et al., 2013a. Evaluating the toxicity of hydroxyapatite nanoparticles in catfish cells and zebrafish embryos. *Small* 9(9-10), 1734–1741. doi: 10.1002/smll.201200639.
- Zhao, X., Wang, S., Wu, Y., You, H., Lv, L., 2013b. Acute ZnO nanoparticles exposure induces developmental toxicity, oxidative stress and DNA damage in embryo-larval zebrafish. *Aquatic Toxicology* 136-137, 49–59. doi: 10.1016/j.aquatox.2013.03.019.
- Zhu, X., Tian, S., Cai, Z., 2012. Toxicity assessment of iron oxide nanoparticles in zebrafish (*Danio rerio*) early life stages. *PLoS ONE* 7(9), e46286. doi: 10.1371/journal.pone.0046286.g003.
- Zhu, X., Zhu, L., Duan, Z., Qi, R., Li, Y., Lang, Y., 2008. Comparative toxicity of

several metal oxide nanoparticle aqueous suspensions to zebrafish (*Danio rerio*)  
early developmental stage. Journal of Environmental Science and Health, Part A  
43(3), 278–284. doi: 10.1080/10934520701792779.

## APPENDICES

### Supplemental Tables

**Table S2-1. Product information provided by Vive Crop Protection Inc.** Lot number, particle size (nm), pH, total metal (%), and purity (%) of vnTiO<sub>2</sub>, vnZnO, vnFe<sub>2</sub>O<sub>3</sub>, and vnCeO<sub>2</sub> NPs.

NP <sup>a</sup>	Lot Number	Size (nm) <sup>b</sup>	pH	Total Metal (%) <sup>c</sup>	Purity (%) <sup>d</sup>
vnTiO <sub>2</sub>	PB 42	3-9	7.0	46.0	98.0
vnZnO	PB-14,15,16	3-9	8.9	18.0	99.7
vnFe <sub>2</sub> O <sub>3</sub>	PB 27	4.5	9.6	24.2	97.8
vnCeO <sub>2</sub>	JD0712SRFD	3-9	8.9	17.0	88.0

<sup>a</sup>NP = Nanoparticle

<sup>b</sup>Exclusive of poly (acrylic) acid coating

<sup>c</sup>Total metal, Ti, Zn, Fe, or Ce

<sup>d</sup>Purity is exclusive of Na<sup>+</sup> stabilizer and poly (acrylic acid) coating

Note: Properties were not measured for vnCAP (Lot Number: PB 47) due to the absence of a metal core.

**Table S2-2. pH values of vnCAP exposure suspensions.** The vnCAP stock suspension (10,000 mg/L) was serially diluted to 400, 800, 1200, 1600, or 2000 mg/L with DTW and half of the exposure suspensions were pH-adjusted from slightly acidic to near neutral values.

<b>Concentration (mg/L)</b>	<b>vnCAP</b>	<b>pH-adjusted vnCAP</b>
400	5.5	7.4
800	4.8	7.5
1200	4.4	7.6
1600	4.1	7.5
2000	4.0	7.5

Note: A DTW control was pH-adjusted from 7.5 to 4.0 to match the pH of the 2000 mg/L vnCAP suspension.

**Table S2-3. Trace metal content present in NP stock suspensions,** as analyzed by the manufacturer. Percent trace metal ( $\geq 0.1\%$ ), excluding  $\text{Na}^+$ , present in  $\text{vnTiO}_2$ ,  $\text{vnZnO}$ ,  $\text{vnCAP}$ ,  $\text{vnFe}_2\text{O}_3$ , and  $\text{vnCeO}_2$  stock suspensions.

<b>Trace Metal (%)</b>	<b>vnTiO<sub>2</sub></b>	<b>vnZnO</b>	<b>vnCAP</b>	<b>vnFe<sub>2</sub>O<sub>3</sub></b>	<b>vnCeO<sub>2</sub></b>
Ag	0.5	-	-	-	-
Al	0.3	-	0.3	0.5	0.7
B	0.1	-	3.5	0.3	0.6
Ca	-	-	10.4	0.4	1.2
Co	0.1	-	-	-	-
Cr	-	-	-	-	0.6
Ga	-	-	-	-	2.7
Gd	-	-	-	-	0.4
Ho	-	-	-	-	1.2
Ir	-	-	-	-	0.2
K	-	-	-	0.4	0.9
Li	-	0.4	-	-	-
Mg	-	0.3	-	-	-
P	-	-	-	-	0.4
Pr	-	-	-	-	0.3
Rb	-	-	-	-	0.2
Si	-	1.8	-	-	1.4
Zn	-	-	-	-	0.3

Note: Dash indicates trace metal not present or below ICP-MS detection limit.

**Table S2-4. Lethal concentration 50 values and 95% confidence intervals.**

Zebrafish were exposed to vnTiO<sub>2</sub> (n = 5), vnZnO (n = 5), vnCAP (n = 10), vnFe<sub>2</sub>O<sub>3</sub> (n = 7), or vnCeO<sub>2</sub> (n = 5) for 72 h.

NP <sup>a</sup>	LC50 <sup>b</sup> (mg/L)	95% CI <sup>c</sup>
vnTiO <sub>2</sub>	> 2000	-
vnZnO	1589.04	1145.51-2676.88
vnCAP	1234.86	312.40-1873.75
vnFe <sub>2</sub> O <sub>3</sub>	> 2000	-
vnCeO <sub>2</sub>	> 2000	-

<sup>a</sup>NP = Nanoparticle

<sup>b</sup>LC50 = Lethal concentration 50 value

<sup>c</sup>CI = Confidence interval

Note: Regression equations in log probit scale are  $y = 1.23x + 1.09$  and  $y = 0.037x + 4.31$  for vnZnO and vnCAP, respectively.

**Table S3-1. Gene-specific primers for zebrafish.** NCBI reference sequence, forward (F) and reverse (R) primer sequence (5' – 3'), amplicon length in base pairs, and amplification efficiency (E) of the endogenous control gene (*ef1α*) and genes of interest (*hif1ab*, *α-ttp*, *gclc*, and *hsp70*) measured using quantitative polymerase chain reaction.

Gene Name (Abbreviation)	Reference Sequence	F / R	Primer Sequence (5' – 3')	Length	E
<i>elongation factor 1 alpha (ef1α)</i> <sup>1</sup>	NM_131263.1	F	GCTGGCAAGGTCACAAAGTCT	76	1.99
		R	CCTTTGGAACGGTGTGATTGA		
<i>hypoxia-inducible factor 1 alpha subunit b (hif1ab)</i> <sup>2</sup>	NM_200233.1	F	CCACCACCCAAAAACTCCCT	77	2.20
		R	GGAGTGGGGGCGATAAAACA		
<i>alpha-tocopherol transport protein (α-ttp)</i> <sup>2</sup>	NM_212590.1	F	AAGGTGGCGCACATGGA	75	2.12
		R	CGGTAGAAGGTCAGTAGCAATAATAAAG		
<i>glutamate-cysteine ligase catalytic subunit (gclc)</i> <sup>2</sup>	NM_199277.2	F	CGAAAGCTCCTCTGCATGAGA	80	1.92
		R	AAACGTTTCCATTTTCGTTGCT		
<i>heat shock protein 70 kDa (hsp70)</i> <sup>2</sup>	AB062116.1	F	GGGCAGGCTGAGCAAAGAG	75	2.03
		R	TGCAGATCGTCTTCAGCTTTGT		

<sup>1</sup>Endogenous control

<sup>2</sup>Gene of interest

**Table S4-1. Gene-specific primers for zebrafish.** NCBI reference sequence, forward (F) and reverse (R) primer sequences (5' – 3') designed for this study, amplicon length in base pairs, and amplification efficiency (E) of endogenous control gene (*ef1α*) and genes of interest (*cat*, *gpx1a*, and *sod2*) measured using quantitative polymerase chain reaction.

Gene Name (Abbreviation)	Reference Sequence	F / R	Primer Sequence (5' – 3')	Length	E
<i>Elongation factor 1 alpha (ef1α)</i> <sup>1</sup>	NM_131263.1	F	TTCTCAGGCTGACTGTGCTG	83	2.01
		R	GGGTCTGTCCGTTCTTGGAG		
<i>Catalase (cat)</i> <sup>2</sup>	NM_130912.1	F	AACAACCCTCCAGACAGACC	115	1.92
		R	TCCGTCGACTTTTCTCTGTCG		
<i>Glutathione peroxidase 1a (gpx1a)</i> <sup>2</sup>	NM_001007281.2	F	TTTACGACCTGTCCGCGAAA	108	2.02
		R	CTGTTGTGCCTCAAAGCGAC		
<i>Superoxide dismutase 2 (sod2)</i> <sup>2</sup>	NM_199976.1	F	GAGCCTCACATCTGTGCTGA	111	2.04
		R	CTTGCCAGAGCCTCTTGAT		

<sup>1</sup> Endogenous control

<sup>2</sup> Gene of interest

## Supplemental Figures

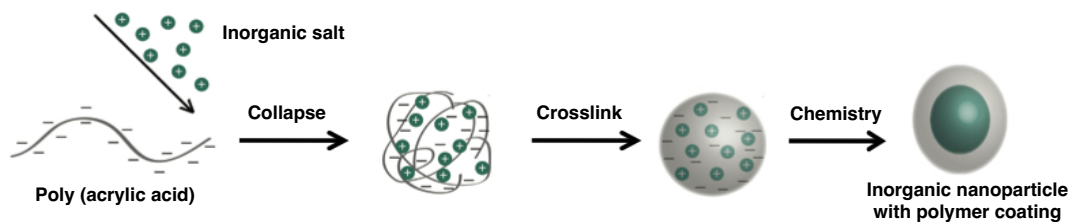


**Figure S2-1. Schematic diagram of polymer-coated NP synthesis**, provided by Vive Crop Protection Inc. Interaction between oppositely charged polymer chains and counterions resulted in condensed orb-like structures. These structures were then stabilized by cross-linking polymer chains either chemically or through ionizing radiation. Redox and precipitation reactions were used to convert the counterions encapsulated within the cross-linked coating to inorganic NPs (Pham et al., 2010).

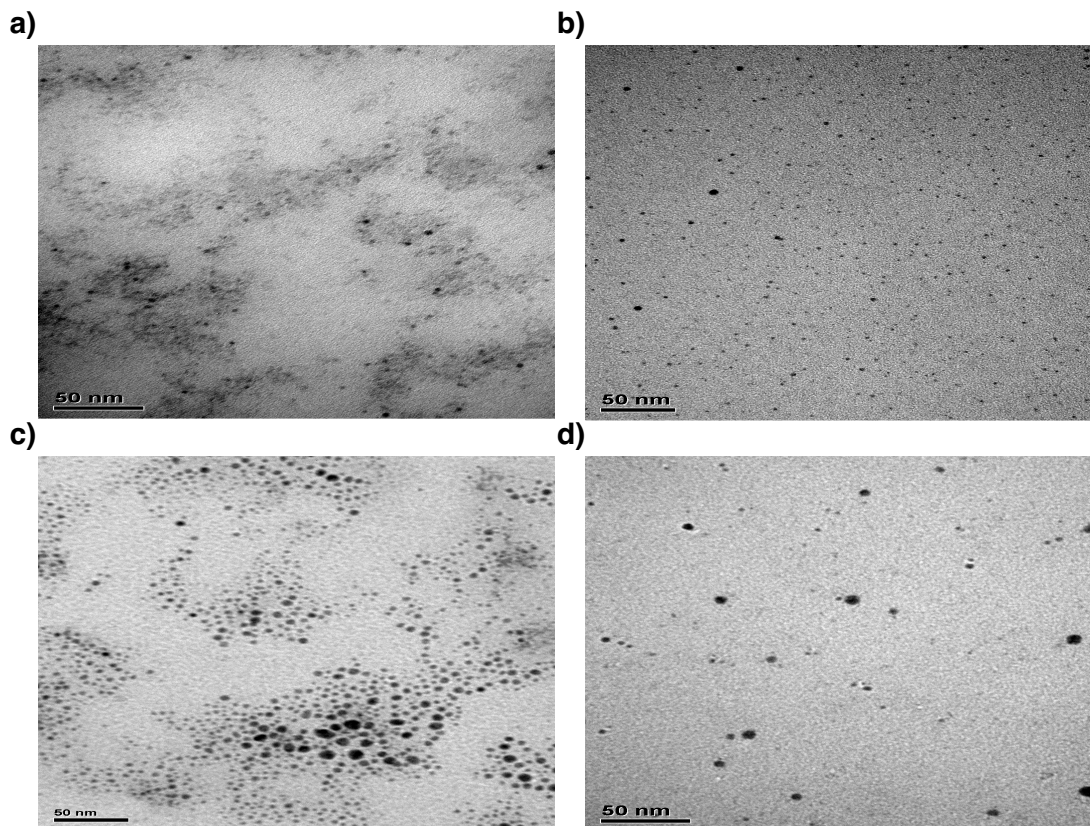


**Figure S2-2. TEM images of MeO NPs.** a) vnTiO<sub>2</sub>, b) vnZnO, c) vnFe<sub>2</sub>O<sub>3</sub>, and d) vnCeO<sub>2</sub> NPs, provided by Vive Crop Protection Inc. Scale bars are 50 nm.

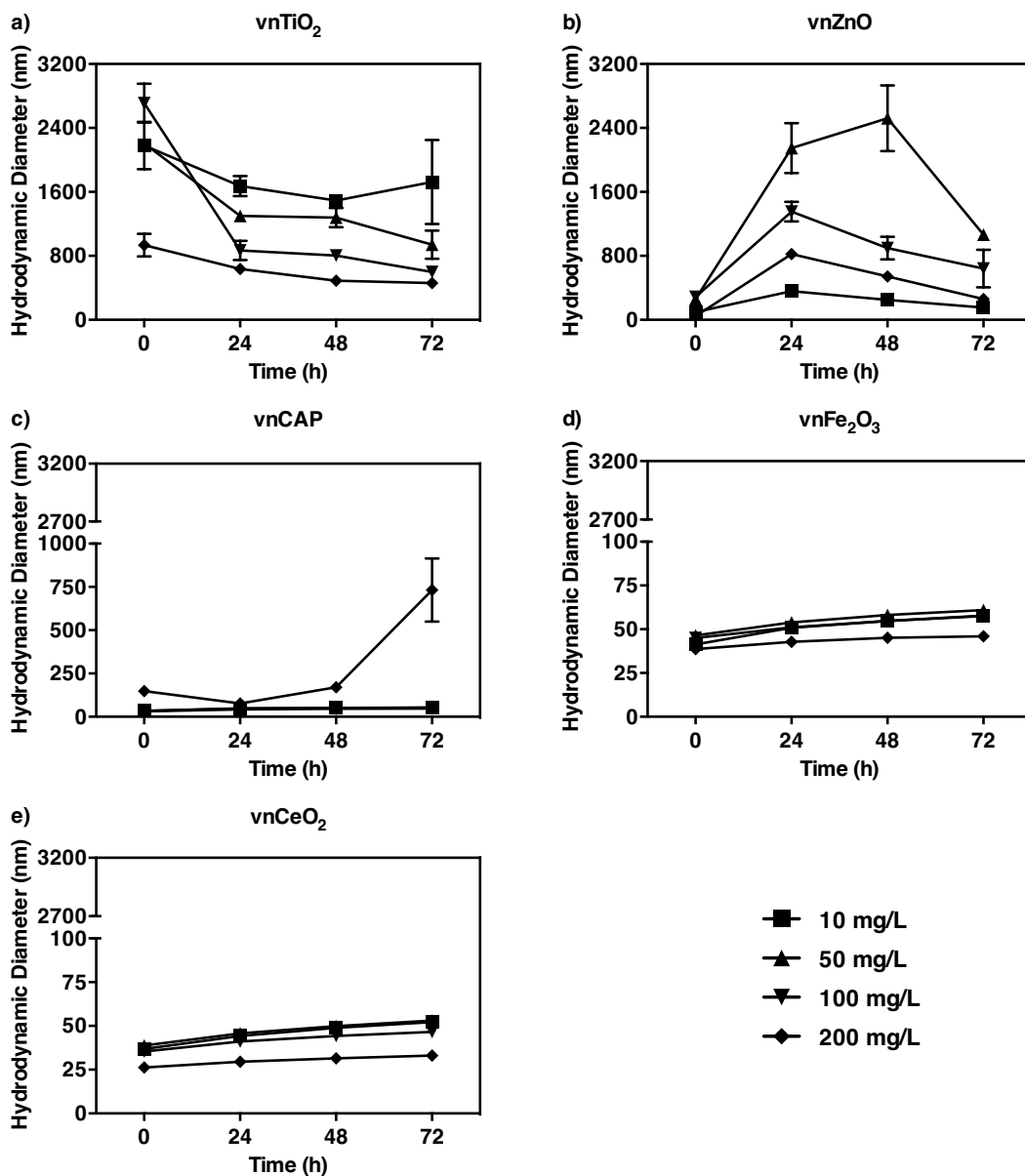


**Figure S2-3. Time-dependent changes in hydrodynamic diameter.** a) vnTiO<sub>2</sub>, b) vnZnO, c) vnCAP, d) vnFe<sub>2</sub>O<sub>3</sub>, and e) vnCeO<sub>2</sub> diluted to 10, 50, 100, or 200 mg/L with DTW (pH ~ 7.6) at 0, 24, 48, and 72 h. Sample values are the average of three replicates (mean ± SEM).

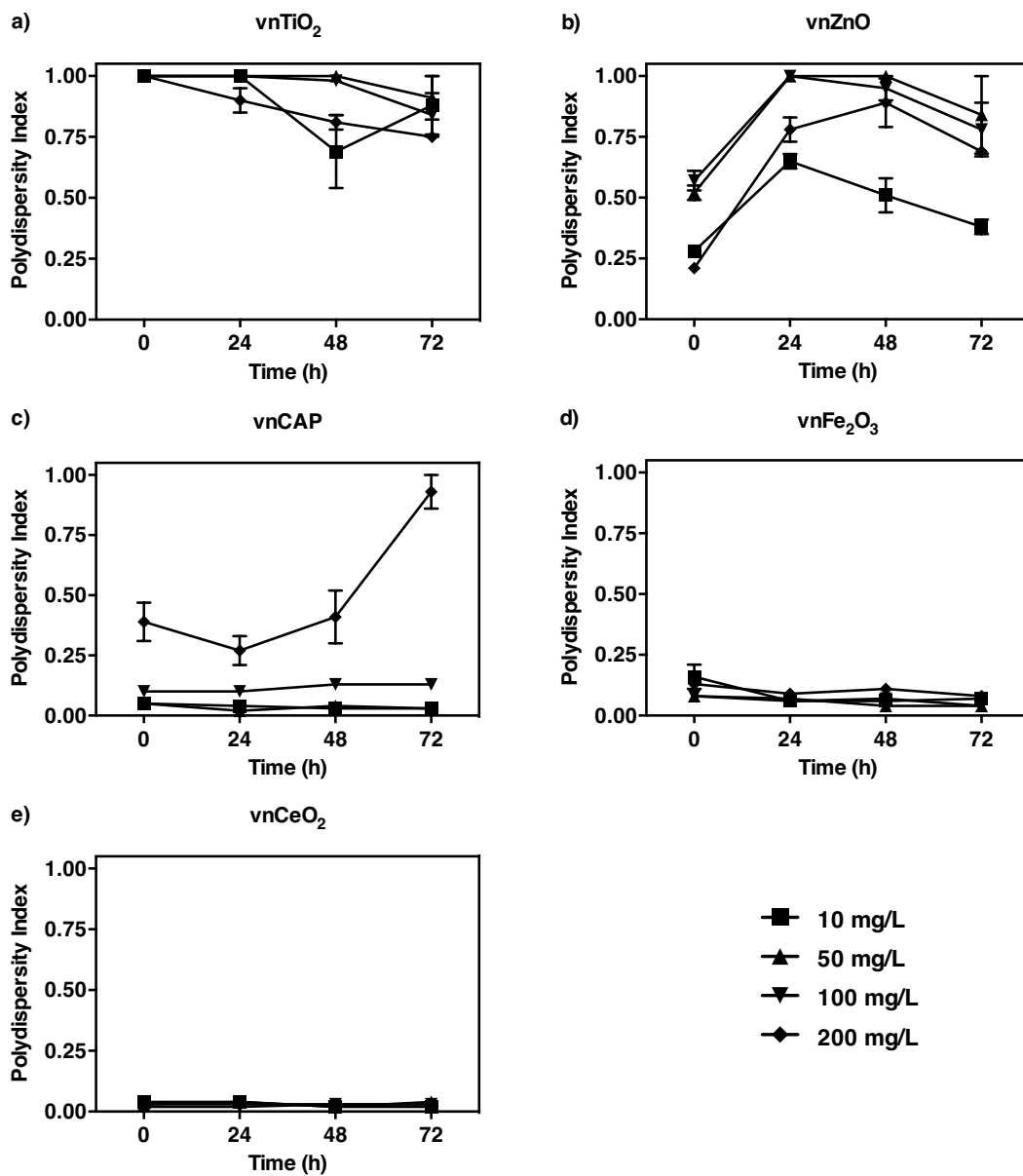


**Figure S2-4. Time-dependent changes in polydispersity index.** a) vnTiO<sub>2</sub>, b) vnZnO, c) vnCAP, d) vnFe<sub>2</sub>O<sub>3</sub>, and e) vnCeO<sub>2</sub> diluted to 10, 50, 100, or 200 mg/L with DTW (pH ~ 7.6) at 0, 24, 48, and 72 h. Sample values are the average of three replicates (mean ± SEM).

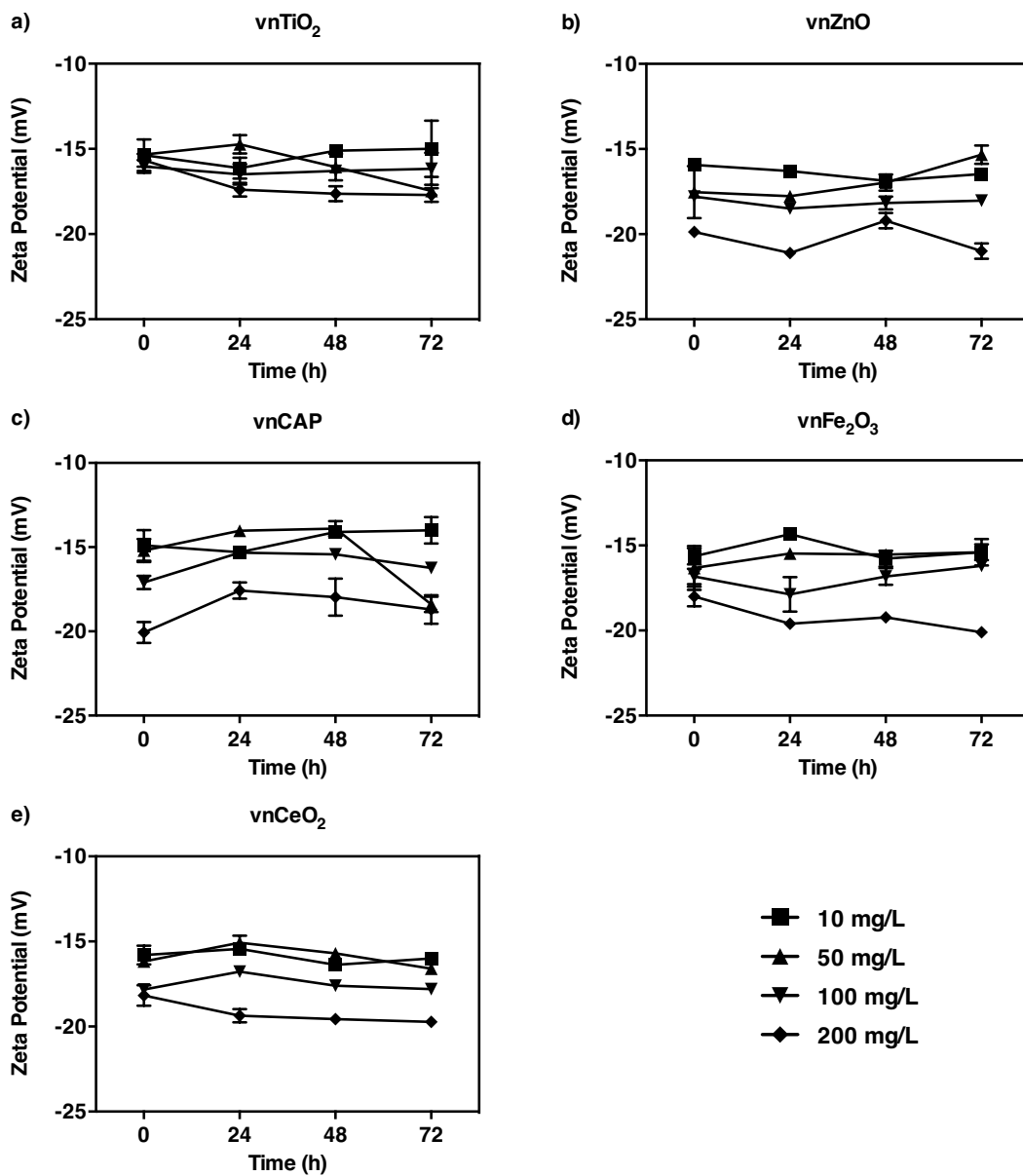


**Figure S2-5. Time-dependent changes in zeta potential.** a) vnTiO<sub>2</sub>, b) vnZnO, c) vnCAP, d) vnFe<sub>2</sub>O<sub>3</sub>, and e) vnCeO<sub>2</sub> diluted to 10, 50, 100, or 200 mg/L with DTW (pH ~ 7.6) at 0, 24, 48, and 72 h. Sample values are the average of three replicates (mean ± SEM).

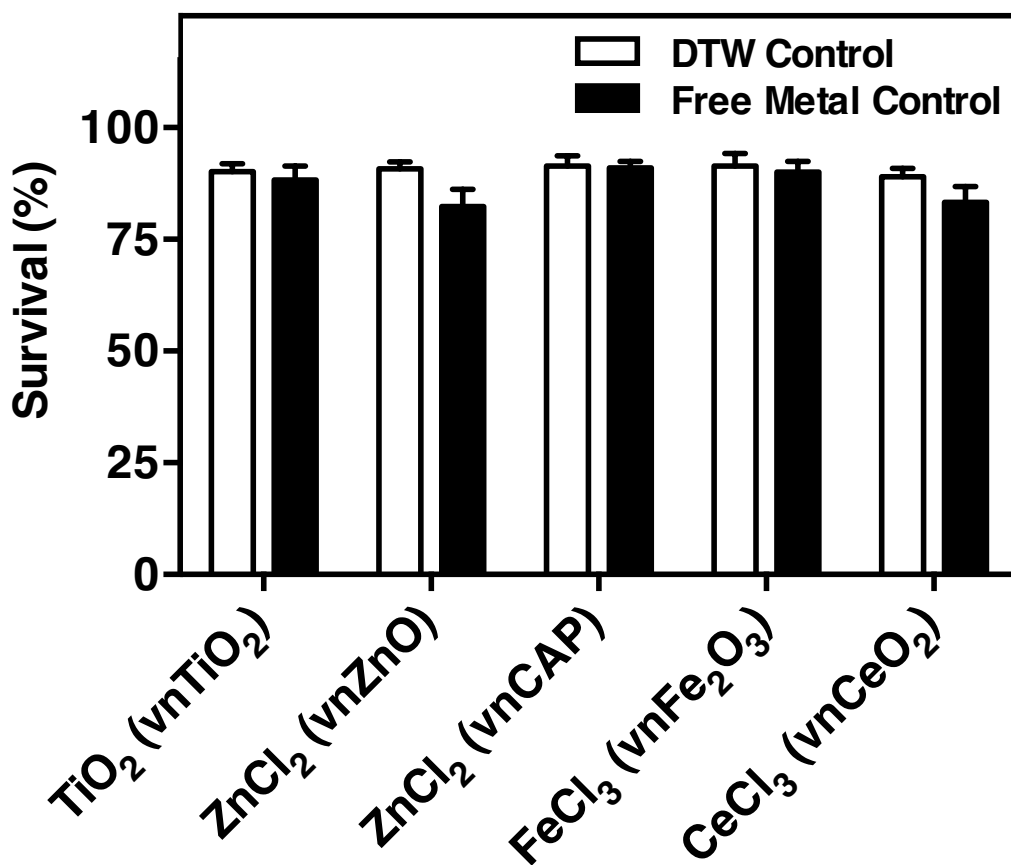


**Figure S2-6. Cumulative percent survival of free metal exposed zebrafish.** Embryos were exposed to the equivalent amount of free metal present in 200 mg/L of vnTiO<sub>2</sub> (bulk TiO<sub>2</sub>; 16.44 mg/L; n = 10), vnZnO at pH 7.0 (ZnCl<sub>2</sub>; 0.03 mg/L; n = 14), vnCAP (ZnCl<sub>2</sub>; 0.08 mg/L; n = 10), vnFe<sub>2</sub>O<sub>3</sub> (FeCl<sub>3</sub>; 0.85 mg/L; n = 8), or vnCeO<sub>2</sub> (CeCl<sub>3</sub>; 14.87 mg/L; n = 9) for 72 h. Each n represents 30 embryos/DTW or free metal control groups. Values are mean ± SEM (ANOVA, Dunnett's, *p* > 0.05).

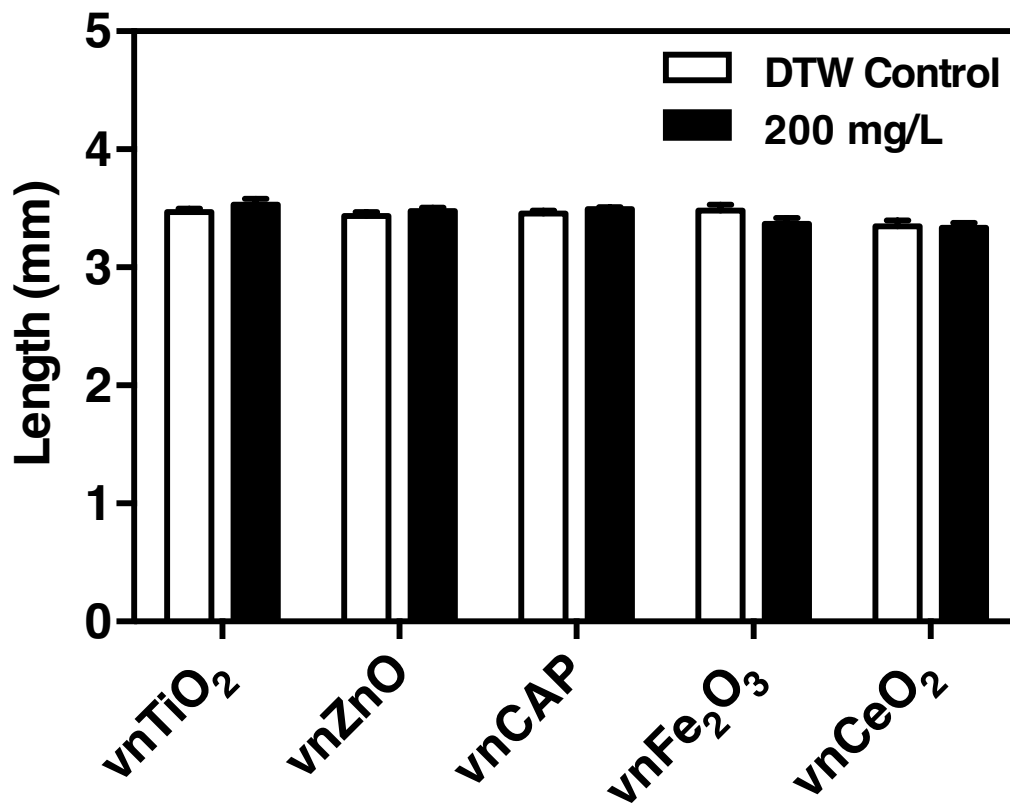


**Figure S2-7. Length of 72 hpf zebrafish larvae**, relative to control, following exposure to 200 mg/L of vnTiO<sub>2</sub> (n = 3), vnZnO (n = 3), vnCAP (n = 3), vnFe<sub>2</sub>O<sub>3</sub> (n = 3), or vnCeO<sub>2</sub> (n = 3). Each n represents 6 randomly selected larvae/well/treatment group. Values are mean ± SEM (ANOVA, Dunnett's, *p* > 0.05).

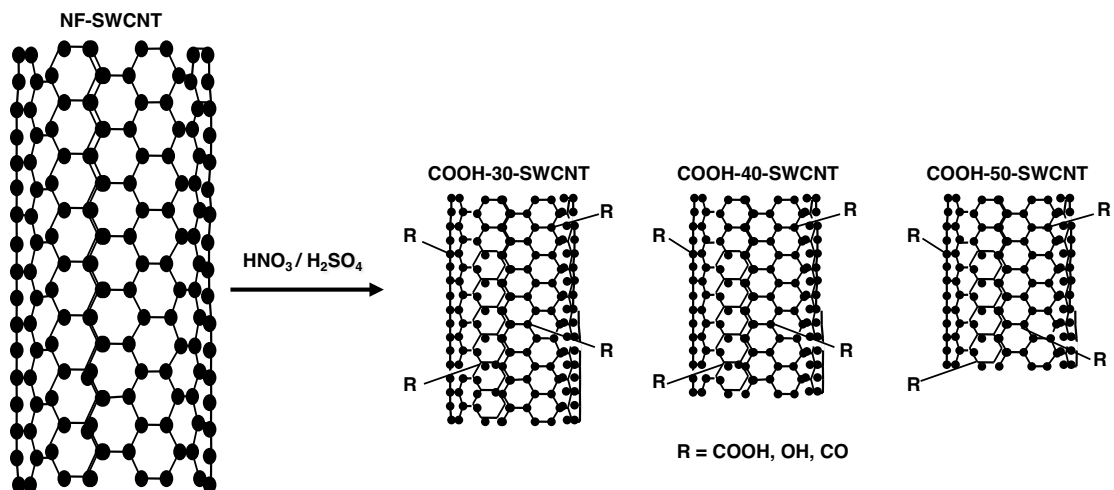


**Figure S3-1. A schematic diagram of the oxidation process.** NF-SWCNTs were oxidized with a mixture of  $\text{HNO}_3$  and  $\text{H}_2\text{SO}_4$  for 2 h at 30 (COOH-30-SWCNTs), 40 (COOH-40-SWCNTs), or 50 °C (COOH-50-SWCNTs), yielding ultra-short bundles with mostly carboxylic acid groups (-COOH) and some hydroxyl (-OH) and carbonyl (-CO) groups covalently bound to their sidewalls. A negative correlation between oxidative temperature and bundle length is depicted.

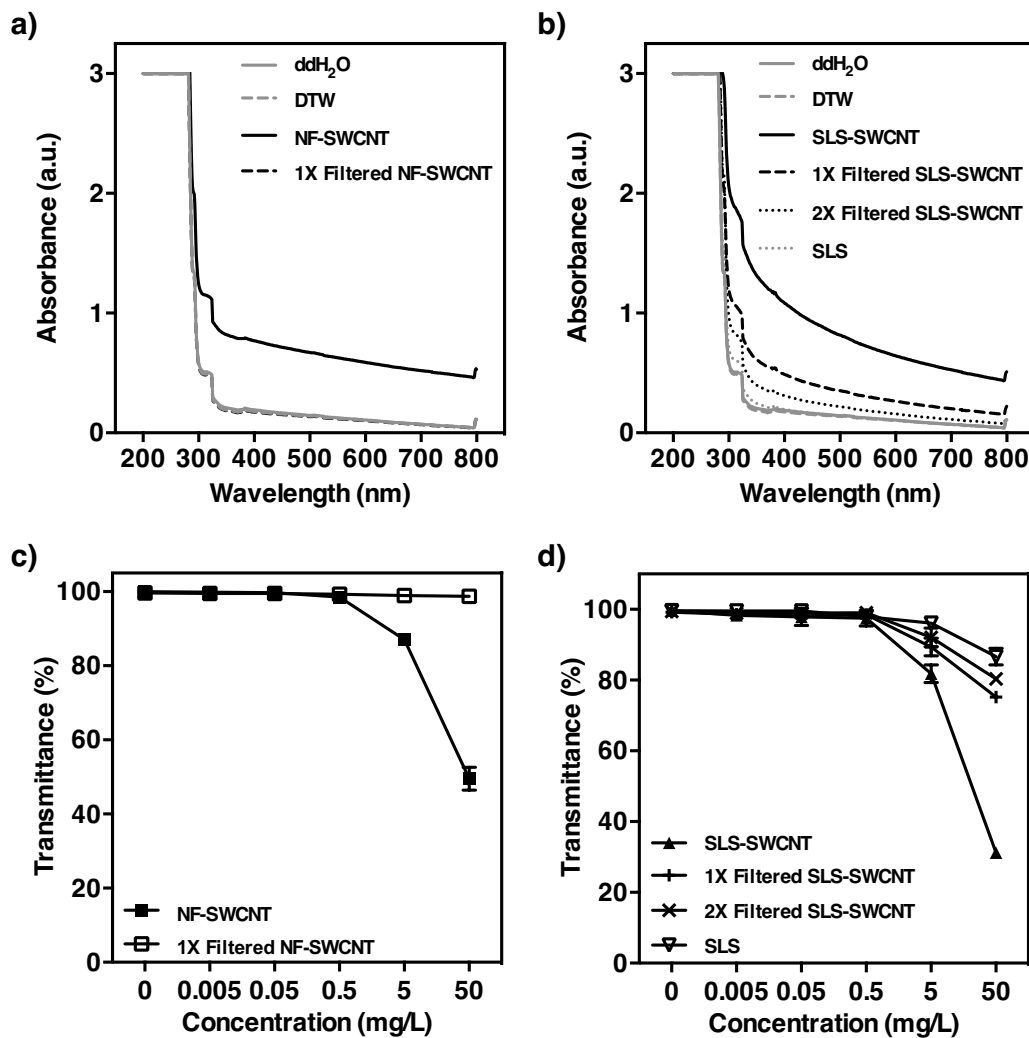
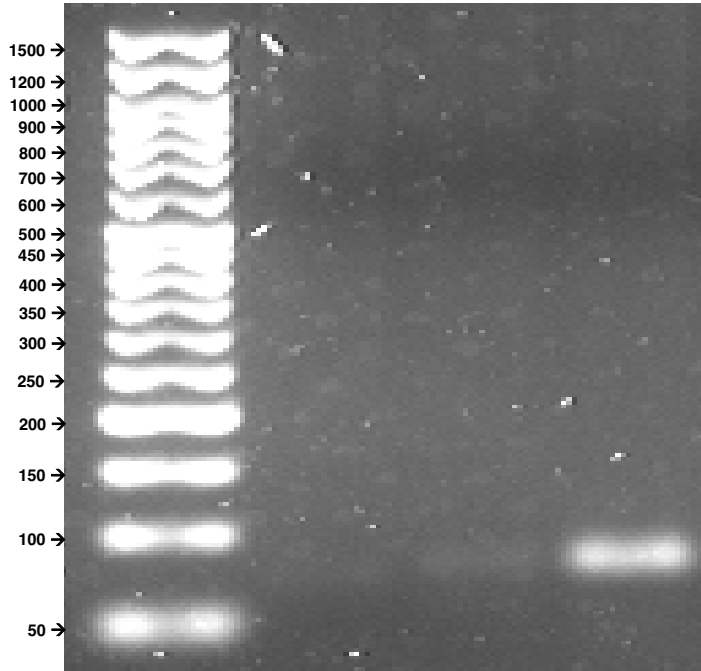


**Figure S3-2. Optical properties of SWCNT and SLS test suspensions.** (a, b) Representative absorption spectral scans (200-800 nm) of ddH<sub>2</sub>O, DTW, and 50 mg/L NF-SWCNT, once (1X) filtered NF-SWCNT, SLS-SWCNT, once and twice (2X) filtered SLS-SWCNT, and SLS test suspensions. (c, d) Percent transmittance at 260 nm of 0, 0.005, 0.05, 0.5, 5 and 50 mg/L NF-SWCNT, 1X filtered NF-SWCNT, SLS-SWCNT, 1X and 2X filtered SLS-SWCNT, and SLS test suspensions. All test suspensions were probe sonicated on ice for  $3 \times 20$  s with a 20 s pause in between and then mixed by vortex for 20 s. Sample values are the average of three replicates and are presented as mean  $\pm$  SEM.

a)



b)

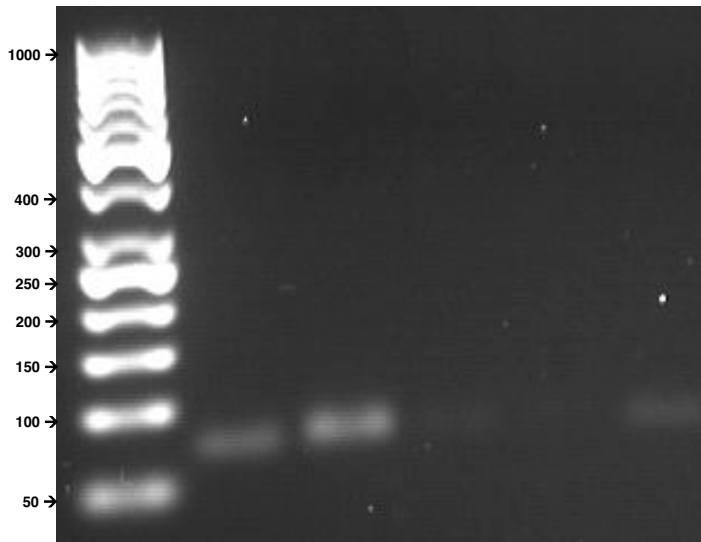


**Figure S3-3. Screening of endogenous control genes and genes of interest by polymerase chain reaction amplification.** Amplification was performed with 2% agarose gel electrophoresis at 60 V for 2 h. cDNA was synthesized from five 72 hpf larvae immediately following exposure to the DTW control. Bands from left to right for each panel are as follows: a) DNA marker (GeneDirex 50 bp DNA Ladder), *beta actin*, *ef1a*, *hif1ab*, b) DNA marker (GeneRuler 50 bp DNA Ladder), *bactin1*, *ef1a*, *alpha-ttp*, *gclc*, and *hsp70*. Note that beta actin was not employed as a housekeeping gene for quantitative molecular based studies.

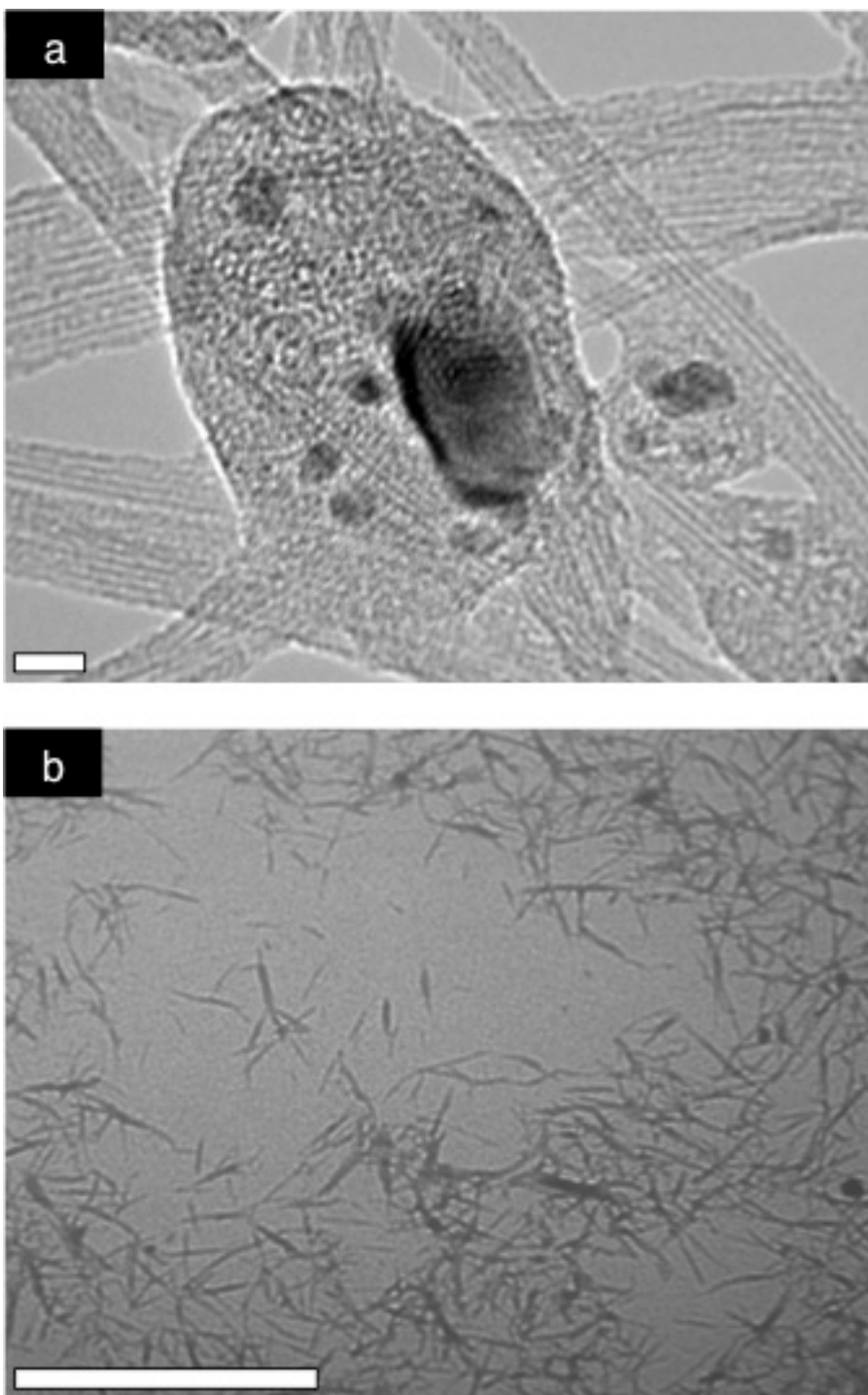


**Figure S3-4. Representative TEM images of SWCNTs and CNCs.** (a) FETEM image of NF-SWCNTs produced by induction thermal plasma technology (scale bar = 10 nm) and (b) LVTEM image of COO<sup>-</sup>-CNCs produced by APS treatment of MCC (scale bar = 1000 nm).

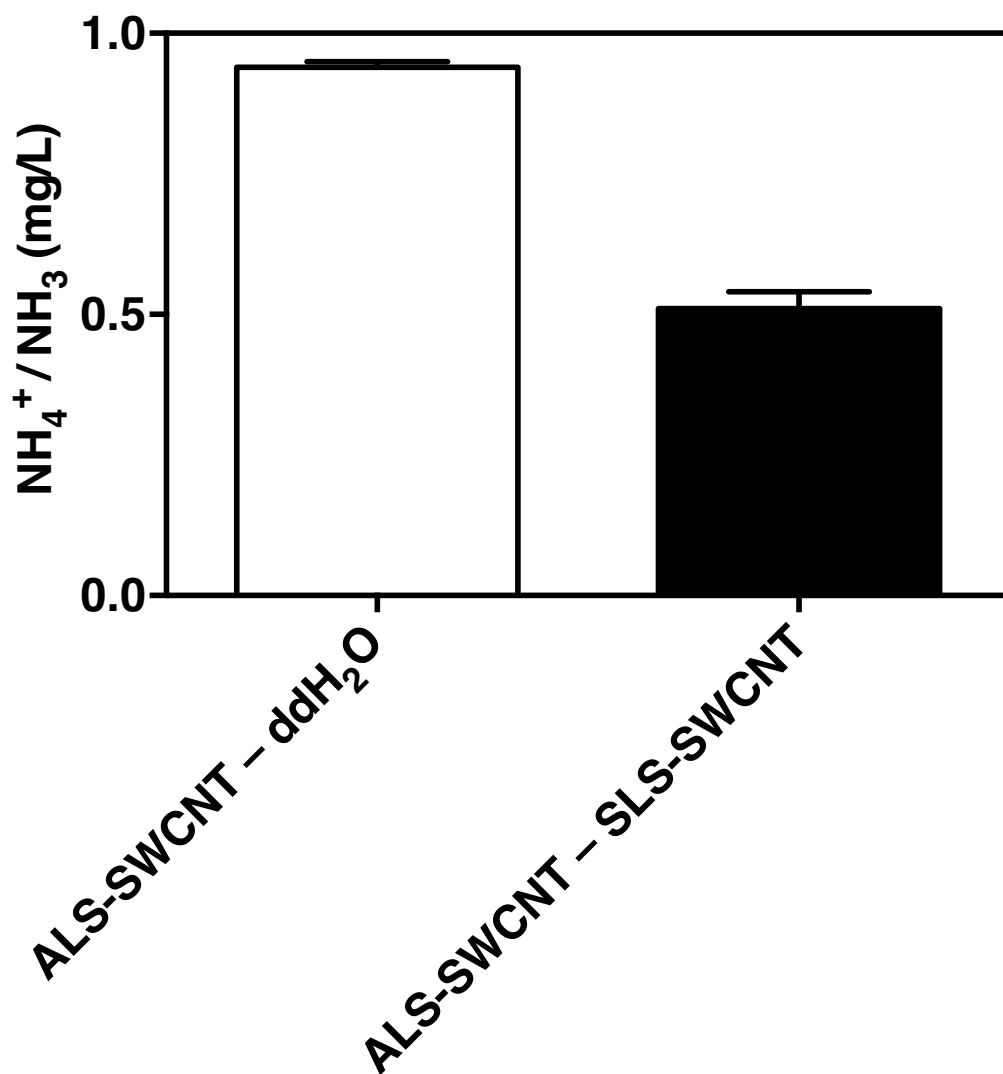


**Figure S3-5. Ammonia concentration in SWCNT suspension.** Concentration of NH<sub>4</sub><sup>+</sup>/NH<sub>3</sub> (mg/L) present in 5 mg/L filtered ALS-SWCNTs when measured against a blank containing ddH<sub>2</sub>O (white bar) or 5 mg/L filtered SLS-SWCNTs (black bar). Values are mean ± SEM.

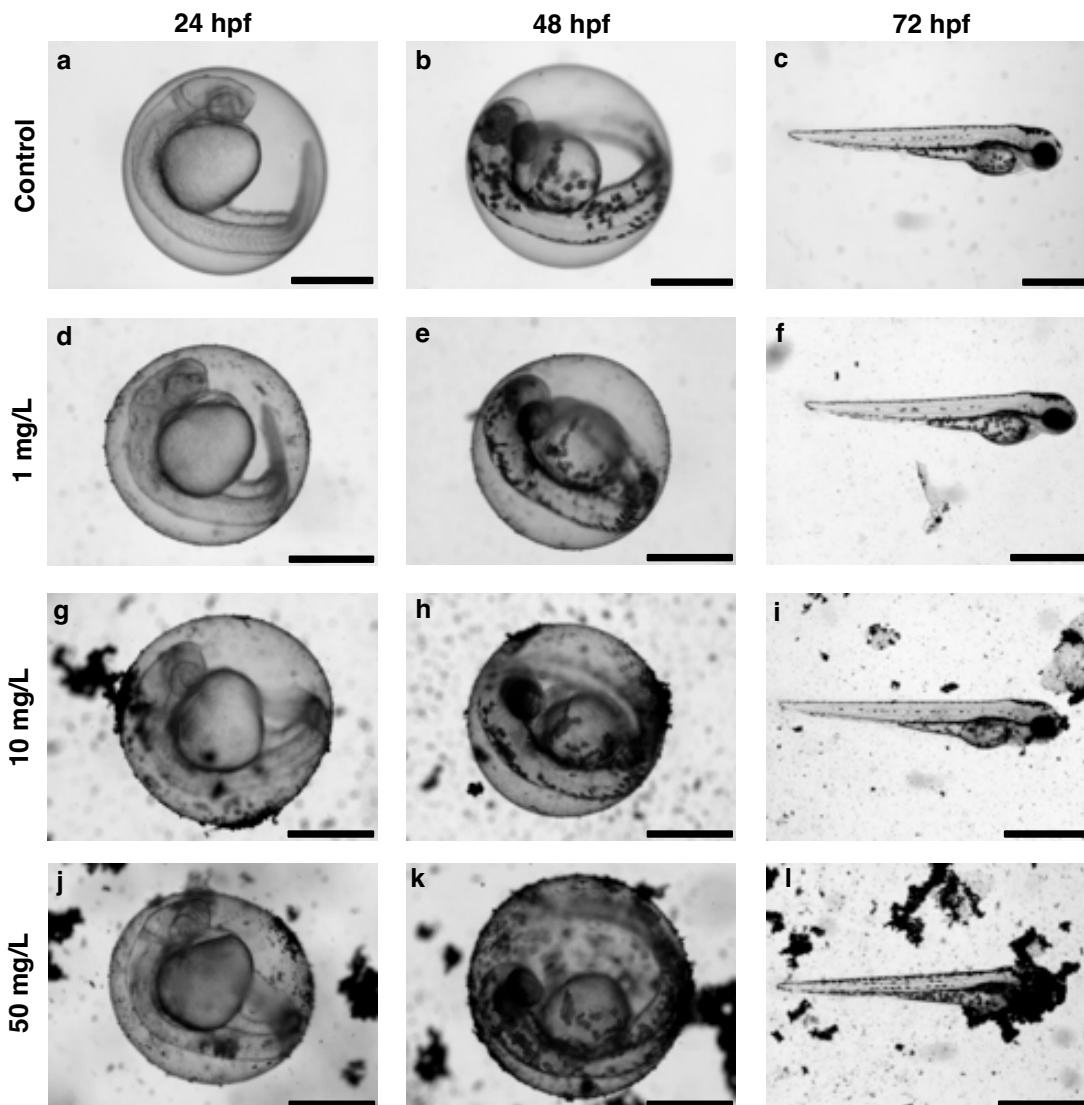


**Figure S3-6. Adsorption of NF-SWCNTs to zebrafish embryos and larvae.** Zebrafish were imaged at 24, 48 and 72 hpf following exposure to the DTW control (a-c) and 1 (d-f), 10 (g-i), or 50 (j-l) mg/L NF-SWCNTs. Scale bars are 0.5 mm for embryos and 1 mm for larvae.

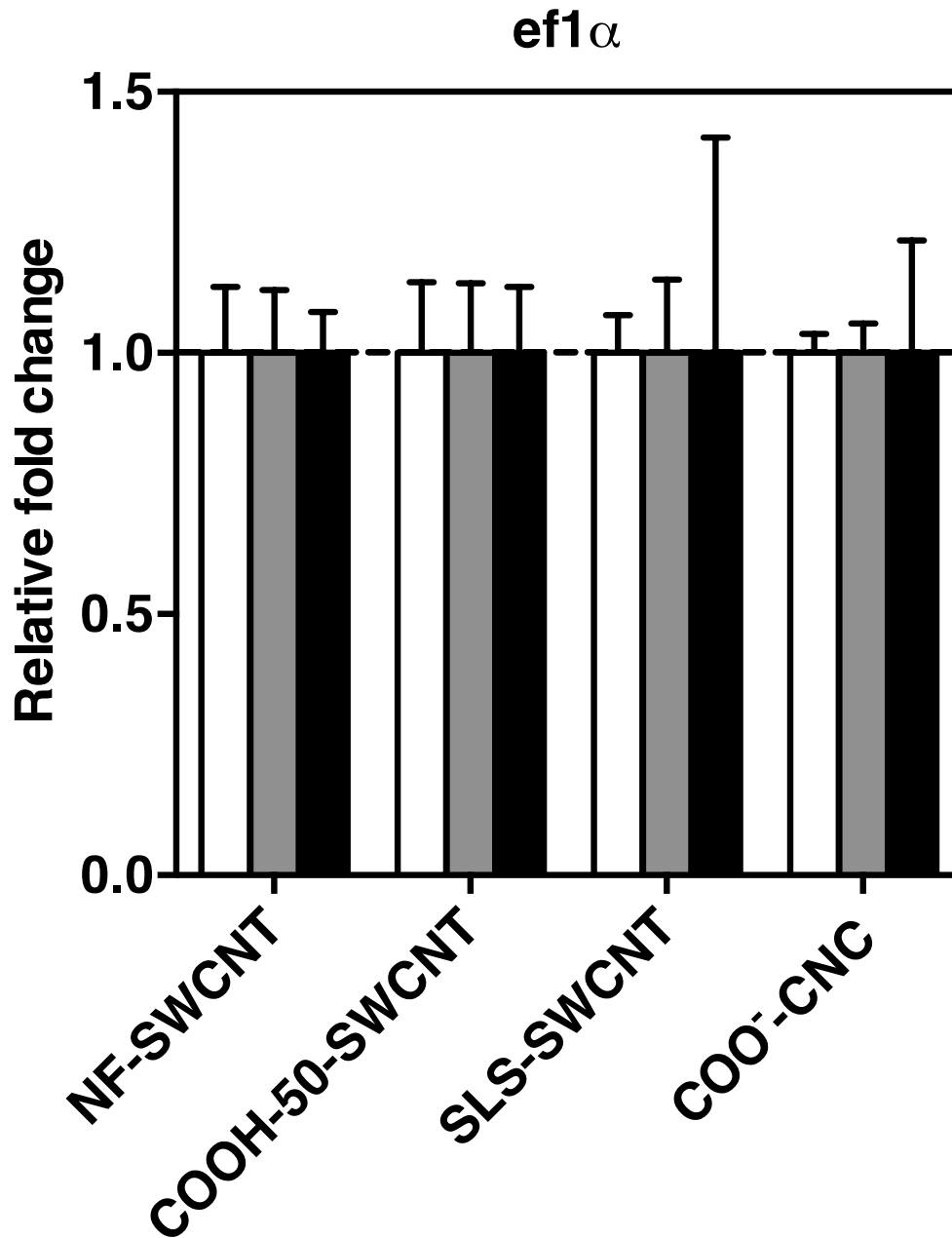


**Figure S3-7. Changes in endogenous control gene expression patterns following exposure to SWCNT and CNC test suspensions.** Relative fold change of *ef1 $\alpha$*  in zebrafish larvae exposed to 0 (DTW), 100 or 200 mg/L NF-SWCNT (n = 4), COOH-50-SWCNT (n = 4), SLS-SWCNT (n = 4), or COO-CNC (n = 4) test suspensions for 72 h from 1 to 2 hpf. Data are relative to unexposed DTW control larvae (dotted line; n = 4). Each n represents five pooled 72 hpf zebrafish larvae. Values are mean  $\pm$  SEM (ANOVA, Tukey's,  $p > 0.05$ ).

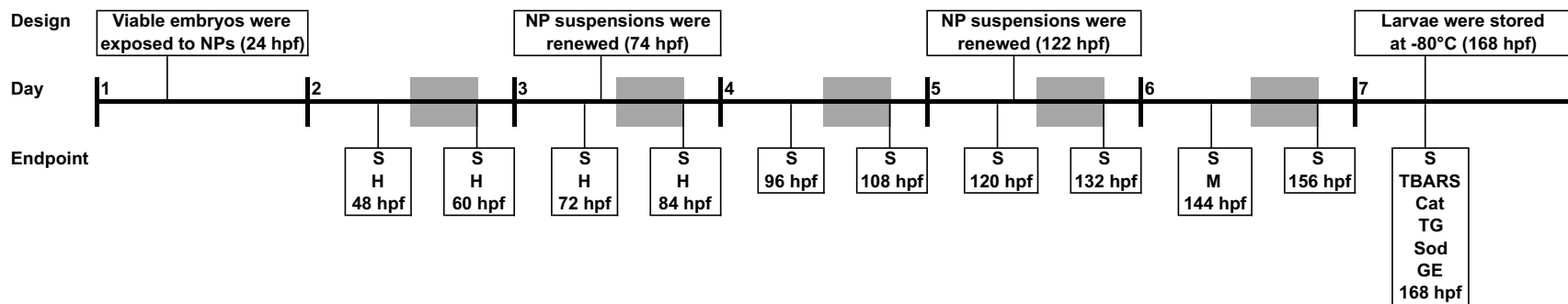


**Figure S4-1. Schematic of experimental design and endpoints examined.** Zebrafish embryos (24 hpf) were exposed to uncoated TiO<sub>2</sub> NPs, polymer-coated TiO<sub>2</sub> NPs, or polymer NPs from 24 to 168 hpf. NP suspensions were renewed at 74 and 122 hpf. Larvae (168 hpf) were washed thrice with DTW, snap frozen in liquid nitrogen, and stored at -80 °C immediately after the experimental period. Measured endpoints included survival (S), hatching success (H), malformation (M), TBARS, Cat activity, TG levels, Sod activity, as well as alteration of gene expression (GE). A gray rectangle indicates an 8 h UV light exposure period.

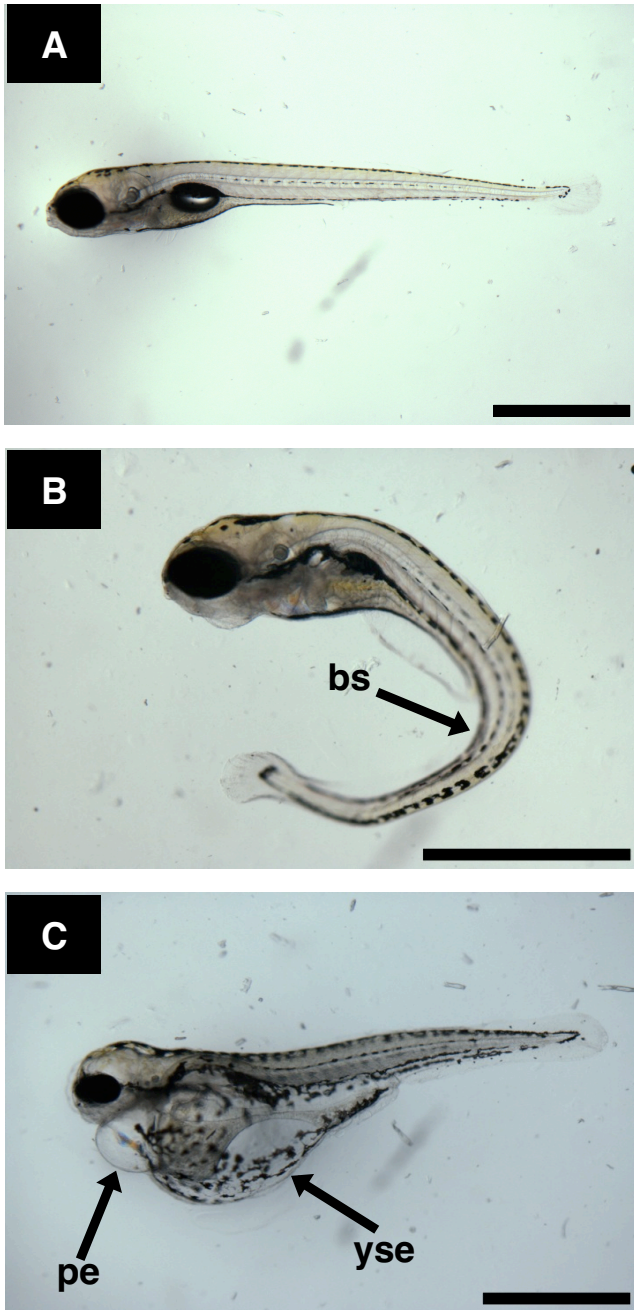


**Figure S4-2. Representative micrographs of 144 hpf larvae.** (A) Normal development and incidences of malformation including (B) bs, (C) pe, and yse. Scale bars are 1 mm.

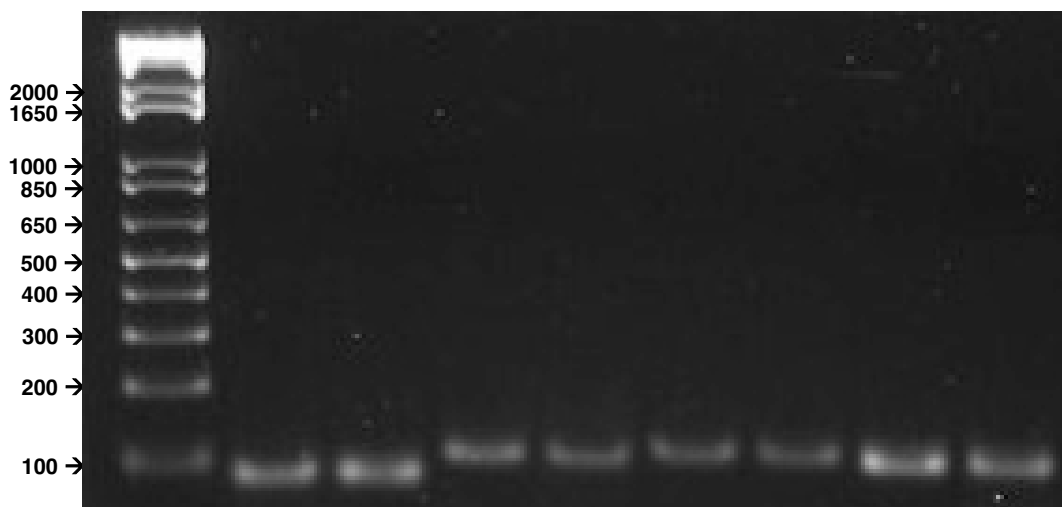


**Figure S4-3. Screening of endogenous control genes and genes of interest by polymerase chain reaction (PCR) amplification.** PCR amplification was performed with 2% agarose gel electrophoresis at 80 V for 1.5 h. cDNA was synthesized from five 72 hpf larvae immediately following exposure to the DTW control. Bands from left to right for each panel are as follows: DNA marker (O'GeneRuler 1 kb Plus DNA Ladder), *efl $\alpha$*  (2 columns), *CAT* (2 columns), *GPX1a* (2 columns) and *SOD2* (2 columns).

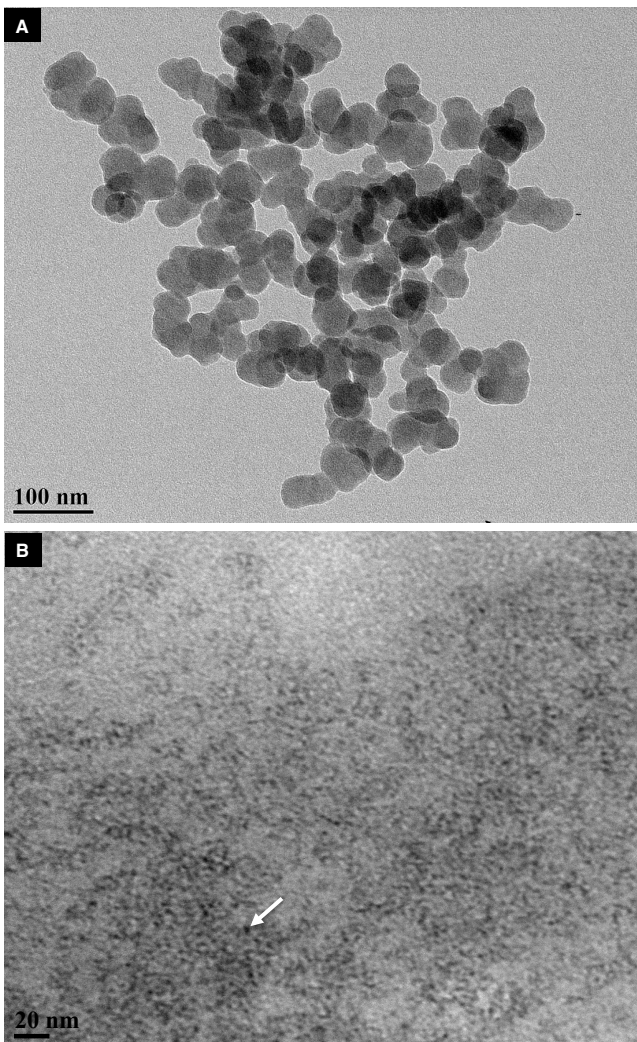


**Figure S4-4. Representative TEM images of NPs.** (A) Uncoated TiO<sub>2</sub> NPs (scale bar = 100 nm) and (B) polymer-coated TiO<sub>2</sub> NPs (scale bar = 20 nm). White arrow denotes an individual particle.

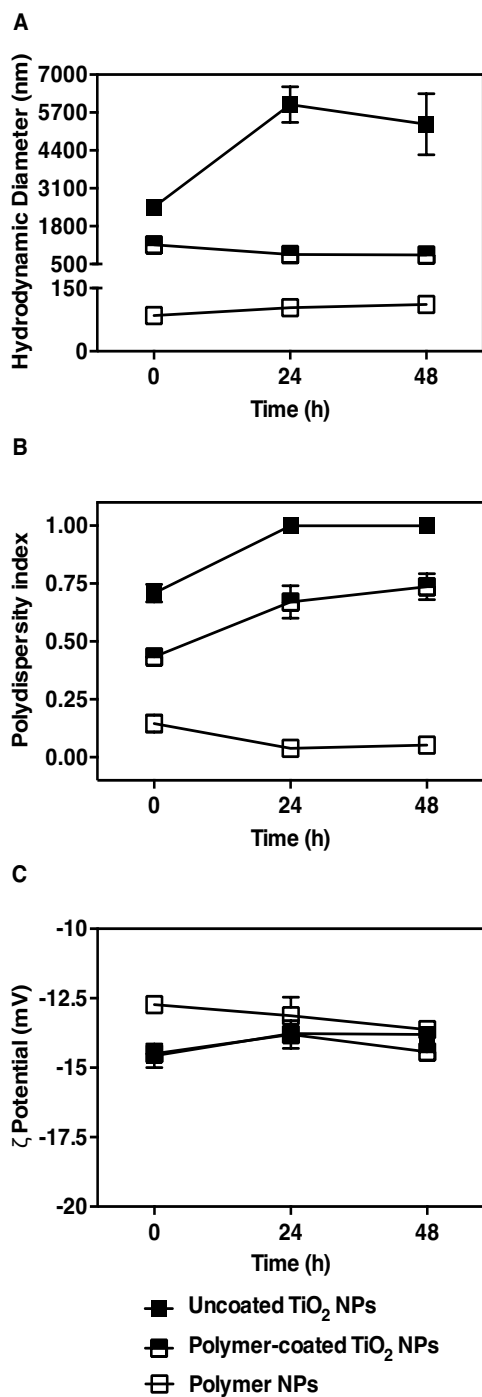


**Figure S4-5. Physicochemical characteristics of NP suspensions over time.** Time-dependent changes in (A) hydrodynamic diameter (nm), (B) polydispersity index, and (C)  $\zeta$  potential (mV) of uncoated TiO<sub>2</sub> NPs (pH 7.97), polymer-coated TiO<sub>2</sub> NPs (pH 7.95), and polymer NPs (pH 7.70) diluted to 10 mg/L with DTW (pH 8.00) at 0, 24, and 48 h. Data are presented as mean  $\pm$  SEM of three independent replicates.

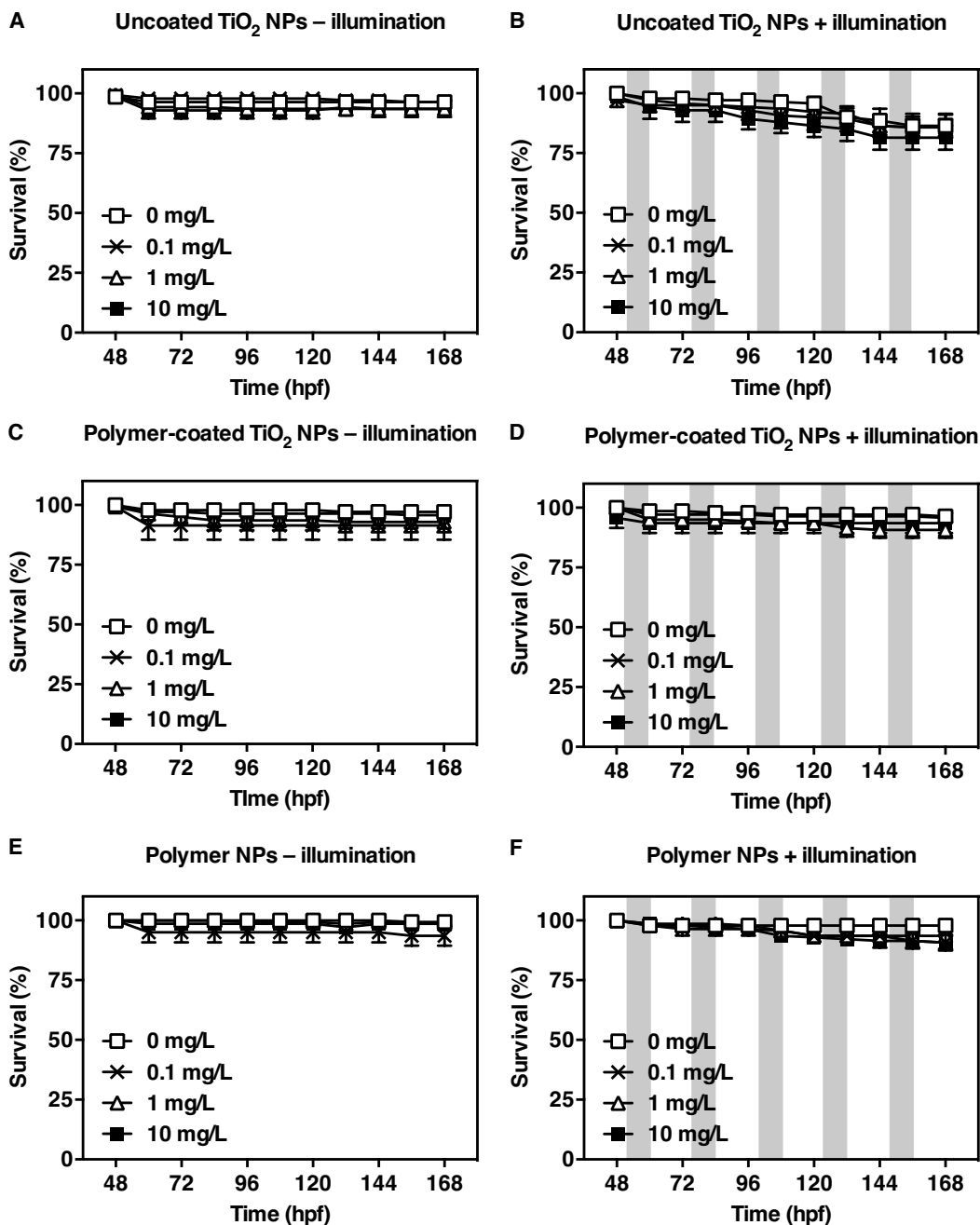


**Figure S4-6. Percent survival of zebrafish exposed to NPs in the absence (–) or presence (+) of UV illumination.** Embryos were exposed to 0 (DTW), 0.1, 1 or 10 mg/L (A, B) uncoated TiO<sub>2</sub> NPs, (C, D) polymer-coated TiO<sub>2</sub> NPs, or (E, F) polymer NPs (n = 7) for 6 d from 24 hpf. Half of the NP exposed zebrafish were illuminated for 8 h / d for 5 subsequent days, as indicated by the gray bars. The other half was kept under ambient fluorescent lighting. Each n represents 4-well plate replicate consisting of 80 embryos (20 embryos/well). Values are mean ± SEM (two-way ANOVA, Dunnett’s, unpaired t-test, *p* > 0.05).

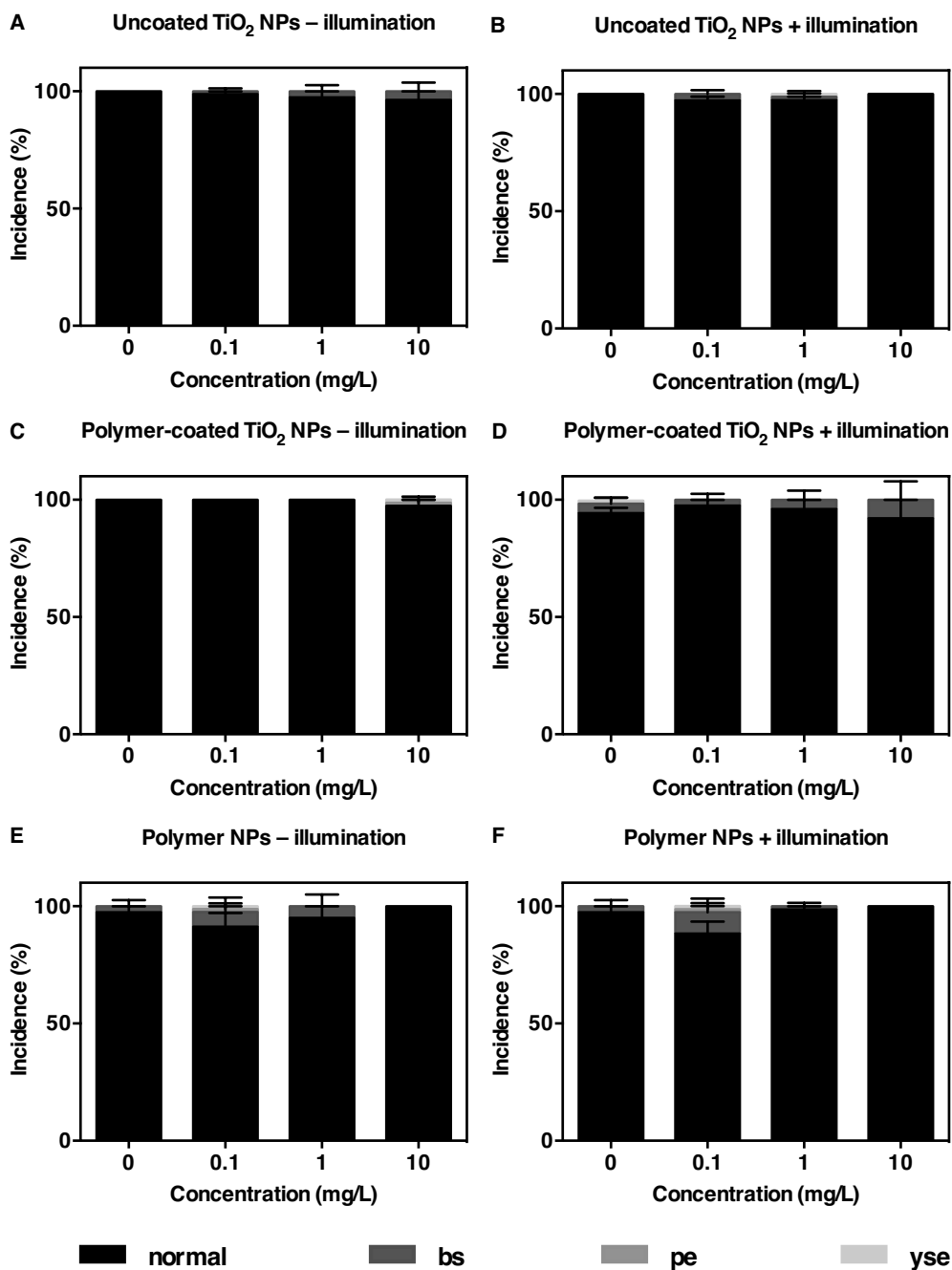


**Figure S4-7. Malformations caused by NP and UV light co-exposure.** Percent incidence of malformation observed in 144 hpf larvae exposed to 0 (DTW), 0.1, 1 or 10 mg/L (A, B) uncoated TiO<sub>2</sub> NPs, (C, D) polymer-coated TiO<sub>2</sub> NPs, or (E, F) polymer NPs (n = 4) in the absence (–) and presence (+) of UV illumination. Each n represents 4-well plate replicate consisting of 80 embryos (20 embryos/well). Malformations were categorized as normal, bs, pe, or yse. Values are mean ± SEM (two-way ANOVA, Dunnett’s, unpaired t-test, *p* > 0.05).

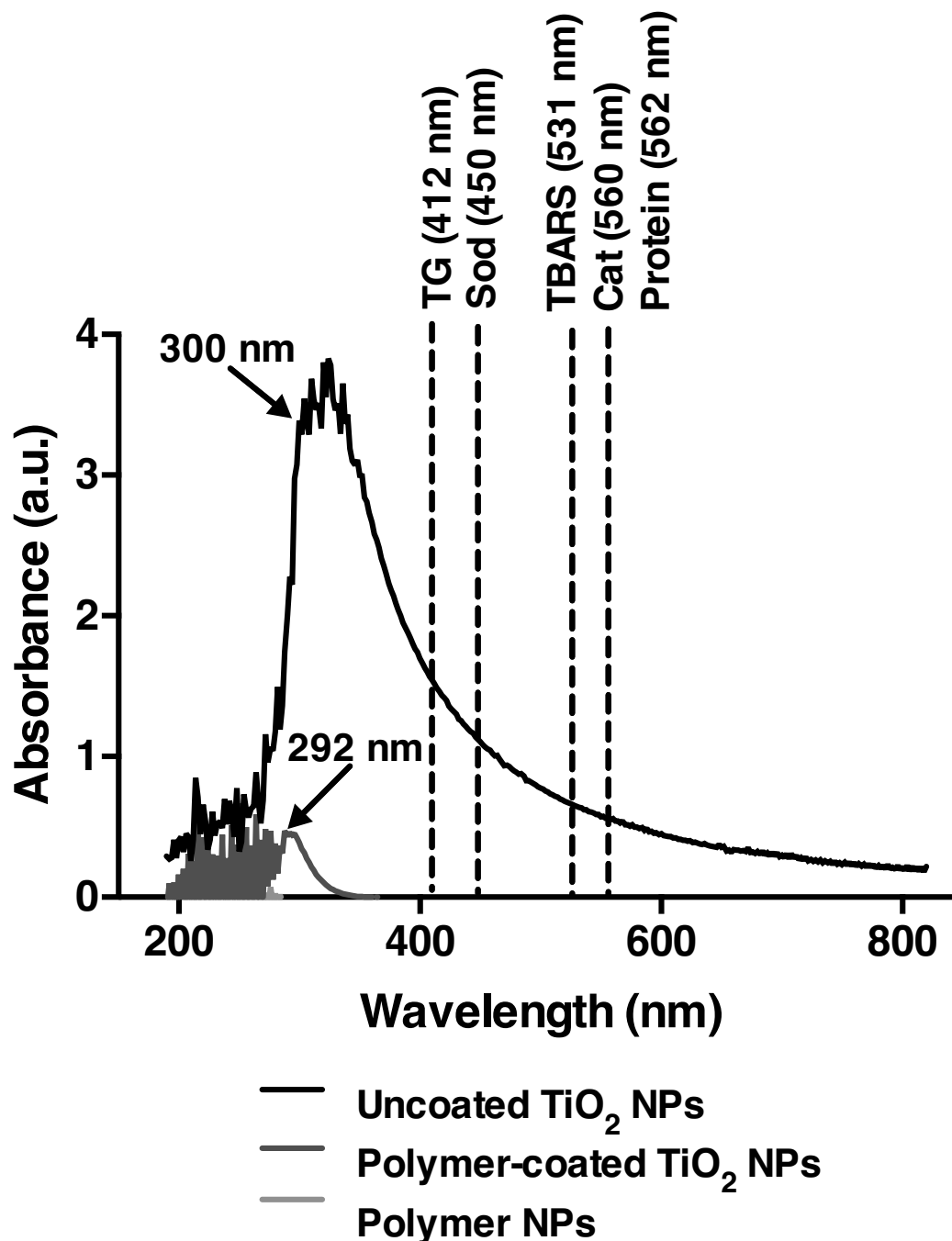


**Figure S4-8. Uncoated TiO<sub>2</sub> NPs absorb at wavelengths used for TG (412 nm), Sod (450 nm), TBARS (531 nm), Cat (560 nm), and protein (562 nm) assay measurements.** Representative absorption spectral scans (200–800 nm) of 100 mg/L uncoated TiO<sub>2</sub> NP, polymer-coated TiO<sub>2</sub> NP and polymer NPs. Spectral scans of NPs diluted with phosphate, 1× reaction, or sucrose buffer were similar. Uncoated and polymer-coated TiO<sub>2</sub> NPs had maximum absorption peaks at 300 and 292 nm, respectively, as indicated by the black arrows.

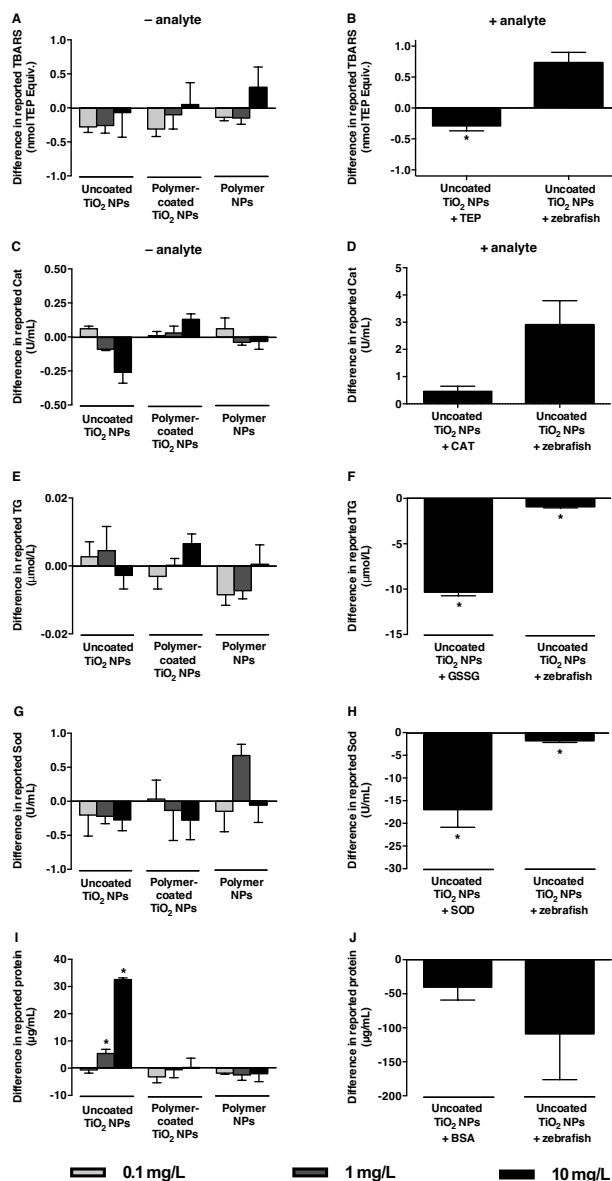


**Figure S4-9. NP interference with biochemical assay components, without (–) and with (+) analyte.** Difference in reported (A) TBARS, (C) Cat, (E) TG, (G) SOD, and (I) protein without analyte addition in the presence of 0.1, 1 or 10 mg/L uncoated TiO<sub>2</sub> NPs, polymer-coated TiO<sub>2</sub> NPs, or polymer NPs (n = 3). Analytes tested included 3.125 uM TEP, 2 U/mL Cat, 20 μmol/L GSSG, 100 U/mL Sod from horseradish, 1000 μg/mL bovine serum albumin (BSA), and 168 hpf zebrafish larvae (n = 11-20). Difference in reported (B) TBARS, (D) Cat, (F) TG, (H) SOD, and (J) protein with analyte addition in the presence of 10 mg/L uncoated TiO<sub>2</sub> NPs (n = 3). Each n represents either a 4-well plate replicate or pooled 168 hpf larvae per treatment. An asterisk (\*) indicates significant difference compared to DTW control (one-way ANOVA, Dunnett's, *p* < 0.05) or between treatment groups (unpaired t-test, *p* < 0.05). Values are mean ± SEM.

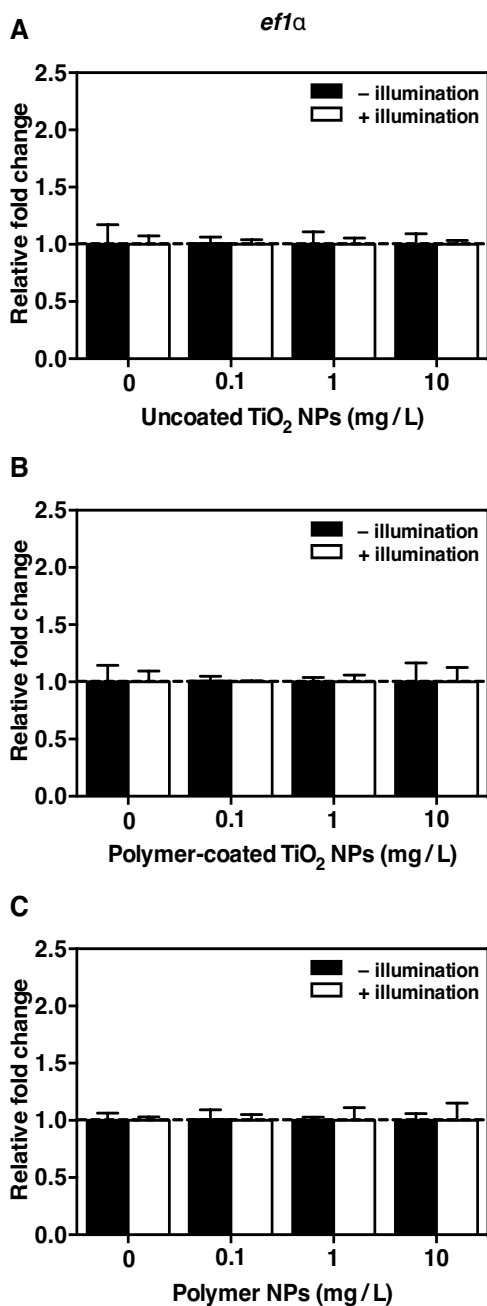


**Figure S4-10. Changes in endogenous control gene expression patterns.** Relative fold change of *eflα* in zebrafish larvae exposed to 0 (DTW), 0.1, 1 or 10 mg/L uncoated TiO<sub>2</sub> NPs (n = 3), polymer-coated TiO<sub>2</sub> NPs (n = 3), or polymer NPs (n = 3) in the absence (–) or presence (+) of illumination for 6 d from 24 hpf. Data are relative to unexposed DTW control larvae (dotted line; n = 3). Each n represents five randomly pooled 168 hpf larvae per treatment. Values are mean ± SEM (two-way ANOVA, Tukey’s,  $p > 0.05$ ).

## Supplemental Text

### *Appendix I*

#### *Physicochemical characterization of polymer-coated nanoparticles*

Physicochemical characteristics, measured by the manufacturer, show a similar size distribution (3-9 nm) (**Table S2-1**) for the spherical shaped vnTiO<sub>2</sub>, vnZnO, vnFe<sub>2</sub>O<sub>3</sub>, and vnCeO<sub>2</sub> NPs tested (**Figure S2-2**). The cross-linked PAA polymer coating enveloping the metal oxide NPs and the PAA that comprises the vnCAPs themselves have low contrast and cannot be resolved well by TEM imagery. The pH of the stock suspension containing vnTiO<sub>2</sub> was neutral (7.0) whereas vnZnO, vnFe<sub>2</sub>O<sub>3</sub> and vnCeO<sub>2</sub> were slightly alkaline, measuring 8.9, 9.6, and 8.9, respectively (**Table S2-1**). The total metal in the stock suspension measured 46.0, 18.0, 24.2, and 17.0% for vnTiO<sub>2</sub>, vnZnO, vnFe<sub>2</sub>O<sub>3</sub>, and vnCeO<sub>2</sub>, respectively (**Table S2-1**). The purity, as measured by the fraction of primary metal, i.e., Ti, Zn, Fe, and Ce, to the total metal, was as follows: vnTiO<sub>2</sub> (98.0%), vnZnO (99.7%), vnFe<sub>2</sub>O<sub>3</sub> (97.8%) and vnCeO<sub>2</sub> (88.0%) (**Table S2-1**). This does not include the presence of the Na<sup>+</sup> stabilizer and the polymer. A variety of trace metals and excess unreacted synthesis reagents, that are present in small portions (> 0.1%), were detected in each NP type (**Table S2-3**).

## *Appendix II*

### *Physicochemical characterization*

For TEM imaging, uncoated and polymer-coated TiO<sub>2</sub> NP stock suspensions (1000 mg/L) were gently mixed by vortex for 30 s, diluted to 10 mg/L in ddH<sub>2</sub>O, drop-coated onto a 200 nm carbon-coated copper grid, and air-dried for 1 min at room temperature. Particle size and morphology of uncoated TiO<sub>2</sub> NPs were examined using a Philips FEI Morgagni 268 TEM operating at 80 kV connected to a Gatan Orius CCD camera (Gatan DigitalMicrograph software, v. 1.81.78) while TEM images of polymer-coated TiO<sub>2</sub> NPs were obtained using the procedure described by Ortega et al. (2015).

Dynamic light scattering (DLS; Zetasizer Nano Series, Malvern Instruments Ltd.) in 173° backscatter mode (Zetasizer software, v. 7.01) was used to characterize the size and charge of uncoated TiO<sub>2</sub> NPs, polymer-coated TiO<sub>2</sub> NPs, and polymer NPs diluted to 10mg/L with DTW at 28.5 °C. Mean z-average hydrodynamic diameter, polydispersity index, and zeta ( $\zeta$ ) potential were measured by DLS at 0, 24, and 48 h under fluorescent laboratory light, and pH was measured with a calibrated digital pH meter (Accumet Basic, AB15, Fisher Scientific) at 0 h. All samples remained static and were covered with Parafilm between daily measurements.

### *Simulated sunlight apparatus and irradiance measurements*

The simulated sunlight apparatus consisted of a blue-spectrum metal halide lamp (mogul base; XM 250 W; 10,000 K; [www.xmlighting.com](http://www.xmlighting.com)) mounted in a

reflective fixture and lit by electronic ballast (LK250; part # 12-01-006706; [www.lumatekballast.com](http://www.lumatekballast.com)). The spectral irradiance emitted by the lamp was measured daily using a handheld UVX digital radiometer fitted with a UVA (UVX-36; calibrated at 365 nm) or UVB (UVX-31; calibrated at 310 nm) sensor (Ultra-Violet Products Ltd., CA, USA). The irradiance for UVA was, on average,  $3.55 \pm 0.38 \text{ W/m}^2$  and, for UVB,  $1.48 \pm 0.17 \text{ W/m}^2$  at the sample level. Typical maximum (clear-sky, mid-day, late-June) UVA and UVB irradiances in Edmonton ( $53^{\circ}31'46'' \text{ N}$ ,  $113^{\circ}31'35'' \text{ W}$ ) were 11.42 and  $6.18 \text{ W/m}^2$ , respectively. The simulated sunlight apparatus was located in a temperature- and light-controlled room ( $25 \text{ }^{\circ}\text{C}$ ; 16 h light: 8 h dark photoperiod). While the UV light output of the lamp far exceeded that of ambient fluorescent lighting ( $0.00 \text{ W/m}^2$ ), the irradiance emitted by the lamp was slightly lower than natural sunlight and thus approximates natural phototoxicity.

#### *Zebrafish husbandry and embryo collection*

Adult zebrafish (wild type strain AB) aged 6 to 18 months were housed in 30 L tanks ( $\sim 20$  fish/tank; pH: 7.4, conductivity:  $1260 \mu\text{S/cm}$ , temperature:  $28.5 \pm 1 \text{ }^{\circ}\text{C}$ , dissolved oxygen: 6.9 mg/L, hardness: 100 mg/L as  $\text{CaCO}_3$ , salinity: 0.6 ppt). Fertilized embryos were collected after natural mating triggered by the start of the light cycle (14 h light: 10 h dark photoperiod), randomly distributed among multiple Petri dishes, and incubated at  $28.5 \text{ }^{\circ}\text{C}$  under fluorescent fish facility lighting for 24 h until NP exposure.

### *Nanoparticle-assay interference*

To determine whether the NPs tested in this study were interfering with the biochemical assays, the intrinsic absorbance of each NP type in the assay buffer was measured, and the absorbance when NPs were added to the assay components in the presence and absence of the analyte (i.e. assay standard or supernatant from 11-20 pooled zebrafish tissue) was also measured. Spectral scans (200-800 nm) of 100 mg/L uncoated TiO<sub>2</sub> NPs, polymer-coated TiO<sub>2</sub> NPs, and polymer NPs were recorded immediately after dilution in phosphate, 1× reaction, or sucrose buffer via a UV-Vis diode array spectrophotometer (8452A UV Visible System, Hewlett Packard) and data collected with UV-Visible ChemStation software (A.09.01, Agilent). NP-assay interference was determined using a procedure outlined by Ong et al. (2014a). Results are presented as ‘difference in reported TBARS/Cat/TG/Sod/protein, calculated by subtracting the actual value of TBARS/Cat/TG/Sod/protein added to the microplate in the absence of NPs from the value reported by the assay in the presence of NPs. These experiments were repeated at least three times, and each experimental condition was repeated in triplicate wells for each experiment.

### ***Appendix III***

#### *Physicochemical characteristics*

Various physicochemical properties intrinsic to NPs themselves including particle size, size distribution and surface charge, as well as extrinsic environmental factors like solar radiation modulate NP toxicity (Shin et al., 2015). TEM images showed that the average diameter of dried, spherical uncoated TiO<sub>2</sub> NPs was 34.98 ± 1.63 nm (mean ± SEM, n = 25 particles; **Figure S4-4A**) while the diameter of the spherical polymer-coated TiO<sub>2</sub> NPs ranged between 3 and 9 nm (**Figure S4-4B**). Sizes of polymer NPs could not be measured by TEM due to the lack of a metal core. Photoreactivity of TiO<sub>2</sub> NPs increases with decreasing particle size mainly due to the band gap energy and large specific surface area of smaller particles (Lin et al., 2006). Lin et al. (2006) reported band gap energies of 3.239 and 3.289 eV for 29 and 3.8 nm TiO<sub>2</sub> NPs, respectively. We expected that polymer-coated TiO<sub>2</sub> NPs would be more photoreactive and generate more ROS than their slightly larger uncoated counterparts.

Aggregation of TiO<sub>2</sub> NPs decreases the production of OH• in aqueous suspension (Jassby et al., 2012). Dispersion was confirmed by DLS immediately after preparation of the 100-fold serial dilutions and again at 24 and 48 h to characterize NP behaviour between medium renewals (**Figure S4-5**). Size profiles indicated that 10 mg/L polymer-coated TiO<sub>2</sub> NPs and polymer NPs were more constant in DTW over 48 h than uncoated TiO<sub>2</sub> NPs, which showed visible signs of flocculation at 24 h and thereafter (**Figure S4-5A**). For example, uncoated TiO<sub>2</sub>, polymer-coated TiO<sub>2</sub>, and polymer NP suspensions had aggregate sizes of 2460.00 ± 25.51, 1165.00 ±

15.04, and  $84.82 \pm 0.97$  nm, respectively, at 0 h and  $5300.67 \pm 1047.48$ ,  $814.27 \pm 29.76$ , and  $111.00 \pm 1.40$  nm, respectively, at 48 h. Ma et al. (2012) reported an aggregate size of  $190 \pm 8$  nm at 0 h and  $171 \pm 11$  nm at 24 h for 0.1 mg/L uncoated TiO<sub>2</sub> NPs under simulated solar radiation and confirmed that these particles remained in suspension during this period. The polydispersity index describes the relative width of the particle size distribution curve (Miglietta et al., 2009). While uncoated TiO<sub>2</sub> NP suspensions were very polydisperse ( $> 0.70$ ) at 24 h, polymer-coated TiO<sub>2</sub> NP formulations showed mid-range polydispersity (0.08-0.70), and polymer NP aggregates were quite monodisperse ( $< 0.05$ ) in DTW (**Figure S4-5B**).

The  $\zeta$  potential is an indicator of the electrostatic interaction between particle surfaces and is thus a useful measure of the colloidal stability of NP suspensions (White et al., 2007). All NPs had a narrow  $\zeta$  potential range from  $-14.57 \pm 0.43$  to  $-12.73 \pm 0.23$  mV in near-neutral water (pH  $\sim 8.00$ ) over time (**Figure S4-5C**). Negatively charged NPs bind to cationic sites on the cell membrane due to electrostatic interactions, which has implications for uptake and toxicity (Wilhelm et al., 2003). Furthermore, the polymer coating can sterically hinder the interaction between the anionic NPs and the positively charged domains on the plasma membrane (Wilhelm et al., 2003). Our previous research has shown similar physicochemical characteristics (i.e. size, polydispersity index, and  $\zeta$  potential) for 10 mg/L polymer-coated TiO<sub>2</sub> NPs and polymer NPs in suspension (Felix et al., 2013). NP suspensions at concentrations  $< 10$  mg/L produced highly variable results and were considered below DLS detection limits (data not shown). Free metal controls were not included in this study because dissolution or release of free metal

ions from polymer-coated TiO<sub>2</sub> and polymer NPs was previously reported by our research group to be negligible ( $\leq 1.07 \pm 0.84\%$  of total metal present in the NP stock suspensions) (Felix et al., 2013). Although we cannot rule out the possibility that dissolved metal or some combination of NPs and metal ions played a role in noted effects, our intent was to examine the effect of polymer coating in determining NP toxicity rather than to distinguish between NP-specific and dissolution-based effects.